MULTIMODAL EXAMINATION OF BRAIN NETWORKS INVOLVED IN ATTENTIONAL

BIASING IN SCHIZOPHRENIA

by

PAUL D. METZAK

B.A., Simon Fraser University, 2006

M.Sc., The University of British Columbia, 2011

A DISSERTATION SUBMITTED IN PARTIAL FULFILLMENT OF THE REQUIREMENTS

FOR THE DEGREE OF

DOCTOR OF PHILOSOPHY

in

THE FACULTY OF GRADUATE AND POSTDOCTORAL STUDIES

(Neuroscience)

THE UNIVERSITY OF BRITISH COLUMBIA

(Vancouver)

July 2017

© Paul D. Metzak, 2017

Abstract

Schizophrenia is a serious, chronic mental illness that is characterized by perceptual abnormalities and cognitive deficits. Although the illness is commonly associated with perceptual abnormalities, the cognitive deficits have the greater impact on functional outcomes in patients. Some of the most profound deficits in schizophrenia have been observed in a domain referred to as cognitive control. Cognitive control is defined as the ability to adaptively adjust behaviour in response to environmental changes. Given the broadness of this definition, cognitive control is often fractionated into constituent cognitive operations, such as goal representation and maintenance, attentional biasing, conflict resolution, and stimulus-response mapping. In this study, the goal was to examine the brain basis for deficits in the attentional biasing aspect of cognitive control in schizophrenia. Behavioural and brain mechanisms of attentional biasing were assessed by manipulating the number of features that participants would have to ignore for each experimental trial. As schizophrenia is characterized by changes to both brain structure and function, a further aim was to use multi-modal brain imaging to develop a comprehensive picture of changes that underlie difficulties in attentional biasing. The results of this study indicated that although schizophrenia patients exhibit changes in brain structure, they still utilized the same brain networks as neurologically healthy individuals to bias attention towards relevant stimulus features. For the functional magnetic resonance imaging results, a functional brain network underlying attentional biasing, which included the dorsal anterior cingulate cortex, was identified and showed a positive relationship between the number of irrelevant stimulus features and increases in brain activity. Patients, however, showed reduced compensatory modulations in brain activity as the number of irrelevant stimulus dimensions increased. The magnetoencephalography results showed differences between the schizophrenia

ii

patients and healthy participants, but these differences were not as hypothesized, and may reflect cognitive differences related to language processing in schizophrenia. This work suggests that brain activity in patients is less efficient at higher levels of task difficulty when performing an attentional biasing task but these results are clouded by underlying changes in brain structure and a high variability in task activity in the patients.

Lay Summary

The goal of this project was to use multiple brain imaging modalities to examine differences between healthy participants and schizophrenia patients while performing a task designed to engage varying degrees of attentional biasing. In this task, the amount of attentional biasing required was varied by manipulating the number of relevant aspects in a figure presented on the screen from trial to trial, and participants were cued to respond to a specific aspect on each trial. On the basis of previous research revealing inefficiency in brain activity in schizophrenia, we expected to find that the patients had increased activity in attention-related areas relative to healthy participants when the number of relevant aspects were low, but lower activity than healthy volunteers when the number of relevant aspects was high. The results indicated that this pattern was present in the functional magnetic resonance imaging data but not in the magnetoencephalography data.

Preface

This dissertation is an original intellectual product of the author, Paul D. Metzak. All research was approved by the UBC Clinical Research Board (UBC CREB NUMBER: H10-01250) and the VCH Research Institute (Vancouver Coastal Health Research Study #V10-01250).

Table of Contents

List of Figures

Acknowledgments

I would like to offer my heartfelt gratitude to my supervisor, Dr. Todd Woodward, for his continued support and mentorship over the years. Thank you for all that you have done for me; I would not be here if not for your guidance and encouragement.

Many thanks to all the members of the Woodward Lab, past and present, that have helped me throughout this project, including but not limited to: Katie Lavigne, Jennifer Whitman, Nicole Sanford, Sarah Flann, Jennifer Riley, Emma Davis, Jesse Tinker, Jessica Ferguson-King, Kelsey Block, Kendall McSweeney, John Paiement, Sara Hughes, Susan Kuo, and Quinn Parker.

I owe a sincere thank you to the Down Syndrome Research Foundation for their generous support of my work and for their invaluable help and advice. I would particularly like to thank Dr. Teresa Cheung, Dr. Alexander Moiseev, Dr. Naznin Virji-Babul, Dr. Urs Ribary and Dawn McKenna for their assistance with my project.

Many thanks are owed to the WestGrid subdivision of Compute Canada for providing the high-performance computing resources used in this project.

Thank you to the members of my supervisory committee (Dr. Elton Ngan, Dr. Christine Tipper, and Dr. Ipek Oruc) for your helpful comments and questions throughout this process.

I owe a tremendous thank you to the Canadian Institutes of Health Research and to the University of British Columbia for their financial support during my PhD. It truly made a difference in my life.

Lastly, I would like to offer my deepest thanks to my family for their love and encouragement. I will be forever grateful to all of you for your unwavering support.

This work is dedicated to my parents, Daniel and Anne Metzak,
who always encouraged their children to follow their dreams.

General Introduction

Schizophrenia

Schizophrenia is a severe mental illness affecting about 0.4 to 1.0 % of the population (American Psychiatric Association. Task Force on DSM-IV, 2000; Saha, Chant, Welham, & McGrath, 2005). Schizophrenia is a developmental disorder that manifests in late adolescence and early adulthood (Karlsgodt et al., 2008; Rapoport, Giedd, & Gogtay, 2012), and is characterized by a panoply of symptoms including delusions, hallucinations, lack of volition, and cognitive disorganization (American Psychiatric Association. Task Force on DSM-IV, 2000; Barch, 2005). Diagnoses are made on the basis of two or more of the following symptoms being present for at least one month: delusions, hallucinations, disorganized speech, grossly disorganized or catatonic behavior, and negative symptoms (diminished emotional expression or avolition) (Tandon et al., 2013).

One of the notable features of schizophrenia is the variability in clinical presentation between patients diagnosed with the same disorder (Tandon, Nasrallah, & Keshavan, 2009). Although diagnosis of schizophrenia has historically relied upon a syndromal model, whereby diagnoses are dependent on the presence of multiple discrete symptoms (Jablensky, 2010); many have been critical of this approach (Jablensky, 2010; Maj, 1998; Westen, 2012), because it relies on arbitrary symptom duration thresholds and the exclusion of other mental illnesses rather than a biomarker or a feature specific to schizophrenia. Attempts have been made to reduce symptom dimensionality using multivariate techniques like factor analysis and principal component analysis to identify latent variables that underlie the covariation of multiple discrete symptoms. However, the number of latent variables differs based on the instrument used to measure symptoms and the sample of patients studied (Emsley, Rabinowitz, & Torreman, 2003; Goghari,

Sponheim, & MacDonald, 2010; P. F. Liddle, 1987; Rietkerk et al., 2008; Van den Oord et al., 2006), so no clear consensus has been reached in the field regarding the true number of symptom dimensions. Further exacerbating this issue is the intra-subject variability in symptomatology throughout the course of the illness (Keefe & Harvey, 2012; Tandon et al., 2009), as symptoms do not remain constant within a given individual over the course of weeks and months (Arndt, 1995; Sherwood, Thornton, & Honer, 2006; Weiler, Fleisher, & McArthur-Campbell, 2000; Woodward et al., 2014).

Cognition.

Although symptoms may wax and wane over time, many of the cognitive deficits that are associated with schizophrenia, including impairments in attention, working memory, verbal learning and executive functions, persist over time from the prodrome to the chronic phase of the illness (Hoff, Svetina, Shields, Stewart, & DeLisi, 2005; Keefe & Harvey, 2012; Tandon et al., 2009). These cognitive deficits are: highly prevalent (Keefe, Eesley, & Poe, 2005), generalized across multiple domains (Dickinson, Ramsey, & Gold, 2007; Gold & Dickinson, 2013; Heinrichs & Zakzanis, 1998), present in the prodromal phase of the disease (Heinrichs & Zakzanis, 1998; Seidman et al., 2010; Woodberry, Giuliano, & Seidman, 2008), pronounced relative to neurologically healthy participants (Dickinson et al., 2007; Heinrichs & Zakzanis, 1998), and present to a lesser degree in non-psychotic relatives (Trandafir, Méary, Schürhoff, Leboyer, & Szöke, 2006; Whalley, Harris, & Lawrie, 2007).

Functional relevance of cognitive deficits to schizophrenia.

Although studies have shown that both clinical symptomatology and cognitive deficits influence quality of life in schizophrenia (Mohamed et al., 2008; Savilla, Kettler, & Galletly, 2008; Ueoka et al., 2011), cognition has been found to be a significant predictor of functional

outcomes in many domains including employment (McGurk, Mueser, Harvey, LaPuglia, & Marder, 2003), independent residential status (W. W. Leung, Bowie, & Harvey, 2008; Shamsi et al., 2011), relapse prevention (Jeste et al., 2003), and cost of care (Sevy & Davidson, 1995). Given their substantial influence on functional outcome in schizophrenia as well as their stability over time, cognitive deficits remain a prime target for remedial efforts and interventions in schizophrenia.

Remediation of impaired cognition in schizophrenia.

Schizophrenia patients exhibit deficits relative to healthy volunteers in virtually every aspect of cognition, and these deficits have a pervasive influence on functional outcomes. Therefore, a concerted effort has been put forth to determine which cognitive domains and neuropsychological measures are most worthwhile in assessing rehabilitative efforts or pharmaceutical interventions (M. F. Green et al., 2004). The outcome of these efforts was a standardized clinical battery suited for use in clinical trials and assessing the impact of interventions on cognitive function, termed the Measurement and Treatment Research to Improve Cognition in Schizophrenia (MATRICS) initiative (M. F. Green, Harris, & Nuechterlein, 2014).

These tests have a variety of important attributes including good test-retest reliability, minimal practice effects, and facility and brevity of administration (M. F. Green et al., 2004). However, the tests used in clinical settings often tap into multiple distinct cognitive systems, which can lead to difficulties when attempting to interpret precisely which aspect of the cognitive task is causing the deficits seen in patients. This issue is compounded by differences in motivation (Fervaha et al., 2014; Thornton et al., 2007), and medication effects (Kane & Sharif, 2008). Therefore, a second project was undertaken to examine the cognitive deficits in

schizophrenia from a basic neuroscience perspective. This effort, known as the Cognitive

Neuroscience Treatment Research to Improve Cognition in Schizophrenia (CNTRICS) initiative,

has as its goal the development of cognitive neuroscience paradigms that isolate a specific

cognitive operation (or one particular aspect of a cognitive operation) in need of remediation in

schizophrenia. This goal is important for drug development because it provides a link between

animal and human studies, and specifies a mechanistic framework for the drug's action via a

single neural system (Carter et al., 2008). The CNTRICS initiative identified six discrete

cognitive domains in which patients show specific deficits: working memory, episodic memory,

attention, perception, social and emotional processing, and executive function (Barch et al.,

2009; Carter et al., 2008). These domains were selected on the basis of their prominence in

neuroimaging and animal research, and their promise in delineating the neural substrates

underlying cognitive systems.

Cognitive Control

One of the domains where schizophrenia patients exhibit pronounced deficits is executive

function. Executive function, also known as cognitive control, is the ability to adaptively adjust

behavior in the face of changing environmental demands. A concrete example of cognitive

control is the ability to differentially respond to a stimulus depending on the situational context,

(e.g. a flashing red light means different things if you are driving a car versus attending a hockey

game). These adaptive behaviours are reflected in goal-directed adjustments in a number of

cognitive operations such as response biasing, feature selection, maintenance of online

information, and attention allocation (Botvinick, Braver, Barch, Carter, & Cohen, 2001). This

higher-order cognitive ability is most often measured using complex tasks such as the Wisconsin

card sorting test (Grant & Berg, 1948), the Stroop test (Stroop, 1935), the Eriksen Flanker task

(Eriksen & Eriksen, 1974), and the Simon task (Simon & Wolf, 1963), and has been identified as a core deficit in schizophrenia (Barch & Ceaser, 2012; Carter, Minzenberg, West, & MacDonald, 2012).

The list of cognitive operations that are considered part of executive function make it apparent that cognitive control is complex, and containing multiple facets. Correspondingly, different executive processes are mediated by different regions of the frontal lobes (Stuss & Alexander, 2000), and correlations between different tasks that purport to measure cognitive control are not high (Miyake et al., 2000). Furthermore, the tasks used to measure cognitive control span multiple cognitive domains (Kerns, Nuechterlein, Braver, & Barch, 2008), and, due to the reliance on the deployment of novel cognitive strategies as an aspect of executive function, they may exhibit poor test-retest reliability (Chan, Shum, Toulopoulou, & Chen, 2008).

Theories of cognitive control.

Many of these issues regarding the complexity and span of cognitive control rest upon the fact that cognitive control, much like attention, is a superordinate system relative to sensory or motor systems. Cognitive control alters the processing in these primary systems in order to achieve abstract or higher-order goals (Botvinick et al., 2001; E. K. Miller & Cohen, 2001; Power & Petersen, 2013) but are generally not considered to be part of the primary systems themselves. The prefrontal cortices have long been considered a key component of the cognitive control system (Koechlin, Ody, & Kouneiher, 2003; E. K. Miller, 2000; E. K. Miller & Cohen, 2001) because of their interconnections with other regions of the brain (Croxson et al., 2005; Petrides & Pandya, 2002; Petrides, Tomaiuolo, Yeterian, & Pandya, 2012), and the pattern of deficits in complex planning resulting from PFC lesions in both humans (Alvarez & Emory, 2006), and non-human animals (Passingham, 1972a, 1972b).

Although the prefrontal cortices are considered to be one of the core regions involved in cognitive control, the precise nature of their involvement, as well as which other regions are involved, is still under active debate. One of the earliest theories of cognitive control in the age of neuroimaging was the conflict model proposed by Botvinick and colleagues (Botvinick, 2007; Botvinick & Braver, 2014; Botvinick et al., 2001; Kool & Botvinick, 2013; MacDonald, 2000). The initial hypothesis was that cognitive control was engaged in instances where there exists a conflict between brain processes occurring in parallel (Botvinick et al., 2001), and that this conflict is indexed by increases in blood oxygenation level dependent (BOLD) activity in the dorsal anterior cingulate cortex (dAcc). This conflict-based interpretation of cognitive control is based on the findings that dAcc activity increases when errors are made, when prepotent responses need to be inhibited, when the correct response is underdetermined, and in situations where multiple separate stimuli (or stimulus dimensions) need to be tracked (Botvinick et al., 2001). In this model, the DLPFC was proposed to be responsible for implementing and maintaining top down control over the attentional demands and response rules of the task (MacDonald, 2000). A more formal statement of the function of the DLPFC in cognitive control was elucidated by Braver and colleagues (Braver, 2012; De Pisapia & Braver, 2006). Braver argues that cognitive control can be exerted via two different pathways: one proactive, and the other reactive. Both of these methods involve DLPFC activation; however, the proactive pathway involves sustained activity prior to the control-requiring event, whereas the reactive pathway involves transitory DLPFC activity in response to the control-requiring event, along with activity in a network of other regions including dAcc (Braver, 2012).

Another prominent theory of cognitive control posits that the conflict theory has misunderstood the roles of the DLPFC and dAcc. Petersen and colleagues argued that brain

regions involved in cognitive control need to display at least 3 types of signals: 1) increased

activity at the outset of a new task that should reflect the instantiation of task rules, 2) sustained

increase in activity throughout the task that should reflect the maintenance of the task set/rules,

and 3) transient increases in activity following error commission that should reflect error-related

feedback (Dosenbach et al., 2006, 2007; Dosenbach, Fair, Cohen, Schlaggar, & Petersen, 2008;

Power & Petersen, 2013). This group examined the BOLD responses from multiple mixed

block/event related experiments, and identified 3 'core' regions that showed all three patterns of

activity: the dAcc and the left and right anterior insulae (Dosenbach et al., 2006). Additionally,

they also found many other brain regions of interest (ROIs) that demonstrated a portion of the

signals thought to be associated with cognitive control. Petersen and colleagues then used graph

theoretic analyses of resting state data to identify the BOLD signal correlations between the areas

identified as being related to cognitive control ('core' regions and ROIs), in order to determine

how and whether these regions coalesce and function as networks (Dosenbach et al., 2007). The

results of this work suggested that there are at least 2 control systems in the human brain. The

first control system included the 'core' regions mentioned above, as well as the medial prefrontal

cortex (mPFC; also known as the anterior prefrontal cortex (aPFC), and the ventromedial

prefrontal cortex (vmPFC)) and the anterior thalamus. The other control system was a fronto-

parietal system with ROIs in DLPFC, middle frontal gyrus, mid cingulum, and inferior parietal

lobule/sulcus (Dosenbach et al., 2007). On the basis of the control signals detected in the nodes

of these networks, the authors argue that DLPFC network, which includes the dorsal attention

network (Corbetta & Shulman, 2002), is involved in initializing cognitive control and adjusting

the level on control in response to feedback. In contrast the cinguloopercular network is involved

in all three aspects of cognitive control, and is responsible for maintaining 'task mode', which is

characterized as the stable, outward-focusing of attention and implementation of rules and strategies (Dosenbach et al., 2008; Power et al., 2011).

Attentional biasing.

As mentioned above, one particular aspect of cognitive control involves the attenuation of conflict between competing stimuli (or competing features of a stimulus) via the top-down regulation of attention. This ability has also been referred to as the inhibition of information that is irrelevant to the to-be-performed task (Blasi et al., 2006; Botvinick, 2007; Botvinick et al., 2001; Diamond, 2013; Duque, Labruna, Verset, Olivier, & Ivry, 2012; Duque, Olivier, & Rushworth, 2013; Sandrini, Rossini, & Miniussi, 2008), although some have argued against the use of the term 'inhibition' in this context (Aron, 2007), and suggest that attentional biasing is a more appropriate description. Attentional biasing seeks to reduce the conflict between stimuli or stimulus dimensions, or to diminish the influence of exogenous attentional capture (Lien, Ruthruff, & Johnston, 2010). Some evidence for deficits in attentional biasing in schizophrenia have been found, specifically, attending to irrelevant stimuli has been associated with positive symptoms (Morris, Griffiths, Le Pelley, & Weickert, 2013), and paranoia-related stimuli elicit quicker subsequent responses in schizophrenia patients relative to healthy participants (Moritz & Laudan, 2007). However, a specific deficit or change in neural function in schizophrenia related to this aspect of cognitive control has yet to be identified in schizophrenia.

There is extensive evidence that this process of top-down attentional biasing and attenuation of conflict between competing responses or stimulus dimensions and features is supported by the DLPFC, ventrolateral prefrontal cortices (VLPFC), dAcc, juxtapositional lobule cortices (also referred to as the supplementary motor area (SMA)) and pre-supplementary motor area (pre-SMA), parietal cortices and insula (Bari & Robbins, 2013; Cole et al., 2013; Dias et al.,

2006; Niendam et al., 2012; Sandrini et al., 2008). This network of regions has been referred to as the cognitive control network (Cole et al., 2013; Cole & Schneider, 2007), is closely aligned with the task positive network (TPN) (M. D. Fox et al., 2005), and overlaps with the regions discussed in both the conflict monitoring and control signal theories of cognitive control.

In the magnetoencephalography (MEG) literature, the requirement for cognitive control often elicits a pattern of activity that has been referred to as frontal midline theta. As the name suggests, this is a pattern of slow oscillatory activity detected by sensors overlying the middle frontal portion of the brain. Several studies have localized the frontal midline theta signal to the dAcc/SMA (Botvinick, Cohen, & Carter, 2004; Cavanagh & Shackman, 2015; Gevins, Smith, McEvoy, & Yu, 1997), and have found increases in activity in a variety of experimental contexts where increased cognitive control is required including novelty detection, response conflict, error detection, and post-error slowing (Cavanagh & Frank, 2014; Cavanagh & Shackman, 2015; Cavanagh, Zambrano-Vazquez, & Allen, 2012), as well as during the delay period in working memory experiments (Hsieh & Ranganath, 2014; Jensen & Tesche, 2002). These findings suggest that the frontal midline theta oscillations index the requirement for control in electrophysiological experiments.

Goals of the current study

The goals of the present study were to isolate the brain activity related to differences in levels of attentional biasing, as well as to identify any changes in activity or anatomical loci in schizophrenia patients. In this study, the levels of attentional biasing required were varied from trial-to-trial by manipulating the number of relevant response features, which in keeping with the terminology from previous task switching studies have been termed the valence of a stimulus (Metzak, Meier, Graf, & Woodward, 2013; Woodward, Metzak, Meier, & Holroyd, 2008).

The motivation for using parametric increases in stimulus valence is based on previous working memory research. In these studies, increasing the number of letters to be encoded led to a corresponding increase in brain activity throughout the course of the trial (Metzak et al., 2010, 2011) in both healthy participants and schizophrenia patients. Furthermore, the patients showed increased activity relative to healthy participants at low to medium levels of memory load, and decreased activity relative to healthy participants at high memory loads (Metzak et al., 2011). A similar pattern of activation whereby schizophrenia patients have increased activity relative to healthy participants a low levels of memory load, and higher activity relative to healthy participants at high levels of memory load has been found in other working memory studies (Brandt et al., 2014; Eich, Nee, Insel, Malapani, & Smith, 2014; Potkin et al., 2009), and is thought to reflect inefficiency in brain activity in schizophrenia. This hypothesis was originally developed to account for the conflicting reports of hypo- and hyperactivity in DLPFC in schizophrenia patients relative to healthy participants while performing working memory experiments, and suggested that DLPFC brain activity in response to working memory load resembled an inverted-U, such that activity increased until capacity is reached, at which point it decreased (Callicott et al., 2003). In schizophrenia patients, this inverted-U is left-shifted so that they exhibit hyper-frontality (relative to healthy participants) at low to medium memory loads, and hypo-frontality (relative to healthy participants) at medium to high memory loads.

Working memory and cognitive control tasks involve many overlapping cognitive mechanisms and elicit activity in similar networks, therefore in the current experiment sought to explore whether the same inefficiency phenomenon is present in attentional biasing in schizophrenia patients by presenting stimuli with varying numbers of stimulus dimensions. The

10

stimuli that were presented had one, two, or three relevant stimulus dimensions and are referred to as univalent, bivalent, or trivalent, respectively.

As there is a relationship between brain structure and function (Messé, Rudrauf, Benali, Marrelec, & Honey, 2014; Rubinov, Sporns, van Leeuwen, & Breakspear, 2009), differences in brain structure between healthy volunteers and schizophrenia patients, as measured by both structural magnetic resonance imaging and diffusion weighted imaging, were also examined. In the present study, a number of separate analyses were performed using multiple brain imaging methods and statistical techniques. The first section was focused on the behavioural data, and the response times and accuracy were assessed in order to identify any significant differences between valence levels and the groups. The second section examined differences in structural connectivity between the two groups using structural magnetic resonance imaging and diffusion weighted imaging. Structural magnetic resonance imaging is generally used to assess the overall size of the brain, the size of specific structures, as well as the thickness or volume of specific tissue types. Diffusion weighted imaging exploits the thermal movement of water molecules and the hydrophobic nature of the axons that link neurons together in order to produce a map indexing the integrity of structural connections in the brain. The third section was focused on the functional magnetic resonance imaging (fMRI) data. In this section both univariate and multivariate statistical methods were used to assess differences between the valence levels and groups. These classes of statistical techniques are typically used to obtain different types of answers; univariate analyses seek to identify discrete anatomical loci whose activity differs significantly between conditions and/or groups, whereas multivariate analyses seek to identify networks of brain regions displaying correlated patterns of activity and assess differences in their activity levels between conditions and/or groups. The fourth section was focused on the MEG

11

data. As with the analyses in the fMRI section, the MEG data was also analyzed using both univariate and multivariate statistical methods in order to identify both discrete brain regions displaying significant differences between conditions and groups, as well as group or condition related activity differences in networks of brain areas. In the fifth section, a multimodal analysis of the functional data was performed, whereby the spatial patterns of fMRI activity found in the multivariate analysis in section two were used as a spatial constraint on the MEG data, thus separating the MEG results into networks that are predictable from the fMRI data, and those that are independent of the patterns found in the fMRI results.

<center>**General Methods**</center>

This section describes the imaging methods, recruitment method, samples for each of the subsequent analysis, as well as the task employed in this study.

Functional Brain Imaging

Two functional brain imaging techniques were employed in this study: fMRI, and MEG. These two techniques were chosen since they are non-invasive measures of brain activity suitable for event-related designs, and can assess activity throughout the entire brain. However, fMRI and MEG measure two distinct aspects of brain activity, the first measures a metabolic after-effect of activity and the second measures the magnetic field changes resulting from brain activity itself. The activity found using each measure does not necessarily overlap (Lorig, Freeman, Ahlfors, & Menon, 2009).

   Functional magnetic resonance imaging.

For the past twenty years, fMRI has been an immensely popular neuroimaging method in cognitive neuroscience. fMRI produces images with good spatial resolution (e.g., 1-2 millimeters), and study of the associated BOLD signal provides reasonably good temporal resolution. For this reason, fMRI imaging using the endogenous BOLD contrast has overwhelmingly been the choice for researchers interested in non-invasively mapping structure(s) to function(s) in the human brain. fMRI is most powerfully used in cognitive experiments in which the primary question to be asked is 'Where?' rather than 'When?'.

fMRI detects changes BOLD signal, which is carried by hemoglobin, the molecule in blood that transports oxygen, and BOLD imaging capitalizes on the difference in the magnetic properties of oxygenated versus deoxygenated hemoglobin (Ogawa, Lee, Kay, & Tank, 1990). When hemoglobin becomes deoxygenated, its magnetic properties change, such that it transitions

<center>13</center>

from being diamagnetic to being paramagnetic. This change to paramagnetism causes a decrease in magnetic field (Ogawa et al., 1990; Thulborn, Waterton, Matthews, & Radda, 1982) that is measurable and localized to specific brain regions.

Neural activity leads to an increase in blood flow to that region, and this increases at a rate greater than the consumption of oxygen by that region, thus, more oxygenated blood (hemoglobin) arrives than is deoxygenated (P. T. Fox & Raichle, 1986). Paradoxically, this change leads to active brain regions having a localized increase in magnetic field strength, which is known as the intrinsic BOLD contrast (Kwong et al., 1992; Ogawa et al., 1992) and is the basis for conventional fMRI studies. Although the interplay of many factors is involved in the production of the BOLD response, tight coupling between blood flow and neural activity has consistently been demonstrated (Buxton, 2013; Raichle, 1994). In a seminal work examining the relationship between BOLD signal and neural activity, Logothetis and colleagues (Logothetis, Pauls, Augath, Trinath, & Oeltermann, 2001) used simultaneous BOLD-fMRI and intra-cranial recordings in monkeys to demonstrate that the increase in BOLD contrast directly reflects an increase in neural activity, and that the relationship between neural activity and BOLD was monotonic. Furthermore, they modeled estimated BOLD activity separately from both local field potentials (LFPs), which measure the summation of post-synaptic depolarizations, and multi-unit activity, which measures the firing of action potentials, and found that the model fit suggested that the LFPs were more closely related to BOLD response than spiking activity.

One point that is readily apparent from the above description of the BOLD signal is that it is a metabolic measure of activity that occurs after neural activity has taken place. Since this measure relies on the ratio of oxygenated to deoxygenated hemoglobin, and this ratio is dependent on the underlying relationship between cerebral blood flow and cerebral oxygen

consumption, interpretations of what the BOLD response means in terms of neural activity is necessarily complex (Buxton, 2013; Lorig et al., 2009). This is further compounded by findings that the BOLD response may not be related to energy consumption (Attwell & Iadecola, 2002; Lorig et al., 2009), BOLD responses vary between voxels based on the volume of blood found therein at baseline (S.-G. Kim & Ogawa, 2012), BOLD responses may overestimate the spatial extent of neural activity (Huettel, 2004), BOLD responses exhibit a signal-to-noise ratio at least one order of magnitude smaller than direct measures of neural activity (Logothetis et al., 2001), and the coupling between cerebral blood flow and oxygen consumption may differ between cortical and subcortical areas (Ances et al., 2008).

Aside from these difficulties in interpreting the meaning of changes in the BOLD signal, there are cases where BOLD fMRI is insensitive to changes in brain activity. These situations include image distortions and signal loss which occurs at air/tissue interfaces, such as in the orbitofrontal cortex and inferior temporal lobe (Cordes, Turski, & Sorenson, 2000), and during periods of brief stimulation where neurons can have their energy needs met through anaerobic glycolysis (P. T. Fox, Raichle, Mintun, & Dence, 1988; Lorig et al., 2009).

Magnetoencephalography.

MEG involves measuring the magnetic fields emanating from the human head, which are created by the electric currents generated by neural activity (Herdman & Cheyne, 2009). These magnetic fields are produced by intracellular ionic current flow, can be measured on a timescale of milliseconds (Hämäläinen, Hari, Ilmoniemi, Knuutila, & Lounasmaa, 1993), and are strongest in the most active parts of the brain. However, the magnetic fields produced by a single neuron are miniscule (~20 femtoamperes) (Hall, Robson, Morris, & Brookes, 2013). Thus, the summation of the magnetic fields of many neurons is required for it to be measurable outside the

head. The magnetic fields are thought to result from the post-synaptic (i.e. dendritic) current flow (Hall et al., 2013; Hämäläinen et al., 1993; Herdman & Cheyne, 2009), rather than the action potentials themselves. This is primarily due to two reasons: the first is that action potentials are quadrupolar which means that their magnetic fields fall off inversely with the cube of the distance from the source, whereas post-synaptic potentials are dipoles, whose fields fall off inversely with the square of the distance, which means that the signal from action potentials is detectable at a much shorter range than those from post-synaptic potentials. And secondly, post-synaptic potentials occur over a time frame an order of magnitude larger than action potentials which facilitates temporal summation of the MEG signal (Hall et al., 2013; Hämäläinen et al., 1993; Herdman & Cheyne, 2009). Sampling rates for MEG are typically near 1000Hz, which means that neural activity is measured with a temporal resolution corresponding to the speed of most cognitive processes. Although MEG is most appropriately used in experiments in which the primary question to be asked is 'When?' rather than 'Where?', advancements have been made in estimating the origins of the measured fields (Herdman & Cheyne, 2009).

Although MEG directly measures functional brain activity, it requires the summation of thousands of miniscule magnetic fields in order to achieve a measurable signal (Hämäläinen et al., 1993). Given that magnetic fields are oriented perpendicular to the flow of current (i.e., it follows the 'right hand rule'), in order to be detectable by MEG the dendrites that form the current dipoles must be oriented in a common direction perpendicular to the scalp, and must be asymmetrical (Hall et al., 2013; Hämäläinen et al., 1993; Herdman & Cheyne, 2009; Lorig et al., 2009). Taken together, these requirements suggest that the measured MEG signal is obtained from pyramidal neurons located primarily in the sulci of the cortex (Hämäläinen et al., 1993). Activity in pyramidal neurons that are located in the gyri, and activity in stellate neurons, which

16

have radially symmetric dendrites, is largely undetectable using MEG (Hall et al., 2013). Furthermore, the radial structure and lack of columnar organization in certain brain regions, such as the thalamus and basal ganglia, precludes them for contributing to the measured MEG signal (Schomer & Lopes da Silva, 2005).

In order to generate a measurable signal at the scalp, thousands of pyramidal neurons must act as a functional ensemble, whereby the activity of each individual neuron synchronizes with its neighbors. This synchrony is partially driven by inputs but is also sculpted by the tens of thousands of anatomical pathways that input to, and output from, each neuron, including extensive feedback and feedforward loops (Haider & McCormick, 2009). This synchrony can occur in spatially distributed neuronal assemblies via oscillatory activity, that is the periodic changes in magnetic/electrical activity (Gray, König, Engel, & Singer, 1989) The oscillatory patterns are partially dependent on the balance of excitatory and inhibitory activity within the neuronal ensembles, as research has shown that altering the inhibitory/excitatory balance of a neuronal ensemble via the inhibition of inhibitory interneurons changes the frequency and strength of oscillatory activity (Sohal, Zhang, Yizhar, & Deisseroth, 2009).

MEG (and electroencephalography (EEG)) activity can be quantified by the frequency of the oscillations, although these frequency bands were identified prior to the discovery of the neurophysiological mechanisms that underlie them (Lopes da Silva, 2013). Although there are differences in the precise ranges assigned to each of the bands, those most commonly discussed are: alpha (8-12 Hz), beta (14-30 Hz), gamma (30-90 Hz), and theta (4-7.5 Hz) (Lopes da Silva, 2013; Schomer & Lopes da Silva, 2005). These oscillations are only detectable in large ensembles of neurons, however, these oscillations cannot be explained simply as by-products of the subtypes of neurons that comprise the ensemble. Rather, these oscillations play a functional

17

role in altering synaptic plasticity, modifying the input selectivity of neurons within the ensemble, and consolidating learned information (Buzsáki & Draguhn, 2004).

Structural Brain Imaging

Two structural brain imaging techniques were employed in this study: structural magnetic resonance imaging (sMRI), and diffusion weighted imaging (DWI). These two techniques were chosen since they are non-invasive measures, and offer complementary views of brain structure.

Structural magnetic resonance imaging.

As its name implies, sMRI provides a static and detailed picture of the structure of the brain with clear visible distinctions between grey matter, white matter, and cerebrospinal fluid (CSF) (Hazlett, Goldstein, & Kolaitis, 2012; Symms, Jäger, Schmierer, & Yousry, 2004). In this study we have used T1 weighted sMRI which contrasts the three tissue types on the basis of the time it takes the protons of hydrogen molecules to align to the magnetic field of the MRI scanner after a perpendicular radio frequency pulse has been applied (Buxton, 2013; Gordon, 1999). sMRI can be used to analyze the overall size of the brain, the size of specific structures, as well as the thickness of specific tissue types (usually grey matter). There are several data analysis programs that can automatically segment sMRI images into different tissue types, and even into specific brain structures (Desikan et al., 2006; Fischl, van der Kouwe, et al., 2004; Tzourio-Mazoyer et al., 2002), however, these programs have difficulty when the brains differ from the norm, or when voxels contain more than one tissue type (de Reus & van den Heuvel, 2013).

Diffusion weighted imaging.

DWI is a specialized MRI scanning technique that is used to show the directionality and integrity of white matter pathways in the brain, and is based on the random thermal movement of water molecules (Jeurissen, Leemans, Jones, Tournier, & Sijbers, 2011). As white matter in the

brain is composed of myelinated axons, which are hydrophobic, water diffusion along axons takes place primarily in a single direction (i.e., is anisotropic). DWI exploits this to map white matter tracts as they travel through the brain by identifying a continuous path of anisotropic water diffusion through adjacent voxels. However, the signal to noise ratio is very low in DWI images and they are highly susceptible to artifacts (Jeurissen et al., 2011; Jeurissen, Leemans, Tournier, Jones, & Sijbers, 2013; Tournier, Mori, & Leemans, 2011) which can lead to false positives and false negatives in the estimated white matter tracts. Furthermore, there is difficulty in assessing white matter integrity in voxels where white matter fibres cross or do not run in parallel (Dell'Acqua, Simmons, Williams, & Catani, 2013; Jeurissen et al., 2011, 2013). This means that it is often difficult to know whether the lower measures of white matter integrity are due to abnormalities in axons and/or myelination, or whether the fibre tracts simply do not run in parallel through a voxel.

Combining Brain Imaging Modalities

Although there are multiple methods and techniques to combine the data or results from brain imaging experiments using different modalities, the rationale is simple: capitalize on the strengths of each modality whilst minimizing its inadequacies. As the review of neuroimaging modalities above has illustrated, each technique has limitations that only allow the measurement of select aspects of brain activity or structure (Uludağ & Roebroeck, 2014). Very generally, multimodal imaging combinations can be of three types: structural-structural, structural-functional, and functional-functional. Structural-structural imaging often combines sMRI and DWI, and is used in cases where changes in both grey matter and white matter are expected, for instance, as one might expect in individuals that have suffered a stroke (Copen, 2015). When discussing the fusion of two functional imaging methods, one of the primary motivations is to

improve the temporal or spatial resolution of the analysis (Biessmann, Plis, Meinecke, Eichele, & Müller, 2011; S. Liu et al., 2015), as each functional method exhibits a lack of precision in one of these aspects. Furthermore, each of the functional imaging modalities is insensitive to some aspect of neural activity. MEG (and EEG) primarily measure from pyramidal neurons as the shape of these neurons, and the fact that they lie in parallel in the cortex, allows for summation of the electrical and magnetic fields that emanate from changes in postsynaptic activity (Lopes da Silva, 2013).

A further distinction to be drawn in multimodal analyses is whether they are symmetrical or asymmetrical. Symmetrical analyses involve utilizing the information from both (all) modalities simultaneously. These analyses can be either data-driven or model based but the primary requirement is that the analyses are performed on both modalities simultaneously, or the mutual information from features in each modality is assessed (Biessmann et al., 2011). Conversely, in an asymmetric analysis, the results from an analysis of a single modality is used to inform the subsequent analysis in a different modality. For example, the anatomical location of a significant increase in activity in an fMRI analysis could be used as a spatial prior in an EEG analysis from the same experimental paradigm.

The present study employs an asymmetrical analysis where the pattern of BOLD activity from the fMRI analysis was used as a spatial constraint on the results of the MEG analysis. The aims of this analysis were to identify the oscillatory frequencies underlying the BOLD response using the attentional biasing task we have designed (Stevenson, Brookes, & Morris, 2011; Whitman, Ward, & Woodward, 2013), as well as to identify patterns of activity that differ between the two modalities (Whitman et al., 2015).

Recruitment of Participants

All participants were recruited from the Greater Vancouver Area. Participants with

schizophrenia were recruited from outpatient facilities and community mental health teams

located in the Greater Vancouver Area. Diagnosis was confirmed at time of testing using the

Mini International Neuropsychiatric Interview (Lecrubier et al., 1997; Sheehan & Lecrubier,

1998). Exclusion criteria included a history of traumatic brain injury, low intelligence (IQ < 85),

< 18 or > 55 years of age, a past or present diagnosis of epilepsy, encephalitis, or any other

neurological illness, severe diabetes, hepatitis C, hypothyroidism, and poor eyesight (20/50 or

worse). Any patients with concurrent Axis I diagnoses other than schizophrenia or

schizoaffective disorder were excluded. Substance use was tolerated if it did not meet DSM-IV

criteria for substance-related disorders. All patients were using atypical antipsychotics, and all

medication dosages have been transformed to chlorpromazine equivalent units (Davies, 2012).

Participants with English as a second language were excluded if they had not been using English

every day for a period of at least 5 years. Current symptoms were assessed using the Signs and

Symptoms of Psychotic Illness scale (SSPI) (P. F. Liddle, Ngan, Duffield, Kho, & Warren,

2002). If participants were found to have delusions and/or hallucinations, they were also

administered the psychotic symptom rating scales (PSYRATS) (Haddock, McCarron, Tarrier, &

Faragher, 1999).

The control group was recruited from the Greater Vancouver Area using posters and

advertisements placed in libraries, community centers, hospitals and on the UBC campus. This

group was matched to the patient group on age, gender, premorbid IQ estimated by Ammons

Quick Test (Otto & McMenemy, 1965) and Wechsler Test of Adult Reading (WTAR) (R. E. A.

Green et al., 2008; Mathias, Bowden, & Barrett-Woodbridge, 2007), and parental socioeconomic

status (Blishen, Carroll, & Moore, 2008). In addition to the exclusion criteria for patients, controls were excluded if they were currently taking any psychiatric medication, or had a personal or family history of either schizophrenia or bipolar disorder. All participants in this experiment were right handed. Please see Table 1 for a summary of the demographic information for this sample.

Participant Samples for Each Analysis

The participants differed in many of the analyses due to a variety of factors including early scan termination, MRI contraindications, excessive movement and data recording issues. Please see Table 2 for a description of sample sizes and a statistical analysis of any differences in age and gender between the groups. For the behavioural analyses, 1 schizophrenia patient had MRI contraindications and therefore did not participate in MRI scanning and was not included in the behavioural analysis of the fMRI response times and accuracy. For the structural MRI, 2 healthy volunteers and 6 schizophrenia patients were removed for excessive motion, and 1 schizophrenia patient was excluded for having MRI contraindications. For the DWI analysis, 3 healthy volunteers and 5 schizophrenia patients were removed for moving excessively, 1 schizophrenia patient was excluded for having MRI contraindications, and 1 schizophrenia patient terminated the scanning session at the outset of the DWI scan. For the fMRI analyses, 4 healthy volunteers and 9 schizophrenia patients were removed for excessive motion, and 1 schizophrenia patient was excluded for having MRI contraindications. For the MEG analyses, 2 healthy volunteers and 6 schizophrenia patients were removed for excessive motion, and 2 healthy volunteers and 7 schizophrenia patients were excluded due to having too few trials in each condition and run following artifact rejection.

Task

The task we have developed was based on previous research in our lab on task switching (Grundy et al., 2011; Woodward, Meier, Tipper, & Graf, 2003; Woodward et al., 2008) and working memory (Metzak et al., 2010, 2011), and involves three discrete tasks in alternation, referred to as a task set: judging whether shapes are blue or red, judging whether numbers are odd or even, and judging whether letters are uppercase or lowercase. The manipulation of interest is that the to-be-judged stimuli can contain one stimulus dimension that cues a task in the task set (e.g. the numeral '2' in white ink), two stimulus dimensions (e.g. the numeral '2' in blue ink), or three stimulus dimensions, such that all three tasks in the task set are cued (e.g. the uppercase letter string 'TWO' written in blue ink). Please see Figure 1 for a depiction of the stimuli used in this experiment, and Figure 2 for an illustration of trial structure and timing.

When switching tasks, this manipulation means that for the univalent, bivalent, and trivalent stimuli, in order to perform the currently relevant task, the participants must counter the attentional capture of, zero, one or two task-irrelevant stimulus dimensions, respectively. The currently task-relevant stimulus dimension for a particular stimulus was explicitly cued at the time of stimulus presentation in order to order to avoid the requirement to memorize cue-response associations (e.g., blue, lowercase and odd are left key, others are right key), thereby simplifying task instructions, facilitating task execution, and removing interactions between stimulus dimension conflict and response conflict. This optimized the experiment for isolation of stimulus dimension conflict, which requires top-down control of attention.

Each stimulus was presented in the center of the screen and the judgment to be performed was cued with a single word followed by a question mark at the bottom center of the screen. The possible judgment cue words were: 'Blue?', 'Red?', 'Odd?', 'Even?', 'Lowercase?', or

23

'Uppercase?'. Additionally, the words 'Yes' and 'No' were also present at the lower left and right corners of the screen to remind participants of the response mapping. Each stimulus was presented for 1500 ms and was followed by a blank screen display during the interstimulus interval (ISI) of 500 ms. Longer intertrial intervals (ITI) were also inserted after every 1, 2, 4, or 8 stimuli. The length of these ITIs formed an exponential distribution with most of the ITIs being of the shortest variety, thereby maximizing the efficiency of the design (Serences, 2004). The only difference between the MRI and MEG versions of the experiment was the number of trials, and the length of the ITIs. In the fMRI scans, there were 64 trials per run in each of the three conditions, and the ITIs were 500, 750, 1500, 3000, or 20000 ms. In the MEG version of the experiment, there were 96 trials per run for each of the three conditions, and the ITIs were 500, 750, 1500, 3000, or 6000 ms. Each participant performed two runs of the task in both the fMRI and the MEG version of the experiment. For the fMRI version, each run was 10 minutes and 25 seconds, and for the MEG version, each run was 14 minutes and 17 seconds.

Behavioural Data

The focus of this study was on one particular aspect of cognitive control referred to as attentional biasing. Although the task we have used is novel, previous experiments employing similar paradigms have suggested that this ability may be impacted in schizophrenia. Using the Stroop task (Stroop, 1935), previous studies have identified patterns that suggest that schizophrenia patients have difficulty with biasing attention. For instance, schizophrenia patients show a stronger Stroop effect than healthy volunteers (Cohen, Barch, Carter, & Servan-Schreiber, 1999; Hepp, Maier, Hermle, & Spitzer, 1996), they have lower accuracy in colour naming than healthy volunteers (Cohen et al., 1999; Perlstein, Carter, Barch, & Baird, 1998), and show greater decrease in RTs (i.e. facilitation) when changing from neutral to congruent stimuli

24

than healthy volunteers (Cohen et al., 1999; Perlstein et al., 1998). These results are all suggestive of a failure to bias attention because each of these instances requires the participant to bias attention away from the dominant response (i.e. word reading). In the case of the Stroop effect and the lower accuracy in colour naming, the pre-potent tendency to read the words interferes with the naming of the colour. In the case of the facilitation, the change from a neutral stimulus to a congruent one decreases RTs in patients more than in controls because the patients are able to relie on the dominant response to perform the task.

Similar results have been found in flanker tasks, where schizophrenia patients show facilitation effects when performing a uni-dimensional flanker task (e.g. faster when the flankers are congruent with the target) but showed no facilitation or interference effects when performing a bi-dimensional flanker task (Yücel et al., 2002). The authors argue that this pattern suggests that patients are unable to use behavioural goals to constrain the selection of visual information, that is, they show a deficit in selective attention. Such findings have also been observed in visuospatial working memory paradigms, where schizophrenia patients are able to perform at the level of controls when correct responses are cued using salient stimuli, but show deficits when the cues are less salient and require more top-down control, that is, when attentional biasing is required (Gold, Fuller, Robinson, Braun, & Luck, 2007; Hahn et al., 2010).

Hypothesis

On the basis of pilot testing, the hypothesis for the behavioural results was that increases in stimulus valence (e.g., the number of relevant stimulus features) would lead to concomitant increases in response time and decreases in accuracy. Furthermore, the schizophrenia patients are hypothesized to display significantly slower response times and lower accuracy relative to the healthy participants.

Results

Response times and accuracy.

Response times (RTs) and accuracy were calculated for univalent, bivalent, and trivalent stimulus types for both the fMRI and MEG versions of the experiment. The response times were calculated by using the number of responses to weight the mean response times from each run and modality. For each experimental modality, the RT analysis involved a mixed-model ANOVA with within-subject factors of Valency (univalent, bivalent, or trivalent), and Performance (correct or incorrect), and a between-subject factor of Group (control or patient). The average RTs for each group and condition in each experimental version can be seen in Table 3, where significant differences between the groups are indicated with an asterisk.

The results from the RT analysis for the fMRI experiment indicated that there were main effects of Valency, $F_{(2,92)} = 20.61$, $p < .001$, $\eta^2 = 0.31$; Performance, $F_{(1,46)} = 8.67$, $p < .01$, $\eta^2 = 0.16$; and Group, $F_{(1,46)} = 4.81$, $p < .05$, $\eta^2 = 0.10$. No interactions were significant (all $ps > .25$). Further examination of the effect of Valency revealed that there were significant differences in RTs between univalent (mean = 992 ms) and bivalent (mean = 1042 ms) stimuli, $F_{(1,46)} = 7.74$, $p < .01$, $\eta^2 = 0.14$; and between bivalent (mean = 1042 ms) and trivalent (mean = 1108 ms) stimuli, $F_{(1,46)} = 11.04$, $p < .005$, $\eta^2 = 0.19$, such that increasing Valency led to increased RTs. Furthermore, an examination of the other main effects revealed that Incorrect (mean = 1069 ms) responses were slower than Correct (mean = 1026 ms) responses, $F_{(1,46)} = 8.67$, $p < .01$, $\eta^2 = 0.16$, and patients (mean = 1090 ms) were slower than controls (mean = 1004 ms), $F_{(1,46)} = 4.81$, $p < .05$, $\eta^2 = 0.10$.

Follow-up tests comparing the healthy volunteers and the schizophrenia patients indicated that the RTs for the correct responses in the fMRI experiment differed significantly

26

between the two groups, such that the healthy volunteers responded significantly faster for the univalent (volunteers = 918 ms, patients = 1035 ms), $t_{(55)} = 3.79$, $p < .001$, bivalent (volunteers = 980 ms, patients = 1078 ms), $t_{(55)} = 3.18$, $p < .01$, and trivalent (volunteers = 1030 ms, patients = 1112 ms) stimuli, $t_{(55)} = 2.38$, $p < .05$. There were no significant differences between the groups for the RTs from incorrect responses ($ps > .05$).

The results from the RT analysis for the MEG experiment indicated that there was a main effects of Valency, $F_{(2,106)} = 58.98$, $p < .001$, $\eta^2 = 0.53$. Further examination of the effect of Valency revealed that there were significant differences in RTs between univalent (mean = 1042 ms) and bivalent (mean = 1125 ms) stimuli, $F_{(1,53)} = 31.26$, $p < .001$, $\eta^2 = 0.37$; and between bivalent (mean = 1125 ms) and trivalent (mean = 1185 ms) stimuli, $F_{(1,53)} = 26.13$, $p < .001$, $\eta^2 = 0.33$, such that increasing Valency led to increased RTs. The main effects of Performance and Group were non-significant ($ps > 0.075$).

Follow-up tests comparing the healthy volunteers and the schizophrenia patients indicated that the RTs for the correct responses in the MEG experiment differed significantly between the two groups, such that the healthy volunteers responded significantly faster for the univalent (volunteers = 1004 ms, patients = 1087 ms), $t_{(56)} = 2.52$, $p < .05$, bivalent (volunteers = 1073 ms, patients = 1143 ms), $t_{(56)} = 2.01$, $p < .05$, and trivalent (volunteers = 1115 ms, patients = 1202 ms) stimuli, $t_{(56)} = 2.54$, $p < .05$. There were no significant differences between the groups for the RTs from incorrect responses ($ps > .25$).

For each experiment version (fMRI or MEG), the accuracy analysis examined the percentage of correct responses in each condition. A two-way ANOVA was performed with a within-subject factor of Valency (univalent, bivalent, or trivalent), and a between-subject factor of Group (control or patient). The average accuracy for each group and condition in each

experimental version can be seen in Table 4, where significant differences between the groups are indicated with an asterisk.

The results from the accuracy analysis in the fMRI experiment indicated that there were main effects of Valency, $F_{(2,100)} = 85.04$, $p < .001$, $\eta^2 = 0.63$, and Group, $F_{(1,50)} = 4.72$, $p < .05$, $\eta^2 = 0.09$. Further examination of the effect of Valency revealed that there were significant differences in accuracy between univalent (mean = 89.08%) and bivalent (mean = 86.56%) stimuli, $F_{(1,50)} = 18.60$, $p < .001$, $\eta^2 = 0.27$; and between bivalent (mean = 86.56%) and trivalent (mean = 81.82%) stimuli, $F_{(1,50)} = 85.77$, $p < .001$, $\eta^2 = 0.63$, such that increasing Valency led to decreased accuracy. The main effect of Group was due to the decreased accuracy in patients relative to controls.

Follow-up tests comparing the healthy volunteers and the schizophrenia patients indicated that the accuracy for the correct responses in the fMRI experiment differed significantly between the two groups, such that the healthy volunteers responded significantly more accurately for the univalent (volunteers = 91.83%, patients = 86.33%), $t_{(55)} = 2.09$, $p < .05$, bivalent (volunteers = 90.30%, patients = 82.81%), $t_{(55)} = 2.14$, $p < .05$, and trivalent (volunteers = 86.70%, patients = 77.95%) stimuli, $t_{(55)} = 2.27$, $p < .05$. The accuracy for the incorrect responses differed between the groups as well for the univalent (volunteers = 3.57%, patients = 6.75%), $t_{(55)} = 2.33$, $p < .025$, and bivalent conditions (volunteers = 3.71%, patients = 6.80%), $t_{(55)} = 2.11$, $p < .05$, indicating that the patients committed more errors. All other accuracy differences between the groups were non-significant ($ps > .09$).

The results from the accuracy analysis in the MEG experiment indicated that there were main effects of Valency, $F_{(2,110)} = 42.54$, $p < .001$, $\eta^2 = 0.44$, and Group, $F_{(1,55)} = 8.34$, $p < .01$, $\eta^2 = 0.13$. Further examination of the effect of Valency revealed that there were significant

differences in accuracy between univalent (mean = 87.36%) and bivalent (mean = 85.05%)

stimuli, $F_{(1,55)} = 15.43$, $p < .001$, $\eta^2 = 0.22$; and between bivalent (mean = 85.05%) and trivalent

(mean = 82.06%) stimuli, $F_{(1,50)} = 57.00$, $p < .001$, $\eta^2 = 0.51$, such that increasing Valency led to

decreased accuracy. The main effect of Group was due to the decreased accuracy in patients

(mean = 79.68%) relative to controls (mean = 89.97%).

Follow-up tests comparing the healthy volunteers and the schizophrenia patients

indicated that the accuracy for the correct responses in the MEG experiment differed

significantly between the two groups, such that the healthy volunteers responded significantly

more accurately for the univalent (volunteers = 91.69%, patients = 83.02%), $t_{(56)} = 2.70$, $p < .01$,

bivalent, $t_{(56)} = 3.01$, $p < .005$ (volunteers = 90.50%, patients = 79.61%), and trivalent stimuli,

$t_{(56)} = 2.82$, $p < .01$ (volunteers = 87.73%, patients = 76.40%). The accuracy for the missed

responses differed between the groups as well for the univalent, $t_{(55)} = 2.49$, $p < .025$ (volunteers

= 2.73%, patients = 9.46%), bivalent, $t_{(55)} = 2.75$, $p < .001$ (volunteers = 4.17%, patients =

12.24%), and trivalent (volunteers =6.42%, patients = 15.35%) conditions, $t_{(55)} = 2.58$, $p < .025$,

indicating that the patients failed to respond in time on more trials. All other accuracy differences

between the groups were non-significant (ps > .13).

Symptomatology.

Symptomatology was recorded using the Signs and Symptoms of Psychotic Illness rating

scale (SSPI). The SSPI is a 20-question semi-structured interview designed for the assessment of

symptoms across five domains: anxiety/depression, excitation, psychomotor poverty,

disorganized psychomotor activity, and reality distortion (P. F. Liddle et al., 2002). SSPI scores

on each item range between 0 (no evidence of impairment), and 4 (severe psychopathology). The

mean total SSPI score (and standard error) was 14.52 (1.51) indicating a relatively low level of

psychopathology. The mean scores (and standard errors) for each item, as well as for each of the five domains are reported in Table 5.

Medication information was collected for all but five of the patients and dosages were converted to chlorpromazine equivalents (Davies, 2012). The mean antipsychotic dosage was 188.47 (standard error = 35.62).

Discussion

The behavioural data from this study were the RTs and accuracy rates for the fMRI and MEG versions of the experiment. The most notable and consistent findings are that increasing stimulus valency led to significant increases in the RTs and decreases in accuracy rates, and that healthy volunteers were significantly faster than schizophrenia patients for correct responses at every level of stimulus valence. The correlation between valence and RT is found in the task switching literature (Meier, Woodward, Rey-Mermet, & Graf, 2009; Metzak et al., 2013; Rubin & Meiran, 2005; Woodward et al., 2008), and was anticipated based on the results of the pilot testing carried out for this study, and provided the justification for using differences in stimulus valence as the primary manipulation investigated in this study.

In the fMRI experiment, controls were found to have significantly faster RTs and significantly greater accuracy than the patients. This pattern of results was also apparent in the MEG experiment, although this effect appeared weaker in the RTs than in the accuracy results. One reason this may have been the case is that the fMRI version of the experiment was always performed after the MEG to avoid magnetization effects so perhaps the additional pre-existing practice with the task prior to the fMRI version allowed the controls to become more proficient at responding quickly. The higher levels of missed responses in the patients in the MEG experiment also supports this interpretation.

Another effect worth noting in the fMRI version of the experiment was the presence of a significant difference between RTs based on performance, such that for both patients and controls, correct responses were faster than incorrect responses. This finding is also common in our previous work in task switching (Metzak et al., 2013; Woodward et al., 2003, 2008), and possibly reflects an emphasis on accuracy rather than speed in responding (Wagenmakers, Ratcliff, Gomez, & McKoon, 2008).

<center>**Structural Imaging**</center>

Diffusion Weighted Imaging

      Introduction.

      Diffusion weighted imaging (DWI) is a relatively new brain imaging technique, but there has been a great deal of interest in its application to the study of schizophrenia, as disconnections in the brain have been hypothesized to be a primary cause of the illness (Fornito, Zalesky, Pantelis, & Bullmore, 2012; Stephan, Friston, & Frith, 2009). The findings from meta-analyses of tract- and voxel-based DWI studies suggest that there are widespread changes in measures of white matter integrity in schizophrenia (Wheeler & Voineskos, 2014), such that patients, in all phases of the illness, show decreases in structural connectivity relative healthy controls.

      In chronic schizophrenia patients, meta-analyses have found decreases in fractional anisotropy (FA), an estimate of the direction and magnitude of water diffusion, in the frontal, temporal, parietal, and occipital lobes (Pettersson-Yeo, Allen, Benetti, McGuire, & Mechelli, 2011; Wheeler & Voineskos, 2014). However, the most common finding in these studies are FA reductions in fronto-temporal connections. Apart from fronto-temporal connections, the areas most associated with reductions in FA in schizophrenia are the white matter connections to the corpus callosum and to the cingulate gyrus (Kubicki et al., 2005; Nestor et al., 2007; Pettersson-Yeo et al., 2011).

      An important consideration in these studies is whether the patients have been chronically ill or whether they are still in their first episode, as antipsychotic medication can also produce changes in brain structure and connectivity (Szeszko et al., 2014). Deficits in white matter integrity relative to controls are also found in first episode patients in similar regions (Yao et al., 2013), but the results are far more equivocal in this population (Pettersson-Yeo et al., 2011). It is

<center>32</center>

speculated that this may be due to medication effects, or simply because it is much easier to find chronic schizophrenia patients than first episode patients. At any rate, the presence of similar, but less severe deficiencies in white matter integrity suggests that this structural change is an intrinsic feature of the disease rather than an effect of medication.

Hypothesis.

Although literature indicates that FA deficits in schizophrenia patients exhibit considerable variability from study to study, the hypothesis for the DWI results was that patients will show decreases in FA relative to healthy volunteers, particularly in the white matter tracts with connections to the dAcc.

Methods.

Scanning.

Diffusion weighted imaging was performed at the University of British Columbia's MRI Research Centre on a Phillips Achieva 3.0 Tesla MRI Scanner equipped with an 8-channel head coil. Diffusion encoding was achieved using a single-shot spin-echo echo planar sequence with a spatial resolution of $2.24 \times 2.24 \times 2.20$ mm, relaxation time / echo time (TR/TE) = 7015/60 ms, field of view (FOV) = 224×224 mm, acquisition matrix 100×99, 70 contiguous transverse slices 2.2 mm thick. Diffusion weighted images were acquired along 60 noncollinear directions, with a b factor of 700 s/mm^2, and one image with b = 0 s/mm^2 (reference image). Total scan time was 7 minutes and 22 seconds.

Preprocessing.

DWI data were processed using the fMRIB Software Library (FSL) Version 5.0 (S. M. Smith et al., 2004). The processing steps incorporated in the fMRIB Diffusion Toolbox (FDT) included skull stripping the raw DWI images to leave only images of the brain itself, correcting

for eddy current induced distortions and head movements using affine registration to a reference

volume (the b0 image mentioned above), and fitting diffusion tensors to each voxel (Behrens et

al., 2003). Fitting the diffusion tensors to each voxel produces a variety of measures including

the fractional anisotropy (FA) in each voxel as well as the principal diffusion direction. The

fractional anisotropy value is a unit between 0 and 1 that indexes the ability of water to diffuse

along a particular axis. For instance, a value of 0 means that water diffuses equally well in any

direction, and a value of 1 means that water diffuses only along a single axis and is fully

impeded from diffusing in other directions. These FA images from each subject were used in a

voxelwise statistical analysis using FSL's Tract-Based Spatial Statistics (TBSS) (S. M. Smith et

al., 2006). The FA images from each subject were normalized to the MNI152 template using the

FSL nonlinear registration tool FNIRT, then these normalized FA images were used to create a

mean FA image, and thinned to create a mean FA skeleton by taking only the center of the white

matter tracts common to each participant. The relevant FA values from each participant (i.e.

those co-localized with the mean FA skeleton) were then projected onto the skeleton by

searching the local maxima along the perpendicular direction from the skeleton, thus creating a

set of 'skeletonized' FA values for each participant. The skeletonized FA values were used as

input in a non-parametric permutation test (Winkler, Ridgway, Webster, Smith, & Nichols,

2014) to identify any voxels displaying significant differences in FA between healthy volunteers

and schizophrenia patients.

Results.

The DWI data was analyzed using FDT and TBSS. TBSS was used to avoid any issues in

the alignment of tracts between subjects, and to facilitate the use of a voxelwise analysis to

detect any between-group changes in FA. from Mean FA values in each group were examined

using a voxelwise non-parametric permutation test, and results were thresholded to $p < 0.05$

(FWE-corrected) using threshold-free cluster enhancement (S. M. Smith & Nichols, 2009).

Please see Figure 3 for a depiction of the significant results. Although there was significant

difference in age between the healthy volunteers and the schizophrenia patients, age was not

used a covariate as this does not appropriately control for preexisting differences in attributes

between the groups (G. A. Miller & Chapman, 2001; Woodward & Menon, 2011).

This analysis was focused on identifying areas in the FA skeleton where controls had

significantly higher values than patients, and vice versa. There were no clusters in which the

patients' FA was significantly greater than that of the controls. However, the healthy participants

did have significantly greater FA was found in the healthy volunteers relative to the

schizophrenia patients in three clusters in the white matter skeleton. These clusters were located

in the right hemisphere, impacting the right inferior and superior longitudinal fasciculi, and the

right inferior fronto-occipital fasciculus, and the right corticospinal tract.

Discussion.

The DWI results show reduced FA in patients relative to healthy controls. Although the

FA deficits are found in multiple tracts, all of the clusters showing lower FA in patients are

found in posterior portion of the right hemisphere. However, contrary to the hypothesis, deficits

in FA were not found in the cingulum bundle, which is the primary white matter connection to

the dorsal anterior cingulate cortex (Croxson et al., 2005).

Previous studies of FA in schizophrenia find WM widespread deficits in FA in regions

similar to the ones found in the present study, including the inferior longitudinal fasciculus (Seitz

et al., 2016; Tamnes & Agartz, 2016; Wheeler & Voineskos, 2014), and inferior fronto-occipital

fasciculus (Nestor et al., 2007; Tamnes & Agartz, 2016). FA deficits in schizophrenia patients

are also found in the cingulum bundle (Wheeler & Voineskos, 2014; Whitford et al., 2014).

However, reviews have noted that almost all major WM tracts have been found to show

deficits in schizophrenia relative to healthy volunteers (Kubicki et al., 2007; Tamnes & Agartz,

2016; Wheeler & Voineskos, 2014), and furthermore, in cases where these deficits are not

observed, it is likely that significant differences have been obfuscated in many studies by a lack

of statistical power (Melicher et al., 2015). These FA changes in schizophrenia are present in

medication naïve patients undergoing their first psychotic episode (Lee et al., 2013; Melicher et

al., 2015; Ohtani et al., 2015; Zhang et al., 2016), suggesting that the changes in structural

connectivity predate, and indeed may contribute to, the development of schizophrenia.

In the current project, the differences in structural connectivity between healthy

volunteers and patients were found in right lateralized tracts in the brain. Although there is not a

direct mapping between structural and functional connectivity, there is a robust relationship

between the two (Honey et al., 2009; Honey, Kötter, Breakspear, & Sporns, 2007), such that

functional connectivity is thought to be constrained by structure of the anatomical connections in

the brain. The tracts found to be impacted in this study serve to connect sensory and cognitive

brain regions, it is possible that deficits in attentional biasing (as indexed behaviourally or using

functional imaging) could be exacerbated by disease-related changes to white matter

microstructure. However, the results of the current study should be weighed carefully in light of

the small sample size and the diversity of the results from previous research. The deficits found

in the present study may reflect differences that are idiosyncratic to the particular sample

recruited for this study, and other 'true' differences may exist between the samples that were

obfuscated via a lack of power. Structural connectivity is more reliable than functional

connectivity, but it is still malleable (Scholz, Klein, Behrens, & Johansen-Berg, 2009), which suggests that some differences in FA between schizophrenia patients and healthy volunteers may be attributable to differences in lifestyle and behaviour between the two groups, rather than being specifically related to the illness. Furthermore, the presence of a significant difference in age between the groups is a confound that limits the strength of the conclusions that can be drawn from these results.

As was mentioned earlier in the Diffusion Weighted Imaging section of the General Methods, care must be taken in the interpretation of FA. FA is often understood as an index of white matter integrity but lower measures of FA are also obtained via crossing of fibre tracts in a voxel, or a lack of parallel orientation in multiple fibres traveling through a voxel, and there is no way to disentangle these possibilities (Jeurissen et al., 2011, 2013). This issue, along with the presence of a significant difference in age between the groups, suggests that the present results be interpreted with caution.

Structural Magnetic Resonance Imaging

      Introduction.

      Although the brains of schizophrenia patients do not show gross abnormalities, such as those that can be seen with the naked eye, the disease is associated with subtle and widespread differences in brain structure (Wright et al., 2000) that can be identified when compared with the brains of individuals without the disease. Although there are many structural aspects of the brain that may be measured, including regional volume, surface area, and gyrification patterns, one of the most commonly used is the measurement of cortical thickness in discrete brain areas. Cortical thickness is typically defined as the distance between the grey matter/white matter boundary and the grey matter/*pia mater* boundary (Mills & Tamnes, 2014), which typically spans between 2 and 4 mm and shows regionally specific variability (Ribeiro et al., 2013). A recent study examining the developmental trajectory of cortical thickness found a linear decrease in the majority of brain regions beginning around age 5 and lasting until early adulthood. Cortical thickness in bilateral temporo-parietal junction and right prefrontal cortex peaked around age 8 and then showed a similar pattern of linear decrease as other brain regions (Ducharme et al., 2016). Cortical thickness has been found to correlate with general intelligence in multiple samples of typically developing individuals, and at multiple points during development (Choi et al., 2008; Karama et al., 2009; Menary et al., 2013; Shaw et al., 2006).

      In schizophrenia, the most common deficits in cortical thickness relative to those unaffected by the disease are found in frontal and temporal regions, specifically in the prefrontal cortices, the dAcc, and the superior and middle temporal gyri (Goldman et al., 2009; Rimol et al., 2010). However, it should be noted that these deficits in cortical thickness are also found in the parietal and occipital lobes, albeit with lower frequency (Rimol et al., 2010). Changes in frontal

38

and temporal cortical thickness are found in first episode patients (Narr et al., 2005; Schultz et al., 2010; Xiao et al., 2015), which suggests that this feature of the illness is not simply due to medication effects. There is some evidence that cortical thickness may be related to cognition in schizophrenia, specifically working memory (Ehrlich et al., 2012), however, this relationship requires further testing using multiple samples and cognitive domains.

Hypothesis.

The results from structural imaging studies suggest that cortical thickness changes in schizophrenia exhibit considerable heterogeneity, therefore the hypothesis for these results was that decreases in cortical thickness will be found in schizophrenia patients relative to healthy participants.

Methods.

Scanning.

Structural imaging was performed at the University of British Columbia's MRI Research Centre on a Phillips Achieva 3.0 Tesla MRI Scanner equipped with an 8-channel head coil. Each scan consisted of a whole brain T1-weighted Fast Field Echo (FFE) sequence (TE = 3.7 ms; TR = 8.1 ms; flip angle = 8°; matrix = 256 × 200; field of view (FOV) = 200 mm; slice thickness = 1 mm with no gap; 1 × 1 × 1 mm voxels; 182 coronal slices). Total scanning time was 6 minutes and 22 seconds.

Preprocessing.

Structural MRI data were preprocessed using Freesurfer image analysis suite, which is documented and freely available for download online (http://surfer.nmr.mgh.harvard.edu/). The technical details of these procedures are described in prior publications (Dale, Fischl, & Sereno, 1999; Dale & Sereno, 1993; Fischl et al., 2002a; Fischl, Liu, & Dale, 2001; Fischl, Salat, et al.,

2004; Fischl, van der Kouwe, et al., 2004; Fischl & Dale, 2000; Fischl, Sereno, & Dale, 1999; Fischl, Sereno, Tootell, & Dale, 1999; Han et al., 2006; Jovicich et al., 2006; Reuter, Rosas, & Fischl, 2010; Reuter, Schmansky, Rosas, & Fischl, 2012; Ségonne et al., 2004). Briefly, this processing includes motion correction and averaging (Reuter et al., 2010) of multiple volumetric T1 weighted images (when more than one is available), removal of non-brain tissue using a hybrid watershed/surface deformation procedure (Ségonne et al., 2004), automated Talairach transformation, segmentation of the subcortical white matter and deep gray matter volumetric structures (including hippocampus, amygdala, caudate, putamen, ventricles) (Fischl et al., 2002b; Fischl, Salat, et al., 2004) intensity normalization (Sled, Zijdenbos, & Evans, 1998), tessellation of the gray matter white matter boundary, automated topology correction (Fischl et al., 2001; Ségonne, Pacheco, & Fischl, 2007), and surface deformation following intensity gradients to optimally place the gray/white and gray/cerebrospinal fluid borders at the location where the greatest shift in intensity defines the transition to the other tissue class (Dale et al., 1999; Dale & Sereno, 1993; Fischl & Dale, 2000).

Once the cortical models are complete, a number of deformable procedures can be performed for further data processing and analysis including surface inflation (Fischl, Sereno, & Dale, 1999), registration to a spherical atlas which is based on individual cortical folding patterns to match cortical geometry across subjects (Fischl, Sereno, Tootell, et al., 1999), parcellation of the cerebral cortex into units with respect to gyral and sulcal structure (Desikan et al., 2006; Fischl, van der Kouwe, et al., 2004), and creation of a variety of surface based data including maps of curvature and sulcal depth. This method uses both intensity and continuity information from the entire three dimensional MR volume in segmentation and deformation procedures to produce representations of cortical thickness, calculated as the closest distance from the

gray/white boundary to the gray/CSF boundary at each vertex on the tessellated surface (Fischl & Dale, 2000). The maps are created using spatial intensity gradients across tissue classes and are therefore not simply reliant on absolute signal intensity. The maps produced are not restricted to the voxel resolution of the original data thus are capable of detecting submillimeter differences between groups. Procedures for the measurement of cortical thickness have been validated against histological analysis (Rosas et al., 2002) and manual measurements (Kuperberg et al., 2003; Salat et al., 2004). Freesurfer morphometric procedures have been demonstrated to show good test-retest reliability across scanner manufacturers and across field strengths (Han et al., 2006; Reuter et al., 2012).

Results.

Using the Freesurfer analysis package, cortical thickness measurements for 34 brain areas in each hemisphere (Desikan et al., 2006) were obtained from 22 controls and 26 patients. A regression analysis using the qdec tool provided with Freesurfer was performed with the between-subject variable of Diagnosis (control or patient) and within-subject variables of Cortical Thickness at each vertex. The analysis conducted involved examining the effect of Diagnosis on cortical thickness. This analysis revealed multiple significant clusters ($p < .001$, cluster-corrected) where controls showed increased cortical thickness relative to patients. There were no significant clusters where patients showed increased cortical thickness relative to controls. Although there was significant difference in age between the healthy volunteers and the schizophrenia patients, age was not used a covariate as this does not appropriately control for preexisting differences in attributes between the groups (G. A. Miller & Chapman, 2001; Woodward & Menon, 2011). Please see Table 6 for a list of all the regions with significant

differences between healthy volunteers and schizophrenia patients, and Figure 4 for a visual depiction of these cluster locations.

Discussion.

The sMRI results from this study indicate that the schizophrenia patients show a significant reduction in cortical thickness in multiple regions throughout the cortex, particularly the frontal cortices including the cingulate gyri. There is extensive evidence that brain volume and intracranial volume are reduced in schizophrenia, even in medication-naïve patients (Haijma et al., 2013). Decreases in cortical thickness, particularly in the frontal cortices and the anterior cingulate, are often found in schizophrenia patients (Knöchel et al., 2016; Kuperberg et al., 2003; Sugihara et al., 2016), a relationship that holds even in the first-episode, medication-naïve state (Narr et al., 2005). This pattern of cortical thinning is also found in unaffected siblings of schizophrenia patients (Goghari, Rehm, Carter, & MacDonald, 2007), and those at high genetic risk for acquiring schizophrenia (Byun et al., 2012).

Structural Imaging General Discussion

Taken together, the structural results suggest that the schizophrenia patients display widespread changes in brain structure. In terms of structural connectivity, these changes were detectable as reductions of FA in many tracts throughout the right hemisphere of the brain. Although there are many different physiological changes which are detectable as a change in FA, patients were found to have deficits, not increases, relative to controls which suggests that the white matter tracts are more disorganized in the patient group. The impacted tracts were found in the right hemisphere, which suggests a lateralized deficit, but this lateralization is likely to be specific to the sample employed in the present study as results from meta-analyses and studies employing large samples do not show a similar pattern (Pettersson-Yeo et al., 2011; Wheeler &

Voineskos, 2014). Notably, no deficits were found in the cingulum bundle, the primary white matter tract linked to dorsal anterior cingulate cortex.

In the cortical thickness analysis, decreases in cortical thickness were found in patients relative to controls throughout the cortex, including deficits in the cingulate gyrus, a region known for its extensive connections to motor, emotional and cognitive subsystems (Paus, 2001). Given the importance of the cingulate and paracingulate gyrus in models of cognitive control, deficits in cortical thickness in the patient group could have wide ranging implications for cognitive functioning in this group. However, the present results must be interpreted with caution, due to the difference in age between the groups.

It is tempting to suggest that the WM connectivity and cortical thickness results could be related; this theory is particularly salient in light of recent work demonstrating the influence of neuronal activity on myelin growth (Gibson et al., 2014); however, further evidence is required to advance this claim.

<center>**Functional Magnetic Resonance Imaging**</center>

Univariate Functional Magnetic Resonance Imaging

      Introduction.

      Although many studies of schizophrenia have examined structural changes in the brain, others have focused on changes in brain function using fMRI (for a review see Gur & Gur, 2010). Many of these studies have focused on executive function and cognitive control, as deficits in these domains have long been recognized to be an aspect of the disorder. Although diverse paradigms have been employed to measure these abilities, many of these studies do find that schizophrenia patients exhibit functional deficits relative to healthy volunteers when performing tasks involving executive functions and selective attention (Minzenberg, Laird, Thelen, Carter, & Glahn, 2014; Orellana & Slachevsky, 2013). The vast majority of these studies find that schizophrenia patients show alterations in functional activity in the prefrontal cortices (Lesh, Niendam, Minzenberg, & Carter, 2011; Minzenberg et al., 2014; Orellana & Slachevsky, 2013), with most of the studies localizing the difference to the DLPFC (Lesh et al., 2011). The finding of DLPFC involvement is not unexpected, given that patients with prefrontal lobe damage often display difficulties in performing these tasks (Gläscher et al., 2012).

      However, these results are not entirely unambiguous; some studies have failed to find a difference in DLPFC activity (Mayer et al., 2015), whereas others have found that other prefrontal regions such as dAcc are selectively impacted (Adams & David, 2007), still others have found both hyper- and hypoactivity in DLPFC in patients (relative to healthy controls) using the same paradigm (Weiss et al., 2007). Thus, while the evidence from meta-analyses strongly suggest the involvement of the DLPFC in attentional biasing, evidence from individual studies seems equivocal: it is dependent on both sample size, severity of illness, and paradigm

<center>44</center>

choice. Furthermore, although the DLPFC is the region whose activity is most commonly found to be altered in schizophrenia, it is clearly not the only locus for functional changes in schizophrenia.

Hypothesis.

Schizophrenia patients will display increases in dAcc activity relative to healthy volunteers at low levels of stimulus valence, and decreases in dAcc activity relative to healthy volunteers at high levels of stimulus valence.

Methods.

Scanning.

Functional imaging was performed at the University of British Columbia's MRI Research Centre on a Phillips Achieva 3.0 Tesla MRI scanner with Quasar Dual Gradients (maximum gradient amplitude 80mT/m and a maximum slew rate of 200mT/m/s). The participant's head was firmly secured using a custom head holder and stimuli were presented on a screen at the end of the bore of the magnet which were reflected on to a mirror positioned on the head holder. Functional image volumes were collected using a T2*-weighted gradient echo spin pulse sequence (TR/TE=2000/30ms, flip angle 90º, 36 slices, 3mm thick, 1mm gap, sense factor 2, 80×80 matrix reconstructed at 128, FOV 240.0mm, measured voxel is 1.875mm × 1.875mm × 3.972mm, actual band width = 53.4 Hz per pixel) effectively covering the whole brain (145mm axial extent).

Preprocessing.

Functional images were reconstructed offline, and the images from the scan series were slice timing corrected, realigned, co-registered to the participant's high definition structural MRI image, normalized to the MNI152 T1 template using the method implemented in Statistical

Parametric Mapping 8 (SPM8; http:/www.fil.ion.ucl.ac.uk/spm). Translation and rotation

corrections did not exceed 3mm or 3º for any of the participants. Voxels were normalized to

2mm × 2mm × 2mm for univariate fMRI analyses, and the normalized functional images were

smoothed with an 8mm full width at half maximum Gaussian filter.

Results.

A univariate analysis of the fMRI data was performed using SPM8

(http://www.fil.ion.ucl.ac.uk/spm/). The following classes of stimuli were modeled in the SPM

analyses: univalent colour, univalent parity, univalent case, bivalent colour, bivalent parity,

bivalent case, trivalent colour, trivalent parity, and trivalent case. Only those stimuli that elicited

a correct response were included in the analysis. These individual stimuli classes were

concatenated to create univalent, bivalent, trivalent conditions which encompassed each of the

three tasks. Brain activity from healthy controls and schizophrenia patients were analyzed

separately, as well as in a combined analysis to assess group level differences. All the results

presented here used a statistical threshold of $p < .05$, FWE-corrected). The contrasts that were

examined were: 1) all stimuli greater than baseline, 2) baseline greater than all stimuli, 3)

bivalent greater than univalent stimuli, 4) trivalent greater than bivalent stimuli, and 5) trivalent

greater than univalent stimuli. The anatomical loci of the significant activations resulting from

each contrast are presented in Table 7 and the cluster information from significant contrasts for

the healthy volunteers, the schizophrenia patients, and the contrast between the two can be found

in Table 8, Table 9, and Table 10, respectively . The brain images for all significant contrasts for

the healthy volunteers can be found in Figure 5, and the brain images for all significant contrasts

in the schizophrenia patients can be found in Figure 6. For the patients, the bivalent greater than

univalent stimuli, and the trivalent greater than bivalent stimuli contrasts yielded no significant

activations, so are not included in the figures. The brain images for the contrast of the healthy

volunteers greater than schizophrenia patients can be found in Figure 7. For this set of results, the

contrast of trivalent greater than bivalent yielded no significant activations therefore, it is not

included in the figure. The brain images for the contrast of the healthy volunteers greater than

schizophrenia patients can be found in Figure 8, and display only the all stimuli greater than

baseline contrast, as only this contrast yielded significant activations.

Discussion.

The univariate fMRI results suggest that the experiment activated similar regions in both

schizophrenia patients and healthy volunteers. In the all stimuli greater than baseline contrasts,

both patients and controls had bilateral activations in the supplementary motor area, frontal eye

fields, dAcc, hippocampi, angular gyri, superior and inferior occipital gyri, and cerebellum, as

well as left lateralized activations in the putamen, pre- and post-central gyri, superior and inferior

parietal lobules, and thalamus. This pattern of activity is broadly consistent with the dorsal

attention network (M. D. Fox, Corbetta, Snyder, Vincent, & Raichle, 2006; Petersen & Posner,

2012; Posner & Petersen, 1990), which is reliably activated by voluntary, goal-directed orienting

of attention. The core nodes of the dorsal attention network are thought to be the inferior parietal

sulci and the frontal eye fields (Vossel, Geng, & Fink, 2014); both of these sets of regions were

present in the all stimuli greater than baseline conditions.

In addition to the dorsal attention network, the all stimuli greater than baseline contrasts

also reveal activity in the occipital lobes, which are fundamentally concerned with the processing

of visual information (Grill-Spector, Kourtzi, & Kanwisher, 2001; Miki et al., 2001; Tong,

2003), and the left pre-central gyrus, which has been associated with making motor responses

with the contralateral (i.e. right) hand (Bucy & Fulton, 1933; Horenstein, Lowe, Koenig, & Phillips, 2009; Witt, Laird, & Meyerand, 2008).

In the baseline greater than all contrasts, the healthy volunteers and schizophrenia patients show similar patterns of activity; in both groups, the medial prefrontal cortices, and posterior cingulate/precuneus are more active during the non-trial periods than during the trials themselves. These regions comprise core nodes of the default mode network (Buckner, Andrews-Hanna, & Schacter, 2008; Raichle et al., 2001), an assembly of brain regions that show task related decreases in activity.

In terms of contrasts examining the activity changes in response to changes in valence, the results suggest that increasing the stimulus valence led to a significant increase in activity in the primary visual cortex (calcarine sulcus). This pattern of significant increases in activity in the calcarine sulcus was present for all the valence increases in both healthy volunteers and schizophrenia patients. However, the patients appear to have a smaller number of voxels showing this significant difference. In the healthy volunteers, the activity related to the contrast of trivalent stimuli greater than univalent stimuli revealed activity in the left inferior frontal gyrus (IFG), specifically in pars triangularis and pars opercularis. The inferior frontal gyrus has been hypothesized to be involved in several inhibitory processes including: inhibiting responses during Go/NoGo tasks (Garavan, Ross, Murphy, Roche, & Stein, 2002) and task switching paradigms (Dove, Pollmann, Schubert, Wiggins, & Yves Von Cramon, 2000), inhibiting interference effects in working memory (D 'esposito, Postle, Jonides, & Smith, 1999), and inhibiting the recollection of unwanted memories (Anderson et al., 2004). Although some have argued that these inhibitory effects are primarily localized to, and stronger in the right IFG

(Aron, Robbins, & Poldrack, 2004), others have found that the left IFG is also critically important for inhibitory behaviours (Swick, Ashley, & Turken, 2008; Swick & Chatham, 2014).

The left IFG activity found in the current study is possibly related to the increased requirement for inhibition (or attentional biasing) during the processing of multivalent stimuli relative to univalent stimuli. However, the left IFG is also the location of Broca's Area, and is known to be critically involved in language production (Price, 2000; Rosen et al., 2000). Additionally, the left IFG has been implicated in the revision of beliefs (Sharot et al., 2012), which suggests that the precise functional role played by the left IFG in this contrast requires further study to fully disambiguate. Notably, we did not find the same significant left IFG activity when examining the same contrast in the patient data.

In terms of the contrasts between the healthy volunteers and the schizophrenia patients, the primary hypothesis that patients would display increased activity in the dAcc relative to healthy controls at low levels of stimulus, and decreased activity in the dAcc relative to healthy controls at high levels of stimulus valence was not supported. The results from the univariate fMRI analysis indicate that many of the regions found to be active in the all greater than baseline contrast and the valence level contrasts were significantly more active in the healthy volunteers than in the schizophrenia patients. In contrast, patients only displayed significantly greater activity than controls in the all stimuli greater than baseline contrast, and the results indicate that this increased activity was present in medial prefrontal cortex, posterior cingulate/precuneus, and middle and superior temporal gyri. As mentioned above, these regions are nodes in the DMN, and were found in both the healthy volunteers and schizophrenia patients when contrasted baseline greater than all stimuli. This pattern of results indicates that the schizophrenia patients had more activity in regions which are usually inactive during task states than the healthy

volunteers. Previous studies have found stronger DMN activity in schizophrenia patients relative to healthy controls when performing effortful cognitive tasks (Broyd et al., 2009; D. Il Kim et al., 2009; Metzak et al., 2011; Whitfield-Gabrieli et al., 2009), and have argued that this hyperactivity is indicative of the inefficiency in cognitive processing in the disease.

Multivariate Functional Magnetic Resonance Imaging

Introduction.

The choice of analysis technique in neuroimaging studies is non-trivial. Univariate and multivariate methods of data analysis yield answers to different questions regarding the relations between brain activity and behaviour. Univariate analyses are ideal for asking questions regarding the functional specificity of discrete brain regions, whereas multivariate methods are generally used to specify the relationships between voxels over time. In other words, univariate methods are excellent for assessing significant changes in activity within any given brain region in response to a stimulus, whereas multivariate methods are excellent for identifying networks of regions whose activity correlates together over stimulus changes, a relationship that is known as functional connectivity. However, there are multivariate methods that examine a priori defined causal relationships between brain regions as well, and this form of analysis is referred to as effective connectivity. Multivariate methods have been especially appealing to schizophrenia researchers given that the illness has often been described as one of 'dysconnectivity' (Fornito et al., 2012; Lynall et al., 2010; Stephan et al., 2009).

Functional connectivity analyses in schizophrenia patients have largely supported this view, with the most common finding being alterations in connectivity between prefrontal cortex and dAcc with the parietal lobes while performing cognitive control tasks (Fornito, Yoon, Zalesky, Bullmore, & Carter, 2011; Libby & Ragland, 2012; Minzenberg et al., 2014). However,

the precise nature of these changes is not invariant; although most studies report that patients show decreased connectivity between prefrontal and temporal regions, some find increases in connectivity as well (Libby & Ragland, 2012; Lynall et al., 2010; Pettersson-Yeo et al., 2011). As this variability in connectivity may be related to the task and design of the experiment being performed, many researchers have capitalized on the intrinsic organization of the brain into functionally connected networks in order to examine how brain activity differs in patients in the resting state. These investigations into differences in resting state connectivity have found that patients generally show deficits in fronto-temporal connectivity even when no task is being performed, but these results are somewhat inconsistent (Fornito et al., 2011; Pettersson-Yeo et al., 2011), as some studies fail to find deficits in fronto-temporal connectivity in schizophrenia.

Hypothesis.

The hypothesized results for the multivalent fMRI analysis were that: 1) the increase in task-irrelevant stimulus dimensions (i.e., valence), and the attendant increase in demand for attentional biasing, will lead to stronger activity for both groups in the TPN (including the dAcc) and 2) schizophrenia patients will show greater activity relative to controls at low levels of valence and decreased activity relative to controls at high levels of valence in the TPN (including the dAcc).

Methods.

Constrained principal component analysis.

The multivariate data analysis method used in this study is called Constrained Principal Component Analysis (CPCA). CPCA is a general method for structural analysis of multivariate data that combines regression analysis and principal component analysis into a unified framework (Takane & Shibayama, 1991). CPCA proceeds in 2 steps: first, the total variability in

51

the criterion data (i.e. the dependent variables) is partitioned into variability related to the predictor data (i.e. the independent variables) and variability that is unrelated to the predictor data via multivariate regression. In step two, PCA is performed on each of the two resulting matrices in order to detect possible underlying structures related (or unrelated) to the predictor variables. As two methods of structure extraction, regression and PCA are complementary as they allow the criterion data to be separated into both known and unknown structures. The regression analysis decomposes the criterion data on the basis of its relationship to known structure in the predictor data, whereas the PCA decomposes the criterion data into unknown structure on the basis of patterns of intercorrelations found within the criterion data itself.

The general form of the CPCA model (the general from is not used in the current study) can be found below:

$$Z = GMH' + BH' + GC + E \tag{1}$$

where Z is the criterion data, G is the matrix of constraints on the rows of Z, H is the matrix of constraints on the columns of Z, and E is the variance in Z that cannot be estimated by G, H or the interaction of G and H. In the full model, the matrices of to-be-estimated parameters are M, B, and C. The first term in the model (GMH) assesses the variance that can be explained by the interaction between G and H, the second term in the model (BH) assesses the variance that can be explained by H, but not G, and the third term in the model (GC) assesses the variance that can be explained by G, but not H.

For the purposes of fMRI experiments, Z is composed of each subject's preprocessed images whereby each column contains data from a single voxel and each row contains data from a single scan (or repetition time, TR), with the rows proceeding temporally so that the first subject's first scan (or TR) comprises row one and the last subject's last scan (or TR) comprises

the last row. So, each row in the Z matrix is m voxels in width and each column is n subjects by s scans in length. The columns of Z should be mean-centered and normalized to unit length prior to analysis. The G matrix can be any type of design matrix as long as it is full rank and has the same number of rows (i.e., n subjects by s scans) as the Z matrix to enable the matrix algebra to proceed. The design matrices that have been used for the G matrix include the canonical HRFs generated using SPM8, and Finite Impulse Response (FIR) basis sets (Woodward et al., 2006; Metzak et al., 2010). The canonical HRF- and FIR-based G matrices both produce images of brain networks that account for a large portion of the variability in the data, however, the HRF design matrices explore how the network activity matches the synthetic HRF shape modeled for each of the experimental conditions represented in the design matrix, whereas the FIR design matrices explore the shape of the HRF underlying network activation changes occurring in post-stimulus time in each of the experimental conditions modeled in the design matrix without making a priori assumptions about the network level HRF shape. In either case, the rows of the FIR G matrix have a width of k conditions by t timepoints, whereas an HRF G matrix has one timepoint per condition. In the current study, we only use an FIR model in G, and t takes a value of 8, representing 8 post-stimulus time points or TRs (with each TR = 2s.).

The H matrix can be used to constrain results to the variance predictable from brain networks of interest. For instance, H matrices may be used to examine brain networks that are lateralized to one hemisphere or the other, brain networks localized dorsal or ventral portions of the cortex, or any other brain network involving areas that can be theoretically pre-specified.

Row constraint matrices similar to the G matrix can also be used to explicitly remove sources of nuisance variance from the data. For instance, subject movement parameters, autocorrelations between adjacent time points, or trends in the data that reflect signals of non-

53

neuronal origin (A. M. Smith et al., 1999) can be included as row constraints in order to remove the variance related to these effects from the measured BOLD response.

Application of CPCA to unimodal data sets.

Although it is possible to use the full model listed in (1) above in the analysis of fMRI data, the CPCA model with only row constraints has been most commonly used:

$$_{n\times s}Z_m = {}_{n\times s}GC_m + {}_{n\times s}E_m \tag{2}$$

where *n* is the number of subjects, *s* is the number of scans, and *m* is the number of voxels.

In this model, the total variance in the data is partitioned into two matrices; the matrix *GC*, which contains the variability that is predictable from the timing of stimulus presentation, and the matrix *E* which contains the variability that cannot be explained by the timing of stimulus presentation. The matrix *G* contains the timing information for the fMRI experiment, where each row of *G* represents a different scan (or TR). *C* is the matrix of condition specific regression weights and is obtained by regressing *Z* onto *G* via the following formula for computation of multivariate ordinary least squares regression weights:

$$_{k\times t}C_m = ({}_{k\times t}G'_{n\times s}G_{k\times t})^{-1}\,{}_{k\times t}G'_{n\times s}Z_m \tag{3}$$

where *k* is the number of conditions, *t* is the number of time points modeled in each condition when using an FIR model (*t* = 1 when using an HRF model), *m* is the number of voxels, *n* is the number of subjects, and *s* is the number of scans.

The set of *m* condition-specific regression weights contained in *C* are often referred to (in conventional univariate fMRI analyses) as beta images. The matrix *GC* is then subjected to PCA in order to identify patterns of intercorrelated voxel activity that are predictable from the presentation of experimental stimuli via the following analysis:

$$[_{n\times s}U_pD_pV'_m] = {}_{n\times s}GC_m \tag{4}$$

where n is the number of subjects, s is the number of scans, p is the number of components extracted, m is the number of voxels, and the square brackets denote the products of singular value decomposition.

This decomposition yields: a) right singular vectors (V) which can be overlaid (after rescaling in the application used here) on a structural brain image to indicate patterns of functionally connected voxel activity related to the presentation of the experimental stimuli, b) the diagonal matrix of singular values (D), and c) the left singular vectors (U) which can be used to produce predictor weights (uppercase P):

$$_{n \times s} U_p = {}_{n \times s} G_{k \times t} P_p \qquad (5)$$

where n is the number of subjects, s is the number of scans, (lowercase) p is the number of components extracted k is the number of conditions, and t is the number of timepoints modeled in each condition. Thus, predictor weights in P are the weights that would be applied to G to produce U. As such, they determine the importance of each column in G for the temporal information in the brain networks represented in U. Since each column in G represents a post-stimulus timepoint, it follows that those columns in G that are more important to U are those coding the peaks of the hemodynamic response shapes. This is why the values in P form hemodynamic response shapes when the analysis of fMRI data is carried out.

In the fMRI-CPCA analysis carried out here, the values of the matrix subscripts were as follows: $n = 44$, $s = 616$ for most participants (308 per run * 2 runs) and 430 for the first few participants (1 run with 430 scans), $k = 3$, $m = 44773$, and $t = 8$.

In order to emphasize the simple structure in the components, all the products of this decomposition were rotated orthogonally using varimax rotation (Kaiser, 1958).

As there is a separate set of predictor weights for each subject, these can be used in conventional statistical analyses (i.e., a repeated measures ANOVA) to assess the group and condition related changes in estimated BOLD activity. The results of the ANOVA indicate whether the brain activity in the components match a biologically plausible HRF shape that does not vary randomly between participants, as well as indexing any significant differences in activity related to group membership or changes in experimental condition.

Results.

This multivariate fMRI-CPCA analysis concatenated the individual stimuli classes (i.e., univalent colour, univalent parity, univalent case, bivalent colour, bivalent parity, bivalent case, trivalent colour, trivalent parity, and trivalent case) to create univalent, bivalent and trivalent conditions. As for the univariate SPM analysis described above, only trials that elicited a correct response were modelled in the design matrix.

An examination of the scree plot (Cattell, 1966) suggested that 3 components should be extracted for further significance testing. The sum of the squared loadings divided by the number of scans (analogous to the percentage of predictable variance accounted for by each component) for the rotated solution was 19.73, 12.70, and 6.93 for components 1, 2, and 3 respectively. Please see Table 11 for the sum of squares and percentages of variances associated with the products of this analysis. The brain regions comprising the functional networks represented by each component (i.e., each row of the rotated and rescaled right singular vector $VD/\sqrt{((n*s)-1)}$, where n is the number of subjects and s is the number of scans), were thresholded to the top 10% of loadings, mapped onto an MNI structural image. These are displayed in the upper panels of Figure 9, Figure 10, and Figure 11, respectively, and the mean predictor weights plotted as a function of poststimulus time, representing the estimated HDR of each functional network, are

depicted in the lower panels of Figure 9, Figure 10, and Figure 11. The repeated-measures ANOVAs of the predictor weights for each component resulted in significant interactions for both components. A $8 \times 3 \times 2$ ANOVA was performed with the within-subject factors of Time Point, and Valence, and a between-subject factor of Group. Any significant interactions with Time Point resulting from this analysis were interpreted using the 'Repeated' option for the Time Point Factor in SPSS, which restricts significance tests of Within-subject contrasts involving the 8 level Time Point factor to changes between adjacent time points, thereby facilitating the break down of all interactions involving this factor to 2×2 interactions.

Component 1.

Component 1, depicted in Figure 9, was comprised of bilateral activations in the middle frontal gyri, inferior frontal gyri (pars opercularis), anterior cingulate gyri, dAcc, paracingulate gyri, juxtapositional lobule cortex (also known as the supplementary motor area (SMA)), superior frontal gyri, precentral gyri, precuneus, superior and inferior lateral occipital cortices, intracalcarine cortices, lingual gyri, fusiform gyri, as well as in the vermis, Crus I and II, and Lobule 6 and 7b of the cerebellum. Lateralized activations were located in the left inferior frontal gyrus (pars opercularis), left postcentral gyrus, left superior parietal lobule, and left angular gyrus.

The statistical analysis of the predictor weights from Component 1 revealed a significant effect of Time Point, $F_{(7,294)} = 20.84$, $p < .001$, $\eta^2 = 0.33$, as well as a significant interaction between Valence and Time Point, $F_{(14,588)} = 2.34$, $p < .05$, $\eta^2 = 0.05$. The significant effect of Time is reflected in the 95% confidence interval of the Grand Mean, which does not span zero (0.06-0.01), and the significant interaction between Valence and Time is reflected in the

difference in mean predictor weight values at 2 seconds post-stimulus time with the Univalent, Bivalent and Trivalent conditions having means of 0.10, 0.15, and 0.05, respectively.

Follow-up tests examining the interaction between Valence and Time Point indicated that there were significant differences between the valence conditions in estimated BOLD signal changes over adjacent time points. Between 0 and 2 seconds, averaged over Group, significant differences were found between the Univalent and Bivalent, and Bivalent and Trivalent conditions, resulting from the initial decrease in the Univalent condition and increase in the Bivalent condition, $F_{(1,42)} = 4.79$, $p < .05$, $\eta^2 = 0.10$, and the initial decrease in the Trivalent condition relative to the increase in the Bivalent condition, $F_{(1,42)} = 5.62$, $p < .025$, $\eta^2 = 0.12$. The mean predictor weight difference scores between 0 and 2 seconds for the Univalent, Bivalent and Trivalent conditions are -0.02, 0.04, and -0.03, respectively. Between 2 and 4 seconds, averaged over Group, the Trivalent condition increased in estimated BOLD activity significantly more than the Bivalent condition, $F_{(1,42)} = 8.98$, $p < .01$, $\eta^2 = 0.18$. The mean predictor weight difference scores between 2 and 4 seconds for the Bivalent and Trivalent conditions are 0.04 and 0.11, respectively.

Component 2.

Component 2, depicted in Figure 10, was characterized by both activations and deactivations. Bilateral activations were found in the juxtapositional lobule cortex/SMA, dAcc, superior and inferior occipital cortices, fusiform gyri, lingual gyri, occipital pole, as well as in the vermis, Crus I and II, and Lobule 6 and 7b of the cerebellum. Lateralized activations were found in the left precentral gyrus, left supramarginal gyrus, and left superior parietal lobule. Bilateral deactivations were found in the frontal pole, medial prefrontal cortex (mPFC), paracingulate gyri, ventral anterior cingulate gyri, middle and superior frontal gyri, middle

temporal gyri, posterior cingulate gyri, precuneus, intracalacarine cortices, cuneus, and superior lateral occipital cortices.

The statistical analysis of the predictor weights from Component 2 revealed significant main effects of Valence, $F_{(2,84)} = 9.80$, $p < .001$, $\eta^2 = 0.19$, and Time Point, $F_{(7,294)} = 28.31$, $p < .001$, $\eta^2 = 0.40$, as well as significant interactions between Valence and Group, $F_{(2,84)} = 3.38$, $p < .05$, $\eta^2 = 0.08$, and Valence and Time Point, $F_{(14,588)} = 2.13$, $p < .05$, $\eta^2 = 0.05$. The significant effect of Valence is due to the changes in mean activity found between the Univalent, Bivalent, and Trivalent conditions, which were 0.12, 0.14, and 0.17, respectively. The significant effect of Time is reflected in the 95% confidence interval of the Grand Mean, which does not span zero (0.16-0.12). The significant interaction between Valence and Group is reflected in the difference scores in mean predictor weight values between the Trivalent and Bivalent conditions which were 0.06 in the healthy volunteers and 0.01 in the schizophrenia patients, and the significant difference in Valence and Time is reflected in the difference in mean predictor weight values at 2 seconds post-stimulus time with the Univalent, Bivalent and Trivalent conditions having means of 0.10, 0.15, and 0.05, respectively.

Follow-up tests for the main effect of Valence indicated that there were significant differences between Bivalent and Trivalent stimuli, $F_{(1,42)} = 13.42$, $p < .005$, $\eta^2 = 0.24$, in that the mean activity in the Trivalent condition was stronger (i.e., predictor weight values were farther from zero) than that of the Bivalent condition (0.14 for the Bivalent condition, and 0.17 for the Trivalent condition). Examination of the interaction between Valence and Group revealed that there were significant Group differences between the Bivalent and Trivalent conditions, $F_{(1,42)} = 5.53$, $p < .025$, $\eta^2 = 0.12$, such that the controls had a larger increase in mean activity in the Trivalent condition relative to the Bivalent condition than was found in the patients, averaged

over Time Point (0.06 in the healthy volunteers and 0.01 in the schizophrenia patients). Follow-up tests examining the interaction between Valence and Time Point indicated that between 4 and 6 seconds post stimulus time there was a greater increase in Bivalent condition than in the Univalent condition, $F_{(1,42)} = 6.40$, $p < .025$, $\eta^2 = 0.13$ (0.07 in the Bivalent condition and 0.03 in the Univalent condition), and between 12 and 14 seconds post stimulus time there was a greater decrease in the Bivalent condition relative to the Univalent condition, $F_{(1,42)} = 4.40$, $p < .05$, $\eta^2 = 0.10$ (0.08 in the Bivalent condition and 0.04 in the Univalent condition). Thus, these differences most likely reflect the increased slope to peak between 4 and 6 seconds, and the steeper slope towards baseline between 12 and 14 seconds in the Bivalent condition relative to the Univalent condition.

Component 3.

Component 3, depicted in Figure 11, was characterized by both activations and deactivations. Bilateral activations were found in the hippocampi, superior and inferior occipital cortices, fusiform gyri, lingual gyri, occipital pole, as well as in the vermis, Crus I and II, and Lobule 6 and 7b of the cerebellum. Lateralized activations were found in the left premotor gyrus and the left supramarignal gyrus. Bilateral deactivations were found in the superior frontal gyri, dorsomedial frontal pole, and middle frontal gyri.

The statistical analysis of the predictor weights from Component 3 revealed a significant main effect of Time Point, $F_{(7,294)} = 19.41$, $p < .001$, $\eta^2 = 0.32$, as well as a significant interaction between Valence and Time Point, $F_{(14,588)} = 5.83$, $p < .001$, $\eta^2 = 0.12$. The significant effect of Time is reflected in the 95% confidence interval of the Grand Mean, which does not span zero (0.01-0.08), and the significant interaction between Valence and Time is reflected in the

difference in mean predictor weight values at 2 seconds post-stimulus time with the Univalent, Bivalent and Trivalent conditions having means of 0.10, 0.01, and 0.03, respectively.

Follow-up tests for the interaction of Valence and Time Point indicated that between 0 and 2 seconds the Univalent condition increased in estimated BOLD activity more than the Bivalent condition, $F_{(1,42)} = 5.34$, $p < .05$, $\eta^2 = 0.11$ (difference scores of 0.04 for the Univalent condition, and -0.02 for the Bivalent condition), whereas between 2 and 4 seconds the Bivalent condition increased more rapidly than the Univalent condition, $F_{(1,42)} = 4.80$, $p < .05$, $\eta^2 = 0.10$ (difference scores of 0.04 for the Univalent condition, and 0.10 for the Bivalent condition). Between 6 and 8 seconds post stimulus time, the Univalent and Bivalent conditions also showed a significant difference as the Univalent condition fell from peak more rapidly than the Bivalent condition, $F_{(1,42)} = 5.18$, $p < .05$, $\eta^2 = 0.11$ (difference scores of -0.06 for the Univalent condition, and -0.01 for the Bivalent condition). During this same time frame (between 6 and 8 seconds post stimulus time), the Trivalent condition also fell from peak more rapidly than the Bivalent condition, $F_{(1,42)} = 5.40$, $p < .05$, $\eta^2 = 0.11$ (difference scores of -0.01 for the Bivalent condition, and -0.07 for the Trivalent condition). Between 10 and 12 seconds post stimulus time, the estimated BOLD activity in Trivalent condition decreased more rapidly than the Bivalent condition, $F_{(1,42)} = 8.21$, $p < .01$, $\eta^2 = 0.16$ (difference scores of -0.05 for the Bivalent condition, and -0.10 for the Trivalent condition), such that the Trivalent condition fell below baseline by 12 seconds post stimulus time.

Discussion.

The scree plot of the fMRI-CPCA results suggested that 3 components should be extracted. Each of these components have predictor weights that show temporally reliable

estimated HRF shapes. In component 1, only positive loadings exceeded the top 10% threshold, whereas components 2 and 3 contain both negative and positive loadings.

Component 1.

Component 1 was characterized by activations in the primary visual cortices, the parietal lobes, primary motor regions, dAcc, SMA, and cerebellum. Statistical analysis of the predictor weights indicated that there was a significant effect of Time, as well as a significant interaction between Valence and Time. The significant effect of Time indicates that the estimated hemodynamic responses are reliable (i.e., they are not random shapes that change between subjects), and visual inspection confirmed that they formed a plausible HDR shape. The significant interaction between Valence and Time was due to the initial dip between 0 and 2 seconds in the Bivalent condition that was not present in the Univalent and Trivalent conditions, as well as the later delayed peak in the Trivalent condition, particularly in the patient group (although there was no significant effect of Group). These differences in early activity likely reflect recovery from previous trials, because activity in this network dips below baseline at the end of the trial. Due to the variability in delays between trials and the inclusion of intermittent 'long' ITIs, this may have resulted in unexpected condition differences at the beginning of the trial.

The pattern of brain activity in this component, especially the left motor cortex and right cerebellar activations, the timing of the peak (~6 seconds), and the absence of difference between conditions and groups suggests that this network is involved in response preparation and execution (Lavigne et al., 2014; Metzak et al., 2011). The delayed peak in the schizophrenia patients relative to the healthy volunteers supports this interpretation, as the patients had significantly longer RTs than the healthy volunteers. The large error bars on the predictor

weights in the latter portion of the trial also support this interpretation as they may reflect the variability in response time in this task. Furthermore, a slower decrease from peak in a response network has been found in schizophrenia patients in previous work using the same multivariate analysis method (Lavigne, Menon, & Woodward, 2016), and was argued to reflect inefficient suppression of motor responses in patients.

Component 2.

Component 2 was characterized by activations in the occipital lobes, dAcc, left parietal lobes and left primary motor regions, and deactivations in the medial prefrontal cortices and the posterior cingulate/precuneus. Statistical analysis of the predictor weights indicated that there were significant main effects of Time, and Valence, as well as significant interactions between Valence and Group, and Time and Valence. The significant effect of Time indicates that the estimated hemodynamic responses are reliable (i.e., they are not random shapes that change between subjects), and visual inspection confirmed they form a plausible HDR. The significant effect of Valence reflects the increases (and decreases in default mode areas) in estimated hemodynamic response as a result of increased number of task-related stimulus features in the Trivalent versus the Bivalent condition. This pattern is present in both healthy volunteers and schizophrenia patients, although the healthy volunteers have higher levels of estimated activity and deactivity (i.e., predictor weight values were were farther from zero) at each of the Valence levels. The interaction between Valence and Group reflects the greater valence-related increases (and decreases) in activity present in the controls relative to the patients. Both groups show similar patterns of increasing overall activity as stimulus valence increases, however the patients show smaller increases than the controls. The significant interaction between Time and Valence reflects differences between the Univalent and Bivalent conditions, and the Bivalent and

63

Trivalent conditions. These differences occur as a result in the difference in slopes to peak, and slopes in return to baseline.

The predictor weights for this component indicate that as the stimulus valence increased and the task grew more difficult, the brain compensated by increasing activity in regions involved in visual processing, attention, vigilance and response preparation (Duncan, 2010; M. D. Fox et al., 2005), while simultaneously decreasing activity in regions involved in internal mentation and self-directed thought (Buckner et al., 2008; M. D. Fox et al., 2005; Greicius, Krasnow, Reiss, & Menon, 2003; Raichle et al., 2001). The pattern of anti-correlation between these two networks is common to many effortful cognitive tasks (M. D. Fox et al., 2005; Uddin, Kelly, Biswal, Xavier Castellanos, & Milham, 2009; Wotruba et al., 2013). The activation/deactivation in this component suggests that the patients were unable to increase the activity/deactivity in this network in the Trivalent condition to the same degree as the controls, which supports the hypothesis that schizophrenia patients display inefficient brain activity in a TPN network involving the dAcc. This is in agreement with previous studies that have suggested that schizophrenia patients display inefficient neural activity which manifests itself most clearly at higher levels of task difficulty (Callicott et al., 2003; Y. Liu et al., 2008; Metzak et al., 2011).

Component 3.

Component 3 was characterized by activations in the occipital lobes, hippocampi, and left parietal and primary motor areas as well as deactivations in superior and middle frontal gyri. The activations in this component in visual areas and hippocampi are frequently encountered in visually based tasks that require the encoding of stimulus-response associations. Similar deactivations in prefrontal regions found in this component have also been found in visual attention and working memory experiments (Tomasi, Ernst, Caparelli, & Chang, 2006), and

64

these deactivations have been found to be correlated with cognitive load (McKiernan, Kaufman, Kucera-Thompson, & Binder, 2003). However, the negative predictor weights at the end of the trial indicate that the prefrontal regions (depicted in blue in Figure 11) were, in fact, active at the end of the trial, suggesting that this component may perform an evaluative function, or may be involved in resolving sematic conflict (V. van Veen & Carter, 2005).

Statistical analysis of the predictor weights indicated that there was a significant main effect of Time, as well as a significant interaction between Valence and Time such that the Univalent and Bivalent conditions, and the Bivalent and Trivalent conditions differed significantly. The significant effect of Time indicates that the estimated hemodynamic responses are reliable (i.e., they are not random shapes that change between subjects). For the interaction between Valence and Time, the differences between the Univalent and Bivalent conditions were located in early in peristimulus time. In the Bivalent condition, the patients decrease in activity initially (although the Group effect was not significant) before rising to peak whereas the Univalent condition does not show this initial negative deflection. In the healthy volunteers, the Bivalent condition is characterized by a slower initial rise than the Univalent condition. The Bivalent and Trivalent conditions show differences late in the trial (i.e., post peak), and are driven by the Trivalent conditions showing a stronger downward slope relative to the Bivalent ones. Similar to Component 1, these differences in early activity likely reflect recovery from previous trials, because activity in this network dips below baseline at the end of the trial. Therefore, due to the variability in delays between trials, and the inclusion of intermittent 'long' ITIs, this may have resulted in unexpected condition differences at the beginning of the trial.

As in component 2, the predictor weights from this component show a load dependent increase, however, this increase is not a significant main effect, as the large standard errors

indicate a greater amount of variability in the neural response than was seen with components 1 or 2. This is possibly related to the potential role of this component in evaluation or resolution of conflict between the stimulus dimensions, since evaluation does not necessarily follow the same timing on every trial. However, even though the main effect of Valence was not significant, the interaction mentioned in the previous paragraph indicates that the rise to peak and the decline below baseline did show significant changes that were related to the Valence conditions. The quicker increase towards the peak in the Trivalent condition, as well as the higher peak, is an indication that there was a load dependent response in this component as well, however, the large standard error indicates that this load dependent response was not present for every participant and/or every trial. Component 3 reaches peak activity between 4 and 6 seconds post-stimulus time which is slightly earlier than component 2, whose peak clearly arrives at 6 seconds. However, the decrease in activity from peak is slower than in Components 1 and 2 which, along with the larger standard errors, suggests greater variability in peak time or ongoing cognitive activity in this network. Given that the BOLD signal has been found to peak approximately 6-8 seconds after stimulus presentation (Logothetis et al., 2001), component 3 was likely to be involved in very early processing of the visual stimuli (Corbetta, Miezin, Dobmeyer, Shulman, & Petersen, 1990), or in feedback to the visual cortices in response to stimulus presentation (Martínez et al., 1999), and maintained activity for a longer period of time than the previous two components. The presence of the early deactivation and late activation of the bilateral superior and middle frontal gyri is consistent with the interpretation that this component is involved in response inhibition/evaluation as these regions have been found to play that role in previous Go/NoGo studies (Li, Huang, Constable, & Sinha, 2006; Simmonds, Pekar, & Mostofsky, 2008). Furthermore, previous research has also found that these regions are involved in semantic

conflict resolution during Stroop tasks (Lavigne, Metzak, & Woodward, 2015; V. van Veen &

Carter, 2005), which is similar to the proposed evaluative function of these regions. In the

current experiment, the decrease below zero in the predictor weights indicates activations in

these areas late in the trial, and these activations display a pattern such that the schizophrenia

patients display less activity than the healthy volunteers, and the trivalent conditions elicit the

strongest activations in both groups. However, the predictor weight pattern does not completely

follow a valence related pattern as bivalent conditions do not show greater activity than the

univalent conditions.

fMRI General Discussion

The hypotheses for the fMRI portion of this experiment were that the increase in task-

irrelevant stimulus dimensions (i.e., valence) would lead to increased activity for both groups in

the TPN (including the dAcc), and that schizophrenia patients would show increased activity

relative to controls at low levels of stimulus valence and decreased activity relative to controls at

high levels of stimulus valence, particularly in dAcc, which is thought to be involved in top-

down attentional biasing. The fMRI results indicated partial support for these hypotheses, as this

pattern was found in the multivariate analysis but not the univariate analysis. Specifically, in the

multivariate fMRI analysis, Component 2 was characterized by positive activity in the TPN (as

well as negative activity in the DMN) and displayed a pattern of stronger activity/deactivity with

increasing task-irrelevant stimulus dimensions. This pattern of results, such that healthy

volunteers have stronger activity/deactivity than patients with increasing cognitive load, has been

found in previous working memory studies at high levels memory load in a TPN/DMN

component (similar to Component 2 in the present analysis) (Metzak et al., 2011). In the working

memory study, patients had stronger activity than controls at low memory loads but this

relationship was reversed at high memory loads, which suggested that patients were unable to further increase brain activity in response to more difficult to retain stimuli. This pattern is consistent with the activity of Component 2 from the current study.

The fMRI results from this experiment suggest that healthy volunteers and schizophrenia patients utilized broadly similar brain regions/networks to perform the task. In the univariate analysis, the primary region that was found to be active in most of the contrasts in this task was the occipital lobe, which is not entirely surprising given its role in visual processing and the visual nature of the stimuli in this experiment. However, in the all greater than baseline contrasts in both the healthy volunteers and the schizophrenia patients, nodes of the task positive network, including SMA/dAcc, can be observed. These results suggest that there was SMA/dAcc activity in the valence level related contrasts, but that the effect was too weak (or the analysis method too conservative) to reach statistical significance. The SMA/dAcc activity found in the all greater than baseline contrasts is consistent with the SMA/dAcc activity found in Components 1 and 2 from the multivariate fMRI analysis. Judging from the predictor weights, the time courses of the two networks appear to perform different roles, with Component 1 showing an early peak and likely to be involved in response preparation and execution, and Component 2 showing a more temporally extended peak.

Both Component 1 and Component 3 exhibited condition related differences early in the trial. These differences in early activity likely reflect recovery from previous trials, because activity in this network dips below baseline at the end of the trial. The variability in delays between trials, and the inclusion of intermittent 'long' ITIs may have resulted in unexpected differences between conditions early in the trial. It is notable that these early trial differences

were not apparent in Component 2, which is congruent with the absence of a dip below baseline

at the end of the trial for Component 2, which was seen in Components 1 and 3.

One additional reason for differences between the univariate and multivariate fMRI

results in this project is that different types of predictors were used in the univariate and

multivariate regressions. The univariate fMRI analysis employed the canonical synthetic HRF as

a predictor whereas the multivariate fMRI analysis employed an FIR model. As the multivariate

fMRI analysis indicated that the three components had somewhat different estimated

hemodynamic response shapes, this raises the possibility that a poor match between the predictor

(i.e., the synthetic HRF) and the criterion (i.e., the hemodynamic responses in each voxel)

variables may underlie the differences in these results, particularly if the schizophrenia patients

displayed more variability in hemodynamic response shape. For example, the multivariate

analysis shows that the SMA/dAcc did show a strong signal for this task (Component 1).

However, it displays a biologically plausible but non-standard HRF shape (see Figure 9) that

would not be captured well by the synthetic HRF shaped employed by SPM, and this would

explain the weak depiction of the SMA/dAcc signal that emerged in the univariate analysis. It

should be noted that the choice of predictor model is independent of the analysis method, either

model could have been used in both the univariate and multivariate analysis.

The univariate and multivariate results both indicate that group related differences were

found in the occipital cortices. In the univariate analyses, the results indicated that increasing

stimulus valence led to increased occipital cortex activity, and the contrast of the controls and

patients found that the controls showed significantly greater increases. This suggests that patients

showed a weaker (or more variable) response to the increase in stimulus dimensions which may

underlie the performance differences found between the two groups. In the multivariate fMRI

69

analysis, group related differences were found only in Component 2, but occipital cortex activity was present in all three of the components. This suggests that the activity in this area may be subserving multiple networks and functions in this task, and that patients only show deficits on some of them. However, it cannot be ruled out that the power level was too low to detect significant differences on the other components.

<center>**Magnetoencephalography**</center>

Univariate Magnetoencephalography

      Introduction.

      Investigators have used MEG to identify differences in functional activity between schizophrenia patients and healthy volunteers while performing attentional biasing tasks, in order to identify which bands and brain regions are affected. One study examining schizophrenia patients and healthy controls performing the Stroop task found that schizophrenia patients showed decreased gamma band activation in the left DLPFC and increased gamma band activity in the right DLPFC relative to healthy controls (Kawaguchi et al., 2005). Another study examining selective visual attention found that schizophrenia patients show smaller decreases in contralateral alpha band power than controls when attending to a cued location (Kustermann, Rockstroh, Kienle, Miller, & Popov, 2016), which suggests that deficits in cognitive control tasks could be related to poor stimulus encoding. This finding is supported by a resting state study which found that patients show deficits in alpha power synchrony in left parietal regions while contrasting eyes-open state with eyes-closed state (Ikezawa et al., 2011). These deficits correlated with scores on a visual memory test, which suggests that it may be related to problems with visual processing and attention. In the beta band, schizophrenia patients show decreased power in the insula relative to controls when encountering task relevant stimuli (E. B. Liddle et al., 2016). The authors argue that this failure in beta band modulation is evidence for a misattribution of salience to stimuli; the failure in generating top-down salience for a currently relevant stimulus supports other accounts of aberrant salience in schizophrenia (Kapur, 2003). Theta band activity, especially in frontal regions, has been hypothesized to support cognitive control and executive functioning (Cavanagh & Frank, 2014; Jensen & Tesche, 2002; Schmiedt,

<center>71</center>

Brand, Hildebrandt, & Basar-Eroglu, 2005). In schizophrenia patients, this hypothesis is supported by findings of decreased in theta power in frontal cortices relative to controls (Schmiedt et al., 2005). The authors argue that this deficit is related to problems in generating, updating, and maintaining task set during a task switching experiment.

Localizing MEG activity to a particular brain region requires the use of beamforming to move from sensor space to source space. Beamforming techniques were originally developed for radar applications, specifically to increase the signals from locations of interest while attenuating signals from other locations (B. D. Van Veen & Buckley, 1988). The primary assumption underlying beamforming is that no two macroscopic sources of neuronal activity are correlated (Herdman & Cheyne, 2009; Hillebrand & Barnes, 2005). If two signals are perfectly correlated and are originating from two proximal tissues, the beamformer will only identify a single source, whereas if the perfectly correlated signals are located distally, the signals cancel each other out (B. D. Van Veen, Van Drongelen, Yuchtman, & Suzuki, 1997). In the case of partially correlated signals, the beamformer identifies the correct number of signals and changes in power, however, the power is diminished. The partial correlations need to be strong in order to cause this attenuation of power, a simulation with the DICS beamforming method (Gross et al., 2001) revealed that the results are robust until correlations reach 0.55, after which the power is attenuated and the localizations begin to blur (Belardinelli, Ortiz, & Braun, 2012). The results of a study using MEG to examine source signal correlations in dorsal attention and default mode networks suggests that correlations of that magnitude are rare (Pasquale et al., 2010).

One feature of beamforming that should be kept in mind is that it achieves increases in spatial resolution at the expense of temporal resolution (Brookes et al., 2011). In order localize changes in power to brain regions, the DICS beamformer uses a frequency based approach

(Gross et al., 2001), meaning that the activity in time segments of tens to hundreds of milliseconds are used to calculate power changes in each beamforming window. This means that the temporal resolution of the beamformed MEG activity is reduced to the time frame required to capture the oscillatory activity of the frequency bands under investigation.

Methods.

Scanning.

Imaging was performed at the Down Syndrome Research Foundation Magnetoencephalography Laboratory on a 151-channel whole-head CTF system (VSM Medtech, Port Coquitlam, Canada) located in a magnetically shielded room. Participants were supine and stimuli were presented on a screen located approximately 40 centimeters above the participant's head. The screen location was optimized for each participant's comfort in order to reduce movement during scanning. A LUMItouch fiber-optic response device (Lightwave Medical, Vancouver, Canada) was used to record the participant's responses. The response box was placed on the participant's abdomen in such a way as to maximize comfort and reduce the need to move to make responses. The participant's right index and middle fingers were used to make all responses. Data were continuously digitized at 1200 Hz, and head movement was measured via fiducial coils placed on the nasion and preauricular points and energized at distinct, high narrow-band frequencies.

Preprocessing.

Using custom written scripts, the MEG data were notch filtered to remove the narrow-band frequencies emitted by the fiducial coils. Following this, the MEG data were preprocessed using FieldTrip software (Oostenveld, Fries, Maris, & Schoffelen, 2011). MEG data were downsampled to 600 Hz from 1200 Hz, and segmented into individual trials. Each trial was then

assessed for head movement; trials with movement exceeding a half centimeter in any direction were removed from further analysis. In order to remove artifacts from the trial segments, a number of steps were undertaken. Firstly, the data were automatically checked for muscle artifacts, clipping artifacts, and SQUID jumping artifacts. Any trials that exceeded a predefined Z-value threshold were removed from subsequent analyses. Next, the remaining valid trials were decomposed using Independent Component Analysis (ICA) (Bell & Sejnowski, 1995). The topographies of the resulting components were manually examined, and components containing eye movement artifacts, blink artifacts, or cardiac artifacts were removed, followed by the remixing of the remaining components. Lastly, the data from each trial were visually inspected to ensure data quality. Following this artifact removal procedure, only participants with at least 25 trials in each condition for each run were included for further analysis.

After artifact removal was complete, the time-frequency plots from each subject and trial type were combined to create average time frequency plots for each group (e.g., patients and controls) and condition (e.g., univalent, bivalent and trivalent). These averaged time-frequency were used to determine the frequency ranges and timing to be used in the subsequent beamforming analyses.

Each participant's structural MRI was segmented into grey matter, white matter, and cerebrospinal fluid (CSF). The segmented MRIs were used to create anatomically accurate head models, these head models define the volume conduction properties of the head and are part of the forward solution. In turn, these head models were used to generate a lead field, which is a matrix indicating the values of the electric potential at the MEG sensors for a given dipole (Vallaghé, Papadopoulo, & Clerc, 2009). In order to assess the beamforming results at a group level, all MEG data was aligned to a common source model template. A source model is used to

represent the set of positions of dipoles that are used as potential loci of magnetic field changes when performing source reconstructions (i.e. during beamforming). The source model used in these analyses were defined using the Montreal Neurological Institute (MNI) coordinate system with grid points placed 5 mm apart. The structural MRI scan from each participant was warped to this source model prior to beamforming. This allowed the beamforming analysis to respect each individual's unique brain structure/function while enabling group-level inferences.

Individual beamforming analyses were performed using a DICS beamformer (Gross et al., 2001) for each frequency band and time course of interest. For all analyses, the prestimulus 'baseline' activity was subtracted from the active task state in order to compensate for the slow drift in MEG signals and lack of a true 'zero' level (Gross et al., 2013). Some follow-up analyses examined the difference between active task states at different levels of stimulus valency (e.g. alpha activity during univalent stimulus presentation vs. alpha activity during bivalent stimulus presentation). For each beamforming analysis, an image file was written out containing the estimated beamforming parameter for each voxel in the brain. These image files were input into SPM8 as individual contrast images for use in a random-effects (second level) analysis. The purpose of this analysis was to determine whether the brain activity elicited by the stimulus presentations was consistently localized to a particular region or network and whether this activity differed significantly between groups and/or conditions.

Hypothesis.

Analogous to the univariate fMRI section, the hypothesis for the univariate MEG results was that both groups would display increases in power in the theta band (i.e., 4-8 Hz) in dAcc/preSMA, and, 2) that schizophrenia patients will show greater theta power in MEG relative to healthy participants at low levels of valence and decreased power relative to healthy

75

participants at high levels of valence in the dAcc/preSMA regions, which are thought to be involved in top-down control of attentional biasing.

Results.

A univariate analysis of the MEG data was performed using the Fieldtrip toolbox (Oostenveld et al., 2011). The following classes of stimuli were modeled in these analyses: univalent colour, univalent parity, univalent case, bivalent colour, bivalent parity, bivalent case, trivalent colour, trivalent parity, and trivalent case. These individual stimuli classes were concatenated to create univalent, bivalent, trivalent conditions which encompassed each of the three tasks.

In order to determine which time points and which frequency ranges to beamform, a time frequency analysis was performed using a multitaper method with Hanning tapers. The frequencies of interest were between 2-160 Hz, increasing in 2 Hz steps, and the time window was 0.5 seconds and these windows were slid 0.05 seconds per analysis, covering the length of the trial (1.5 seconds). The goal of this analysis was to produce an image depicting the average changes in power over frequencies and time points over the trial. This analysis revealed post-stimulus decreases in power in the 20 Hz range and increases in power in the 10 Hz, and 6 Hz ranges. On the basis of the time-frequency plot, beamforming was performed in the beta (20 +/-3 Hz) range between 0.4 and 0.9 seconds, in the alpha (10 +/-3 Hz) range between 0.0 and 0.3 seconds, and in the theta (6 +/-2 Hz) range between 0.75 and 1.25 seconds. Please see Figure 12 for the time frequency plot that has been averaged over all conditions, sensors, and participants.

Brain activity from healthy controls and schizophrenia patients were analyzed separately, as well as in a combined analysis to assess group level differences. All the results presented in

this section contrasted either a condition to the prestimulus baseline, or contrasted two experimental conditions. All analyses used a statistical threshold of $p < .05$ (FWE-corrected). The anatomical loci of the significant activations resulting from each contrast are listed in Table 12 and the cluster information from significant contrasts for the healthy volunteers and the schizophrenia patients can be found in Table 13 and Table 14, respectively.

For the brain images for the significant condition greater than baseline contrasts in the 6 Hz (theta) band in the healthy volunteers, please see Figure 13. For the brain images of the significant condition greater than baseline contrasts from the 20 Hz (beta) band in the healthy volunteers, please see Figure 14. There were no significant brain images resulting from the condition greater than baseline contrasts in the 10 Hz (alpha) band in the healthy volunteers.

For the brain images of the significant contrasts between conditions from the 10 Hz (alpha) band in the healthy volunteers, please see Figure 15. For the brain images of the significant contrasts between conditions from the 20 Hz (beta) band in the healthy volunteers, please see Figure 16. There were no significant brain images resulting from the condition contrasts in the 6 Hz (theta) band in the healthy volunteers.

For the brain images of the significant condition greater than baseline contrasts from the 20 Hz (beta) band in the schizophrenia patients, please see Figure 17. For the schizophrenia patients, there were no other significant condition greater than baseline contrasts, nor were there any significant contrasts between conditions. Also, all contrasts between groups yielded non-significant results.

Discussion.

The univariate MEG results suggest that the experiment activated similar regions in both schizophrenia patients and healthy volunteers but the predicted relationship between increases in

valence and increases in power in the theta band in the dAcc were not supported, nor was there evidence of valence-related inefficiency in theta power in the schizophrenia patients.

In both healthy volunteers and patients, analysis of the 20 Hz (beta) band at all levels of valence versus baseline (as seen in Figure 14 and Figure 17, respectively) revealed widespread decreases in power with the strongest negative deflections found in the left primary motor regions and the bilateral inferior visual cortices and cerebellum. The presence of this decrease in the left motor/sensory cortices is presumed to be a consequence of the requirement to make responses using the right hand, on the basis of decades of research illustrating the relationship between limb movement and decreases in beta power over the contralateral sensorimotor cortex and ipsilateral cerebellum (Brown, 2007; Davis, Tomlinson, & Morgan, 2012; Neuper & Pfurtscheller, 2001; Salmelin & Hari, 1994). In the visual cortices, this decrease in power is thought to reflect attentional demands and release from inhibition, (Bauer et al., 2012; Panagiotaropoulos, Kapoor, & Logothetis, 2013), and is widely reported (Gola, Magnuski, Szumska, & Wróbel, 2013; Whitman et al., 2015). Both of these decreases appear to reflect basic sensory and motor responses associated with the performance of this task.

In the healthy volunteers, these decreases in power (as seen in Figure 16) appear as though they may be load dependent, as the bivalent and trivalent conditions show further decreases in power in posterior regions relative to the univalent condition. This load-dependent pattern of beta activity has been found in primary visual cortex in visual attention experiments requiring to participants to attend to differing numbers of stimuli (Rouhinen, Panula, Palva, & Palva, 2013). Load dependent increases in activity in visual cortex have also been found in fMRI experiments examining working memory (Metzak et al., 2010, 2011). However, it is also possible that the increased size of some of the bivalent stimuli could have led to increased

desynchronization in primary visual cortex in the bivalent condition relative to the univalent condition.

In the trivalent greater than bivalent contrast in healthy volunteers (Figure 16b), decreases in power were found in posterior portions of the brain, including posterior cingulate, fusiform and lingual gyri, calcarine fissure, and the cerebellum. With the exception of the posterior cingulate and the cerebellum, the regions in which these decreases appear are related to visual processing, thus inviting the speculation that these significant decreases are related to the increased numbers of stimuli dimensions that must be encoded (and ignored). However, the pattern of power decreases in this contrast is less well localized to the calcarine fissure than the previously discussed bivalent stimuli greater than univalent stimuli contrast. Furthermore, the lack of significant differences in the contrast of trivalent versus bivalent stimuli in healthy volunteers suggests that the load dependent effect was not as strong, or as consistent as the one between univalent and bivalent stimuli. Beta band activity has been found in the posterior cingulate (J. S. Kim et al., 2014) in previous studies, and there is speculation that this activity indicates the maintenance of the status quo (Engel & Fries, 2010), which suggests that perhaps the reduction of beta power in the PCC is related to the ever-changing nature of the required responses. There was no evidence of load-dependence in this band in the schizophrenia patients.

In the 6 Hz (theta) band (as seen in Figure 13), healthy volunteers showed increases in power in the ventromedial PFC (vmPFC) and medial orbitofrontal cortex (OFC). Significant increases in theta band power in OFC and vmPFC have previously been found in MEG research examining various cognitive operations, for instance, the completion of sentences that involve 'complement coercion' (Pylkkänen & McElree, 2007), during predictive coding mismatches (Garrido, Barnes, Kumaran, Maguire, & Dolan, 2015), and examining prediction violations in

word-picture pairs (Dikker & Pylkkänen, 2013). Other MEG studies have found theta rhythm phase-locking between the hippocampus and the OFC during rewarded decision making (Guitart-Masip et al., 2013). Furthermore, this increase in theta activity in the medial orbitofrontal cortex has also been found in the EEG literature in paradigms including visual oddball tasks (Delorme, Westerfield, & Makeig, 2007; Makeig et al., 2004), and reward based learning (Hauser et al., 2015).

These disparate examples can be unified by viewing the increases in medial orbitofrontal theta activity as being involved in forming, monitoring, and revising associations between stimuli and the anticipated reward value of responses. This hypothesis is supported by the electrophysiological examples cited above; and the role of the OFC in cognition has also been explored in many positron emission tomography (PET) studies as well. For instance, increased OFC activity is found: when expectation violations are detected in visual attention paradigms (Nobre, Coull, Frith, & Mesulam, 1999), when subjects spontaneously devise strategies to categorize stimuli (Savage et al., 2001), when subjects distinguish currently relevant information from previously encountered (and currently irrelevant) information (Schnider & Ptak, 1999), when responses must be guessed prior to receiving complete information (Elliott, Dolan, & Frith, 2000), when there are four possible guessing options versus two possible guessing options (Elliott et al., 2000), and during match-to-sample tasks (Elliott et al., 2000).

Interestingly, there are fewer fMRI studies evaluating this hypothesis than might be expected, but this is perhaps due to the BOLD signal dropout found in air/tissue interfaces in the brain, of which the orbitofrontal cortex is a prime example (Glover & Law, 2001). However, fMRI studies have found significant coupling between the hippocampus and the vmPFC during

an inferential learning task (Zeithamova, Dominick, & Preston, 2012), thus supporting the PET and electrophysiological results mentioned above.

In the current study, the change in event related synchrony (ERS) in the medial OFC and vmPFC in the theta band is most likely related to the requirement to learn the association between the stimulus features (e.g. colour, parity, or case) and the correct button press in a situation where responses must be made rapidly. As mentioned above, one possible reason why we do not see the same activity in the fMRI analyses is due to the poor BOLD signal reliability in the vmPFC. Another potential explanation is that, for all the participants, MEG scanning was performed prior to fMRI scanning to avoid any potential magnetization effects. Thus, it is also possible that scan order effects underlie the lack of significant vmPFC activity in the fMRI version of the experiment.

In the 10 Hz (alpha) band (Figure 15), the only significant differences were found in healthy volunteers in the contrasts between trivalent and univalent stimuli, and bivalent and univalent stimuli. These contrasts identified increases in power in the rectus gyri and medial orbitofrontal gyri. Previous research has associated alpha band activity in this area with the computation of value signals, that is, it codes the valence and magnitude of rewards and punishments (Harris, Adolphs, Camerer, & Rangel, 2011). As the number of to-be-ignored stimulus dimensions increase, this coding becomes more complex as a single stimulus is associated with multiple response dimensions, each of which may have different value depending on the cue that appears with it.

However, it is notable that the 10 Hz (alpha) condition (Figure 15) contrasts find similar patterns of activity in the vmPFC (Figure 13) in the 6 Hz (theta) range. Although the bivalent greater than univalent activations are located more superiorly and posteriorly to the activations in

the healthy volunteers in the 6 Hz conditions in the univalent and trivalent conditions, they do appear to co-localize well with the significant activations in the bivalent condition. This suggests that this region shows task related increases in power in multiple frequencies (Buzsáki & Draguhn, 2004).

Multivariate Magnetoencephalography

Introduction.

Multivariate statistical methods have also been employed in MEG studies to examine connectivity and communication between brain regions (Pizzella et al., 2014). Although there are many different approaches that have been used , the majority can be defined in the same way as those used by fMRI, that is, they assess either functional or effective connectivity. Changes in activity in multiple frequency bands and multiple locations have been detailed using measures of functional connectivity. Increased gamma activity in the right DLPFC has been found in hallucinating patients relative to controls and non-hallucinating patients while performing the Stroop task (Kawaguchi et al., 2005). Others have found deficits in frontal theta power in schizophrenia patients relative to healthy volunteers while performing working memory tasks (Schmiedt et al., 2005), and when experiencing prediction errors (Roa Romero, Keil, Balz, Gallinat, & Senkowski, 2016). Schizophrenia patients also display a reversed pattern of beta band activity in the insula relative to healthy volunteers when performing a salience task (E. B. Liddle et al., 2016). In this experiment, controls had significantly higher levels of beta power while salient stimuli were being presented, whereas patients had significantly higher levels of beta power while irrelevant stimuli were being presented.

Although the experiments listed above all employed task-based designs, many of the MEG studies employing multivariate statistics have examined resting state connectivity. A meta-

analysis of resting state MEG studies found that the most common finding in resting state MEG analyses involving schizophrenia patients is increased theta power in the temporal lobes (Siekmeier & Stufflebeam, 2010). A secondary finding is increased beta power in patients, however, the anatomical loci of these increases was less consistent.

Another recent study involving 46 patients and 45 matched controls found that patients showed hyperconnectivity relative in controls in dAcc and superior frontal areas and hypoconnectivity in the precuneus/posterior cingulate (Houck et al., 2017). Furthermore, this study found beta-band hyperconnectivity in patients relative to controls in multiple functional networks, suggesting that this frequency band may be particularly impacted.

Hypothesis.

The hypothesized results for this experiment were that: 1) the increase in task-irrelevant stimulus dimensions (i.e., valence), and the attendant increase in demand for attentional biasing, will produce a component with increased power in the theta band (i.e., 4-8 Hz) in preSMA/dAcc in both groups and 2) that schizophrenia patients will show greater theta power relative to controls at low levels of valence and decreased theta power relative to controls at high levels of valence in the dAcc/preSMA, which is thought to be involved in top-down attentional biasing.

Methods.

In order to characterize the functional networks underlying this task using MEG, we employed a DICS beamformer (Gross et al., 2001) to identify whole-brain images of changes in oscillatory power. In this analysis, we produced one image for each 500ms post-stimulus window. This window was then temporally displaced by 50ms to create a new image, which resulted in a time series comprising windows of temporally overlapping estimates of oscillatory power. In this analysis, three frequency bands of interest were identified from the literature and

the time-frequency plot. These frequency bands were alpha (10 Hz center frequency +/-3 Hz),

beta (20 Hz center frequency +/- 3 Hz), and theta (6 Hz center frequency +/-2 Hz).

Principal component analysis for magnetoencephalography.

The steps outlining the procedure for an fMRI-CPCA analysis are discussed above.

However, in the case of the MEG data, additional processing steps needed to be taken to prepare

for a PCA analysis. As was mentioned earlier, beamforming was employed to localize the MEG

data to brain space. For the purpose of this PCA analysis, these preparations entailed creating a

series of beamformed images, with each image corresponding to a particular combination of

participant, run, condition, frequency, and timepoint of interest. This set of beamformed images

was created separately for each frequency band under investigation, and the *Z* matrix was made

by concatenating the three frequency-specific set of beamformed images in a row-wise manner.

The use of a *G* matrix was not necessary for this analysis because the rapid nature of the

magnetic field changes precludes overlap in signal between trials. Thus, the *G* matrix is not

required to disentangle the contributions of multiple trials to the observed signal, as it is when

measuring sluggish BOLD responses using fMRI. The MEG time series was split into trials prior

to performing this analysis such the *Z* matrix only contained trial averaged activity organized by

experimental condition, and therefore did not include data from the intertrial intervals. Since we

are not using a *G* matrix, or any other matrix as a constraint, these analysis procedures are best

described as a PCA analysis (not a CPCA analysis), although the structure of the MEG-*Z* matrix

renders it conceptually similar to the fMRI-CPCA analysis. The MEG *Z* matrix was decomposed

directly:

$$[_{n \times s}U_p D_p V'_{m \times f}] = {}_{n \times s}Z_{m \times f} \tag{6}$$

where n is the number of subjects, s is the number of beamforming windows (the MEG

equivalent of scans), m is the number of gridpoints (the MEG equivalent of voxels), f is the

number of frequency bands being examined, p is the number of components extracted, and the

square brackets denote the products of singular value decomposition.

In the current study the values of the matrix subscripts were as follows: $n = 41$, $s = 63$ (21

beamforming windows for each of the univalent, bivalent, and trivalent conditions), $f = 3$ (alpha,

beta, and theta), and $m = 6758$.

Results.

On the basis of the examination of the time-frequency plot, and in order to maintain

consistency with the univariate MEG results, the results described below are organized by

frequency range: beta (20 +/-3) Hz, alpha (10 +/-3) Hz, and theta (6 +/-2) Hz. This MEG-PCA

analysis concatenated the individual stimuli classes (e.g. univalent colour, univalent parity,

univalent case, bivalent colour, bivalent parity, bivalent case, trivalent colour, trivalent parity,

and trivalent case) to create univalent, bivalent and trivalent conditions. An examination of the

scree plot (Cattell, 1966) resulting from the decomposition of the MEG Z matrix suggested that 6

components should be extracted for further significance testing. After rotating the products of the

decomposition using varimax rotation (Kaiser, 1958), the sum of the squared loadings divided by

the number of scans/time points (analogous to the percentage of predictable variance accounted

for by each component) for the solution was 11.79, 6.33, 9.52, 4.32, 4.96, and 3.29 for

components 1, 2, 3, 4, 5, and 6 respectively. For a summary of the variance accounted for by

each component in the overall MEG-PCA solution, please see Table 15. The brain regions

comprising the functional networks represented by each component, were thresholded to the top

10% of loadings, mapped onto an MNI structural image, are displayed in the upper panels of

Figure 18, Figure 19, Figure 20, Figure 21, Figure 22, and Figure 23, respectively, and the mean

predictor weights plotted as a function of post-stimulus time, representing the estimated HDR of

each functional network, are depicted in the lower panels of Figure 18, Figure 19, Figure 20,

Figure 21, Figure 22, and Figure 23. The first timepoint was set to zero for visualization

purposes, therefore, the statistical analysis of the component scores was a $20 \times 3 \times 2$ mixed-

model ANOVA with the within-subject factors of Time Point, and Valence, and a between-

subject factor of Group.

Component 1.

Component 1 was characterized by decreases of power in the 20 Hz (beta) band. Please

see Figure 18 for the brain images and predictor weights from this component. These decreases

were found bilaterally in the angular gyri, inferior parietal lobule, superior, middle, and inferior

occipital gyri, lingual gyri, calcarine sulci, fusiform gyri, cuneus, precuneus, posterior cingulate,

parahippocampal gyrus, and hippocampus, as well as the vermis, crus I & II, and lobules 6, 7b, 8

and 9 of the cerebellum. Left lateralized decreases in power were found in the precentral gyrus,

middle frontal gyrus, superior and middle temporal gyrus, Heschl's gyrus, thalamus, insula, and

putamen.

The statistical analysis of the predictor weights from Component 1 revealed a significant

main effects of Time, $F_{(19,741)} = 15.82$, $p < .001$, $\eta^2 = 0.29$, as well as a trend in the Time by

Group interaction, $F_{(19,741)} = 2.16$, $p = .15$, $\eta^2 = 0.05$. All other main effects and interactions were

non-significant (p's > .25). The significant effect of Time is reflected in the 95% confidence

interval of the Grand Mean, which does not span zero (0.33-0.91).

Component 2.

Component 2 was characterized by decreases of power in the 6 Hz (theta) band. Please see Figure 19 for the brain images and predictor weights from this component. These decreases in power were found bilaterally in precuneus, middle and posterior cingulate, superior, middle, and inferior occipital gyri, lingual gyri, calcarine sulci, fusiform gyri, inferior temporal gyri, parahippocampal gyri, hippocampi, as well as the vermis, crus I & II, and lobules 6, 7b, 8 and 9 of the cerebellum. Left lateralized decreases in power were found in the superior parietal lobule, thalamus, and superior and middle temporal gyri.

The statistical analysis of the predictor weights from Component 2 revealed a significant main effects of Time, $F_{(19,741)} = 45.61$, $p < .001$, $\eta^2 = 0.54$. All other main effects and interactions were non-significant (p's > .35). The significant effect of Time is reflected in the 95% confidence interval of the Grand Mean, which does not span zero (1.20-1.73).

Component 3.

Component 3 was characterized by decreases of power in the 10 Hz (alpha) band. Please see Figure 20 for the brain images and predictor weights from this component. In the 10 Hz band, bilateral decreases in power were found in superior parietal gyri, superior, middle, and inferior occipital gyri, lingual gyri, calcarine sulci, fusiform gyri, precuneus, middle and inferior temporal gyri, as well as the vermis, crus I & II, and lobules 6, 7b, 8 and 9 of the cerebellum.

The statistical analysis of the predictor weights from Component 3 revealed a significant main effects of Time, $F_{(19,741)} = 15.60$, $p < .001$, $\eta^2 = 0.29$, as well as trends in the main effect of Group, $F_{(1,39)} = 2.62$, $p < .15$, $\eta^2 = 0.06$, and in the interaction between Time and Group, $F_{(19,741)} = 2.04$, $p < .15$, $\eta^2 = 0.05$. All other main effects and interactions were non-significant (p's >

.50). The significant effect of Time is reflected in the 95% confidence interval of the Grand Mean, which does not span zero (1.02-1.79).

Component 4.

Component 4 was characterized by decreases of power in the 6 Hz (theta) band and 10 Hz (alpha) band. Please see Figure 21 for the brain images and predictor weights from this component. In the 6 Hz band, bilateral decreases in power were found in superior, middle and inferior frontal (pars orbitalis) gyri, orbitofrontal gyri, rectus gyrus, imsula dAcc, and vmPFC. Right lateralized decreases in power were found in inferior frontal gyrus (pars triangularis and opercularis), temporal pole, superior, middle and inferior temporal gyri, putamen, amygdala and hippocampus.

In the 10 Hz (alpha) band, bilateral decreases in power were found in superior and middle frontal gyri, orbitofrontal gyri, rectus gyrus, dAcc, and vmPFC. Right lateralized decreases in power were found in inferior frontal gyrus (pars orbitalis and triangularis), insula, temporal pole, superior, middle, and inferior temporal gyri and hippocampus.

The statistical analysis of the predictor weights from Component 4 revealed a significant main effect of Time, $F_{(19,741)} = 15.65$, $p < .001$, $\eta^2 = 0.29$, as well as a trend in the interaction between Valence and Time, $F_{(38,1482)} = 1.89$, $p < .10$, $\eta^2 = 0.04$. All other main effects and interactions were non-significant (p's > .20). The significant effect of Time is reflected in the 95% confidence interval of the Grand Mean, which does not span zero (-0.74-(-1.45)).

Component 5.

Component 5 was characterized by increases of power in the 10 Hz (alpha) band. Please see Figure 22 for the brain images and predictor weights from this component. These increases in power were found bilaterally in superior frontal gyrus, SMA/juxtapositional lobule cortex, dAcc,

middle cingulum, posterior cingulate, precuneus. Left lateralized decreases in power were found in superior, middle, and inferior frontal (pars opercularis, triangularis, and orbitalis) gyri, orbitofrontal gyrus, pre- and post-central gyri, superior and inferior parietal lobules, temporal pole, superior, middle, and inferior temporal gyri, caudate, putamen, hippocampus, planum polare, Heschl's gyrus, and insula.

The statistical analysis of the predictor weights from Component 5 revealed a significant main effects of Time, $F_{(19,741)} = 5.44$, $p < .005$, $\eta^2 = 0.12$, and Group, $F_{(1,39)} = 5.51$, $p < .025$, $\eta^2 = 0.12$. All other main effects and interactions were non-significant (p's > .15). In this component, Grand Mean, which does span zero (-0.02-0.82), however, the Grand Mean is larger than the standard error (0.40 to 0.21) which leads to the significant main effect of Time. The main effect of Group is reflected in the large difference between healthy volunteers and schizophrenia patients in mean power changes, -0.09 and 0.89 respectively.

Component 6.

Component 6 was characterized by increases in power in the 10 Hz (alpha) and 20 Hz (beta) bands. Please see Figure 23 for the brain images and predictor weights from this component. In the 10 Hz (alpha) band, right lateralized increases in power were found superior, middle, and inferior frontal (pars triangularis, opercularis, and orbitalis) gyri, pre- and post-central gyri, central opercular cortex, insula, caudate, putamen, thalamus, temporal pole, and superior and middle temporal gyri.

In the 20 Hz (beta) band, right lateralized increases in power were found in superior, middle, and inferior frontal (pars opercularis, triangularis, and orbitalis) gyri, orbitofrontal gyrus, pre- and post-central gyri, inferior parietal lobule, supramarginal gyrus, angular gyrus, central

opercular cortex, insula, superior, middle, and inferior temporal gyrus, Heschl's gyrus, thalamus, caudate, putamen, temporal pole, and hippocampus.

The statistical analysis of the predictor weights from Component 6 revealed a significant main effect of Time, $F_{(19,741)} = 8.13$, $p < .001$, $\eta^2 = 0.17$, as well as a trend in the interaction between Valence and Time, $F_{(38,1482)} = 1.88$, $p < .10$, $\eta^2 = 0.04$. All other main effects and interactions were non-significant (p's > .15). In this component, the 95% confidence interval of the Grand Mean does span zero (-0.57-0.21), but the main effect of Time is driven by the large increase in power at the end of the trial coupled with small standard errors.

Discussion.

Overall, these results suggest that healthy volunteers and schizophrenia patients employ brain networks in a similar way in order to perform the experimental task. The hypothesized results were not observed, as the component with theta activity in the frontal midline was found to decrease in power, rather than the hypothesized increase in power. Furthermore, the expected relationship between valence and theta power in the schizophrenia patients and healthy volunteers was not found.

Only Component 5 showed a significant main effect or interaction with Group; however, Component 3 did display trend level significance for a main effect of Group; and Components 1 and 3 displayed trend level significance for the interaction between Time and Group.

Component 1.

Component 1, which can be seen in Figure 18, was characterized by decreases in power (due to negative loadings) in the 20 Hz (or beta) band. These decreases were located primarily in the occipital and parietal cortices and extended into the left frontal and temporal regions. The predictor weights indicate that for the healthy volunteers, this decrease in power peaked at

approximately 375 ms and then started increasing until it returned to baseline by the end of the trial. In the schizophrenia patients, the peak was less well defined as it appeared to occur slightly later and last longer, particularly in the trivalent condition.

Statistical analysis of the predictor weights indicated that there was a significant main effect of Time, which indicates that the estimated power changes show temporal validity (i.e., they are not random shapes that change between subjects). In the visual cortices, this decrease in beta power is thought to reflect attentional demands and release from inhibition, (Bauer et al., 2012; Panagiotaropoulos et al., 2013), is widely reported (Gola et al., 2013; Whitman et al., 2015), and is common in tasks involving visual stimuli (Hoogenboom, Schoffelen, Oostenveld, Parkes, & Fries, 2006; Medendorp et al., 2007). The presence of decrease of beta power in the left sensorimotor cortices is presumed to be a consequence of the requirement to make responses using the right hand, on the basis of decades of research illustrating the relationship between limb movement and decreases in beta power over the contralateral sensorimotor cortex and ipsilateral cerebellum (Brown, 2007; Davis et al., 2012; Neuper & Pfurtscheller, 2001; Salmelin & Hari, 1994). These decreases appear to reflect basic sensory responses associated with the performance of this task.

The predictor weights indicated that, in general, the patients and controls showed the greatest decreases in power in the trivalent condition, and beta band related changes in power in the insula have been related to cognitive control related functions like post-error slowing and to changes in visual and language related processing (Tops & Boksem, 2011). However, there was no clear evidence of a load dependent effect, as the predictor weights for the univalent and bivalent conditions do not align in the predicted direction. There was a trend towards an interaction between Group and Time, which via inspection of the predictor weights, appears to

be related to the tendency for healthy volunteers to show a greater decrease in beta power than schizophrenia patients, particularly in the early phase of the trials. Previous studies have also found weaker beta desynchronization in schizophrenia in the occipital lobes in an emotional paradigm involving visual stimuli (Csukly, Farkas, Marosi, & Szabó, 2016), suggesting that this may represent a feature of the illness.

Component 2.

Component 2, which can be seen in Figure 19, was characterized by decreases in power in the 6 Hz (or theta) band. These decreases were located primarily in the occipital cortices, and hippocampal/parahippocampal gyri. The predictor weights indicate that this decrease in power peaked just prior to 750 ms in healthy volunteers, and around 800 ms in schizophrenia patients. The negative deflection in power was sustained for the rest of the trial, and the patients appear to display a greater decrease from baseline than the controls, but this difference was not statistically significant (or a trend).

Statistical analysis of the predictor weights indicated that there was a significant main effect of Time, which indicates that the estimated hemodynamic responses show temporal validity (i.e., they are not random shapes that change between subjects). Decreases in theta power in the occipital lobe have been reported previously in studies of multisource attention and in studies of working memory (Meltzer et al., 2008). In the working memory study, theta power decreases in the occipital lobes displayed a load dependent response pattern, a pattern which was not present in the current experiment.

It is notable that the hippocampi were found in this component, as hippocampal theta activity has been crucially linked to learning and memory in non-human animals (Buzsáki, 2002). The data regarding the importance of hippocampal theta rhythms in humans has been

more equivocal (Lega, Jacobs, & Kahana, 2012), but the majority of studies that do detect a

change report increases in hippocampal theta power when performing learning or memory tasks

(Ekstrom et al., 2005; Watrous, Fried, & Ekstrom, 2011), which is the opposite of what we see in

this component.

   Component 3.

   Component 3, which can be seen in Figure 20, was characterized by decreases in power

in the 10 Hz (or alpha) band. These decreases were located primarily in the occipital cortices.

The predictor weights indicate that this decrease in power peaked early in the trial in both

healthy volunteers and schizophrenia patients, and then began returning to baseline over the

course of the rest of the trial, although the patients showed a stronger return to baseline than did

the controls.

   Statistical analysis of the predictor weights indicated that there was a significant main

effect of Time, which indicates that the estimated hemodynamic responses show temporal

validity (i.e., they are not random shapes that change between subjects). Decreases in alpha

power in the occipital lobe when the eyes are open relative to when the eyes are closed was the

earliest finding using EEG, and has been termed the 'Berger Effect' after its discoverer

(Kirschfeld, 2005). This finding has been extended to include alpha band decreases in power in

occipital cortex during tasks requiring visual attention (Rana & Vaina, 2014). These decreases in

alpha power during visual attention are thought to be a sensory gating mechanism signifying the

release from inhibition (Klimesch, 2012; Zumer, Scheeringa, Schoffelen, Norris, & Jensen,

2014). This inhibition is thought to be a mechanism that limits the ability of the occipital cortex

to process potential distractors in the visual environment (Rana & Vaina, 2014).

93

As noted in the Results section for this component, there was a trend towards a significant main effect of Group, and of the interaction between Time and Group. These trends appear to be driven by the smaller decrease in alpha power and in the sharper return to baseline from peak found in patients relative to controls.

Component 4.

Component 4, which can be seen in Figure 21, was characterized by decreases in power in the 10 Hz (alpha) and 6 Hz (theta) bands. These decreases were located primarily in the prefrontal and temporal cortices. The predictor weights indicate that these decreases in power were sustained over the course of the trial with the patients showing an upward inflection approximately 400 ms into the trial that was not seen in the healthy volunteers. Although the volunteers did show, on average, a larger decrease in power, this group related difference was not statistically significant (or a trend).

The statistical analysis of these predictor weights indicated that there was a significant main effect of Time, which indicates that the estimated power changes show temporal validity (i.e., they are not random shapes that change between subjects). Additionally, the statistical analysis also indicated a trend in the interaction between Valence and Time. These effects are likely due to the predictor weights for both the schizophrenia patients and the healthy volunteers evolving in the same way over the course of the trial, that is, the greatest decrease in power is seen in the univalent condition, the bivalent condition shows the least decrease in power initially but crosses over with the trivalent condition in the middle of the trial. The univalent condition showing the greatest decrease in power suggests that the decrease of power in this component was tempered by the requirement to increase activity in this network in response to the increased demand for attentional biasing in the face of multiple response features. It is notable that the

94

patients show a noticeable positive deflection in the predictor weights around 375 ms, as well as an overall increase in activity relative to controls, which may suggest a greater requirement for frontal control in this group.

Decreases in alpha power in the frontal lobes has been found in previous studies and has been attributed to different stimulus features including: greater memory load (Krause et al., 2000; Stipacek, Grabner, Neuper, Fink, & Neubauer, 2003), greater reliance on bottom-up as opposed to top-down processing (Benedek, Bergner, Könen, Fink, & Neubauer, 2011), and reflecting a greater need for activity/less need for inhibition (Cooper, Croft, Dominey, Burgess, & Gruzelier, 2003; Klimesch, Doppelmayr, & Hanslmayr, 2006). In the case of the present experiment, all of these stimulus features were present: the stimuli varied in terms of the numbers of relevant features thus requiring differed memory loads, the stimuli were continuously presented on the screen thus allowing bottom-up features to guide performance, and some activation/release from inhibition was required to identify the relevant stimulus features to follow the correct rule. In the current experiment, the trend in the interaction between Valence and Time suggests that there was a load dependent effect but the design does not rule whether this load dependency is a result of the requirement to use more top-down resources to bias attention, or whether it is the result of greater inhibition of pre-potent responses.

In the theta band, event related increases in power have been found in the dAcc and medial prefrontal regions, and some have related to these increases to cognitive control (Cavanagh & Frank, 2014), however, increases in theta power have also been found when performing mental arithmetic (Ishii et al., 2014), and when retaining items in working memory (Jensen & Tesche, 2002), thus suggesting that activity in this region/band is associated with more difficult cognitive activities in general. In the present experiment, we found a generalized

95

decrease in theta band activity in the prefrontal areas, however, this decrease was marked with transitory increases in activity in the first half of the trial, which suggests that perhaps this component was involved in cognitive control/effortful processing but that the overall difficulty level of the task was too low to generate a strong positive signal in the theta band. The fact that the patients showed a prominent increase in activity supports this interpretation as well.

Component 5.

Component 5, which can be seen in Figure 22, was characterized by increases in power in the 10 Hz (alpha) band. These increases were located primarily in the left parietal and temporal lobes, extending into the prefrontal cortex. The predictor weights indicate that this component showed an initial decrease in power followed by a return to baseline in the healthy volunteers and a steady increase over baseline in the schizophrenia patients. This component is driven primarily by the patients, and statistical analysis of the predictor weights indicated significant main effects of Time and of Group. The significant effect of Time indicates that the estimated power changes show temporal validity (i.e., they are not random shapes that change between subjects). The significant Group effect is due to the increased activity in schizophrenia patients relative to healthy volunteers.

The increase in alpha power in this network included the left inferior frontal gyrus (IFG). This region has been described as a node in the cognitive control network (Cole & Schneider, 2007; Niendam et al., 2012), and could be playing such a role in the current experiment, particularly as this region has been hypothesized to be more active in situations where attentional focus and motor control are deployed on rapidly changing stimuli (Tops & Boksem, 2011). However, the lack of any Valence related effects, as well as the involvement of the left IFG in lexical tasks (Poldrack et al., 1999) speaks against this interpretation.

The increase in alpha power was also observed bilaterally in the insula, a region that is part of the cingulo-opercular control network outlined by Dosenbach and colleagues (Dosenbach et al., 2007, 2008). EEG and MEG evidence suggest that alpha rhythms in the insula play a functional role in the control and deployment of attentional resources. Alpha activity is found bilaterally in the insulae when performing working memory tasks involving retrocues, that is, when the relevant stimulus features are cued after the stimulus has been encoded (Wallis, Stokes, Cousijn, Woolrich, & Nobre, 2015). The authors of the study note that the insula activity occurs relatively late in the trial, which accords to the pattern of increasing power seen in the present experiment. Another recent study has found that alpha band activity in the insula (and the anterior cingulate) influences activity in the visual cortices (Doesburg, Bedo, & Ward, 2016), such that the processing of information from task-irrelevant areas is inhibited.

This hypothesized role for the insula aligns well with its description as part of the salience network (Palaniyappan & Liddle, 2012), which is thought be heavily involved in the development of psychosis. The salience network is comprised of the anterior insula and the dAcc, and this network is involved in integrating sensory input to guide attention by acting to identify motivationally salient stimuli (Kapur, 2003). In normal healthy brain function, the salience network is activated when behaviourally relevant, unexpected, or novel stimuli are detected in order to initiate appropriate behavioural responses. In psychosis, this network is dysfunctional, such that it attributes abnormal and persistent levels of salience to otherwise mundane external stimuli or internal thoughts. Although the mechanism of action of this network is still under debate, there is evidence that the salience network influences the DMN and task-based network activity in order to guide behaviour (Menon & Uddin, 2010). In support of this hypothesis, reviews and meta-analyses have noted widespread changes in both the structure and

function of the insula in individuals suffering from psychosis and other psychiatric disorders (McTeague et al., 2017; Palaniyappan & Liddle, 2012; Peters, Dunlop, & Downar, 2016). These interpretations are relevant to the current experiment, as this component was driven primarily by the patients in this study, and the task involved manipulating the salience of the stimulus features from trial to trial. Furthermore, the hypothesized role of the insula is similar in the cognitive control network (Dosenbach et al., 2008), the ventral attention network (Petersen & Posner, 2012) and the salience network (Palaniyappan & Liddle, 2012), suggesting that all three accounts may be identifying the same mechanism of action in different contexts.

Component 6.

Component 6, which can be seen in Figure 23, was characterized by increases in power in the 20 Hz (beta) and 10 Hz (alpha) bands. These increases were located primarily in the right parietal and temporal lobes, extending into the prefrontal cortex. The predictor weights indicate that this component showed a slight initial decrease in power followed by a return to around baseline and then showed a slow increase from baseline in the latter portions of the trial.

Statistical analysis of the predictor weights indicated significant main effects of Time, which indicates that the estimated changes in power show temporal validity (i.e., they are not random shapes that change between subjects). There was also a trend towards significant interactions between Valence and Time. The interaction between Valence and Time appears to have been driven by the increased power in the trivalent condition in both patients and controls, relative to the bivalent and univalent conditions. This relationship is not in the predicted direction, as the univalent conditions show higher power than the bivalent conditions, and does not appear to exhibit a load dependent relationship. Alpha power increases in ipsilateral motor cortex have been found when planning motor actions (Brinkman, Stolk, Dijkerman, de Lange, &

Toni, 2014), and are thought to reflect an inhibitory mechanism preventing interference with movement selection (Brinkman et al., 2016). However, ipsilateral alpha and beta decreases in power have also been reported when making movements (Rau, Plewnia, Hummel, & Gerloff, 2003), suggesting that there is a need for further research is required to disentangle the precise nature of alpha and beta activity in ipsilateral motor regions.

MEG General Discussion

The hypotheses for the MEG data were that the increase in task-irrelevant features would lead to an increase in theta power in the dAcc in both groups, and that the schizophrenia patients would show increased theta power in this area relative to the healthy volunteers at low levels of stimulus valence and decreased theta power relative healthy volunteers at high levels of stimulus valence. These hypotheses were disconfirmed by the results of both of the MEG analyses. In the univariate analysis, we did find activity in medial prefrontal areas in the 6 Hz (theta) and 10 Hz (alpha) bands when contrasting stimulus valence levels in the healthy volunteers (Figure 13 and Figure 15); this activity was localized to regions inferior to the dAcc but previous EEG and MEG literature has identified the medial prefrontal regions as also being involved in the production of frontal midline theta (Ishii et al., 1999, 2014).

In both the univariate and multivariate MEG results (Figure 13, Figure 17, and Figure 18), decreases of power in the beta band were found in occipital cortices and left sensorimotor regions. These decreases are presumed to be a consequence of the visual attention required in the task, as well as the motor responses being made with the contralateral (i.e., right) hand.

In the multivariate MEG results, Component 4 was characterized by a decrease in power in the 6 Hz (theta) and 10 Hz (alpha) bands in the medial prefrontal cortices (Figure 21), with the decrease in power extending superiorly into the ventral portion of the dAcc and superior frontal

99

gyri. Although these are decreases in power where increases in power were hypothesized, the pattern in the predictor weights suggests that the power decreased less as valence increased, such that a contrast between adjacent valence levels would appear as a positive correlation between valence and power. Notably, the activity time courses for the schizophrenia patients and healthy volunteers show a divergence at approximately 400 ms post stimulus time, with the controls continuing to decrease in power whereas the patients appear to display a brief increase. This may suggest that the patients experienced a greater need for cognitive control than the healthy volunteers but more evidence is required to support this claim.

Component 5 from the multivariate MEG analysis displayed a significant difference between groups, and appeared to be driven primarily by the patients (Figure 22). This component included the left IFG and insula, which have both been implicated in cognitive operations like task switching, word reading, as well as in the pathophysiology of schizophrenia and other psychoses. It is notable that Component 6 is a right lateralized version of a similar network (without the medial frontal regions, including dAcc) and this component shows no differences between patients and controls. This suggests that the activity in the dAcc and other medial frontal structures are more closely related to the left temporal regions, insula and IFG, perhaps due to the lexical demands of the present task.

In the univalent MEG analysis, the power changes in the occipital cortex in the 20 Hz (beta) band closely match the fMRI results, with the MEG results showing decreases in power in the primary visual cortex with some commensurate increases in stimulus valence in the healthy volunteers (e.g., valence level contrasts yielded significant results). This is similar to the fMRI results where increases in BOLD activity were found in the same areas as stimulus valence increased. This pattern was not apparent in the schizophrenia patients which, coupled with the

significant decreases in power found in all valence conditions (Figure 17), suggests that either the occipital cortex in the patients was not sensitive to changes in stimulus valence, or displayed lower SNR. The lack of significant differences when contrasting the power changes in the 20 Hz (beta) band in healthy volunteers with those in the schizophrenia patients suggest the latter interpretation, as significant differences between the groups should be expected if the neural activity in one of the group was not modulated by changes in stimulus valence.

One important issue in attempting to compare the univariate MEG results to the multivariate MEG results is that the univariate MEG results are related to a particular section of the trial, whereas the multivariate results span its entirety. This greatly reduces the comparability of the two, and clearly influences the results in both cases. Selecting an inappropriate time window in a univariate analysis might result in missing important differences between conditions/groups, whereas analyzing the entire trial in a multivariate analysis may obfuscate critical but transitory differences between conditions/groups if they only occur at for a short period of time relative to the trial length. One salient example of this is in Component 4 of the MEG-PCA analysis, where an increase in activity in the schizophrenia patients can been seen at approximately 400 ms. This time segment a good candidate for univalent beamforming, as differences between the groups would likely be apparent as increases in activity in patients relative to controls, and may display Valence related effects. However, when we examine the statistical results from Component 4 of the multivariate MEG analysis, we do not see a significant (or trend level) effect of Group, indicating that the effect was obfuscated by the lack of differences in the rest of the trial.

Multivariate Multimodal MEG-fMRI Analysis

Introduction

Although the multivariate fMRI and MEG results were individually informative, it is difficult to ascertain the relationship between the two sets of results without further analysis. Although different methods have been developed to examine the relationship between data collected using different neuroimaging modalities, the few studies that have examined both MEG and fMRI simultaneously have found that multimodal investigations can offer insights into brain activity and connectivity that are not apparent using a single modality. On one hand, the use of multiple imaging modalities offers an additional degree of confidence, as any networks that correspond between the modalities would be unlikely to result from limitations or deficits of any individual modality. For instance, the detection of a similar network in both fMRI and MEG would suggest that, in the MEG data, the network is not spuriously obtained (for example) due to the ill-defined inverse problem, and, in the fMRI data, the network is not spuriously obtained (for example) due to shared drainage veins, or cardiac/respiratory activity (Brookes et al., 2011). On the other hand, the discovery of networks that are detectable using only one of the two modalities may be spurious, but could also represent true signal changes to which the other modality is insensitive. Thus, there is the potential of finding important differences that might otherwise be missed. For instance, in a paper using combined fMRI-MEG to examine accepting versus rejecting a hypothesis retrieved more detailed networks than was provided by an analysis of fMRI data alone using the same paradigm (Whitman et al., 2015). In a separate study examining resting state data in schizophrenia patients, hyperconnected prefrontal and temporal networks were discovered using a combined MEG-fMRI analysis; networks that were not apparent in the fMRI data alone (Houck et al., 2017).

Hypothesis.

As the application of CPCA to multimodal brain imaging data is relatively novel, the hypothesis for the multivariate multimodal MEG-fMRI analysis was that it would identify components that showed a clear relationship to those obtained from the unimodal multivariate MEG analysis, in terms of the brain regions involved and the pattern of activity depicted in the component scores.

Methods

Application of CPCA to multimodal data sets.

The general framework of the CPCA method can be used with multimodal datasets by including the H column constraints in the model, using a simplified version of Equation (1) which does not include the use of a G matrix.

$$Z = BH' + E \tag{7}$$

where Z is the criterion data, B is the matrix of contrast specific regression weights, H is the matrix of constraints on the columns of Z, and E is the variance in Z that cannot be explained by BH'.

The multimodal analyses that were performed in this project were asymmetrical (Biessmann et al., 2011), which, as mentioned above, means that the results from one modality were used to guide or constrain the subsequent analyses in another modality. In this case, the fMRI results were used to constrain the MEG results, to determine which frequencies of oscillation underlie the fMRI netwoks, and which are specific to MEG.

The first step in the multivariate multimodal fMRI-MEG analysis was to regress the MEG data onto the column constraints representing the spatial patterns of the fMRI networks from the fMRI-CPCA analysis. The matrix H contains the spatial patterns (rescaled right singular

vectors) from the fMRI-CPCA analysis as columns, where each column of *H* represents a different functional network, with a separate set repeat to correspond to each frequency of oscillation. *B* is the matrix of constraint specific regression weights and is obtained by regressing *Z* onto *H* via the following formula:

$$_{n \times s}B_{w \times f} = \ _{n \times s}Z_{m \times f}H_{w \times f}\left(_{w \times f}H'_{m \times f}H_{w \times f}\right)^{-1} \tag{8}$$

where *n* is the number of subjects, *s* is the number of beamforming windows, *m* is the number of gridpoints/voxels, *f* is the number of frequencies, and *w* is the number of fMRI networks used as column constraints.

In this model, the total variance in the MEG data is partitioned into two matrices; the matrix *BH'*, which contains the variability that can be explained by the pattern of fMRI networks (i.e., the MEG data constrained to the fMRI-CPCA networks), and the matrix *E* which contains the variability that cannot be explained by the pattern of fMRI networks.

$$_{n \times s}Z_{m \times f} = \ _{n \times s}BH'_{m \times f} + _{n \times s}E_{m \times f} \tag{9}$$

where *n* is the number of subjects, *s* is the number of beamforming windows, *m* is the number of gridpoints/voxels, and *f* is the number of frequency bands.

Then matrix of predicted scores (*BH'*) is decomposed:

$$\left[_{n \times s}U_p D_p V'_{m \times f}\right] = _{n \times s}BH'_{m \times f} \tag{10}$$

where *n* is the number of subjects, *s* is the number of beamforming windows, *m* is the number of voxels/gridpoints, *p* is the number of components extracted, and the square brackets denote the products of singular value decomposition.

Correlating the right singular vectors from this decomposition with the fMRI-component specific portions of the *H*-matrix yielded *H*-predictor weights that specify the match between the

spatial pattern of the fMRI-constrained MEG networks and those from the original fMRI analysis.

In addition to the portion of the MEG variance that is predictable from the spatial distribution of the fMRI-CPCA results, the variability that could not be explained by the pattern of fMRI networks was also decomposed.

$$[_{n \times s} U_p D_p V'_{m \times f}] = {}_{n \times s} E_{m \times f} \qquad (11)$$

where n is the number of subjects, s is the number of beamforming windows, m is the number of gridpoints/voxels, p is the number of components extracted, and the square brackets denote the products of singular value decomposition.

In the current study the values of the matrix subscripts were as follows: $n = 41$, $s = 63$ (21 beamforming windows for each of the univalent, bivalent, and trivalent conditions), $f = 3$ (alpha, beta, and theta), $m = 6758$ and $w = 3$ (the 3 fMRI-CPCA networks derived above, which were applied to each frequency band separately; Equation 8).

Results

An examination of the scree plot (Cattell, 1966) from this analysis suggested that 2 components should be extracted for further significance testing. The sum of the squared loadings divided by the number of scans (analogous to the percentage of predictable variance accounted for by each component) for the rotated solution was 38.03, and 32.49 for components 1 and 2. For a summary of the variance accounted for by the fMRI-MEG multimodal analysis (*BH'*-CPCA analysis), please see Table 15.

H-predictor weights.

The brain images comprising the functional networks from the fMRI-CPCA analysis, as well as the *H*-predictor weights indicating the relative involvement of the MEG frequency bands

are displayed in the upper panels of Figure 24 and Figure 25 and the component scores, plotted as a function of post-stimulus time, representing the estimated HDR of each functional network, are depicted in the lower panels of Figure 24 and Figure 25. For the statistical analysis of the component scores, a $20 \times 3 \times 2$ mixed-model ANOVA was performed with within-subject factors of Time Point and Valence, and a between-subject condition of Group.

Component 1.

The fMRI-MEG multimodal analysis (*BH'*-CPCA analysis) demonstrated that the fMRI-based networks were characterized by unique combinations of MEG power frequencies. Please see Figure 24 for the fMRI-MEG multimodal Component 1 results. The first component from the original fMRI-CPCA analysis, which will be referred to as fMRI-CPCA-1 for the remainder of this section, was characterized by decreases in MEG power, particularly in the beta and alpha bands. The second component from the original fMRI-CPCA analysis, which will be referred to as fMRI-CPCA-2 for the remainder of this section, was characterized by an increase in MEG power in the theta band and slight decreases in the alpha and beta bands. The third component from the original fMRI-CPCA analysis, which will be referred to as fMRI-CPCA-3 for the remainder of this section, was distinguished by decreases in power in all bands, with the strongest decrease in the alpha band.

The statistical analysis of the component scores from Component 1 indicated that there was a main effect of Time, $F_{(19,741)} = 6.34$, $p < .005$, $\eta^2 = 0.14$. The significant effect of Time is reflected in the 95% confidence interval of the Grand Mean, which does not span zero (0.40-0.99).All other main effects and interactions were non-significant (ps > 0.25). The component scores for Component 1 are very similar to those of Component 1 from the unimodal MEG-PCA analysis. Both timecourses show a stronger peak for controls relative to patients that occurs at

106

approximately 375 ms, as well as an extended peak in the trivalent condition in both patients and controls at approximately 750 ms. Please see the lower panels of Figure 24 and Figure 18 for comparison.

Component 2.

Please see Figure 25 for the fMRI-MEG multimodal Component 2 results. Component 2 from the fMRI-MEG multimodal analysis (*BH'*-CPCA analysis) indicated that fMRI-CPCA-1 was distinguished by decreases in MEG power in all bands. fMRI-CPCA-2 was characterized by slight decreases in MEG power in all bands, particularly in the alpha and theta bands, and fMRI-CPCA-3 was characterized by decreases in the theta and alpha bands, and slight increases in the beta band.

The statistical analysis of the component scores from Component 2 indicated that there was a main effect of Time, $F_{(19,741)} = 4.39$, $p < .05$, $\eta^2 = 0.10$, as well as a trend in the interaction between Group and Time, $F_{(19,741)} = 2.12$, $p < .15$, $\eta^2 = 0.05$. The significant effect of Time is reflected in the 95% confidence interval of the Grand Mean, which does not span zero (0.62-1.33).All other main effects and interactions were non-significant ($ps > 0.25$). The component scores for Component 2 are very similar to those of Component 2 from the unimodal MEG-PCA analysis. Both timecourses show a stronger power for patients relative to controls, as well as a slope that flattens at approximately 375 ms. Please see the lower panels of Figure 25 and Figure 19 for comparison.

Decomposition of *E*.

The scree plot suggested that 3 components should be extracted for further analysis. The sum of the squared loadings divided by the number of scans (analogous to the percentage of predictable variance accounted for by each component) for the rotated solution was 5.58, 4.45,

and 3.87 for components 1, 2, and 3. For a summary of the variance accounted for by each

component in the *E*-CPCA, please see Table 15. The brain images and component score graphs

for each of the 3 *E*-CPCA components can be seen in Figure 26, Figure 27, and Figure 28,

respectively.

Within each condition, the component scores for beamforming windows 2 through 21

were expressed as a difference from the score at beamforming window 1 so that the univalent,

bivalent, and trivalent conditions were equal at stimulus onset. Therefore, the statistical analysis

of the component scores was a $20 \times 3 \times 2$ mixed-model ANOVA was performed with within-

subject factors of Time Point and Valence, and a between-subject condition of Group.

Component 1.

Component 1 from the *E* analysis, which can be seen in Figure 26, was characterized by

increases and decreases in the 6 Hz (theta), 10 Hz (alpha), and 20 Hz (beta) bands.

In the 6 Hz (theta) band, bilateral increases in power were detected in vmPFC, and frontal

pole, and right lateralized activations were found in middle frontal and inferior (pars orbitalis)

gyri, and orbitofrontal gyrus. Left lateralized decreases in power were found in precuneus,

parahippocampal gyrus, and superior, middle and inferior temporal gyri.

In the 10 Hz (alpha) band, bilateral increases in power were detected in vmPFC, and

frontal pole, and right lateralized activations were found in superior, middle and inferior frontal

(pars orbitalis) gyri and orbitofrontal gyri. Left lateralized decreases in power were found in

angular gyrus, Heschl's gyrus, parahippocampal gyrus, hippocampus, and superior, middle and

inferior temporal gyri.

In the 20 Hz (beta) band, bilateral increases in power were found in the Crus I and II of

the cerebellum, and right lateralized increases were found in middle frontal and superior medial

frontal gyri. Left lateralized decreases in power were found in postcentral gyrus, inferior parietal lobule, supramaginal gyrus, Heschl's gyrus, parahippocampal gyrus, hippocampus, and superior, middle and inferior temporal gyri.

The statistical analysis of the predictor weights from Component 1 indicate that there was a significant main effect of Time, $F_{(19,741)} = 52.57$, $p < .001$, $\eta^2 = 0.57$. All other main effects and interactions were non-significant (ps > 0.35). The significant effect of Time is reflected in the 95% confidence interval of the Grand Mean, which does not span zero (1.73-2.16).

Component 2.

Component 2 from the *E* analysis, which can be seen in Figure 27, was characterized by increases and decreases in power in the 6 Hz (theta) and 10 Hz (alpha) bands, and decreases in power in the 20 Hz (beta) bands.

In the 6 Hz (theta) band, right lateralized increases in power were found in the temporal pole, superior, middle, and inferior temporal gyri, putamen, insula, hippocampus, parahippocampal gyrus, and fusiform gyrus, as well as Crus I and Lobule VI of the cerebellum. Bilateral decreases in power were found in the cuneus.

In the 10 Hz (alpha) band, right lateralized increases in power were found in middle and inferior occipital gyri, angular gyrus, temporal pole, superior, middle, and inferior temporal gyri, calcarine sulcus, parahippocampal gyrus, hippocampus, amygdala, putamen, and insula. Bilateral decreases in power were found in juxtapositional lobule cortex/SMA, middle cingulate, and pre- and post-central gyri.

In the 20 Hz (beta) band, bilateral decreases in power were found in pre- and post-central gyri.

The statistical analysis of the predictor weights from Component 2 indicate that there was a significant main effect of Time, $F_{(19,741)} = 24.06$, $p < .001$, $\eta^2 = 0.38$, as well an interaction between Valence and Time, $F_{(38,1482)} = 2.26$, $p < .05$, $\eta^2 = 0.06$. All other main effects and interactions were non-significant ($ps > 0.20$). In this component the 95% confidence interval of the Grand Mean, which does span zero (-0.57-0.19) but this is likely due to the bidirectionality in the power changes over the course of the trial. The interaction between Valence and Time is reflected by the difference scores in the estimated power changes for the Univalent, Bivalent and Trivalent conditions between 0.50-1.00 and 0.55-1.05 seconds, which were 2.1, 1.6, and 0.2, respectively.

Follow-up tests for the significant interaction between Valence and Time indicated that there were significant differences between the Bivalent and Trivalent conditions when comparing the beamformed power between 0.20-0.70 and 0.25-0.75 seconds, $F_{(1,39)} = 5.02$, $p < .05$, $\eta^2 = 0.11$ (difference scores of 0.04 for the Bivalent condition, and 0.20 for the Trivalent condition), between 0.50-1.00 and 0.55-1.05 seconds, $F_{(1,39)} = 6.70$, $p < .025$, $\eta^2 = 0.31$ (difference scores of 0.16 for the Bivalent condition, and -0.05 for the Trivalent condition), and between 0.55-1.05 and 0.60-1.10 seconds, $F_{(1,39)} = 5.02$, $p < .05$, $\eta^2 = 0.11$ (difference scores of -0.08 for the Bivalent condition, and 0.23 for the Trivalent condition).

Component 3.

Component 3 from the *E* analysis, which can be seen in Figure 28, was characterized by increases and decreases in the 10 Hz (alpha) and 20 Hz (beta) bands.

In the 10 Hz band, right lateralized increases in power were detected in middle and inferior frontal (pars triangularis and opercularis) gyri, pre- and post-central gyri, supramarginal gyrus, insula, putamen, central opercular cortex, Heschl's gyrus, superior and middle temporal

gyri and lingual gyrus. Bilateral decreases in power were observed in precuneus and middle temporal gyri, as well as the vermis, Crus I and II, and Lobules VI, VIII, and IX of the cerebellum.

In the 20 Hz (beta) band, right lateralized increases in power were found in middle and inferior frontal (pars triangularis and opercularis) gyri, pre- and post-central gyri, supramarginal gyrus, insula, putamen, central opercular cortex, Heschl's gyrus, and superior and middle temporal gyri. Bilateral decreases in power were observed in precuneus and middle temporal gyri, as well as the vermis, Crus II, and Lobules VI and VIII of the cerebellum.

The statistical analysis of the predictor weights from Component 3 indicate that there was a significant main effect of Time, $F_{(19,741)} = 28.87$, $p < .001$, $\eta^2 = 0.43$, as well as a trend in the interaction between Time and Group, $F_{(19,741)} = 2.27$, $p < .10$, $\eta^2 = 0.06$. All other main effects and interactions were non-significant ($ps > 0.15$). The significant effect of Time is reflected in the 95% confidence interval of the Grand Mean, which does not span zero (0.71-1.50).

Discussion

As predicted, the multimodal multivariate analysis found many of the same patterns present in the unimodal MEG analyses, in terms of the regions showing task-related activity, as well as the frequency bands in those regions. This was anticipated on the basis of previous literature showing broad correspondence in cortical localization using both EEG/MEG and fMRI (Moradi et al., 2003; Puce, Allison, Spencer, Spencer, & McCarthy, 1997; Strelnikov & Barone, 2013). The graphs of the component scores from the *BH'*-CPCA Components 1 and 2 closely resembled the graphs from Components 1 and 2 from the MEG-PCA, suggesting that the spatial patterns found in these components were present in both the MEG and fMRI data.

The *BH'* analysis illustrated the broad overlap in the spatial locations of the areas that showed changes in activity during the task. The two components from *BH'* accounted for over 20% of the variance in the MEG-*Z* matrix (and over 70% of the variance in the MEG-*BH'* matrix). This indicates that there is fairly widespread agreement between the fMRI and MEG CPCA analyses in terms of the neural foci of activity changes.

One of the main findings that emerged from the *BH'* analysis was the negative correlation between BOLD activity and MEG power. For instance, fMRI-CPCA-1 (Figure 9) contains only positive BOLD activity and the *BH'* analysis demonstrated that this component is characterized by decreases in MEG power in almost every band in both of the components from the *BH'* analysis (with the exception of a slight increase in theta power in fMRI-MEG-CPCA Component 1 (Figure 24)). This negative correlation has been identified in the literature for frequencies below 45 Hz, whereas the power in frequencies over 45 Hz tend to display a positive correlation with BOLD responses (Swettenham, Muthukumaraswamy, & Singh, 2013; Zumer, Brookes, Stevenson, Francis, & Morris, 2010). However, this view has been challenged by findings that both positive and negative correlations are present in MEG power/BOLD signal relationships in different cortical regions and in different experimental conditions (Kujala et al., 2014). In the present experiment, the notable exception to the negative correlation between BOLD response and oscillatory power was the activity found in the vmPFC (Figure 21). In the fMRI data, this region, which is part of the DMN, was found to show a task-related reduction in BOLD activity (Figure 10); a pattern which was also found in the same region in alpha and theta bands during the MEG analysis.

The results of the *BH'* analysis suggest that the components were split according to activity in multiple frequency bands. Component 1 (Figure 24) is dominated by activity in the

alpha and beta bands, whereas Component 2 (Figure 25) is dominated by activity in the theta and alpha bands. This pattern is fairly consistent for all three of the fMRI components suggesting that this is a feature distinguishing the *BH'* analysis components from one another. Inspection of the component scores suggests that the components are also distinguishable on the basis of which group showed the stronger pattern of activity. For Component 1, the healthy volunteers had a stronger power increase than the controls, whereas for Component 2, the schizophrenia patients showed a stronger power increase. The relative dominance of the beta band over other bands in Component 1 is in line with previous findings that indicate a general tendency for schizophrenia patients to show abnormal increases in beta power in multiple experiments (E. B. Liddle et al., 2016; Moran & Hong, 2011).

In the *E* analysis, it is notable that the components generally showed both increases and decreases in power in all three frequency bands. This is in contrast to the MEG-PCA analysis where all components displayed only increases or decreases in power, and, with the exception of Components 4 and 6, all the components were characterized by activity in one frequency band. It appears as though the *BH'* components, which were constrained to the spatial patterns from the fMRI-CPCA analysis, accounted for the large band-specific variance components that were found in the unimodal MEG-PCA analysis (for instance, the multi-band power decreases in the occipital cortices in Figure 18, Figure 19, and Figure 20), and exposed more complex patterns in E that were not found in the unimodal MEG analysis.

The spatial patterns from the fMRI-CPCA and the MEG-PCA analyses displayed a high degree of overlap, and these MEG-PCA components were characterized by power changes in the same frequency bands as those found in the *BH'*-CPCA analysis. For instance, in *BH'*-CPCA Component 1 (Figure 24), the alpha and beta bands have the strongest negative deflections in the

fMRI-CPCA-1 condition, which is characterized by strong activity in the occipital cortices. Correspondingly, in the MEG-PCA analysis, decreases in power were found in occipital areas in the beta band (MEG-PCA Component 1), and in the alpha band (MEG-PCA Component 3) (Figure 18 and Figure 20).

The components from the *E*-CPCA analysis were different from those of the MEG-PCA analysis in that activity in multiple frequency bands was localized to a similar brain networks within a component. For instance, in *E*-CPCA Component 1 (Figure 26), increases in power were found in vmPFC, and decreases in power were found in left temporal areas in all three frequency bands, whereas in the MEG-PCA analysis, Components 1, 2, and 3 (Figure 18, Figure 19, and Figure 20) were all localized to the occipital cortices but each component comprised a single frequency band. As both the *BH'*-CPCA and *E*-CPCA analyses are characterized by activity in multiple frequency bands, this suggests that the fMRI constraint may have parcellated the MEG data in such a way that the activity from multiple MEG-PCA components was captured by a *BH'*-CPCA single component. The component scores graph from *BH'*-CPCA Component 2 (Figure 25), which is dominated by theta and alpha power changes, appears to be a mixture of the component scores graphs from MEG-PCA Components 1 and 2 (Figure 18 and Figure 19), which are characterized by decreases in theta and alpha power, respectively.

The two components from the *BH'*-CPCA analysis accounted for 21.54% of the total variance in the MEG dataset, which suggests that there was considerable spatial overlap between the largest variance components in the fMRI and MEG results, but also that much of the MEG variance resides in smaller components that do not align with those from the fMRI analysis. For instance, there is overlap in the left temporal regions found to be decreasing in power in the 20 Hz (beta) band in both Component 1 from the MEG-PCA analysis (Figure 18) and Component 1

114

from the *E*-CPCA analysis (Figure 26). However, in this same component we see that the results of the overall MEG-PCA analysis do not always coincide with those from the *E* analysis. Specifically, in Component 4 from the MEG-PCA analysis (Figure 21), the vmPFC shows a decrease in activity whereas in Component 1 from the *E*-CPCA analysis (Figure 26) shows an increase in activity in this region, although there is not perfect correspondence between the anatomical loci. Although these results can appear paradoxical, these signals were generated from the rhythmic activity of thousands of neurons per voxel/gridpoint that need only share a spatial location, not a functional role. It is possible that localized increases in power can take place within a more widespread area with decreasing power, as well as for these previously unseen components to emerge if the data is constrained/parcellated in different ways.

General Discussion

The goal of this experiment was to identify differences between healthy volunteers and schizophrenia patients while performing an experiment that was designed to examine changes in neural activity in response to variable levels of stimulus valence (attentional biasing). In the univalent condition, the stimuli had only one relevant response feature, in the bivalent condition there were two relevant response features, and in the trivalent condition, there were three relevant response features.

Both structural and functional imaging were used in this study, in order to obtain a more complete picture of where and when any salient differences emerged between healthy volunteers and schizophrenia patients. In general, the results indicated that patients used the same regions in similar ways to perform the task. Although we did find many differences between the groups in both the structural and functional analyses, the majority of the statistical tests indicated broad similarity between the patients and the healthy volunteers.

The hypotheses for the functional imaging sections of this experiment were that: 1) the increase in task-relevant stimulus dimensions would lead to increased activity for both groups in the SMA/dAcc as measured by fMRI, and increased theta power in SMA/dAcc in both groups as measured by MEG, and that 2) schizophrenia patients will show increased activity (BOLD response in fMRI and theta power in MEG) relative to controls at low levels of valence and decreased activity relative to controls at high levels of valence, particularly in the regions thought to be involved in top-down attentional biasing (particularly the dAcc/SMA). These predictions were based on the cognitive control literature, which posits the dAcc as a key node in a network associated with top-down control, that is generally found to be active in demanding cognitive tasks. The hypotheses were partially supported by the results of this experiment. Specifically, the multivariate fMRI analysis did show the predicted effect of Valence, such that Component 2 was characterized by activity in the dAcc and the predictor weights indicated that there was a significant effect of Valence such that it was positively correlated with BOLD signal. The examination of the predictor weights suggests that the patients modulated their brain activity less than the healthy volunteers as Valence increased. That is, patients showed increased activity relative to controls for univalent stimuli (although these differences were not significant), patients and controls had equivalent activity for bivalent stimuli, and patients showed decreased activity relative to controls for the bivalent stimuli. This pattern has been described previously in the schizophrenia working memory literature as a left shifted inverted-U pattern (Callicott et al., 2003), which was theorized to account for the finding that schizophrenia patients showed hyperactive DLPFC activity (relative to controls) at low levels of task difficulty but hypoactive DLPFC activity at high levels of task difficulty. This account was extended to other brain regions

in schizophrenia (Metzak et al., 2011) and appears similar to the pattern detected in Component 2 from the multivariate fMRI analysis.

The behavioural data displayed the hypothesized pattern; that is, the patients were slower than controls, errors were slower than correct responses, and increasing valence led to increases in RT and decreases in accuracy. Although not all of these changes were statistically significant differences (depending on the measure and experiment modality), the general trend for these differences suggested that a valence based analysis would yield differences at the neural level. The behavioural findings are consistent with our pilot studies of this experiment, as well as with our previous work on task switching. It is notable that the controls were faster than the patients for correct responses in all conditions, as this demonstrates that the controls were consistently better at the task, even during the MEG version of the experiment which was always performed prior to the fMRI experiment.

Structural Imaging

In the structural analyses, we found support for previous research indicating widespread changes in structural connectivity and grey matter volume. In the DWI data, we observed decreases in FA in patients relative to controls in tracts in the posterior right hemisphere, including the right inferior longitudinal fasciculus, and the right inferior fronto-occipital fasciculus. However, we did not find the predicted deficits in FA in the cingulum bundle.

Deficits in FA have been repeatedly observed in these tracts in schizophrenia (Wheeler & Voineskos, 2014), and have been associated with multiple symptoms and outcomes. Deficits in the inferior longitudinal fasciculus have been associated with decreased verbal processing speed in never-medicated schizophrenia patients (X. Liu et al., 2014), and have been associated with poorer social functioning in those at high risk of developing schizophrenia (along with

lower FA in inferior fronto-occipital fasciculus) (Karlsgodt, Niendam, Bearden, & Cannon, 2009), and FA changes in the inferior fronto-occipital fasciculus have previously been associated with increased risk for hallucinations (Szeszko et al., 2008). However, the heterogeneity of these findings calls into question the value of these associations, particularly since many were obtained using small samples and variable methodology (Wheeler & Voineskos, 2014).

The structural MRI analysis in this study found many deficits in cortical thickness in schizophrenia patients, primarily in the frontal cortices, including the left cingulate gyrus, an area included as part of the dAcc. Deficits in cingulate gyrus thickness are found in the first episode (Koo et al., 2008) and in chronic schizophrenia (Torres et al., 2016), although the results are not unequivocal (Goghari et al., 2007; McIntosh et al., 2004). It is interesting to note that the DWI and structural MRI results from this study localize the FA deficits and some of the cortical thickness changes in the schizophrenia patients to adjacent locations as this pattern of grey matter/white matter deficit overlap has been noted in a previous review (Bora et al., 2011), although the authors do mention that this overlap could be due to multiple causes and may not be causally related. Furthermore, the sample from the present study included only outpatients whose symptoms were well controlled by medication, thus raising the possibility that the pattern of changes observed is a result of medication effects and/or a selection bias towards those individuals that exhibit less severe symptomatology or whose illness is responsive to medication.

In the present study, the decreases in cortical thickness in the schizophrenia patients occurred in the cingulate gyrus, a brain region that was hypothesized to show differences in functional activity in both the fMRI and MEG analyses. The relationship between cortical thickness and functional activity is poorly understood (Haier, Karama, Leyba, & Jung, 2009; Hunt et al., 2016; Kochunov et al., 2011), but the possibility that these structural changes may

118

contribute to activity differences between the schizophrenia patients and the healthy volunteers cannot be dismissed.

Functional Imaging

The functional analyses in this project can be subdivided on the basis of two features: the first is whether the statistical analysis method was univariate or multivariate, and the second distinction is whether the functional imaging modality was fMRI or MEG. The fMRI and MEG analyses offered independent yet largely complementary views of the brain activity underlying performance in this study, regardless of the statistical methodology. One notable example of this overlap, regardless of differences in statistical and imaging methods, is the presence of the occipital cortex in every analysis. This was a visual task and occipital cortex activity was expected, however, the activity in the occipital cortices was found to differ between valence conditions in many of the analyses. Although there were some differences in stimulus properties that could have influenced this, the presence of the significant activity in non-occipital regions suggests that the visual cortices are also involved in biasing attention towards relevant stimulus features. In the univalent fMRI analyses, in both patients and controls, there were increases in occipital cortex activity as Valence increased. In the univalent MEG analyses, this Valence related change in power was present (somewhat) in the 20 Hz (beta) band for the healthy volunteers, but not for the schizophrenia patients. In the multimodal fMRI analysis, the occipital cortex was found to be active in all three components, and all three components showed an interaction between Valence and Time, such that increasing stimulus Valence led to increased activity in the network. In the multivariate MEG analysis, the first three components were dominated by occipital cortex activity, one for each of the three frequency bands investigated. In the fMRI literature, attending to a point in the visual field leads to increased activity in

retinotopically corresponding portion of visual cortex (Martínez et al., 1999), and these increases in activity shift retinotopic location in conjunction with shifts in visual attention (Brefczynski & DeYoe, 1999). In the MEG literature, the effects of visual attention on activity in the occipital lobes have been identified as decreases in power in the alpha band contralateral to the target stimulus (Thut, Nietzel, Brandt, & Pascual-Leone, 2006). In contrast, there are increases in alpha power contralateral to task-irrelevant distractors (Worden, Foxe, Wang, & Simpson, 2000), suggesting that alpha activity may act as a sensory gating mechanism. In the present experiment, location of the cue did not vary so it is not possible to examine for alpha increases/decreases in the relevant hemispheres but the valence-related increases in fMRI activity and decreases in MEG power are suggestive.

Relevance to schizophrenia.

Group related differences in activity were also found in the occipital cortices. Specifically, in some of the univariate fMRI analyses, the controls were found to have higher occipital cortex activity than the patients when contrasting valence levels, which means that controls increased activity in these regions significantly more than the patients as the valence levels increased. In the multivariate fMRI analysis, Component 2 was characterized by a Valence by Group interaction, and in the multivariate MEG analysis, Component 1 showed a trend towards an interaction between Group and Time, and Component 3 showed a trend in the main effect of Group, as well as a trend in the interaction between Group and Time. In each of these cases, the healthy volunteers had larger BOLD increases, and larger MEG power reductions, than the patients. This pattern of results over multiple analyses suggests that the controls were able to modulate their occipital cortical activity to enhance visual attention during the performance of the task. It is notable that Component 2 from the multivariate MEG analysis is also characterized

120

by decreases in power in the occipital cortices (in the 6 Hz (theta) band), however, although the predictor weight pattern suggests that the patients had larger decreases in activity than controls, there was no effect of Group and this effect did not even reach trend level significance. The presence of a component that is localized to the same anatomical locations but shows a differing pattern of activity is indicative that any potential group-related confounds are not distributed evenly throughout the components/analyses.

Another region which is found to be active in a majority of the analyses, regardless or statistical methodology or imaging modality, is the left inferior frontal gyrus (IFG). Left IFG activity is found in the healthy volunteers in the univariate fMRI contrast of trivalent stimuli greater than univalent stimuli, in Components 1 and 2 in the multivariate fMRI analysis, and in Component 5 from the multivariate MEG analysis. In the multivariate fMRI analysis, both Components with increasing left IFG activity showed a significant interaction between Valence and Time, such that the estimated BOLD activity was positively correlated with Valence, and in Component 2, there was also a significant interaction between Valence and Group, which was due to the greater BOLD increase (or decrease in areas in negative predictor weights) in this network between Bivalent and Trivalent stimuli in healthy volunteers relative to the patients. In the multivariate MEG analysis, Component 5 was characterized by a significant difference in Group such that the patients had higher activity in this Component than the healthy volunteers. In this Component, there was no evidence of the predicted effect of Valence, although in the patients, it appears that the time courses of the bivalent and trivalent conditions are very similar, and display a pattern where the multivalent conditions have lower power for the first half of the trial before crossing with the univalent condition for the second half of the trial. Based on both the fMRI (Derrfuss, Brass, Neumann, & von Cramon, 2005; Derrfuss, Brass, & Yves Von

121

Cramon, 2004; C. Kim, Johnson, Cilles, & Gold, 2011; Sundermann & Pfleiderer, 2012) and

MEG literatures (Hedge et al., 2015; Heinrichs-Graham & Wilson, 2015; Periáñez et al., 2004),

there is considerable evidence that the IFG is involved in cognitive control, including attentional

biasing, task switching, and inhibition. Some have argued that the left and right IFG has separate

roles; such that the left IFG is involved in switching and the right IFG is specialized for

inhibition (Aron, 2007; Aron et al., 2004; H.-C. Leung & Cai, 2007), however, multiple accounts

have found that left IFG is also critically involved in inhibition, using both fMRI (Dodds,

Morein-Zamir, & Robbins, 2011; Hampshire, Chamberlain, Monti, Duncan, & Owen, 2010) and

lesion studies (Swick et al., 2008). These studies suggest that the bilateral IFG are involved in

switching and inhibiting behaviours, although this is still under debate (Aron, Robbins, &

Poldrack, 2014). Furthermore, there is some evidence via effective connectivity modeling that

shows that left IFG modulates visual attentional control via the frontal eye fields (DiQuattro &

Geng, 2011). However, the left IFG, also known as Broca's area, is critically involved in word

reading and comprehension (Cornelissen et al., 2009; Friederici, Rüschemeyer, Hahne, &

Fiebach, 2003; Poldrack et al., 1999). As the current experiment involved reading a word cueing

the relevant stimulus feature, the activity in this region could relate to lexical processing.

Control-related and language-related switching activity also appear to share a common neural

substrate (De Baene, Duyck, Brass, & Carreiras, 2015), which further compounds the issue. In

the present experiment, these alternatives cannot be disambiguated using the temporal activity

profile as the cue was present on the screen at the same time as the responses were made.

Multimodal multivariate analysis.

The multimodal analysis generally supported previous research indicating that power in

low frequency MEG bands is negatively correlated with BOLD signal, and identified a

relationship between frequency bands, such that one of the components was dominated by alpha and beta activity and the other was dominated by theta and alpha activity. As predicted these results were concordant with the results from the MEG-PCA analysis, as the anatomical locations and power changes in specific frequency bands overlapped considerably. For instance, in *BH'*-CPCA Component 1 (Figure 24), the alpha and beta bands have the strongest negative deflections in the fMRI-CPCA-1 condition, which is characterized by strong activity in the occipital cortices. Correspondingly, in the MEG-PCA analysis, decreases in power were found in occipital areas in the beta band (MEG-PCA Component 1, Figure 18), and in the alpha band (MEG-PCA Component 3, Figure 20). Another feature that emerged from the *BH'*-CPCA analysis was the finding that theta power increases were detected in components with anatomical loci that spanned the region the frontal midline. This is in accordance with the previous literature on the involvement of frontal midline theta activity in cognitive control experiments (Cavanagh & Frank, 2014; Ishii et al., 2014), and also detected in Component 1 from the *E* analysis, indicating that increases in theta activity were related to, but not completely overlapping with, the anatomical loci from the multivalent fMRI analysis. This differed from the MEG-PCA analysis which found only decreases in theta power in the vmPFC. Another notable feature from the *E* analysis is the involvement of multiple frequency bands, and their anatomical overlap, in each component. This is in contrast to the multivariate MEG analysis, where all the components, with the exception of Components 4 and 6, were linked to only a single frequency band. This is likely to be partially due to the altered parcellation of the variance in the MEG data due to the presence of the fMRI constraints.

Univariate versus multivariate results.

As there are substantial methodological differences in how they are carried out, univariate and multivariate methods yield different results. In the current experiment, one of the notable differences between the univariate and multivariate analyses, regardless of imaging modality, is that the multivariate analyses resulted in more foci of activation. One reason for this is more restrictive control over Type I errors in the univariate analyses. While this strict control is admirable in the sense that it stands on firm statistical ground, it is likely that many relevant foci of activity are obfuscated by underpowered studies and small effect sizes. This is particularly relevant when attempting to address differences in heterogeneous clinical populations. In the case of the present experiment, the differences between levels of Valence were only able to detect the strongest, and most consistent of activations, which were most often found in the occipital cortices.

A concern with the multivariate analyses is that small (but possibly important) effects may be overlooked. This is particularly relevant in studies with clinical populations, since the groups may utilize different networks to perform a given task. In this case, the networks that are linked to specific regions and specific groups would likely account for a much smaller percentage of the overall variance than a network that is common to both. Furthermore, there is not always a useful way to interrogate the roles of the individual clusters/nodes of activity. It is possible to examine the activity of individual clusters by masking that region in the original dataset and calculating the condition specific differences (see Whitman et al., 2015), but this will capture the sum of every component's activity in those regions, and not the activity that is specifically related to the component of interest. Although this may not be problematic in cases where the component of interest accounts for a large percentage of the variance, it is possible

124

that important (but small) effects may be lost when examining the individual clusters, thus rendering it difficult to identify the most relevant nodes in the network. In the case of the current experiment, it seems as though the patients and controls used largely the same networks in similar ways when performing the task, but it is unknown whether there is a small variance component in the data that may have identified a meaningful difference between the groups.

Differences between the univariate and multivariate methods can also make it difficult to assess the relationship between the two, as was mentioned in the modality-specific fMRI and MEG discussion sections above. In the case of the fMRI analysis, the use of a synthetic HRF in the univariate analysis and the use of an FIR model in the multivariate analysis renders comparisons difficult, as differences between the two will emerge due to poor goodness-of-fit between the synthetic HRF and the measured hemodynamic responses. Furthermore, the choice of time points for the FIR model are subject to the same interpretational problems in that choosing a different number can yield different results. In a similar vein, the interpretation of the MEG analyses is problematic due to the difference in how much of the trial is being beamformed. Also, as mentioned above, in the univariate MEG analysis, specific points within the trial are selected for further evaluation, whereas in the multivariate MEG analysis, the entire trial is beamformed and then any differences are identified using statistical methods (i.e., a repeated measures ANOVA).

MEG versus fMRI results.

In terms of the differences between the imaging modalities, the fMRI and MEG analyses displayed broadly overlapping results. The fMRI and MEG analyses identified activations/power changes in overlapping areas, notably the occipital cortices, IFG, insula, mPFC, and pre-central gyri. One area that was hypothesized, but notably absent from both the univariate and

multivariate MEG analyses was the dAcc. Although this region did appear as part of the network in Component 5 from the multivariate MEG analysis, this component did not show any Valence related modulations, which suggests that it was not responding in the hypothesized manner, or that this component is playing a different functional role in the experiment. This is in contrast to the multivariate fMRI analysis, where the dAcc figures prominently in Component 2 (i.e. it shares the highest loadings with the occipital cortices) and displays the hypothesized Valence related effect.

Another salient difference between the fMRI and MEG analyses is the lack of significant Group and Valence related effects in the MEG analyses relative to the fMRI analyses. In the univariate analyses, Valence and Group related effects were detected in almost every contrast in the fMRI data but much fewer were significant in the MEG data. There are likely at least two reasons for this difference: the first is related to statistical power or illness heterogeneity, as the significant Valence-related contrasts in the MEG data were all found in the healthy volunteers (Figure 15 and Figure 16). As the number of patients and controls were approximately equivalent in this experiment, this suggests that there was greater variability in the patient data. A second reason for this difference is the choice of the frequency bands for use in the beamformer analyses. In the present experiment, the frequency bands were chosen in an effort to match the frequency ranges that are typically described in the literature to the power changes that were seen in the time frequency plot. In the multivariate analyses, Valence and Group related effects were less prominent/significant in the MEG data. As mentioned in the discussion of the univariate analyses, this may be partly due to greater variability in the patient data, as well as the choice of frequency bands to examine. Furthermore, in both the univariate and multivariate MEG analyses, the rapid nature of the MEG signal may have also led to poorer statistical power. In the present

experiment, the responses occurred over a range of time and thus were variable on a trial to trial basis. Although the standard deviations were small, the differences in response times, coupled with the temporally rapid nature of the MEG signal means that there may have been insufficient numbers of trials/participants to obtain strong estimates of estimates of interest. This temporal variability is less worrisome in the fMRI data, as the sluggish nature of the BOLD response should result in overlap between cognitive operations/responses and more robust estimates.

Limitations

There were several limitations in the current experiment. One limitation was the size of the sample for this study, as this affected the level of power for the analyses. The sample was limited in two ways. The first limit was due to the closure of the MEG Research Centre at the Down Syndrome Research Foundation, which placed a time constraint on our ability to recruit participants. The second limit on the sample was in the large number of participants, particularly patients, whose data was removed due to excessive movement or other scanning artifacts that limited the number of clean trials available for analysis.

Another limitation related to a possible lack of power in the MEG data was due to variability in the timing of responses, as well as potentially increased variability in the brain activity of the schizophrenia patients. Pursuant to this, another potential reason for the lack of significance of many of the predicted effects in the MEG data, particularly the multivariate analysis, could be due to the data analysis procedure employed in this study. In the multivariate analysis, the entire 1.5 seconds trial was modeled whereas the longest average RT was ~1.2 seconds. Since the MEG signal is very quick, this means that the inclusion of the data from later timepoints does not (typically) reflect trial related processes, and may have dampened the signal

to noise ratio by adding non-task related variability to the data and increasing the error term in the statistical test.

A limitation related to the experimental design is the temporal overlap between the cognitive and motor requirements of the task. The participants made their response on the basis of the stimulus and cue which remained present on the screen thus making it challenging to assess whether changes in brain activity were related to one function or the other. A further difficulty associated with running a multivalent analysis with this type of experiment is that the predictor weights are difficult to interpret unless they align perfectly with the hypotheses. For instance, in the absence of an effect of Valence, it is unclear whether other significant effects are task-related, or group-related, or the result of random measurement error. One way to improve the current experiment would have been to add a temporal delay between the presentation of the stimulus and the presentation of the cue, or to restrict responses until after the stimulus and the cue had been presented. Alternatively, 'blank' trials where all features of the stimuli save for the probe (i.e. "Blue?") could have been used to isolate brain activity related to stimulus presentation from those involved in attentional biasing. In these cases, it would be easier to assess whether the post-stimulus changes in brain activity were associated with the decision-making processes, or with the motor response preparation processes.

An associated limitation was revealed during the course of this experiment was the role of the left IFG in the performance of the task. As was mentioned earlier, the left IFG was found to be active in many of the analyses. However, as the left IFG is hypothesized to play a crucial role in both cognitive control and reading, it is unclear whether the activity in this region reflects one or the other, or a combination of both. Given the experimental design that was employed, there is no apparent way to resolve this ambiguity. A future experiment that inserted delays

128

between the stimulus, cue, and response would add clarity to the role of the IFG in experiments of this nature. Furthermore, the stimuli could be manipulated such that the requirement for reading could be minimized. For instance, the stimuli could be shapes that could be a combination of 1) red or blue, 2) triangle or square, and/or 3) striped/solid. Each of these features could be present or absent, and could be cued by a non-word indicating which feature is currently relevant. Another concern in the present experiment is the presence of ceiling effects. The accuracy in each condition ranged from 92% - 86% in healthy volunteers, and 86% - 76% in the schizophrenia patients. Although the pilot testing, and the behavioural data suggested the manipulation was effective, these high success rates raise the possibility that the task was too simple to elicit a robust control-related signal.

Conclusions

This experiment was designed to examine the neural substrate of attentional biasing in healthy volunteers and schizophrenia patients using stimuli with varying levels of task-relevant features. The hypothesis was that the increase in task-relevant stimulus dimensions would lead to increased activity in the task positive network (specifically in the dAcc) in the fMRI results, and increased theta power in the preSMA/dAcc, and that schizophrenia patients would show increased activity relative to healthy volunteers in low stimulus valence conditions and decreased activity relative to healthy volunteers in high stimulus valence conditions. The hypotheses were partially supported by the results of this experiment. Specifically, the multivariate fMRI analysis did show the predicted effect of Valence, such that Component 2 was characterized by activity in the dAcc and the predictor weights indicated that there was a significant effect of Valence such that it was positively correlated with BOLD signal. The interaction between Group and Valence also conformed with the hypothesis, as the healthy volunteers showed a significant increase in

129

the Trivalent condition over the Bivalent condition, relative to the schizophrenia patients, which was the predicted pattern of results. The predicted significant increase in activity in the schizophrenia patients relative to healthy volunteers in the univalent condition was not observed in this component, however, visual inspection of the predictor weights indicate that the patients did display lower mean BOLD activity at this level of stimulus valence. In the MEG data, the hypothesis was disconfirmed, as there was no evidence of a load-dependent increase in theta power in the preSMA/dAcc. The schizophrenia patients appeared to exhibit lower signal to noise ratio in the functional analyses, particularly those involving MEG, which was likely related to the lack of significant group related differences in these analyses. The results of the structural analyses suggested that the patient sample exhibited widespread changes in structural connectivity, as well as a deficit in cortical thickness in many frontal areas including the left cingulate gyrus; however, the impact of these structural deficits on the functional results are unclear and remains an important topic of investigation for future studies.

Tables

Table 1. Demographic Information for the healthy volunteers and schizophrenia patients in the current study.

	Healthy Volunteers (25 Total)	Schizophrenia Patients (33 Total)	Test Statistic for Group Differences	p-value for Group Differences
Age	32.68 (2.12)	38.00 (1.47)	$t_{(56)} = 2.13$	0.038
Gender	12 M, 13 F	20 M, 13 F	$\chi^2_{(1)} = 0.91$	0.34
Watt's Socio-economic Status	57.42 (4.37)	72.32 (5.33)	$t_{(56)} = 2.08$	0.043
Years of Education	15.27 (0.48)	14.31 (0.39)	$t_{(56)} = 1.58$	0.12
Age of Illness Diagnosis	N/A	23.19 (1.00)	N/A	N/A
Illness Duration in Years	N/A	14.65 (1.63)	N/A	N/A
Total SSPI Score	N/A	14.52 (1.51)	N/A	N/A

Missing values: Watt's Socio-economic Status - 1 healthy volunteer and 2 schizophrenia patients; Years of Education – 1 healthy volunteer and 2 schizophrenia patients, Age of Illness onset – 2 schizophrenia patients, Illness Duration in Years - 2 schizophrenia patients

Table 2. Number of participants, and statistical test for group-level differences in age and gender for each analysis.

Analysis	Healthy Volunteers	Schizophrenia Patients	t-test for Age Differences	p-value for Age Differences	Chi-Square Test for Gender Differences	p-value for Gender Differences
Behavioural (MEG)	25	33	$t_{(56)} = 2.13$	0.038	$\chi^2_{(1)} = 0.91$	0.34
Behavioural (fMRI)	24	33	$t_{(55)} = 2.13$	0.017	$\chi^2_{(1)} = 0.64$	0.43
Structural MRI	23	26	$t_{(47)} = 3.04$	0.004	$\chi^2_{(1)} = 1.54$	0.22
Diffusion Weighted Imaging	22	26	$t_{(46)} = 2.36$	0.02	$\chi^2_{(1)} = 0.24$	0.62
fMRI (Univariate and Multivariate)	21	23	$t_{(42)} = 1.59$	0.12	$\chi^2_{(1)} = 0.73$	0.39
MEG (Univariate and Multivariate)	21	20	$t_{(39)} = 1.74$	0.09	$\chi^2_{(1)} = 0.03$	0.85
Multivariate MEG-fMRI	21 (fMRI) 21 (MEG)	23 (fMRI) 20 (MEG)	$t_{(42)} = 1.59$ (fMRI) $t_{(39)} = 1.74$ (MEG)	0.12 (fMRI) 0.09 (MEG)	$\chi^2_{(1)} = 0.73$ (fMRI) $\chi^2_{(1)} = 0.03$ (MEG)	0.39 (fMRI) 0.85 (MEG)

Table 3. Mean response times (RTs) for the fMRI and MEG versions of the experiment. RTs are in milliseconds, and standard errors are in parentheses.

	Univalent		Bivalent		Trivalent	
	fMRI					
	Correct	Incorrect	Correct	Incorrect	Correct	Incorrect
Controls	918 (22)*	966 (53)	980 (23)*	992 (56)	1030 (26)*	1139 (53)
Patients	1035 (24)	1047 (38)	1078 (23)	1118 (35)	1112 (24)	1149 (36)
	MEG					
	Correct	Incorrect	Correct	Incorrect	Correct	Incorrect
Controls	1004 (23)*	1031 (41)	1073 (23)*	1116 (37)	1115 (23)*	1201 (24)
Patients	1087 (23)	1048 (31)	1143 (24)	1170 (35)	1202 (23)	1222 (31)

Note: * = $p < .05$ for between-group comparisons

Table 4. Mean accuracy for the fMRI and MEG versions of the experiment. Accuracy rates are in percentages, and standard errors are in parentheses.

	Univalent			Bivalent			Trivalent		
	fMRI								
	Correct	Incorrect	Miss	Correct	Incorrect	Miss	Correct	Incorrect	Miss
Controls	91.83* (2.08)	3.57* (1.02)	2.44 (1.63)	90.30* (2.62)	3.71* (1.09)	2.61 (2.18)	85.70* (2.55)	4.48 (1.15)	3.35 (2.01)
Patients	86.33 (1.85)	6.75 (0.91)	5.64 (1.45)	82.81 (2.33)	6.80 (0.97)	7.14 (1.94)	77.95 (2.27)	7.11 (1.02)	7.94 (1.79)
	MEG								
	Correct	Incorrect	Miss	Correct	Incorrect	Miss	Correct	Incorrect	Miss
Controls	91.69* (2.41)	5.65 (1.23)	2.73* (2.02)	90.50* (2.71)	5.33 (1.38)	4.17* (2.20)	87.73* (3.01)	5.85 (1.45)	6.42* (2.59)
Patients	83.02 (2.13)	8.17 (1.09)	9.46 (1.79)	79.61 (2.40)	8.15 (1.22)	12.24 (1.95)	76.40 (2.66)	8.25 (1.28)	15.35 (2.29)

Note: $* = p < .05$ for between-group comparisons

Table 5. Mean SSPI Item Scores, Mean Factor Scores, and Mean Total Score.

SSPI Item	Mean	Standard Error
Anxiety	1.18	0.19
Depression	0.82	0.18
Anhedonia	1.15	0.23
Elated Mood	0.27	0.21
Insomnia	0.82	0.21
Somatic Concerns	0.33	0.13
Delusions	2.21	0.32
Hallucinations	1.97	0.32
Attentional Impairment	1.09	0.19
Disorientation	0.63	0.63
Overactivity	0.24	0.11
Underactivity	1.03	0.21
Flattened Affect	1.00	0.18
Inappropriate Affect	0.12	0.12
Pressure of Speech	0.12	0.09
Poverty of Speech	0.48	0.15
Disordered Thought	0.48	0.17
Peculiar Behaviour	0.18	0.09
Irritability	0.24	0.76
Insight	0.70	0.17
Factors	Mean	Standard Error
Anxiety/Depression	2.00	0.30
Excitation	1.88	0.40
Psychomotor Poverty	3.67	0.56
Psychomotor Disorganization	1.76	0.41
Reality Distortion	4.18	0.54
Total	14.52	1.51

Table 6. Clusters displaying decreased cortical thickness in schizophrenia patients relative to healthy volunteers (p < .001, cluster-corrected). No significant increases in cortical thickness in patients relative to volunteers were found.

Cluster	Size (mm^2)	MNI Coordinates of Peak	Anatomical Location of Peak	Brodmann Area of Peak
1	3140	-8, 30, 55	L Superior Frontal Gyrus	8
2	2325	50, -24,-18	R Middle Temporal Gyrus	20
3	1600	-22, 41, 24	L Middle Frontal Gyrus	9
4	1556	-40, 20, 8	L Inferior Frontal Gyrus (pars opercularis)	45
5	1106	36, -14, 14	R Insula	13
6	1066	42, 34, 8	R Inferior Frontal Gyrus (pars triangularis)	46
7	1051	32, -62, -9	R Fusiform Gyrus	37
8	990	-26, 26, 4	L Insula	13
9	977	40, 6, 24	R Inferior Frontal Gyrus (pars opercularis)	44
10	949	52, -22, 38	R Postcentral Gyrus	1
11	891	-12, -90, 6	L Superior Occipital Gyrus	17
12	779	60, -40, 12	R Superior Temporal Gyrus	22
13	578	-34, -32, 17	L Anterior Transverse Temporal Gyrus	41

Table 7. Contrasts yielding significant brain activity in univariate fMRI analysis. The brain images for all significant contrasts in the healthy volunteers can be found in Figure 5. The brain images for all significant contrasts in the schizophrenia patients can be found in Figure 6. The brain images for the contrast of the healthy volunteers greater than schizophrenia patients can be found in Figure 7. The brain images for the contrast of the healthy volunteers greater than schizophrenia patients can be found in Figure 8.

Group	Contrast	Regions with Significant Brain Activity
Controls		
	All > Baseline	Bilateral: supplementary motor area, frontal eye fields, dorsal anterior cingulate cortex, hippocampi, angular gyri, superior and inferior occipital gyri, calcarine sulci, fusiform gyri, and the vermis, Crus I, and lobule VI of the cerebellum Left: putamen, pre- and post-central gyri, superior and inferior parietal lobules, and thalamus
	Baseline > All	Bilateral: medial prefrontal cortices, angular gyri, precuneus/posterior cingulate Right: superior temporal gyrus, insula, inferior frontal gyrus (pars triangularis and orbitalis)
	Bivalent > Univalent	Bilateral: lingual gyri and calcarine fissure
	Trivalent > Bivalent	Bilateral: lingual gyri and calcarine fissure
	Trivalent > Univalent	Bilateral: lingual gyri, calcarine fissure, superior occipital gyri, and superior parietal lobules Left: Crus I of the cerebellum
Patients		
	All > Baseline	Bilateral: supplementary motor area, frontal eye fields, dorsal anterior cingulate cortex, hippocampi, thalamus, angular gyri, superior parietal lobules, superior and inferior occipital gyri, calcarine sulci, fusiform gyri, and the vermis, Crus I, Crus II, and lobule VI of the cerebellum
	Baseline > All	Bilateral: medial prefrontal cortices, superior frontal gyri, precuneus/posterior cingulate
	Trivalent > Univalent	Bilateral: lingual gyrus Left: Crus I of the cerebellum Right: Superior occipital gyrus
Controls > Patients		
	All > Baseline	Bilateral: hippocampi, fusiform gyri, lingual gyri, calcarine sulci, and Crus I and lobule 6 of the cerebellum Left: putamen and inferior parietal lobule

Group	Contrast	Regions with Significant Brain Activity
	Bivalent > Univalent	Bilateral: lingual gyri and calcarine fissure
	Trivalent > Univalent	Bilateral: lingual gyri, calcarine fissure and lobule VI of the cerebellum
Patients > Controls		
	All > Baseline	Bilateral: medial prefrontal cortices, insula, and posterior cingulate/precuneus Right: middle and superior temporal gyri

Table 8. Cluster information for contrasts yielding significant brain activity in univariate fMRI analysis in healthy volunteers.

Group	Contrast	Cluster	Cluster Size (mm^3)	Peak t-value	MNI Coordinates of Peak (X, Y, Z)	Anatomical Location of Peak	Brodmann Area of Peak
Healthy Volunteers							
	All > Baseline						
		1	3352	12.56	32, -54, -28	R Lobule VI (Cerebellum)	N/A
		2	2173	14.48	-36, -54, -24	L Lobule VI (Cerebellum)	N/A
		3	288	9.21	-28, -72, 44	L Middle Occipital Gyrus	19
		4	248	8.03	-34, -60, 58	L Inferior Parietal Lobule	7
		5	173	11.00	-32, -22, 66	L Precentral Gyrus	6
		6	148	9.75	-24, -34, -2	L Hippocampus	27
		7	108	9.88	-46, 6, 34	L Inferior Frontal Gyrus (pars opercularis)	44
		8	76	8.33	32, -64, 42	R Angular Gyrus	7
		9	66	9.99	-8, 2, 54	L Medial Frontal Gyrus	6
	Baseline > All						
		1	1278	10.81	6, 42, -4	R Orbitofrontal Gyrus	10
		2	427	9.34	-8, -46, 50	L Posterior Cingulate	23
		3	240	8.87	44, -66, 20	R Middle Temporal Gyrus	39
		4	163	9.34	6, 48, 34	R Superior Frontal Gyrus	9
		5	71	7.91	-42, -80, 32	L Middle Occipital Gyrus	19

Group	Contrast	Cluster	Cluster Size (mm³)	Peak t-value	MNI Coordinates of Peak (X, Y, Z)	Anatomical Location of Peak	Brodmann Area of Peak
	Bivalent > Univalent						
		1	199	10.56	2, -82, -4	R Lingual Gyrus	17
	Trivalent > Bivalent						
		1	58	7.62	2, -80, -6	R Lingual Gyrus	17
	Trivalent > Univalent						
		1	482	11.04	2, -86, -2	R Calcarine Gyrus	17
		2	86	9.36	30, -74, 40	R Middle Occipital Gyrus	7
		3	50	8.65	-22, -74, 46	L Superior Parietal Lobule	7

Table 9. Cluster information for contrasts yielding significant brain activity in univariate fMRI analysis in schizophrenia patients.

Group	Contrast	Cluster	Cluster Size (mm³)	Peak t-value	MNI Coordinates of Peak (X, Y, Z)	Anatomical Location of Peak	Brodmann Area of Peak
Patients							
	All > Baseline						
		1	5290	10.99	-38, -70, -16	L Lobule VI (Cerebellum)	N/A
		2	631	10.13	-42, -34, 46	L Inferior Parietal Lobule	40
		3	363	8.40	-48, 2, 44	L Precentral Gyrus	6
		4	261	8.66	-12, -20, 0	L Thalamus	N/A
		5	173	7.08	-2, 2, 62	L Medial Frontal Gyrus	6
		6	54	7.67	30, -56, 42	R Angular Gyrus	7
	Baseline > All						
		1	2060	11.74	16, 56, 2	R Medial Prefrontal Gyrus	10
		2	261	8.84	-8, -54, 32	L Posterior Cingulate	23
	Trivalent > Univalent						
		1	101	7.40	-2, -86, -10	L Lingual Gyrus	17

Table 10. Cluster information for contrasts yielding significant brain activity in univariate fMRI analysis in comparisons of healthy volunteers to schizophrenia patients.

Group	Contrast	Cluster	Cluster Size (mm^3)	Peak t-value	MNI Coordinates of Peak (X, Y, Z)	Anatomical Location of Peak	Brodmann Area of Peak
Volunteers > Patients							
	All > Baseline						
		1	912	8.22	10, -68, -18	R Lobule VI (Cerebellum)	N/A
		2	728	8.10	-36, -70, -16	L Lobule VI (Cerebellum)	N/A
		3	172	5.93	10, -76, -26	R Lobule VIII (Cerebellum)	N/A
	Bivalent > Univalent						
		1	321	6.86	12, -80, -4	R Lingual Gyrus	18
	Trivalent > Univalent						
		1	690	8.44	12, -78, 2	R Lingual Gyrus	18
Patients > Volunteers							
	All > Baseline						
		1	539	7.43	-8, -48, 50	L Precuneus	23
		2	124	6.31	12, 54, 8	R Medial Prefrontal Gyrus	10
		3	65	6.09	-14, 52, 0	L Medial Prefrontal Gyrus	10

Table 11. Sums of squares and percentages of variance accounted for by the fMRI-CPCA analysis. The External column lists the sum of squares for the total dataset (*Z*) as well as the sum of squares predictable from task timing (*G*), and the proportion of total variance predictable from task timing. The internal columns list the sum of squares and percentage of predictable variance accounted for by each component. The totals column lists the total sum of squares for all components as well as the proportion of predictable variance that they account for.

| | | Internal | | | |
Source	External	1	2	3	Totals
Total (*Z*)	44773.00				
Predictable (*G*)	2879.86	568.20	365.74	199.57	1133.51
	6%	19.73%	12.70%	6.93%	39.36%

Table 12. Contrasts yielding significant changes in power in univariate MEG analysis. For the brain images for the significant condition greater than baseline contrasts in the 6 Hz band in the healthy volunteers, please see Figure 13. For the brain images of the significant condition greater than baseline contrasts from the 20 Hz band in the healthy volunteers, please see Figure 14. For the brain images of the significant contrasts between conditions from the 10 Hz band in the healthy volunteers, please see Figure 15. For the brain images of the significant contrasts between conditions from the 20 Hz band in the healthy volunteers, please see Figure 16. For the brain images of the significant condition greater than baseline contrasts from the 20 Hz band in the schizophrenia patients, please see Figure 17.

Group	Contrast	Frequency Band	Regions with Significant Brain Activity
Controls			
	Univalent > Baseline		
		6 (theta)	Bilateral increases in power: orbitofrontal gyri and rectus gyri Right increases in power: middle orbitofrontal gyrus
		20 (beta)	Bilateral reductions in power: inferior, middle and superior occipital gyri, calcarine sulci, lingual gyri, fusiform gyri, angular gyri, inferior parietal lobules, supramarginal gyri, dAcc, supplementary motor area, frontal eye fields, caudate, thalamus, hippocampi, parahippocampal gyri, as well as Crus I and II, lobule 6 and 9, and the vermis of the cerebellum Left decreases in power: precentral and postcentral gyri, middle frontal gyrus, superior, middle and inferior temporal gyri, pallidum, Heschl's gyrus and amygdala.
	Bivalent > Baseline		
		6 (theta)	Bilateral increases in power: medial and superior orbitofrontal gyri, and rectus gyri
		20 (beta)	Bilateral reductions in power: inferior, middle and superior occipital gyri, calcarine sulci, lingual gyri, fusiform gyri, angular gyri, inferior parietal lobules, supramarginal gyri, dAcc, supplementary motor area, frontal eye fields, caudate, thalamus, hippocampi, parahippocampal gyri, as well as Crus I and II, lobule 6 and 9, and the vermis of the cerebellum Left decreases in power: precentral and postcentral gyri, middle frontal gyrus, superior, middle and inferior temporal gyri, pallidum, Heschl's gyrus and amygdala
	Trivalent > Baseline		

Group	Contrast	Frequency Band	Regions with Significant Brain Activity
		6 (theta)	Bilateral increases in power: medial and superior orbitofrontal gyri, and rectus gyri Right increase in power: inferior orbitofrontal gyrus
		20 (beta)	Bilateral reductions in power: inferior, middle and superior occipital gyri, calcarine sulci, lingual gyri, fusiform gyri, angular gyri, inferior parietal lobules, supramarginal gyri, dAcc, supplementary motor area, frontal eye fields, caudate, thalamus, hippocampi, parahippocampal gyri, as well as Crus I and II, lobule 6 and 9, and the vermis of the cerebellum Left decreases in power: precentral and postcentral gyri, middle frontal gyrus, superior, middle and inferior temporal gyri, pallidum, Heschl's gyrus and amygdala
	Bivalent > Univalent		
		10 (alpha)	Bilateral increases in power: rectus gyri, and medial orbitofrontal gyri
		20 (beta)	Bilateral reductions in power: calcarine fissure and the cuneus
	Trivalent > Univalent		
		10 (alpha)	Bilateral increases in power: rectus gyri, and medial orbitofrontal gyri
		20 (beta)	Bilateral decreases in power: posterior cingulate, fusiform gyri and Crus I of the cerebellum Left decreases in power: calcarine fissure, lingual gyrus, and Crus II and lobe 6 of the cerebellum
Patients			
	Univalent > Baseline		
		20 (beta)	Bilateral reductions in power: superior, middle, and inferior occipital gyri, calcarine sulci, lingual gyri, fusiform gyri, inferior parietal lobules, angular gyri, supramarginal gyri, dAcc, supplementary motor area, frontal eye fields, caudate, hippocampi, parahippocampal gyri, and thalamus, as well as the as Crus I and II, lobule 6 and 9, and the vermis of the cerebellum. Left decreases in power: precentral and postcentral gyri, middle frontal gyrus, superior, middle and inferior temporal gyri, pallidum, Heschl's gyrus and amygdala
	Bivalent > Baseline		
		20 (beta)	Bilateral reductions in power: superior, middle, and inferior occipital gyri, calcarine sulci, lingual gyri, fusiform gyri, inferior parietal lobules, angular gyri, supramarginal gyri, hippocampi, parahippocampal gyri, and thalamus, as well as the as Crus I and II, lobule 6 and 9, and the vermis of the cerebellum.

Group	Contrast	Frequency Band	Regions with Significant Brain Activity
			Left decreases in power: precentral and postcentral gyri, middle frontal gyrus, superior, middle and inferior temporal gyri, pallidum, Heschl's gyrus and amygdala
	Trivalent > Baseline	20 (beta)	Bilateral reductions in power: inferior, middle and superior occipital gyri, calcarine sulci, lingual gyri, fusiform gyri, angular gyri, inferior parietal lobules, supramarginal gyri, dAcc, supplementary motor area, frontal eye fields, caudate, thalamus, hippocampi, parahippocampal gyri, as well as Crus I and II, lobule 6 and 9, and the vermis of the cerebellum. Left decreases in power: precentral and postcentral gyri, middle frontal gyrus, superior, middle and inferior temporal gyri, pallidum, Heschl's gyrus and amygdala

Table 13. Cluster information for contrasts yielding significant brain activity in univariate fMRI analysis in healthy volunteers.

Group	Frequency	Contrast	Cluster	Cluster Size (mm³)	Peak t-value	MNI Coordinates of Peak (X, Y, Z)	Anatomical Location of Peak	Brodmann Area of Peak
Healthy Volunteers								
	6 Hz (theta)							
		Univalent > Baseline						
			1	88	6.64	20, 38, -26	R Orbitofrontal Gyrus	11
		Bivalent > Baseline						
			1	1007	7.41	-4, 48, -28	L Gyrus Rectus	11
		Trivalent > Baseline						
			1	66	6.38	-6, 58, -26	L Gyrus Rectus	11
	10 Hz (alpha)							
		Bivalent > Univalent						
			1	260	7.04	0, 34, -26	Gyrus Rectus	11
		Trivalent > Univalent						
			1	647	7.03	2, 34, -22	R Gyrus Rectus	11
	20 Hz (beta)							
		Univalent > Baseline						
			1	114232	13.20	-40, -32, 54	L Postcentral Gyrus	3
		Bivalent > Baseline						
			1	104162	14.27	-30, -74, 28	L Middle Occipital Gyrus	19
		Trivalent > Baseline						

Group	Frequency	Contrast	Cluster	Cluster Size (mm³)	Peak t-value	MNI Coordinates of Peak (X, Y, Z)	Anatomical Location of Peak	Brodmann Area of Peak
			1	109938	13.56	-28, -68, -10	L Fusiform Gyrus	19
		Bivalent > Univalent						
			1	137	7.44	-4, -76, 26	L Calcarine Sulcus	18
		Trivalent > Univalent						
			1	157	6.99	46, -54, -22	R Crus I (Cerebellum)	N/A
			2	156	7.05	-20, -80, -16	L Lobule VI (Cerebellum)	N/A

Table 14. Cluster information for contrasts yielding significant brain activity in univariate fMRI analysis in schizophrenia patients.

Group	Frequency	Contrast	Cluster	Cluster Size (mm^3)	Peak t-value	MNI Coordinates of Peak (X, Y, Z)	Anatomical Location of Peak	Brodmann Area of Peak
Schizophrenia Patients								
	20 Hz (beta)							
		Univalent > Baseline						
			1	105823	12.14	-34, -84, -16	L Crus I (Cerebellum)	N/A
		Bivalent > Baseline						
			1	80504	14.43	-16, -64, 2	L Lingual Gyrus	17
		Trivalent > Baseline						
			1	80790	14.11	-26, -62, -26	L Lobule VI (Cerebellum)	N/A

Table 15. Percentages of variance accounted for by the MEG-PCA, *BH'*-CPCA, and *E*-CPCA analyses. The External column lists the sum of squares for the total dataset (Z), the sum of squares and percentage of total variance predictable from the spatial distribution of fMRI networks (*BH'*), and the sum of squares and percentage of total variance that was not predictable from the spatial distribution of fMRI networks (*E*). The internal columns list the sum of squares and percentage of predictable variance accounted for by each component. The totals column lists the total sum of squares for all components as well as the proportion of predictable variance that they account for.

	External	Internal 1	2	3	4	5	6	Totals
Total (Z)	19309.00	2276.53	1222.26	1838.22	834.15	957.73	635.27	7764.15
% Total	100%	11.79%	6.33%	9.52%	4.32%	4.96%	3.29%	40.21%
BH'	5897.40	2242.78	1916.07					4158.85
% Total	30.54%	11.62%	9.92%					21.54%
% of *BH'*	100%	38.03%	32.49%					70.52%
E	13411.60	748.37	596.82	519.03				1864.21
% Total	69.46%	3.88%	3.09%	2.69%				9.65%
% of *E*	100%	5.58%	4.45%	3.87%				13.90%

Figures

Figure 1. Sample stimuli from the fMRI and MEG experiments. For each task type, stimuli can contain zero, one, or two currently task-irrelevant dimensions. The cue at the bottom of the stimulus indicates which type of stimulus dimension is currently relevant. For example, in the Trivalent Case condition presented here, the correct response would be 'yes' and is made by pressing a button with the right index finger.

	Colour	Parity	Case
Univalent	✠ Blue?	2 Odd?	d Lower?
Bivalent	4 Blue? Q Red?	5 Odd? seven Even?	NINE Lower? a Upper?
Trivalent	FIVE Red?	three Even?	six Lower?

Figure 2. Graphical depiction of the experimental procedure for both the MEG and fMRI versions of the experiment. Each stimulus was displayed for 1500ms, with a blank screen displayed for 500ms during the inter-stimulus interval (ISI). The variable presentation and duration of intertrial intervals (ITIs) forms an approximately exponential distribution, with the most trials at the shortest ITIs, thereby maximizing the efficiency of the design in detecting the hemodynamic response to each stimulus. The words 'yes' and 'no' appeared on the bottom of the screen to cue participants as to which button to press for the relevant response. Note: the 20000ms variable ITI was only present in the fMRI version of the experiment. Please see General Methods – Task for more details.
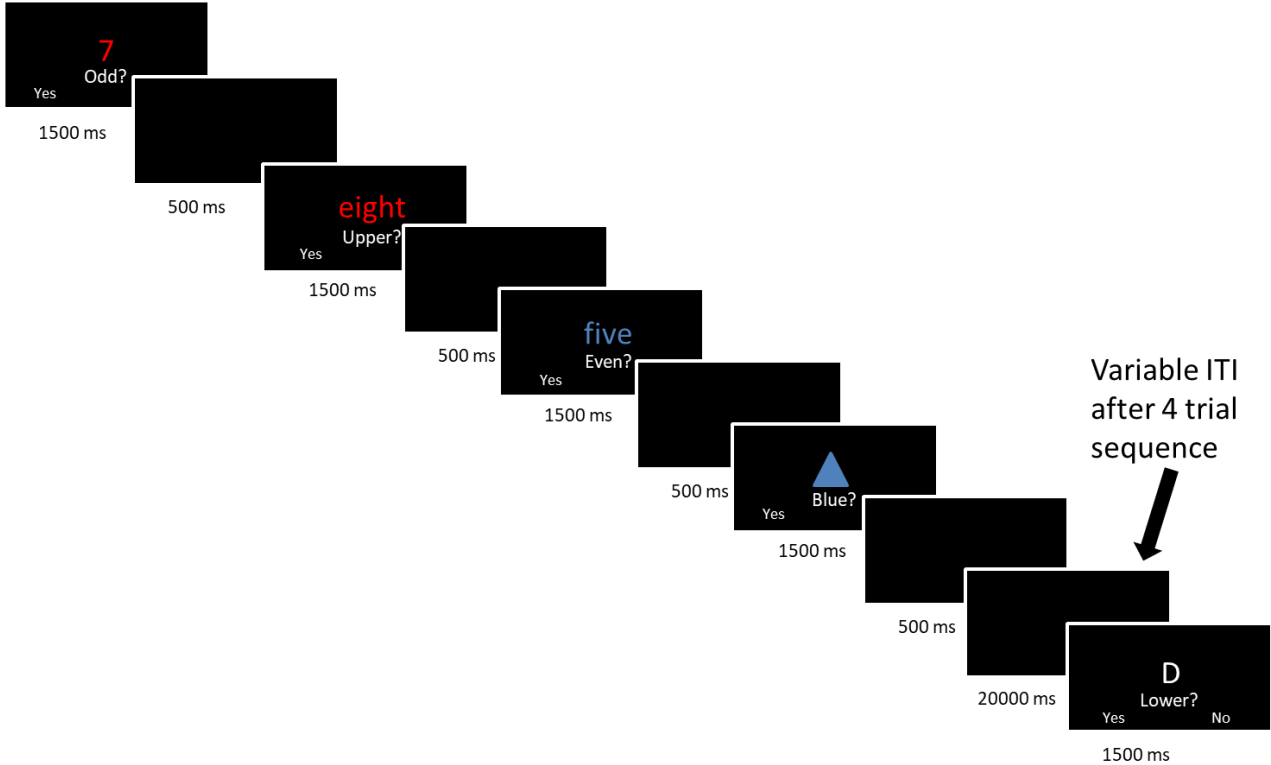
Figure 3. Comparison of skeletonized FA in healthy volunteers and schizophrenia patients when controlling for age and gender. The FSL-TBSS FA skeleton is depicted in green. Areas in red/yellow indicate tracts where healthy volunteers have significantly greater FA than patients ($p < 0.05$, TFCE). NOTE: This figure uses radiological convention, meaning that the right side of the image is the left side of the brain.
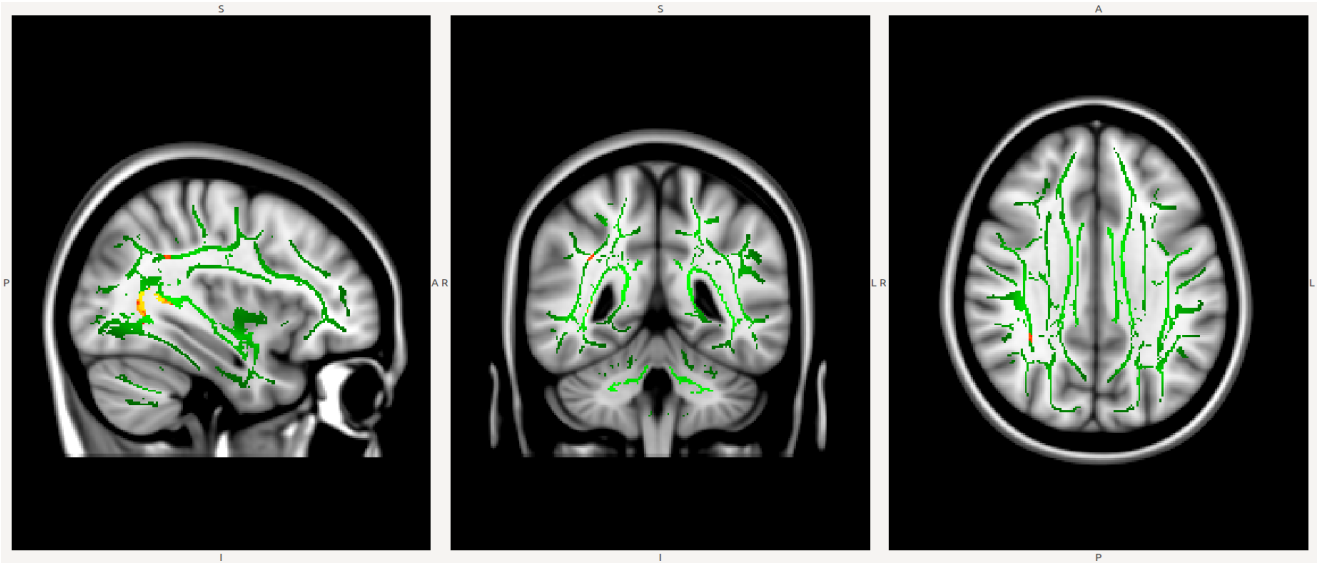
Figure 4. Comparison of cortical thickness between healthy volunteers and schizophrenia patients when controlling for the effects of age and gender. Only decreases in cortical thickness were found in patients, and are depicted in yellow-red (p < 0.001, cluster-corrected). The top row depicts the lateral and medial views of the left hemisphere, and the bottom row depicts the lateral and medial views of the right hemisphere.
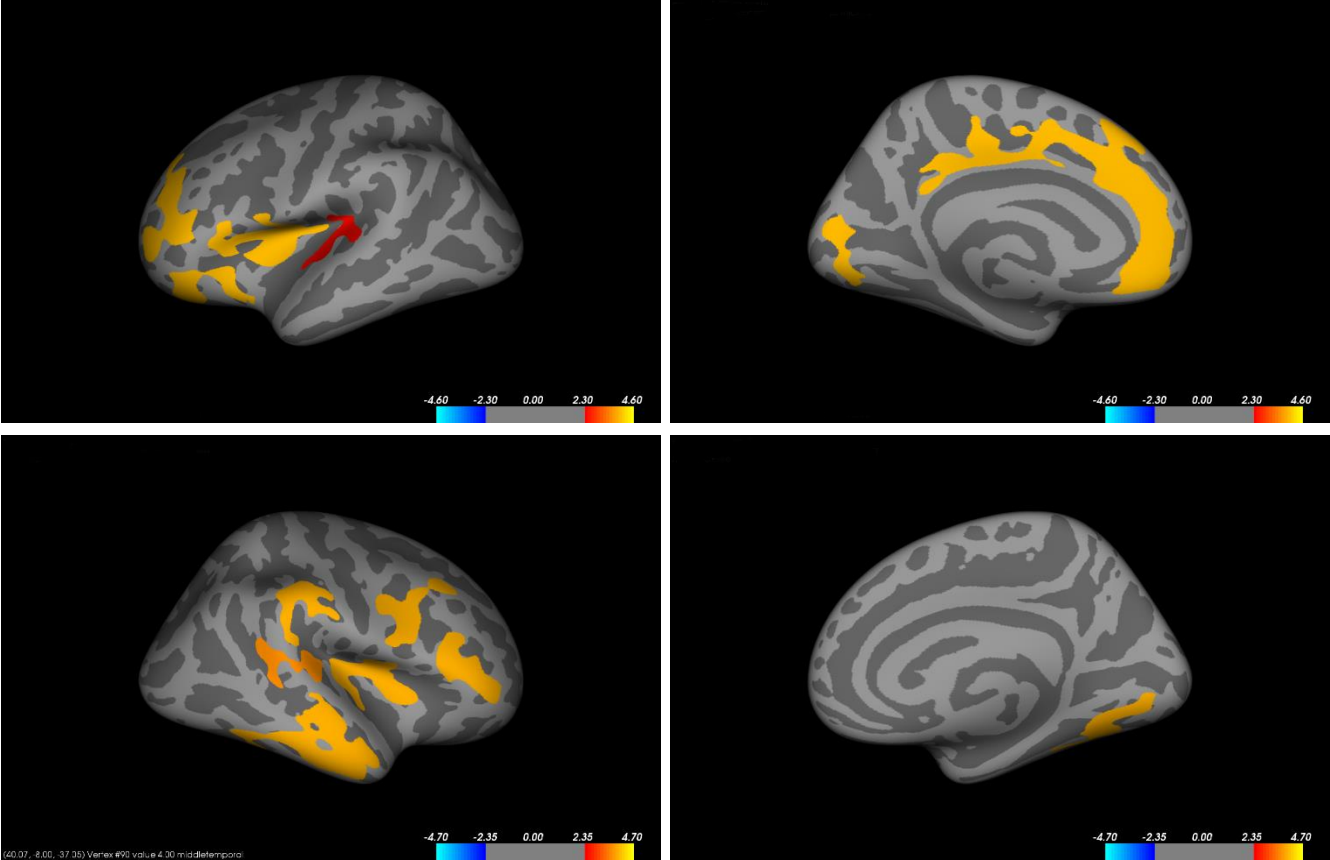
Figure 5. Significant results from the univariate fMRI analysis, healthy controls. Activations are displayed in red/yellow (p < .05, FWE-corrected). Images are in neurological convention (i.e., the right side of the image is the right side of the brain).

   a. All stimuli greater than baseline. The axial slices in the image are located at the MNI z-axis coordinates: -22, -2, 38, and 58.
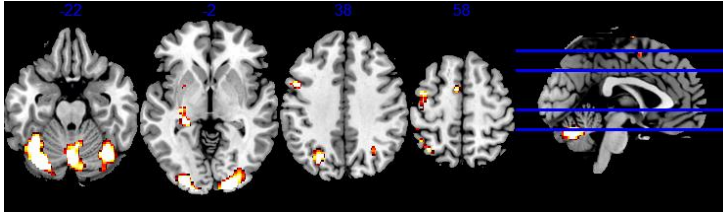
    b. Baseline greater than all stimuli. The axial slices in the image are located at the MNI z-axis coordinates: -22, -2, 38, and 58.
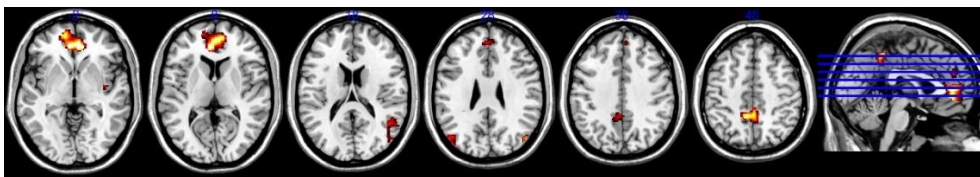
    c. Bivalent stimuli greater than univalent stimuli. The axial slices in the image are located at the MNI z-axis coordinates: -7, -2, and 3.
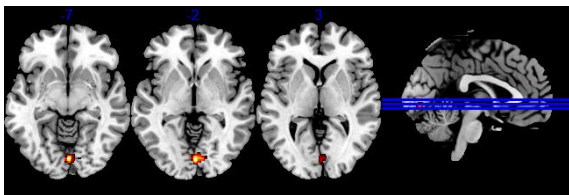
    d. Trivalent stimuli greater than bivalent stimuli. The axial slices in the image are located at the MNI z-axis coordinates: -7, and -2.
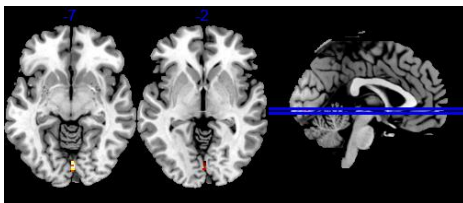
    e. Trivalent stimuli greater than univalent stimuli. The axial slices in the image are located at the MNI z-axis coordinates: -17, -2, 18, and 40.
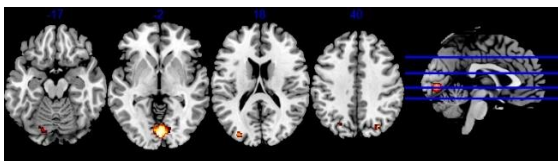
Figure 6. Significant results from the univariate fMRI analysis, schizophrenia patients. Activations are displayed in red/yellow (p < .05, FWE-corrected). Images are in neurological convention (i.e., the right side of the image is the right side of the brain).

a. All stimuli greater than baseline. The axial slices in the image are located at the MNI z-axis coordinates: -12, 8, 28, 38, and 58.
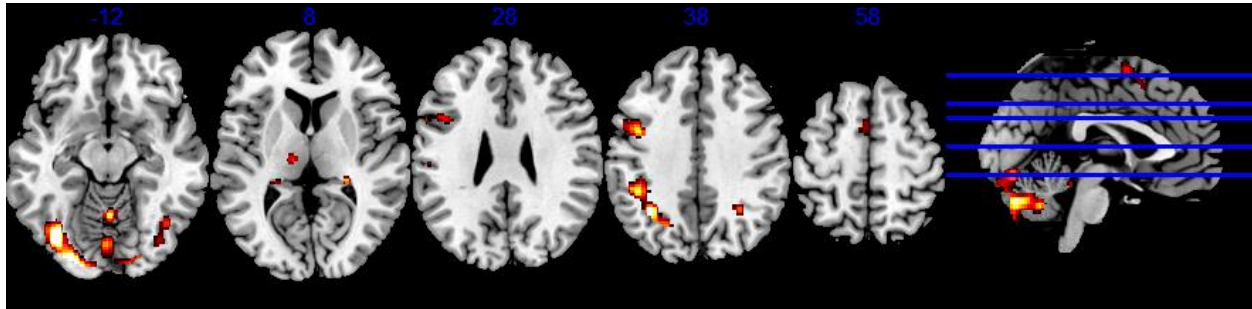
b. Baseline greater than all stimuli. The axial slices in the image are located at the MNI z-axis coordinates: -12, 8, 28, 38, and 58.
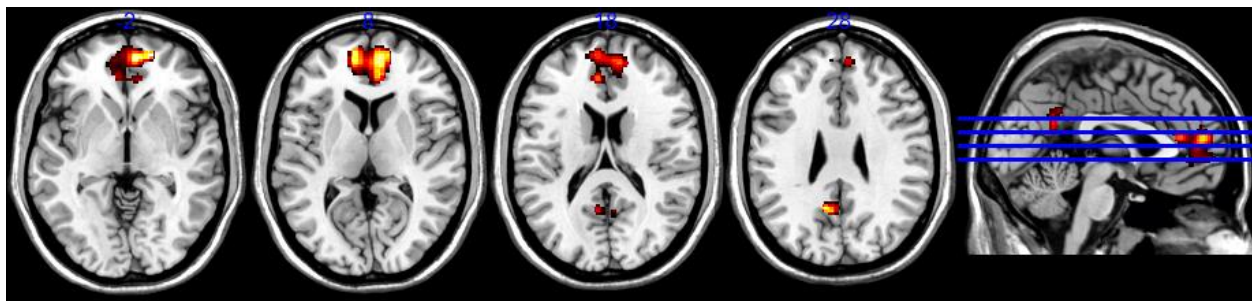
c. Trivalent stimuli greater than univalent stimuli. The axial slices in the image are located at the MNI z-axis coordinates: -16, -10, -6.
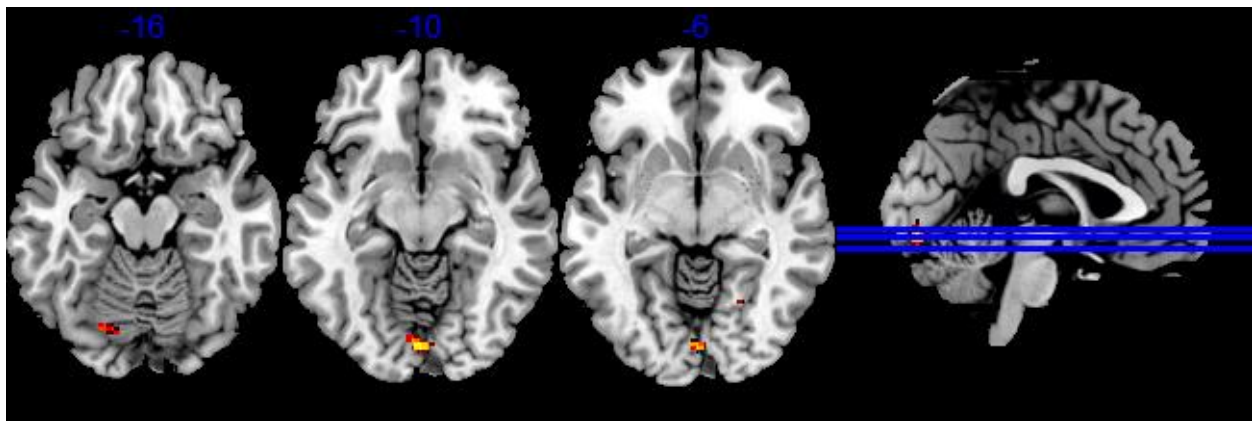
Figure 7. Significant results from the univariate fMRI analysis, controls greater than patients. Activations are displayed in red/yellow (p < .05, FWE-corrected). Images are in neurological convention (i.e., the right side of the image is the right side of the brain).

    a. All stimuli greater than baseline. The axial slices in the image are located at the MNI z-axis coordinates: -17, -7, 4, 10, and 44.
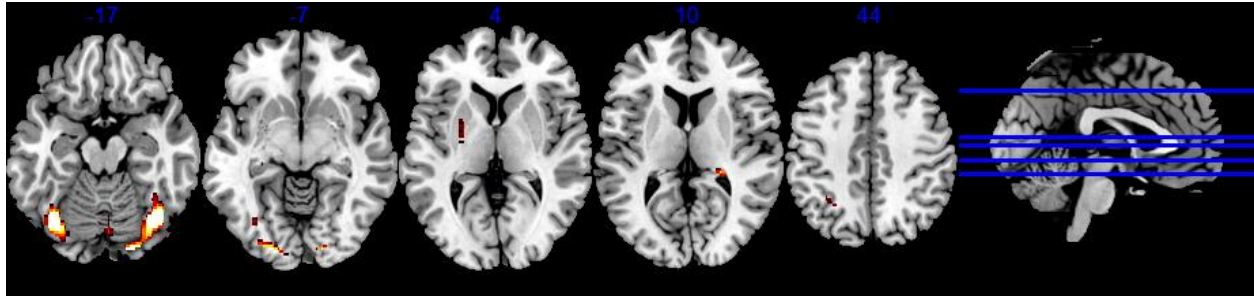
    b. Bivalent stimuli greater than univalent stimuli. The axial slices in the image are located at the MNI z-axis coordinates: -12, -7, -2, and 50.
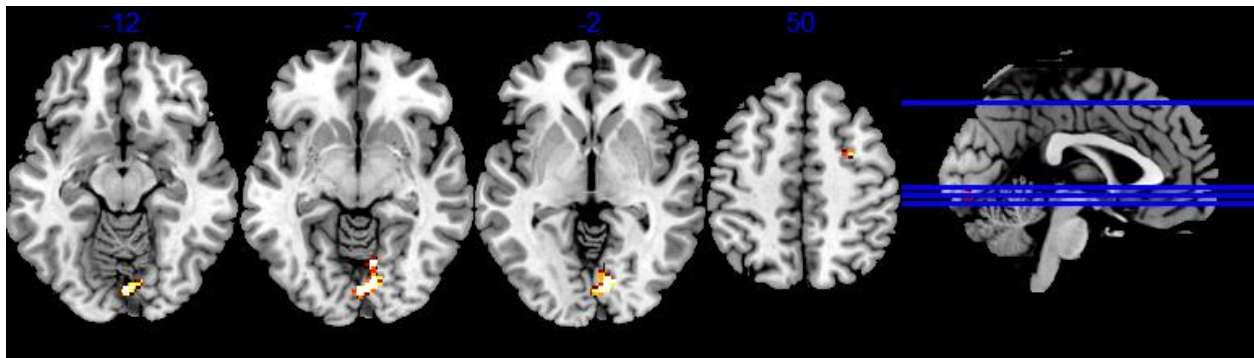
    c. Trivalent stimuli greater than univalent stimuli. The axial slices in the image are located at the MNI z-axis coordinates: -7, -2, and 3.
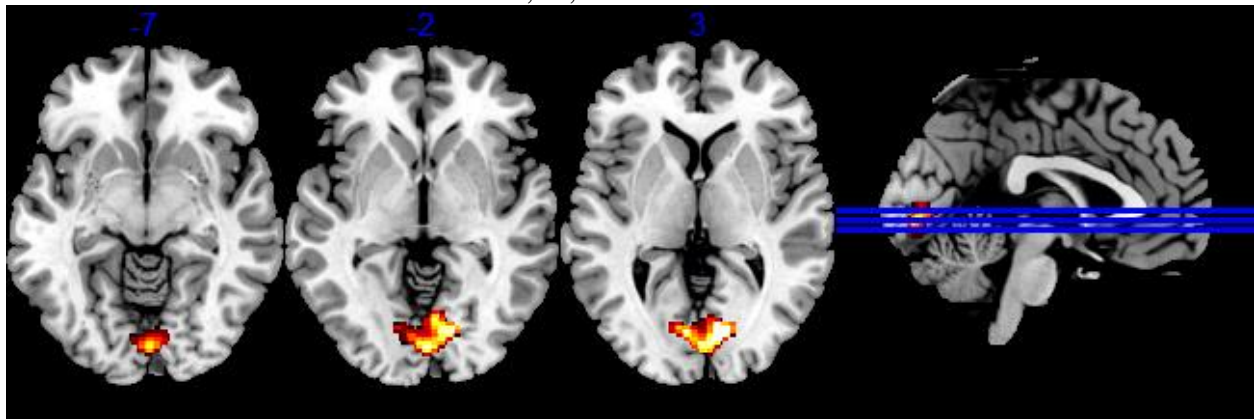
Figure 8. Significant results from the univariate fMRI analysis, patients greater than controls. All stimuli greater than baseline. Activations are displayed in red/yellow (p < .05, FWE-corrected). The axial slices in the image are located at the MNI z-axis coordinates: -1, 3, 43, and 51. Images are in neurological convention (i.e., the right side of the image is the right side of the brain).
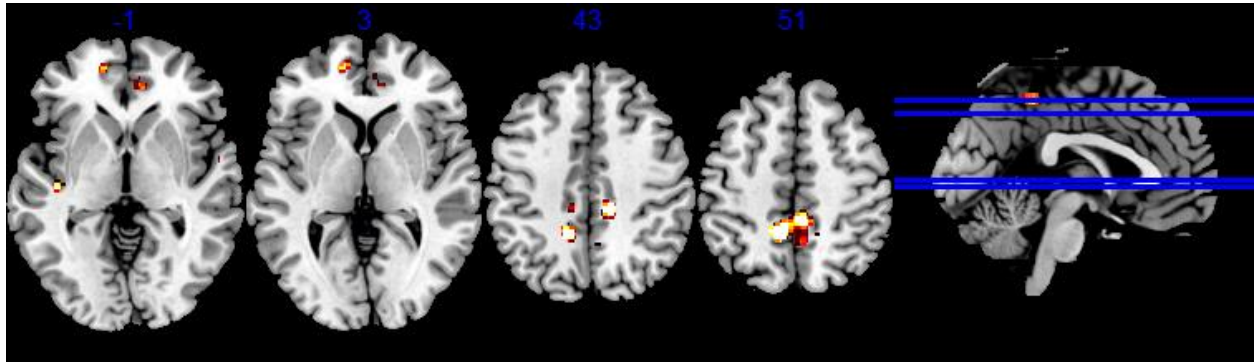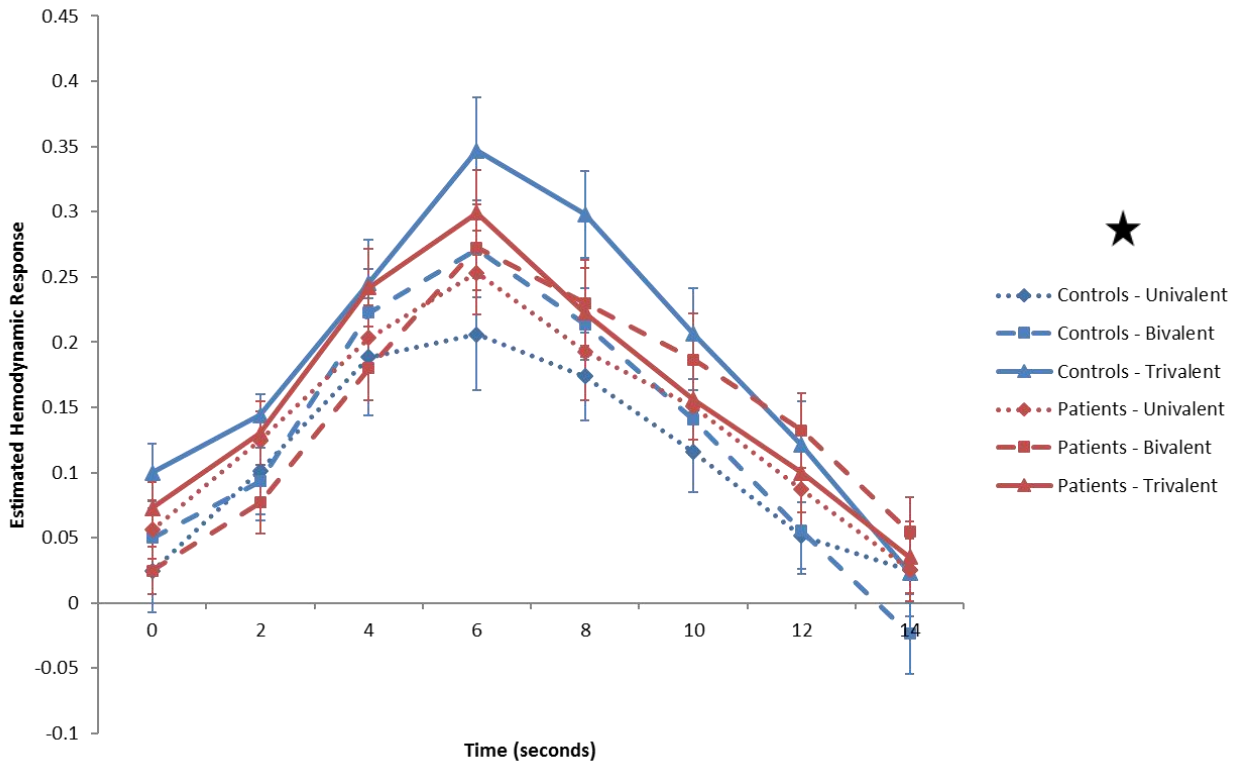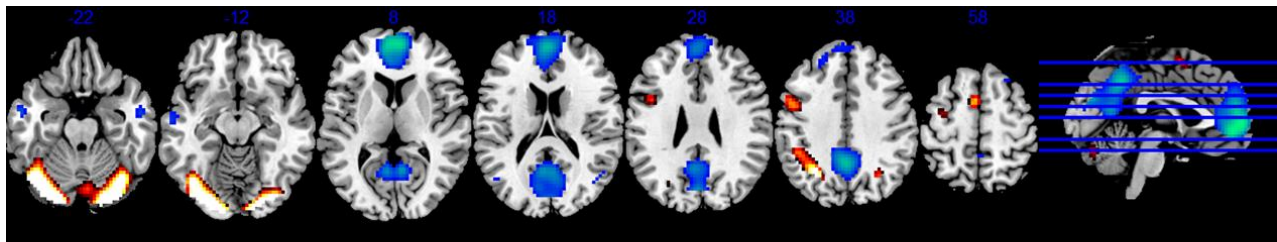
Figure 9. Component 1 from the fMRI-CPCA analysis. The upper image depicts the dominant 10% of component loadings for Component 1 from the fMRI-CPCA analysis. Positive loadings are depicted in red/yellow and represent task-based increases in BOLD signal. This is reversed when the estimated HRF crosses the baseline. No negative loadings exceeded the 10% threshold. The lower image depicts the mean FIR-based predictor weights plotted as a function of post-stimulus time. Data from control subjects are plotted in blue, and data from schizophrenia patients are plotted in red. The axial slices in the image are located at the MNI z-axis coordinates: -22, -12, 28, 38, 48, 58, and 68. Images are in neurological convention (i.e., the right side of the image is the right side of the brain). This component exhibited a significant main effect of Time, and a significant interaction between Valence and Time.
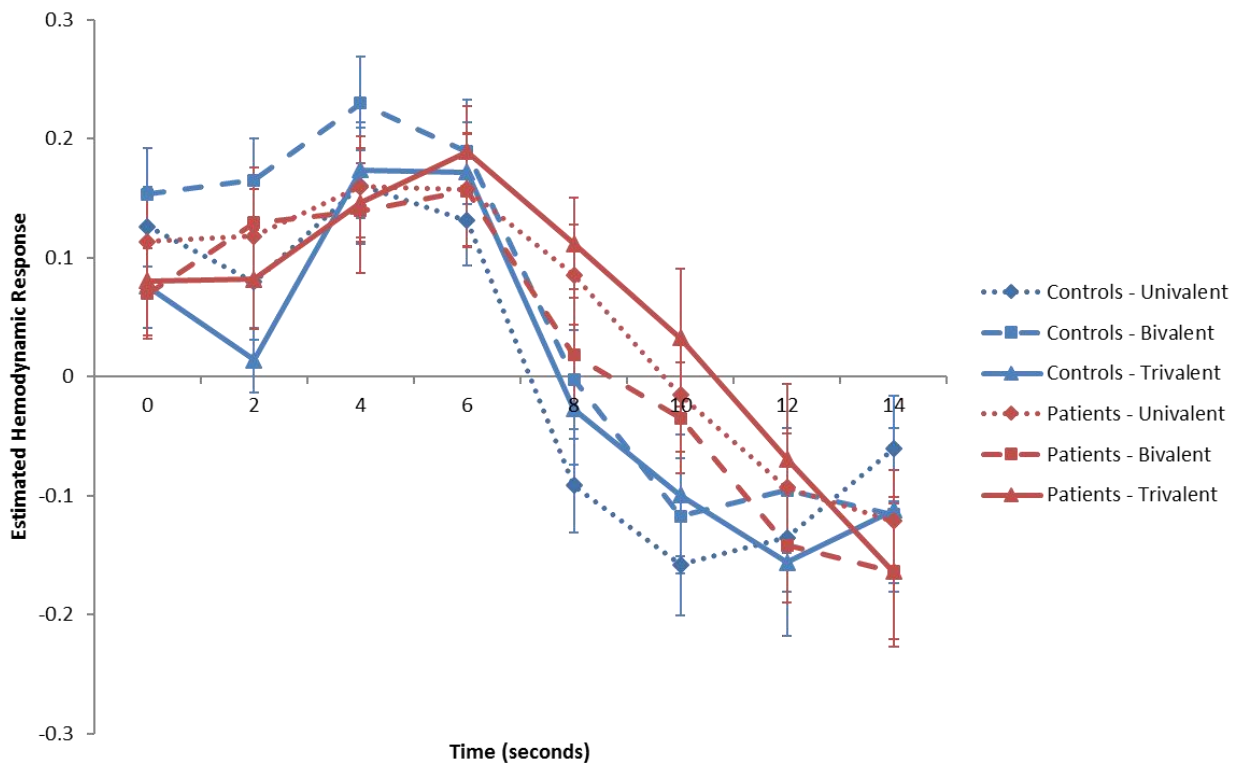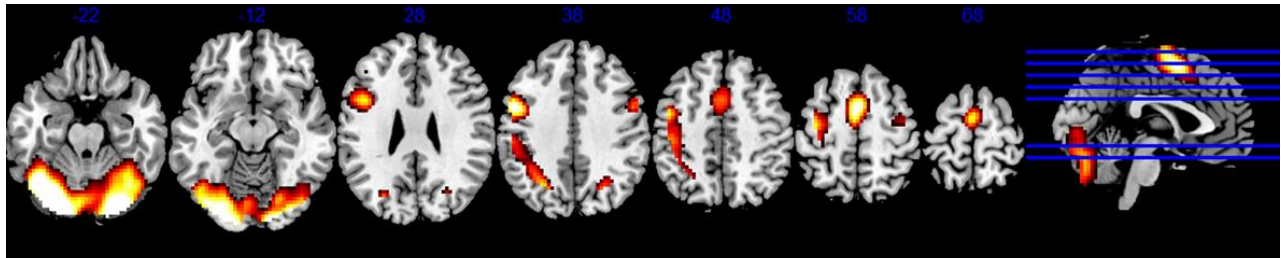
Figure 10. Component 2 from the fMRI-CPCA analysis. The upper image depicts the dominant 10% of component loadings for Component 2 from the fMRI-CPCA analysis. Positive loadings are depicted in red/yellow, and negative loadings are depicted in blue/green, and represent task-based increases and decreases (respectively) in BOLD signal. The lower image depicts the mean FIR-based predictor weights plotted as a function of post-stimulus time. Data from control subjects are plotted in blue, and data from schizophrenia patients are plotted in red. The axial slices in the image are located at the MNI z-axis coordinates: -22, -12, 8, 18, 28, 38, and 58. Images are in neurological convention (i.e., the right side of the image is the right side of the brain). This component exhibited a significant main effects of Time and Valence, as well as significant interactions between Valence and Time, and Valence and Group. Note: The star above the legend indicates a Group effect, in this case, a significant interaction between Valence and Group.

Figure 11. Component 3 from the fMRI-CPCA analysis. The upper image depicts the dominant 10% of component loadings for Component 3 from the fMRI-CPCA analysis. Positive loadings are depicted in red/yellow, and negative loadings are depicted in blue/green, and represent task-based increases and decreases (respectively) in BOLD signal. This is reversed when the estimated HRF crosses the baseline. The lower image depicts the mean FIR-based predictor weights plotted as a function of post-stimulus time. Data from control subjects are plotted in blue, and data from schizophrenia patients are plotted in red. The axial slices in the image are located at the MNI z-axis coordinates: -22, -12, -2, 18, 28, 38 and 48. Images are in neurological convention (i.e., the right side of the image is the right side of the brain). This component exhibited a significant main effect of Time, and a significant interaction between Valence and Time.
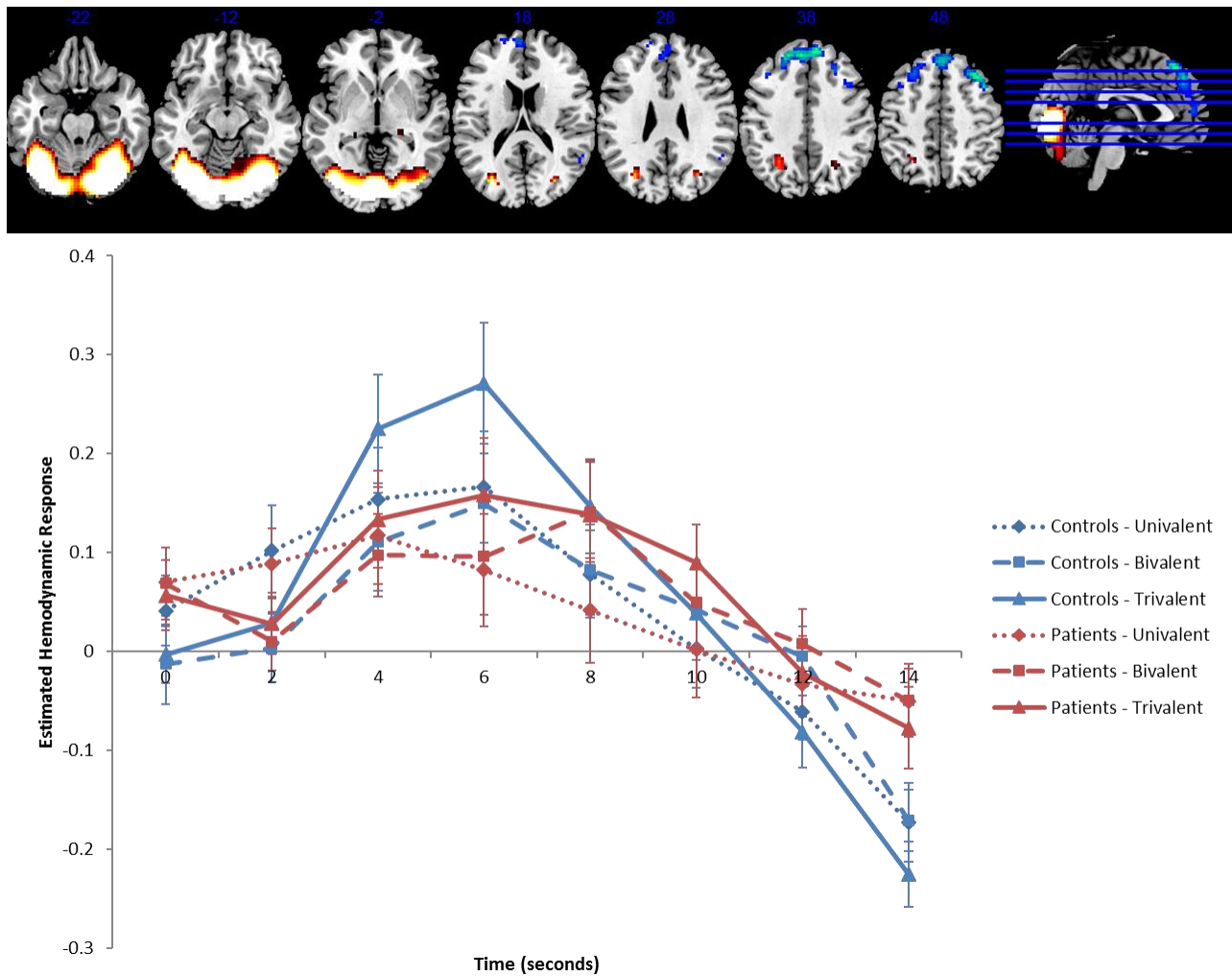
Figure 12. Time-frequency plot averaged over all participants, all frequencies, all trials, and all sensors. Blue areas indicate time-frequencies with decreased power, red areas indicate time-frequencies with increased power. White boxes indicate the alpha (10 +/-3 Hz), beta (20 +/-3 Hz), and theta (6 +/-2 Hz) time-frequencies selected for univariate beamforming analyses. The multivariate MEG analysis examined identical frequency ranges, but a sliding window approach was used to obtain beamforming results that spanned the entire trial.
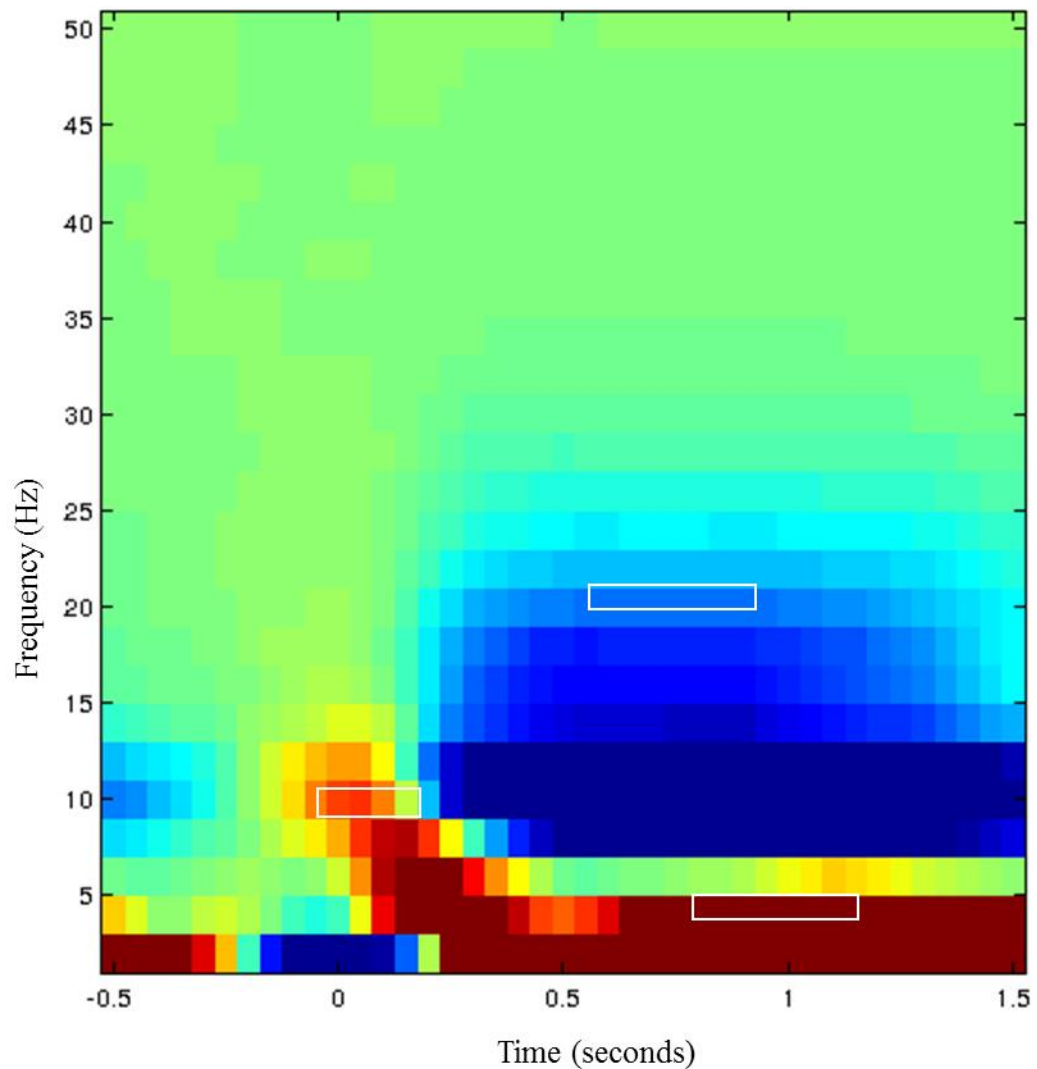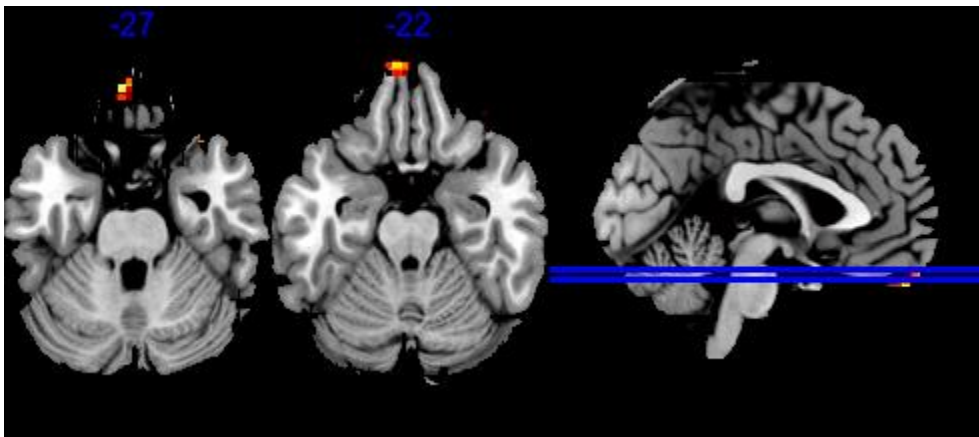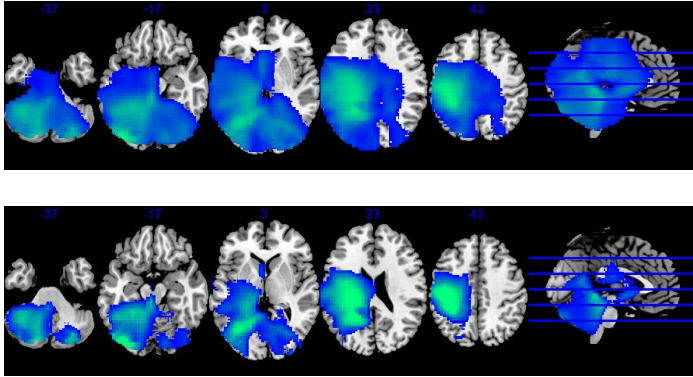
Figure 13. Significant results from the univariate beamformer localized brain activity of the source of 6 Hz (theta) power greater than baseline changes in healthy volunteers. Red/yellow colour indicates an increase in power in this frequency band and condition. Only power changes that exceeded the $p < 0.05$ (FWE) threshold are displayed. Images are in neurological convention (i.e., the right side of the image is the right side of the brain).

    a.   Univalent greater than baseline. The axial slices in both images are located at the MNI z-axis coordinates: -27, -22, 3, and 22.
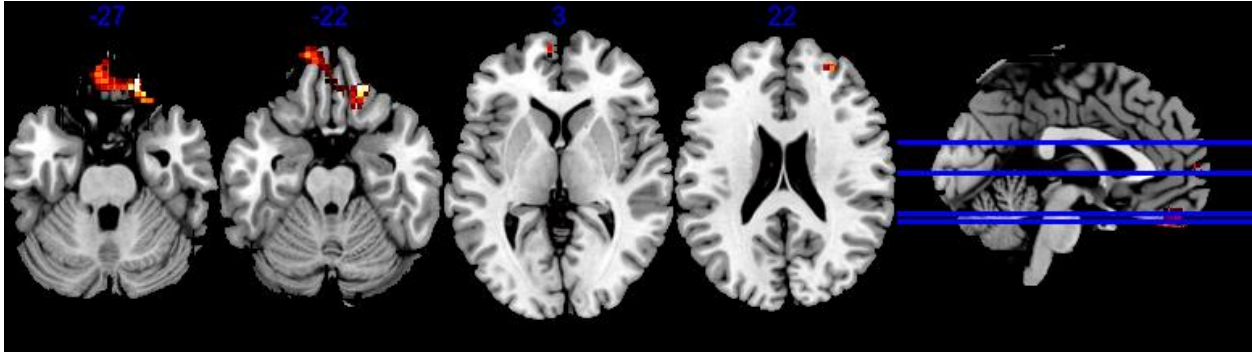
    b.   Bivalent greater than baseline. The axial slices in the image are located at the MNI z-axis coordinates: -27, -22, -17, -12, and -7.
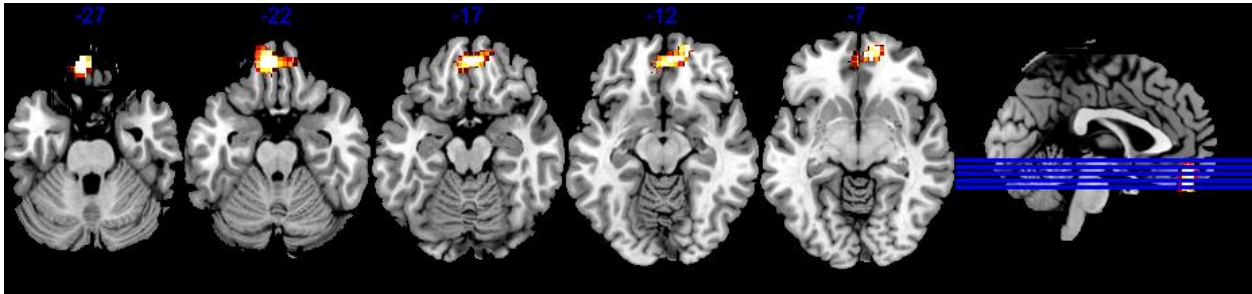
    c.   Bivalent greater than baseline. The axial slices in the image are located at the MNI z-axis coordinates: -27 and -22.
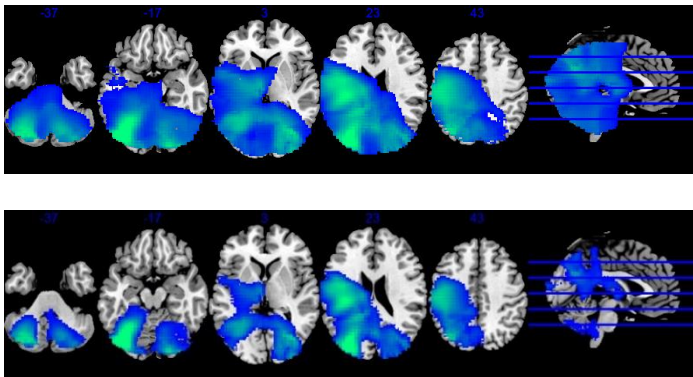
Figure 14. Significant results from the univariate beamformer localized brain activity of the source of 20 Hz (beta) power changes in valence level greater than baseline in healthy volunteers. Blue/green colour indicates a decrease in power in this frequency band and condition. In the upper images, only power changes that exceeded the $p < 0.05$ (FWE) threshold are displayed. In the lower images, the threshold has been increased to show only the largest power changes. Images are in neurological convention (i.e., the right side of the image is the right side of the brain).

    a. Univalent greater than baseline. The axial slices in both images are located at the MNI z-axis coordinates: -37, -17, 3, 23, and 43.

    b. Bivalent greater than baseline. The axial slices in both images are located at the MNI z-axis coordinates: -37, -17, 3, 23, and 43.

    c. Trivalent greater than baseline. The axial slices in both images are located at the MNI z-axis coordinates: -37, -17, 3, 23, and 43.
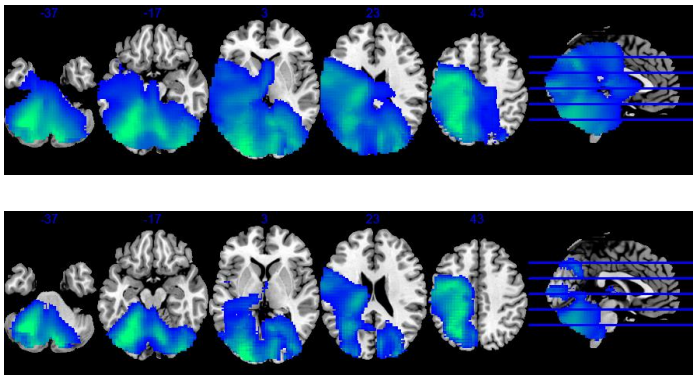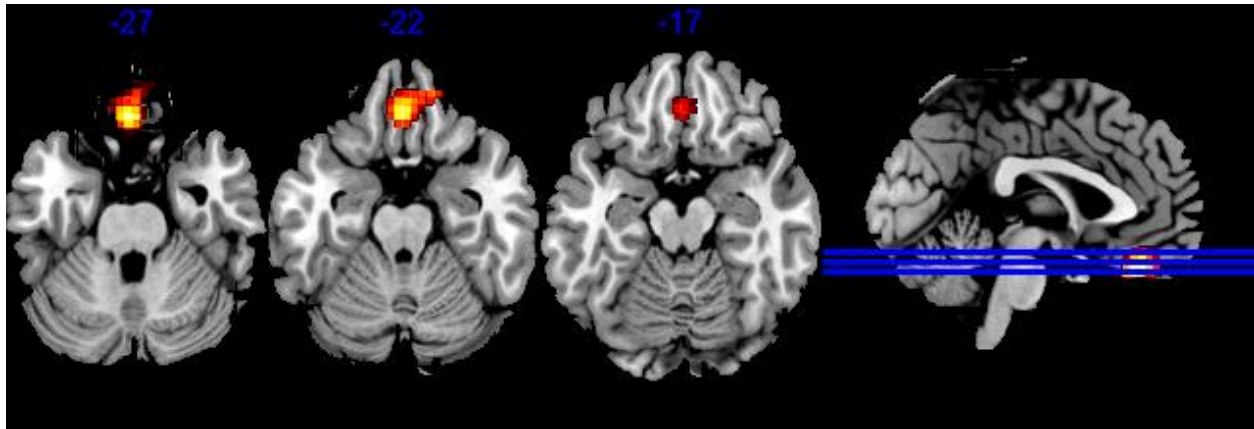
Figure 15. Significant results from the univariate beamformer localized brain activity of the source of the 10 Hz (alpha) power changes in valence related contrasts in healthy volunteers. Only power changes that exceeded the $p < 0.05$ (FWE) threshold are displayed. Red/yellow colour indicates an increase in power in this frequency band. Images are in neurological convention (i.e., the right side of the image is the right side of the brain).

    a. Bivalent stimuli greater than univalent stimuli. The axial slices in the image are located at the MNI z-axis coordinates: -27, -22, and -17.

    b. Trivalent greater than univalent stimuli. The axial slices in this image are located at the MNI z-axis coordinates: -27 and -22.
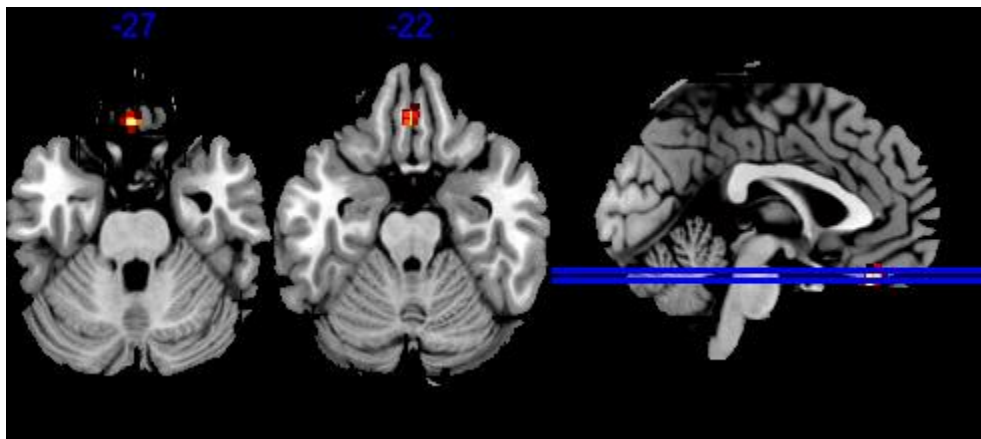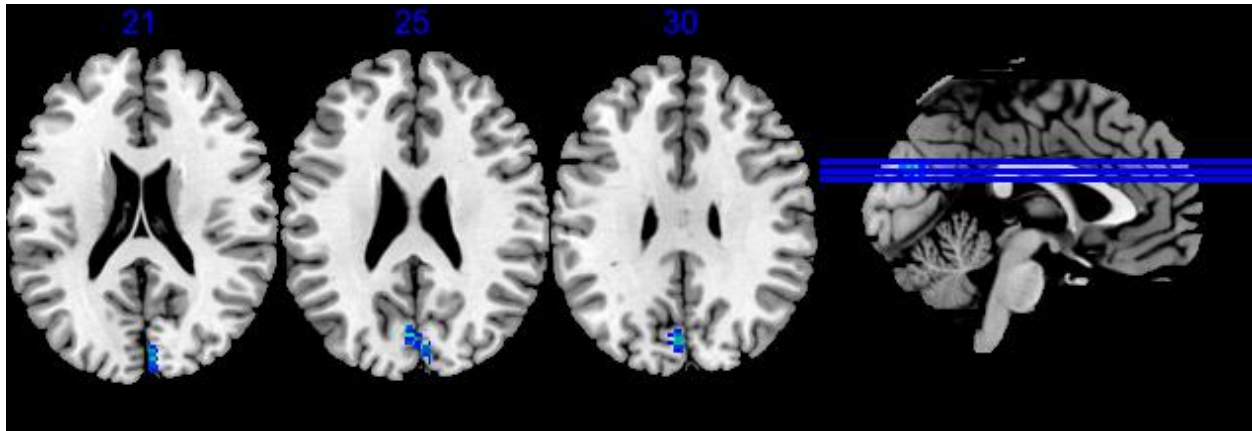
Figure 16. Significant results from the univariate beamformer localized brain activity of the source of the 20 Hz (beta) power changes in valence related contrasts in healthy volunteers. Only power changes that exceeded the $p < 0.05$ (FWE) threshold are displayed. Blue/green colour indicates a decrease in power in this frequency band. Images are in neurological convention (i.e., the right side of the image is the right side of the brain).

a. Bivalent stimuli greater than univalent stimuli. The axial slices in the image are located at the MNI z-axis coordinates: 21, 25, and 30.

b. Trivalent greater than univalent stimuli, The axial slices in the image are located at the MNI z-axis coordinates: -27, -22, -17, 1, and 33.
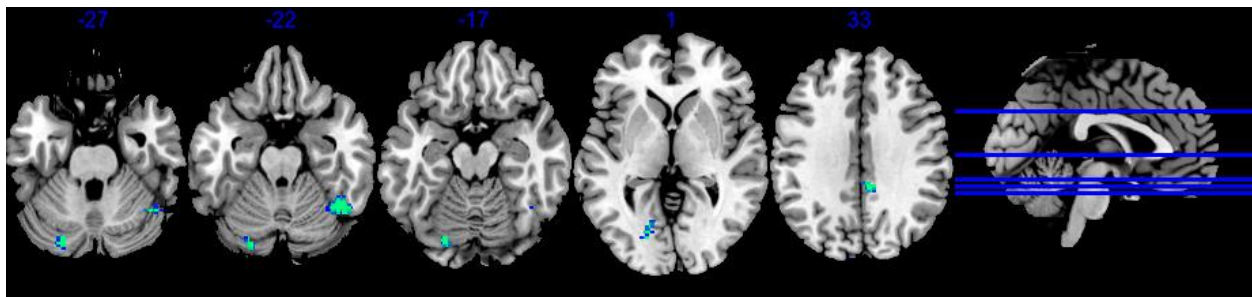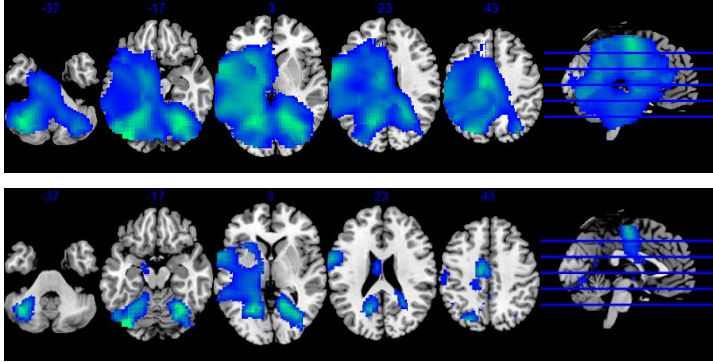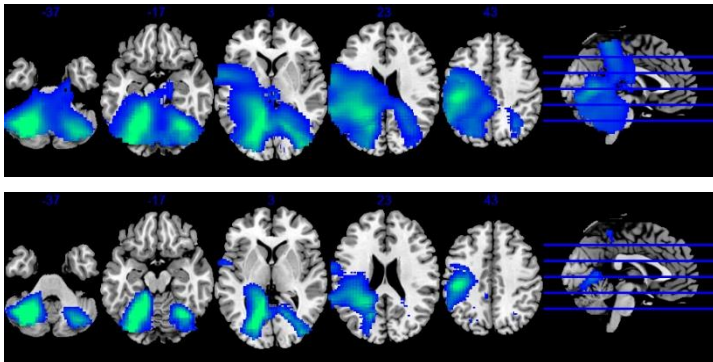
Figure 17. Significant results from the univariate beamformer localized brain activity of the source of 20 Hz (beta) power changes in valence level greater than baseline in schizophrenia patients. Blue/green colour indicates a decrease in power in this frequency band and condition. In the upper images, only power changes that exceeded the $p < 0.05$ (FWE) threshold are displayed. In the lower images, the threshold has been increased to show only the largest power changes. Images are in neurological convention (i.e., the right side of the image is the right side of the brain).

  a. Univalent greater than baseline. The axial slices in both images are located at the MNI z-axis coordinates: -37, -17, 3, 23, and 43.

  b. Bivalent greater than baseline. The axial slices in both images are located at the MNI z-axis coordinates: -37, -17, 3, 23, and 43

  c. Trivalent greater than baseline. The axial slices in both images are located at the MNI z-axis coordinates: -37, -17, 3, 23, and 43.
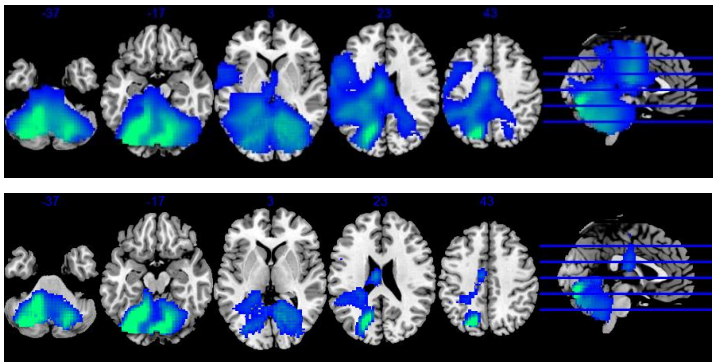
Figure 18. Component 1 from the MEG-PCA analysis. The upper brain images depict the dominant 10% of component loadings for the 20 Hz (beta) band from Component 1 from the MEG-PCA analysis. Negative loadings are depicted in blue/green. These loadings represent task-based decreases in power. This is reversed when the estimated power crosses the baseline. The lower image depicts the mean component scores plotted as a function of post-stimulus time. Data from control subjects are plotted in blue, and data from schizophrenia patients are plotted in red. The axial slices in the image are located at the MNI z-axis coordinates: -22, -12, -2, 8, 18, 28, 38, 48, and 58. Images are in neurological convention (i.e., the right side of the image is the right side of the brain). This component exhibited a significant main effect of Time, and a trend in the interaction between Time and Group. Note: The star above the legend indicates a Group effect, in this case, a trend in the interaction between Time and Group.
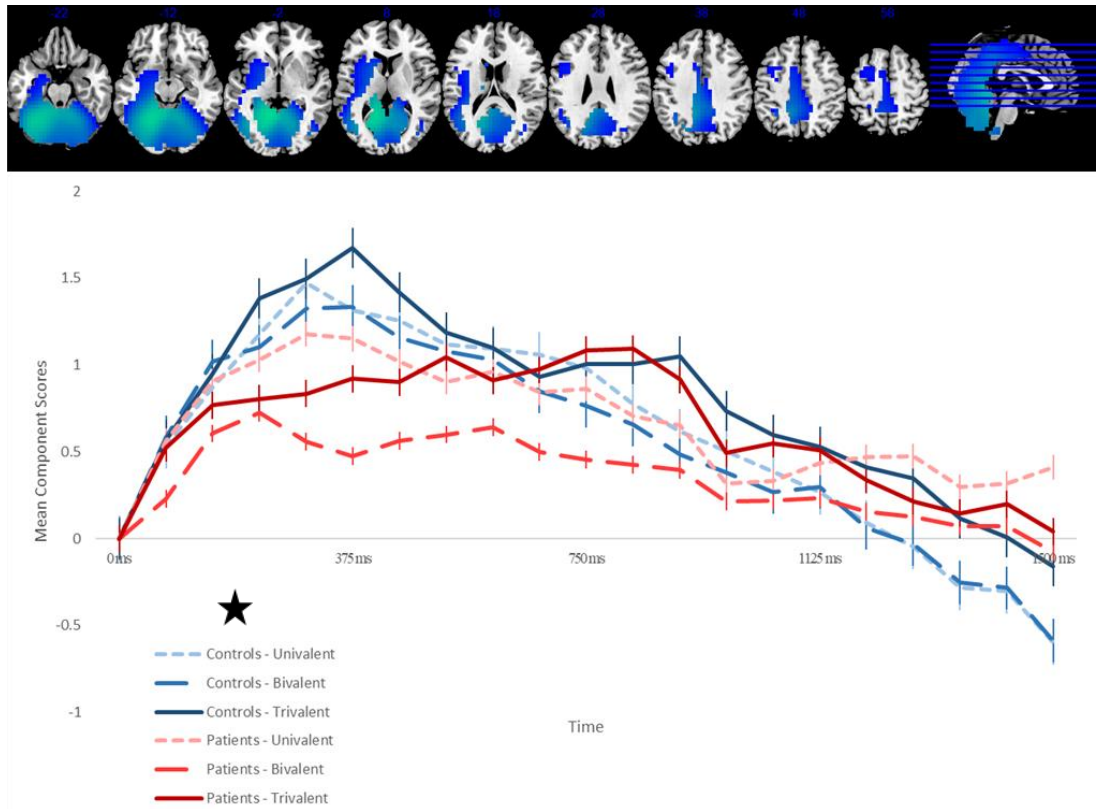
Figure 19. Component 2 from the MEG-PCA analysis. The upper brain images depict the dominant 10% of component loadings for the 6 Hz (theta) band from Component 2 from the MEG-PCA analysis. Negative loadings are depicted in blue/green. These loadings represent task-based decreases in power. The lower image depicts the mean component scores plotted as a function of post-stimulus time. Data from control subjects are plotted in blue, and data from schizophrenia patients are plotted in red. The axial slices in the image are located at the MNI z-axis coordinates: -22, **-**12, -2, 8, 18, 28, and 38. Images are in neurological convention (i.e., the right side of the image is the right side of the brain). This component exhibited a significant main effect of Time.
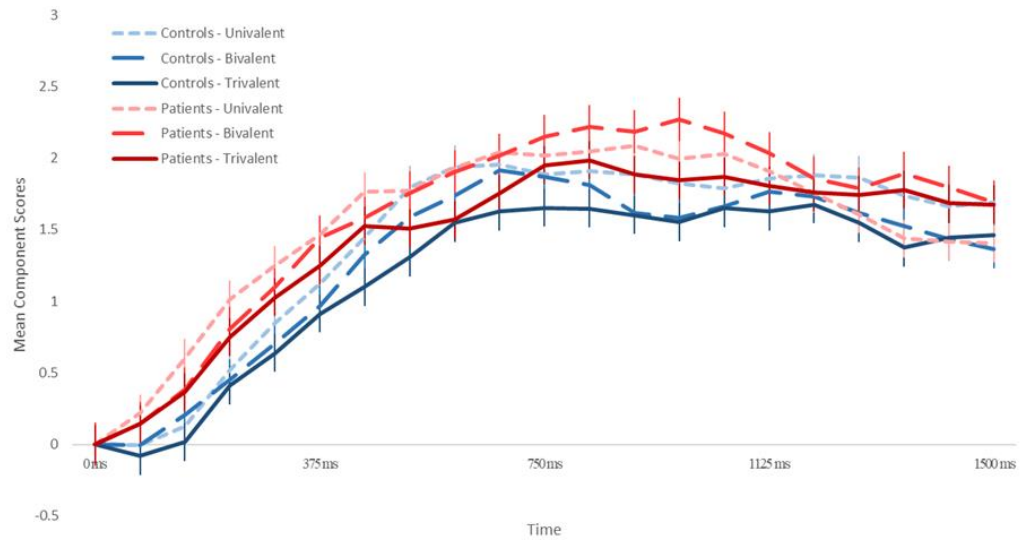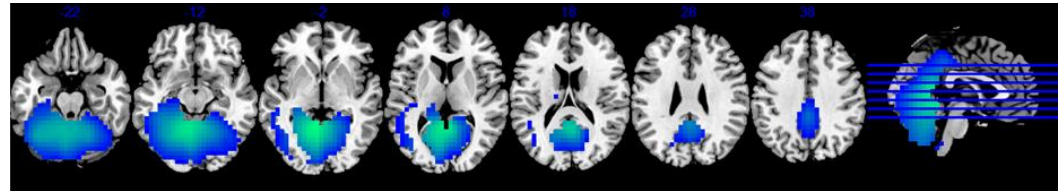
Figure 20. Component 3 from the MEG-PCA analysis. The upper brain images depict the dominant 10% of component loadings for the 10 Hz (alpha) band from Component 3 from the MEG-PCA analysis. Negative loadings are depicted in blue/green. These loadings represent task-based decreases in power. The lower image depicts the mean component scores plotted as a function of post-stimulus time. Data from control subjects are plotted in blue, and data from schizophrenia patients are plotted in red. The axial slices in the image are located at the MNI z-axis coordinates: -32, -22, **-**12, -2, 8, 18, and 28. Images are in neurological convention (i.e., the right side of the image is the right side of the brain). This component exhibited a significant main effect of Time, a trend towards a main effect of Group, and a trend-level interaction between Time and Group. Note: The star beside the legend indicates a Group effect, in this case, trends in the main effect of Group, and in the interaction between Time and Group.

Figure 21. Component 4 from the MEG-PCA analysis. The upper brain images depict the dominant 10% of component loadings for the 6 Hz (theta) and 10 Hz (alpha) bands from Component 4 from the MEG-PCA analysis. Negative loadings are depicted in blue/green. These loadings represent task-based decreases in power. The lower image depicts the mean component scores plotted as a function of post-stimulus time. Data from control subjects are plotted in blue, and data from schizophrenia patients are plotted in red. The axial slices in both of the images are located at the MNI z-axis coordinates: -12, -2, 8, 18, 28, and 38. Images are in neurological convention (i.e., the right side of the image is the right side of the brain). This component exhibited a significant main effect of Time, and a trend towards an interaction between Valence and Time.
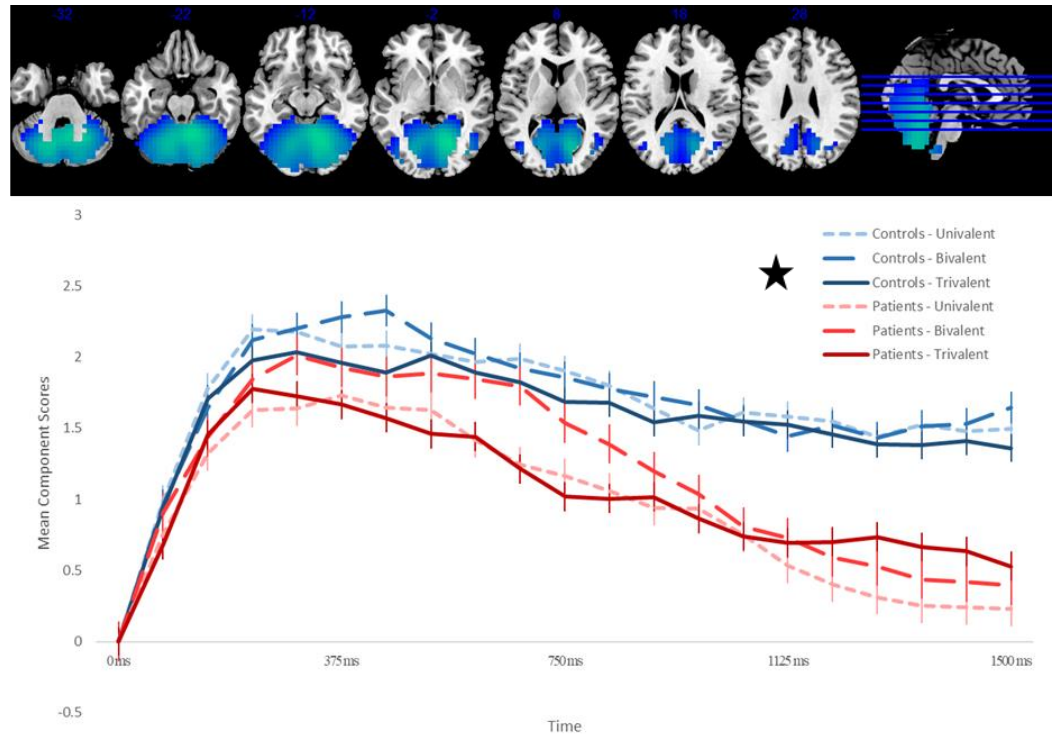
Figure 22. Component 5 from the MEG-PCA analysis. The upper brain images depict the dominant 10% of component loadings for the 10 Hz (alpha) band from Component 5 from the MEG-PCA analysis. Positive loadings are depicted in red/yellow. These loadings represent task-based increases in power. The lower image depicts the mean component scores plotted as a function of post-stimulus time. Data from control subjects are plotted in blue, and data from schizophrenia patients are plotted in red. The axial slices in the image are located at the MNI z-axis coordinates: -2, 8, 18, 28, 38, 48, and 58. Images are in neurological convention (i.e., the right side of the image is the right side of the brain). This component exhibited significant main effects of Time and Group. Note: The star beside the legend indicates a Group effect, in this case, a significant main effect of Group.
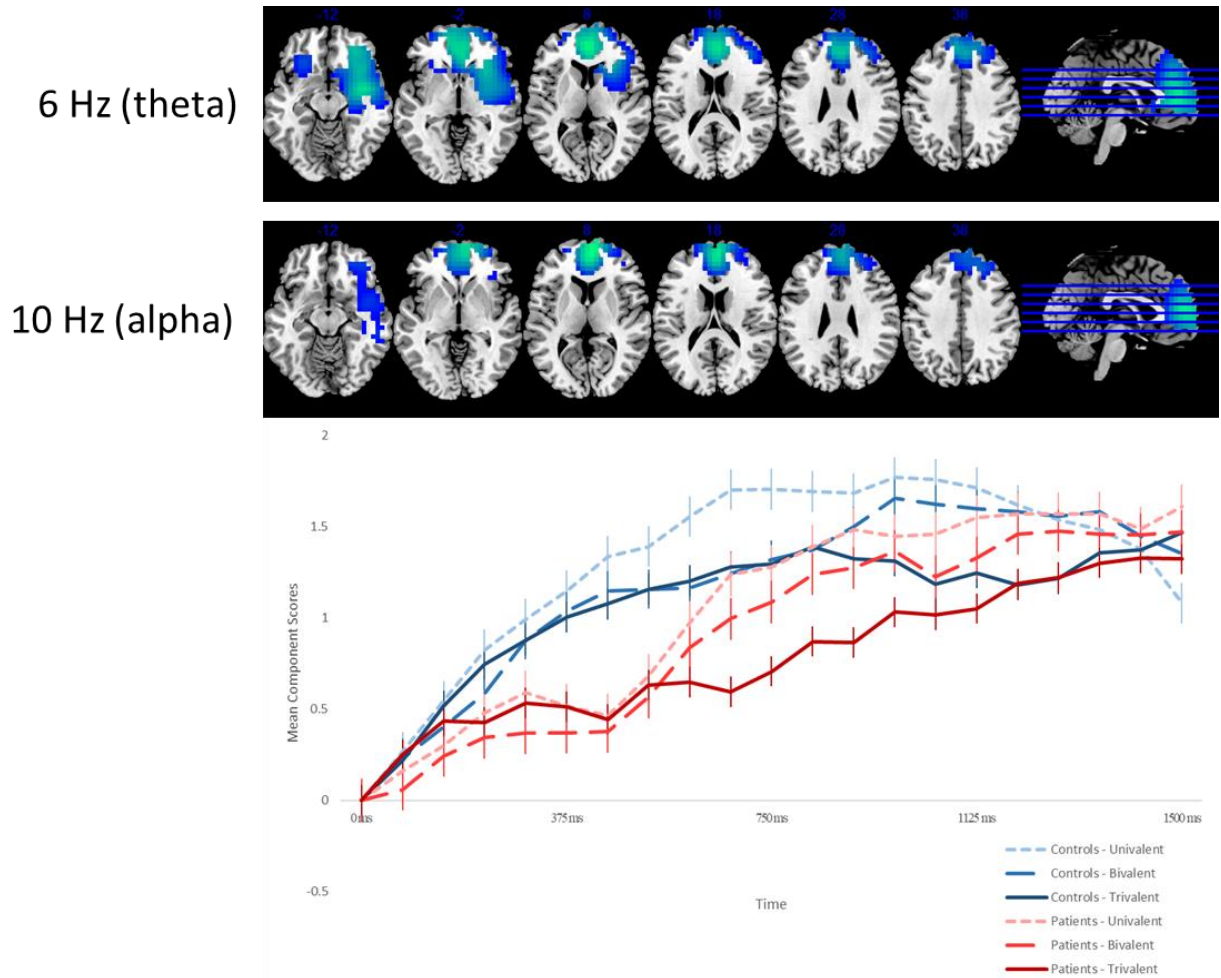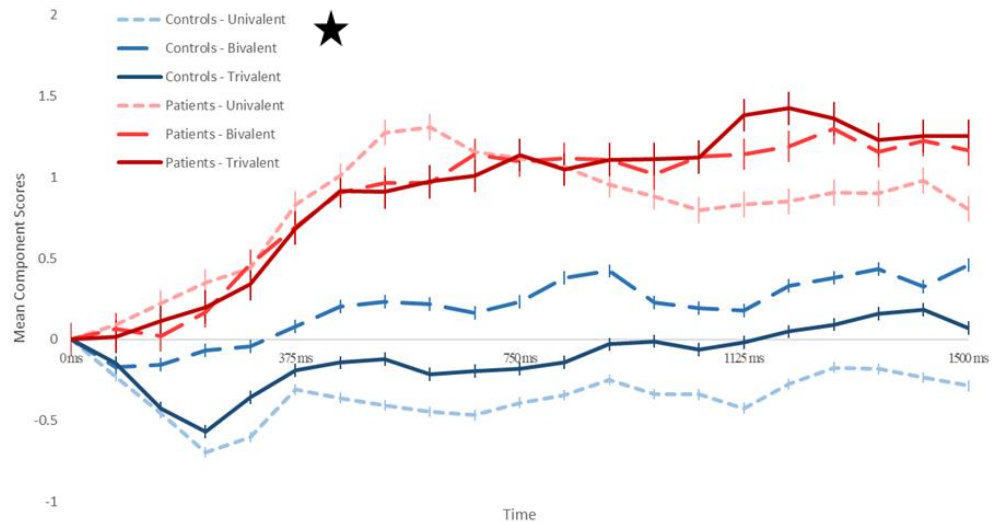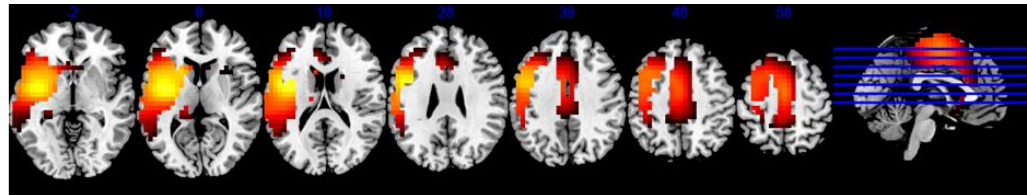
Figure 23. Component 6 from the MEG-PCA analysis. The upper brain images depict the dominant 10% of component loadings for the 10 Hz (alpha) and 20 Hz (beta) bands from Component 6 from the MEG-PCA analysis. Positive loadings are depicted in red/yellow and represent task-based increases in power. The lower image depicts the mean component scores plotted as a function of post-stimulus time. Data from control subjects are plotted in blue, and data from schizophrenia patients are plotted in red. The axial slices in both the images are located at the MNI z-axis coordinates: -2, 8, 18, 28, 38, 48, and 58. Images are in neurological convention (i.e., the right side of the image is the right side of the brain). This component exhibited a significant main effect of Time, and a trend in the interaction between Valence and Time.

Figure 24. Component 1 of the multivariate multimodal MEG-fMRI-CPCA (*BH'*-CPCA) analysis. The brain images are the dominant 10% of loadings from the components from the original fMRI-CPCA analysis and the bar graphs specify the correlations between the spatial patterns of the fMRI-CPCA (*H*) and MEG-PCA components (*V*) and index the relative contributions of each MEG frequency band. The line graphs below depict the mean component scores (*U* from the Equation 10) plotted as a function of post-stimulus time. Images are in neurological convention (i.e., the right side of the image is the right side of the brain). This component exhibited a significant main effect of Time.
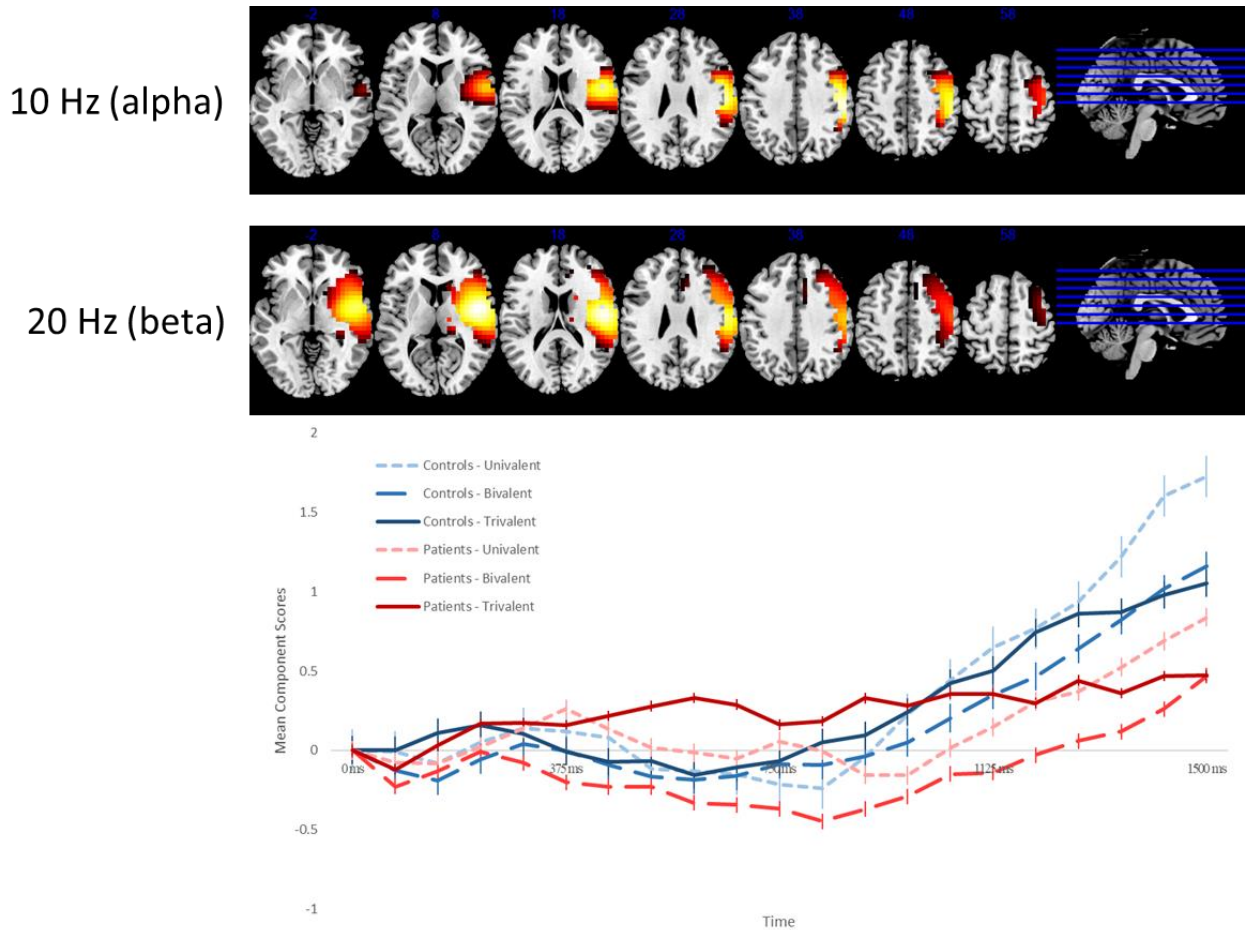

fMRI-CPCA-1

fMRI-CPCA-2

fMRI-CPCA-3

Figure 25. Component 2 of the multivariate multimodal MEG-fMRI-CPCA (*BH'*-CPCA) analysis. The brain images are the dominant 10% of loadings from the components from the original fMRI-CPCA analysis and the bar graphs specify the correlations between the spatial patterns of the fMRI-CPCA (*H*) and MEG-PCA components (*V*) and index the relative contributions of each MEG frequency band. The line graphs below depict the mean component scores (*U* from the Equation 10) plotted as a function of post-stimulus time. Images are in neurological convention (i.e., the right side of the image is the right side of the brain). This component exhibited a significant main effect of Time, and a trend in the interaction between Time and Group. Note: The star beside the legend indicates a Group effect, in this case, a trend in the interaction between Time and Group.

fMRI-CPCA-1   fMRI-CPCA-2   fMRI-CPCA-3

175

Figure 26. Component 1 from the multivariate multimodal *E*-CPCA analysis. The upper brain images depict the dominant 10% of component loadings for the 6 Hz (theta), 10 Hz (alpha), and 20 Hz (beta) bands from Component 1 from the multivariate multimodal *E*-CPCA analysis. Positive loadings are depicted in red/yellow and represent task-based increases in power, and negative loadings are depicted in blue/green, and represent task-based decreases in power. The lower image depicts the mean component scores plotted as a function of post-stimulus time. Data from control subjects are plotted in blue, and data from schizophrenia patients are plotted in red. The line graphs depict the mean component scores plotted as a function of post-stimulus time. The axial slices in the image are located at the MNI z-axis coordinates: 6 Hz: -2, 8, and 18; 10 Hz: -12, -, 8, 18, and 28; 20 Hz: -32, -12, -2, 8, and 18. Images are in neurological convention (i.e., the right side of the image is the right side of the brain). This component exhibited a significant main effect of Time.
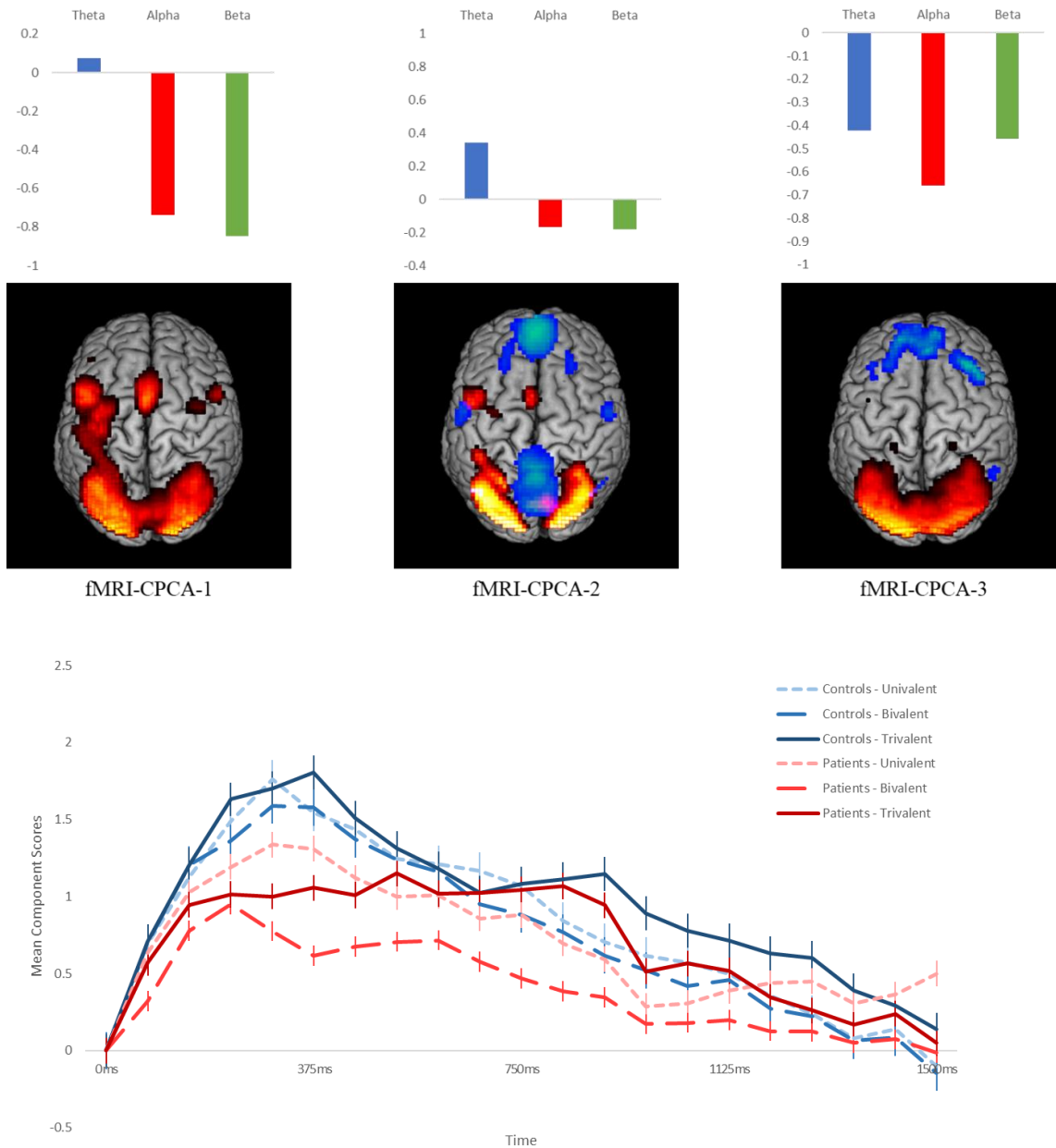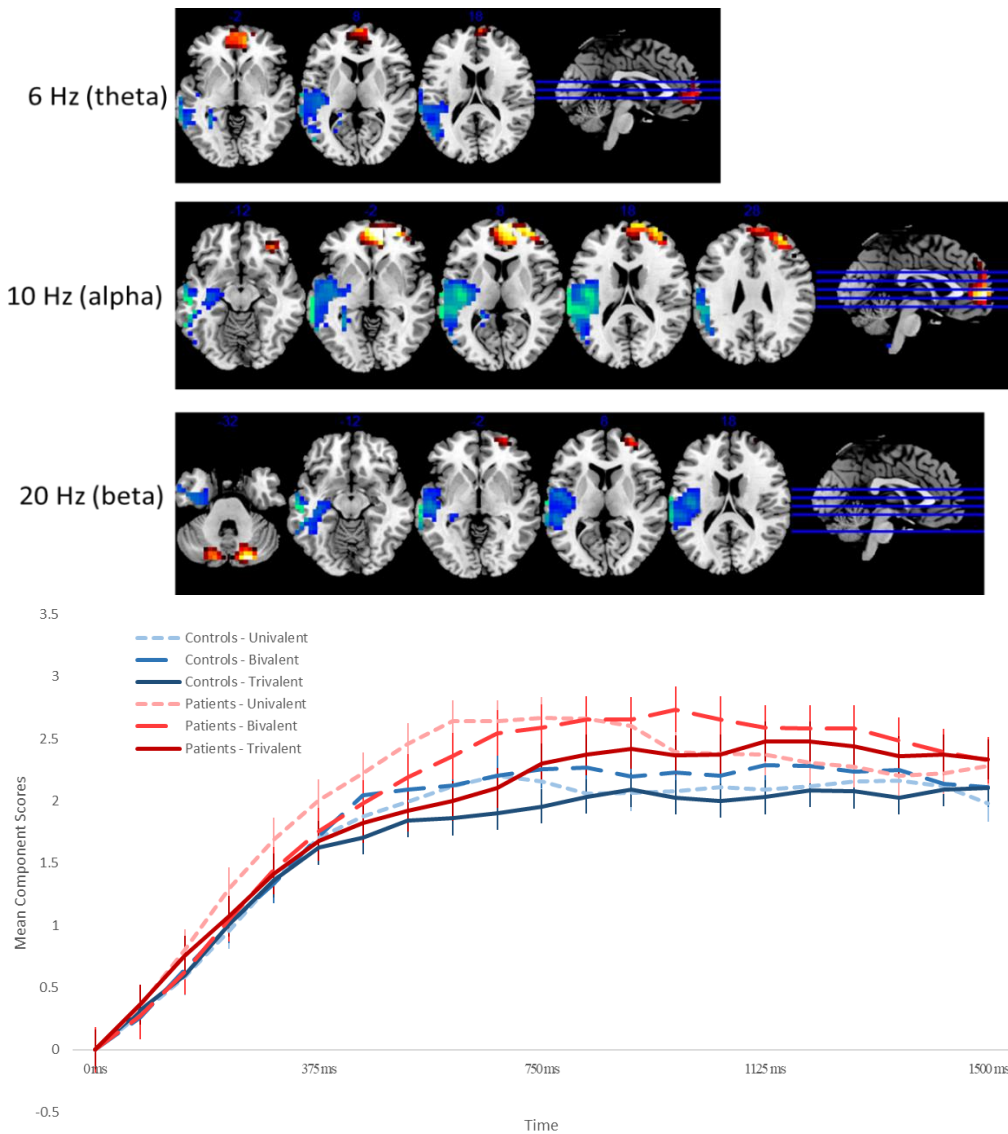
Figure 27. Component 2 from the multivariate multimodal *E*-CPCA analysis. The upper brain images depict the dominant 10% of component loadings for the 6 Hz (theta), 10 Hz (alpha), and 20 Hz (beta) bands from Component 2 from the multivariate multimodal *E*-CPCA analysis. Positive loadings are depicted in red/yellow and represent task-based increases in power, and negative loadings are depicted in blue/green, and represent task-based decreases in power. The lower image depicts the mean component scores plotted as a function of post-stimulus time. Data from control subjects are plotted in blue, and data from schizophrenia patients are plotted in red. The line graphs depict the mean component scores plotted as a function of post-stimulus time. The axial slices in the image are located at the MNI z-axis coordinates: 6 Hz: -22, **-**12, -2, 18 and 28; 10 Hz: -2, 8, 18, 48, and 58; 20 Hz: 48 and 58. Images are in neurological convention (i.e., the right side of the image is the right side of the brain). This component exhibited a significant main effect of Time, and a significant interaction between Valence and Time.
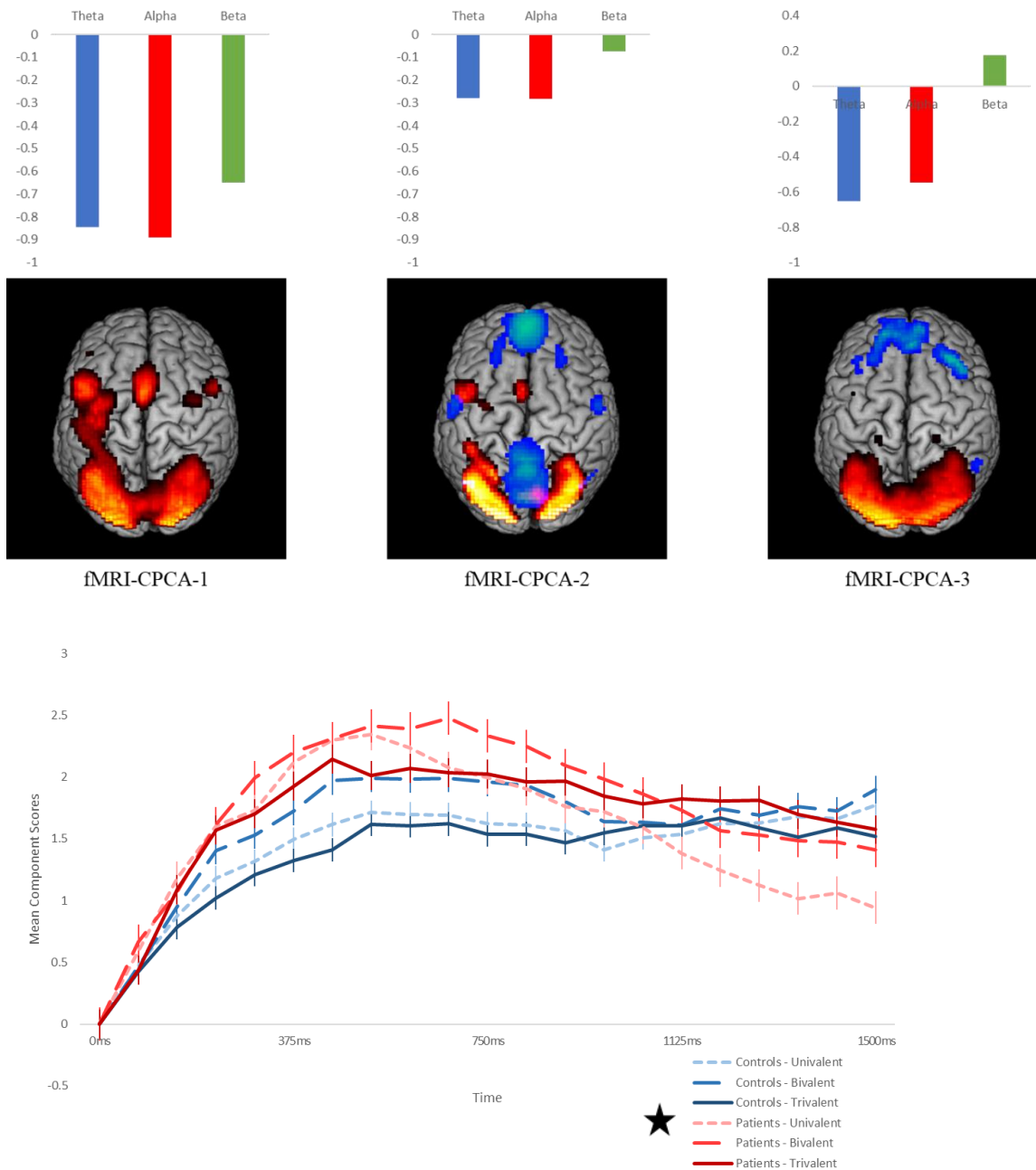

177
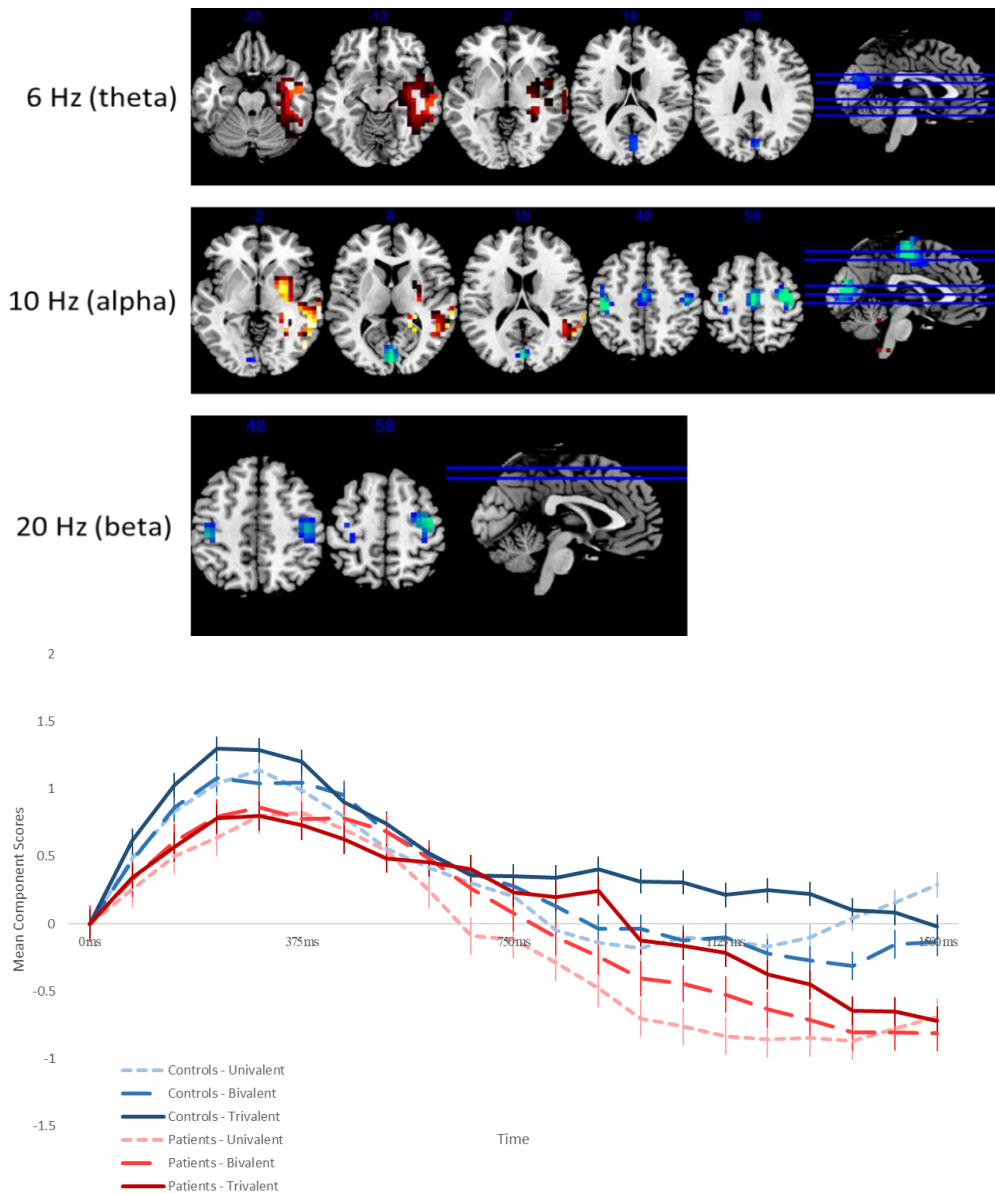
Figure 28. Component 3 from the multivariate multimodal E-CPCA analysis. The upper brain images depict the dominant 10% of component loadings for the 10 Hz (alpha) and 20 Hz (beta) bands from Component 3 from the multivariate multimodal E-CPCA analysis. Positive loadings are depicted in red/yellow and represent task-based increases in power, and negative loadings are depicted in blue/green, and represent task-based decreases in power. The lower image depicts the mean component scores plotted as a function of post-stimulus time. Data from control subjects are plotted in blue, and data from schizophrenia patients are plotted in red. The line graphs depict the mean component scores plotted as a function of post-stimulus time. The axial slices in both the images are located at the MNI z-axis coordinates: -32, 18, 28, 38, 48, and 58. Images are in neurological convention (i.e., the right side of the image is the right side of the brain). This component exhibited a significant main effect of Time, and a trend towards an interaction between Time and Gro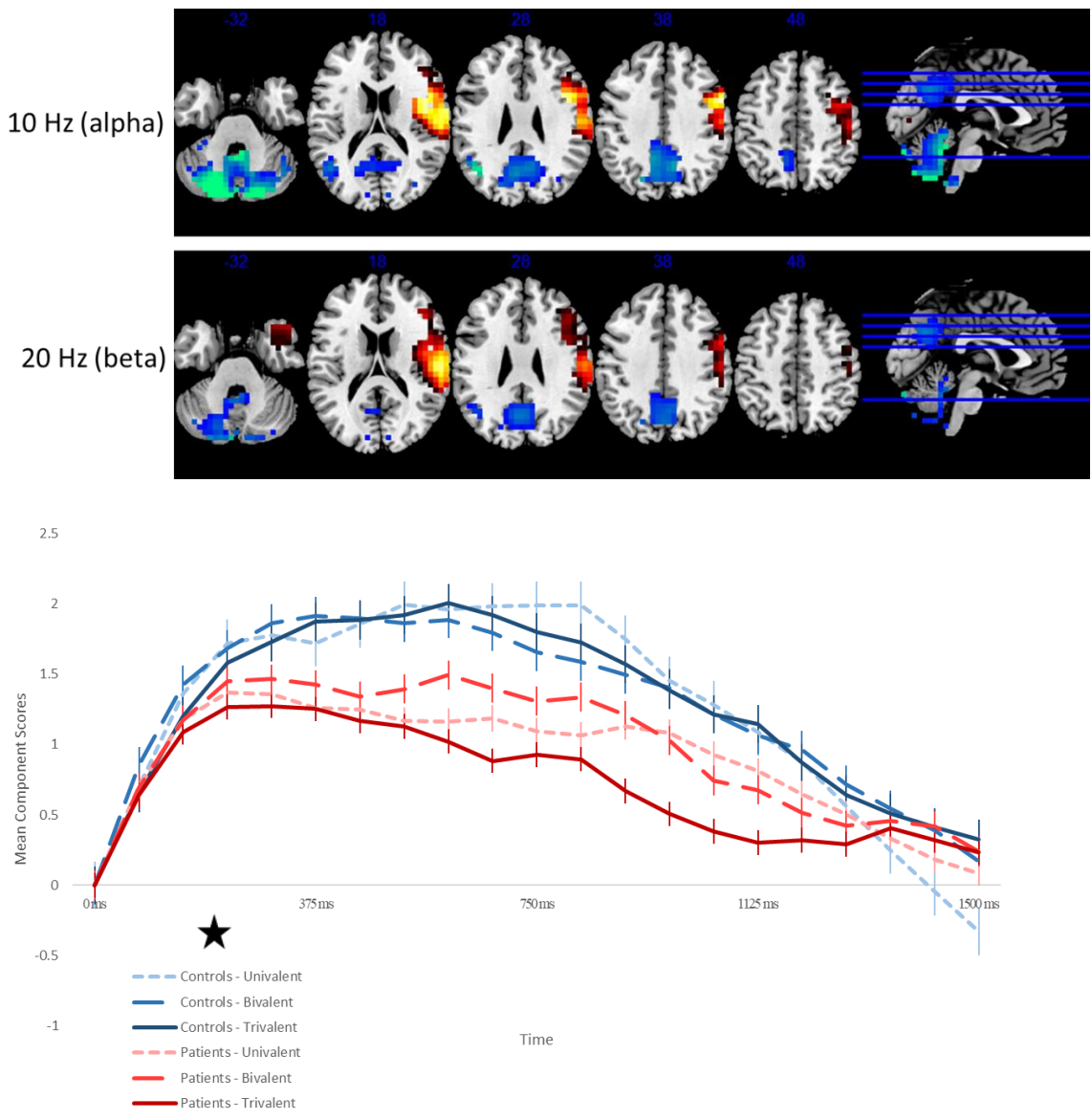up. Note: The star beside the legend indicates a Group effect, in this case, a trend in the interaction between Time and Group.

References

Adams, R., & David, A. S. (2007). Patterns of anterior cingulate activation in schizophrenia: a selective review. *Neuropsychiatric Disease and Treatment*, *3*(1), 87–101.

Alvarez, J. A., & Emory, E. (2006). Executive Function and the Frontal Lobes: A Meta-Analytic Review. *Neuropsychology Review*, *16*(1), 17–42.

American Psychiatric Association. Task Force on DSM-IV, A. P. A. (2000). *Diagnostic and statistical manual of mental disorders : DSM-IV-TR.* Washington, DC: American Psychiatric Association.

Ances, B. M., Leontiev, O., Perthen, J. E., Liang, C., Lansing, A. E., & Buxton, R. B. (2008). Regional differences in the coupling of cerebral blood flow and oxygen metabolism changes in response to activation: implications for BOLD-fMRI. *NeuroImage*, *39*(4), 1510–21.

Anderson, M. C., Ochsner, K. N., Kuhl, B., Cooper, J., Robertson, E., Gabrieli, S. W., … Gabrieli, J. D. E. (2004). Neural systems underlying the suppression of unwanted memories. *Science (New York, N.Y.)*, *303*(5655), 232–235.

Arndt, S. (1995). A Longitudinal Study of Symptom Dimensions in Schizophrenia. *Archives of General Psychiatry*, *52*(5), 352.

Aron, A. R. (2007). The neural basis of inhibition in cognitive control. *The Neuroscientist : A Review Journal Bringing Neurobiology, Neurology and Psychiatry*, *13*(3), 214–28.

Aron, A. R., Robbins, T. W., & Poldrack, R. A. (2004). Inhibition and the right inferior frontal cortex. *Trends in Cognitive Sciences*, *8*(4), 170–7.

Aron, A. R., Robbins, T. W., & Poldrack, R. A. (2014). Inhibition and the right inferior frontal cortex: one decade on. *Trends in Cognitive Sciences*, *18*(4), 177–185.

Attwell, D., & Iadecola, C. (2002). The neural basis of functional brain imaging signals. *Trends in Neurosciences*, *25*(12), 621–625.

Barch, D. M. (2005). The cognitive neuroscience of schizophrenia. *Annual Review of Clinical Psychology*, *1*, 321–53.

Barch, D. M., Carter, C. S., Arnsten, A., Buchanan, R. W., Cohen, J. D., Geyer, M., … Heinssen, R. (2009). Selecting paradigms from cognitive neuroscience for translation into use in clinical trials: proceedings of the third CNTRICS meeting. *Schizophrenia Bulletin*, *35*(1), 109–14.

Barch, D. M., & Ceaser, A. (2012). Cognition in schizophrenia: core psychological and neural mechanisms. *Trends in Cognitive Sciences*, *16*(1), 27–34.

Bari, A., & Robbins, T. W. (2013). Inhibition and impulsivity: behavioral and neural basis of response control. *Progress in Neurobiology*, *108*, 44–79.

Bauer, M., Kluge, C., Bach, D., Bradbury, D., Heinze, H. J., Dolan, R. J., & Driver, J. (2012). *Cholinergic Enhancement of Visual Attention and Neural Oscillations in the Human Brain*. *Current Biology* (Vol. 22).

Behrens, T. E. J., Woolrich, M. W., Jenkinson, M., Johansen-Berg, H., Nunes, R. G., Clare, S., … Smith, S. M. (2003). Characterization and propagation of uncertainty in diffusion-weighted MR imaging. *Magnetic Resonance in Medicine : Official Journal of the Society of*

Magnetic Resonance in Medicine / Society of Magnetic Resonance in Medicine, *50*(5), 1077–88.

Belardinelli, P., Ortiz, E., & Braun, C. (2012). Source activity correlation effects on LCMV Beamformers in a realistic measurement environment. *Computational and Mathematical Methods in Medicine*, *2012*, 190513.

Bell, A. J., & Sejnowski, T. J. (1995). An information-maximization approach to blind separation and blind deconvolution. *Neural Comput*, *7*(6), 1129–1159.

Benedek, M., Bergner, S., Könen, T., Fink, A., & Neubauer, A. C. (2011). EEG alpha synchronization is related to top-down processing in convergent and divergent thinking. *Neuropsychologia*, *49*(12), 3505–3511.

Biessmann, F., Plis, S. M., Meinecke, F. C., Eichele, T., & Müller, K.-R. (2011). Analysis of multimodal neuroimaging data. *IEEE Reviews in Biomedical Engineering*, *4*, 26–58.

Blasi, G., Goldberg, T. E., Weickert, T. W., Das, S., Kohn, P. D., Zoltick, B., … Mattay, V. S. (2006). Brain regions underlying response inhibition and interference monitoring and suppression. *The European Journal of Neuroscience*, *23*(6), 1658–64.

Blishen, B. R., Carroll, W. K., & Moore, C. (2008). The 1981 socioeconomic index for occupations in Canada. *Canadian Review of Sociology/Revue Canadienne de Sociologie*, *24*(4), 465–488.

Bora, E., Fornito, A., Radua, J., Walterfang, M., Seal, M., Wood, S. J., … Pantelis, C. (2011). Neuroanatomical abnormalities in schizophrenia: A multimodal voxelwise meta-analysis and meta-regression analysis. *Schizophrenia Research*, *127*(1), 46–57.

Botvinick, M. M. (2007). Conflict monitoring and decision making: Reconciling two perspectives on anterior cingulate function. *Cognitive, Affective, & Behavioral Neuroscience*, *7*(4), 356–366.

Botvinick, M. M., & Braver, T. S. (2014). Motivation and cognitive control: from behavior to neural mechanism. *Annual Review of Psychology*, *66*, 83–113.

Botvinick, M. M., Braver, T. S., Barch, D. M., Carter, C. S., & Cohen, J. D. (2001). Conflict monitoring and cognitive control. *Psychological Review*, *108*(3), 624–52.

Botvinick, M. M., Cohen, J. D., & Carter, C. S. (2004). Conflict monitoring and anterior cingulate cortex: An update. *Trends in Cognitive Sciences*.

Brandt, C. L., Eichele, T., Melle, I., Sundet, K., Server, A., Agartz, I., … Andreassen, O. A. (2014). Working memory networks and activation patterns in schizophrenia and bipolar disorder: comparison with healthy controls. *The British Journal of Psychiatry : The Journal of Mental Science*, *204*(4), 290–8.

Braver, T. S. (2012). The variable nature of cognitive control: a dual mechanisms framework. *Trends in Cognitive Sciences*, *16*(2), 106–113.

Brefczynski, J. A., & DeYoe, E. A. (1999). A physiological correlate of the "spotlight" of visual attention. *Nature Neuroscience*, *2*(4), 370–374.

Brinkman, L., Stolk, A., Dijkerman, H. C., de Lange, F. P., & Toni, I. (2014). Distinct roles for alpha- and beta-band oscillations during mental simulation of goal-directed actions. *The Journal of Neuroscience : The Official Journal of the Society for Neuroscience*, *34*(44),

14783–92.

Brinkman, L., Stolk, A., Marshall, T. R., Esterer, S., Sharp, P., Dijkerman, H. C., … Toni, I. (2016). Independent Causal Contributions of Alpha- and Beta-Band Oscillations during Movement Selection. *The Journal of Neuroscience : The Official Journal of the Society for Neuroscience*, *36*(33), 8726–33.

Brookes, M. J., Hale, J. R., Zumer, J. M., Stevenson, C. M., Francis, S. T., Barnes, G. R., … Nagarajan, S. S. (2011). Measuring functional connectivity using MEG: methodology and comparison with fcMRI. *NeuroImage*, *56*(3), 1082–104.

Brown, P. (2007). Abnormal oscillatory synchronisation in the motor system leads to impaired movement. *Current Opinion in Neurobiology*.

Broyd, S. J., Demanuele, C., Debener, S., Helps, S. K., James, C. J., & Sonuga-Barke, E. J. S. (2009). Default-mode brain dysfunction in mental disorders: A systematic review. *Neuroscience & Biobehavioral Reviews*, *33*(3), 279–296.

Buckner, R. L., Andrews-Hanna, J. R., & Schacter, D. L. (2008). The brain's default network: anatomy, function, and relevance to disease. *Annals of the New York Academy of Sciences*, *1124*, 1–38.

Bucy, P. C., & Fulton, J. F. (1933). Ipsilateral representation in the motor and premotor cortex op monkeys. *Brain*, *56*(3), 318–342.

Buxton, R. B. (2013). The physics of functional magnetic resonance imaging (fMRI). *Reports on Progress in Physics. Physical Society (Great Britain)*, *76*(9), 96601.

Buzsáki, G. (2002). Theta oscillations in the hippocampus. *Neuron*.

Buzsáki, G., & Draguhn, A. (2004). Neuronal oscillations in cortical networks. *Science (New York, N.Y.)*, *304*(5679), 1926–9.

Byun, M. S., Kim, J. S., Jung, W. H., Jang, J. H., Choi, J. S., Kim, S. N., … Kwon, J. S. (2012). Regional cortical thinning in subjects with high genetic loading for schizophrenia. *Schizophrenia Research*, *141*(2–3), 197–203.

Callicott, J. H., Mattay, V. S., Verchinski, B. A., Marenco, S., Egan, M. F., & Weinberger, D. R. (2003). Complexity of prefrontal cortical dysfunction in schizophrenia: More than up or down. *American Journal of Psychiatry*, *160*(12), 2209–2215.

Carter, C. S., Barch, D. M., Buchanan, R. W., Bullmore, E. T., Krystal, J. H., Cohen, J. D., … Heinssen, R. (2008). Identifying cognitive mechanisms targeted for treatment development in schizophrenia: an overview of the first meeting of the Cognitive Neuroscience Treatment Research to Improve Cognition in Schizophrenia Initiative. *Biological Psychiatry*, *64*(1), 4–10.

Carter, C. S., Minzenberg, M. J., West, R., & MacDonald, A. W. (2012). CNTRICS imaging biomarker selections: Executive control paradigms. *Schizophrenia Bulletin*, *38*(1), 34–42.

Cattell, R. B. (1966). The Scree Test For The Number Of Factors. *Multivariate Behavioral Research*, *1*(2), 245–276.

Cavanagh, J. F., & Frank, M. J. (2014). Frontal theta as a mechanism for cognitive control. *Trends in Cognitive Sciences*, *18*(8), 414–421.

Cavanagh, J. F., & Shackman, A. J. (2015). Frontal midline theta reflects anxiety and cognitive

control: Meta-analytic evidence. *Journal of Physiology Paris*, *109*(1–3), 3–15.

Cavanagh, J. F., Zambrano-Vazquez, L., & Allen, J. J. B. (2012). Theta lingua franca: A common mid-frontal substrate for action monitoring processes. *Psychophysiology*, *49*(2), 220–238.

Chan, R. C. K., Shum, D., Toulopoulou, T., & Chen, E. Y. H. (2008). Assessment of executive functions: review of instruments and identification of critical issues. *Archives of Clinical Neuropsychology : The Official Journal of the National Academy of Neuropsychologists*, *23*(2), 201–16.

Choi, Y. Y., Shamosh, N. A., Cho, S. H., DeYoung, C. G., Lee, M. J., Lee, J.-M., … Lee, K. H. (2008). Multiple Bases of Human Intelligence Revealed by Cortical Thickness and Neural Activation. *Journal of Neuroscience*, *28*(41).

Cohen, J. D., Barch, D. M., Carter, C., & Servan-Schreiber, D. (1999). Context-processing deficits in schizophrenia: Converging evidence from three theoretically motivated cognitive tasks. *Journal of Abnormal Psychology*, *108*(1), 120–133.

Cole, M. W., Reynolds, J. R., Power, J. D., Repovs, G., Anticevic, A., & Braver, T. S. (2013). Multi-task connectivity reveals flexible hubs for adaptive task control. *Nature Neuroscience*, *16*(9), 1348–55.

Cole, M. W., & Schneider, W. (2007). The cognitive control network: Integrated cortical regions with dissociable functions. *NeuroImage*, *37*(1), 343–60.

Cooper, N. R., Croft, R. J., Dominey, S. J. ., Burgess, A. P., & Gruzelier, J. H. (2003). Paradox lost? Exploring the role of alpha oscillations during externally vs. internally directed attention and the implications for idling and inhibition hypotheses. *International Journal of Psychophysiology*, *47*(1), 65–74.

Copen, W. A. (2015). Multimodal imaging in acute ischemic stroke. *Current Treatment Options in Cardiovascular Medicine*, *17*(3), 368.

Corbetta, M., Miezin, F. M., Dobmeyer, S., Shulman, G. L., & Petersen, S. E. (1990). Attentional modulation of neural processing of shape, color, and velocity in humans. *Science (New York, N.Y.)*, *248*(4962), 1556–9.

Corbetta, M., & Shulman, G. L. (2002). Control of goal-directed and stimulus-driven attention in the brain. *Nature Reviews. Neuroscience*, *3*(3), 201–215.

Cordes, D., Turski, P. A., & Sorenson, J. A. (2000). Compensation of susceptibility-induced signal loss in echo-planar imaging for functional applications☆. *Magnetic Resonance Imaging*, *18*(9), 1055–1068.

Cornelissen, P. L., Kringelbach, M. L., Ellis, A. W., Whitney, C., Holliday, I. E., & Hansen, P. C. (2009). Activation of the Left Inferior Frontal Gyrus in the First 200 ms of Reading: Evidence from Magnetoencephalography (MEG). *PLoS ONE*, *4*(4), e5359.

Croxson, P. L., Johansen-Berg, H., Behrens, T. E. J., Robson, M. D., Pinsk, M. A., Gross, C. G., … Rushworth, M. F. S. (2005). Quantitative investigation of connections of the prefrontal cortex in the human and macaque using probabilistic diffusion tractography. *The Journal of Neuroscience : The Official Journal of the Society for Neuroscience*, *25*(39), 8854–66.

Csukly, G., Farkas, K., Marosi, C., & Szabó, Á. (2016). Deficits in low beta desynchronization

reflect impaired emotional processing in schizophrenia. *Schizophrenia Research*, *171*(1), 207–214.

D 'esposito, M., Postle, B. R., Jonides, J., & Smith, E. E. (1999). The neural substrate and temporal dynamics of interference effects in working memory as revealed by event-related functional MRI. *Neurobiology*, *96*(13), 7514–7519.

Dale, A. M., Fischl, B., & Sereno, M. I. (1999). Cortical surface-based analysis. I. Segmentation and surface reconstruction. *NeuroImage*, *9*(2), 179–94.

Dale, A. M., & Sereno, M. I. (1993). Improved Localizadon of Cortical Activity by Combining EEG and MEG with MRI Cortical Surface Reconstruction: A Linear Approach. *Journal of Cognitive Neuroscience*, *5*(2), 162–76.

Davies, S. J. C. (2012). Clinical Handbook of Psychotropic Drugs, 19th Revised Edition Edited by Adil Virani, Kalyna Z. Bezchlibnyk-Butler, J. Joel Jeffries, Ric M. Procyshyn, PB - Hogrefe Publishing , Göttingen. Price £53.96, pp 362 + pp 50 printable PDF patient informa. *Human Psychopharmacology: Clinical and Experimental*, *27*(6), 632.

Davis, N. J., Tomlinson, S. P., & Morgan, H. M. (2012). The Role of Beta-Frequency Neural Oscillations in Motor Control. *Journal of Neuroscience*, *32*(2), 403–404.

De Baene, W., Duyck, W., Brass, M., & Carreiras, M. (2015). Brain Circuit for Cognitive Control Is Shared by Task and Language Switching. *Journal of Cognitive Neuroscience*, *27*(9), 1752–1765.

De Pisapia, N., & Braver, T. S. (2006). A model of dual control mechanisms through anterior cingulate and prefrontal cortex interactions. *Neurocomputing*, *69*(10–12), 1322–1326.

de Reus, M. A., & van den Heuvel, M. P. (2013). The parcellation-based connectome: limitations and extensions. *NeuroImage*, *80*, 397–404.

Dell'Acqua, F., Simmons, A., Williams, S. C. R., & Catani, M. (2013). Can spherical deconvolution provide more information than fiber orientations? Hindrance modulated orientational anisotropy, a true-tract specific index to characterize white matter diffusion. *Human Brain Mapping*, *34*(10), 2464–83.

Delorme, A., Westerfield, M., & Makeig, S. (2007). Medial Prefrontal Theta Bursts Precede Rapid Motor Responses during Visual Selective Attention. *Journal of Neuroscience*, *27*(44), 11949–11959.

Derrfuss, J., Brass, M., Neumann, J., & von Cramon, D. Y. (2005). Involvement of the inferior frontal junction in cognitive control: Meta-analyses of switching and Stroop studies. *Human Brain Mapping*, *25*(1), 22–34.

Derrfuss, J., Brass, M., & Yves Von Cramon, D. (2004). Cognitive control in the posterior frontolateral cortex: Evidence from common activations in task coordination, interference control, and working memory. *NeuroImage*, *23*(2), 604–612.

Desikan, R. S. R., Ségonne, F., Fischl, B., Quinn, B. T., Dickerson, B. C., Blacker, D., … Killiany, R. J. (2006). An automated labeling system for subdividing the human cerebral cortex on MRI scans into gyral based regions of interest. *NeuroImage*, *31*(3), 968–80.

Diamond, A. (2013). Executive functions. *Annual Review of Psychology*, *64*, 135–68.

Dias, E. C., McGinnis, T., Smiley, J. F., Foxe, J. J., Schroeder, C. E., & Javitt, D. C. (2006).

Changing plans: neural correlates of executive control in monkey and human frontal cortex. *Experimental Brain Research*, *174*(2), 279–91.

Dickinson, D., Ramsey, M. E., & Gold, J. M. (2007). Overlooking the obvious: a meta-analytic comparison of digit symbol coding tasks and other cognitive measures in schizophrenia. *Archives of General Psychiatry*, *64*(5), 532–42.

Dikker, S., & Pylkkänen, L. (2013). Predicting language: MEG evidence for lexical preactivation. *Brain and Language*, *127*(1), 55–64.

DiQuattro, N. E., & Geng, J. J. (2011). Contextual Knowledge Configures Attentional Control Networks. *Journal of Neuroscience*, *31*(49), 18026–18035.

Dodds, C. M., Morein-Zamir, S., & Robbins, T. W. (2011). Dissociating Inhibition, Attention, and Response Control in the Frontoparietal Network Using Functional Magnetic Resonance Imaging. *Cerebral Cortex*, *21*(5), 1155–1165.

Doesburg, S. M., Bedo, N., & Ward, L. M. (2016). Top-down alpha oscillatory network interactions during visuospatial attention orienting. *NeuroImage*, *132*, 512–519.

Dosenbach, N. U. F., Fair, D. A., Cohen, A. L., Schlaggar, B. L., & Petersen, S. E. (2008). A dual-networks architecture of top-down control. *Trends in Cognitive Sciences*, *12*(3), 99–105.

Dosenbach, N. U. F., Fair, D. A., Miezin, F. M., Cohen, A. L., Wenger, K. K., Dosenbach, R. A. T., … Petersen, S. E. (2007). Distinct brain networks for adaptive and stable task control in humans. *Proceedings of the National Academy of Sciences of the United States of America*, *104*(26), 11073–8.

Dosenbach, N. U. F., Visscher, K. M., Palmer, E. D., Miezin, F. M., Wenger, K. K., Kang, H. C., … Petersen, S. E. (2006). A core system for the implementation of task sets. *Neuron*, *50*(5), 799–812.

Dove, A., Pollmann, S., Schubert, T., Wiggins, C. J., & Yves Von Cramon, D. (2000). Prefrontal cortex activation in task switching: An event-related fMRI study. *Cognitive Brain Research*, *9*(1), 103–109.

Ducharme, S., Albaugh, M. D., Nguyen, T.-V., Hudziak, J. J., Mateos-Pérez, J. M., Labbe, A., … Karama, S. (2016). Trajectories of cortical thickness maturation in normal brain development — The importance of quality control procedures. *NeuroImage*, *125*, 267–279.

Duncan, J. (2010). The multiple-demand (MD) system of the primate brain: mental programs for intelligent behaviour. *Trends in Cognitive Sciences*, *14*(4), 172–9.

Duque, J., Labruna, L., Verset, S., Olivier, E., & Ivry, R. B. (2012). Dissociating the role of prefrontal and premotor cortices in controlling inhibitory mechanisms during motor preparation. *The Journal of Neuroscience : The Official Journal of the Society for Neuroscience*, *32*(3), 806–16.

Duque, J., Olivier, E., & Rushworth, M. F. S. (2013). Top-down inhibitory control exerted by the medial frontal cortex during action selection under conflict. *Journal of Cognitive Neuroscience*, *25*(10), 1634–48.

Ehrlich, S., Brauns, S., Yendiki, A., Ho, B.-C., Calhoun, V., Schulz, S. C., … Sponheim, S. R. (2012). Associations of Cortical Thickness and Cognition in Patients With Schizophrenia

and Healthy Controls. *Schizophrenia Bulletin*, *38*(5), 1050–62.

Eich, T. S., Nee, D. E., Insel, C., Malapani, C., & Smith, E. E. (2014). Neural Correlates of Impaired Cognitive Control over Working Memory in Schizophrenia. *Biological Psychiatry*, *76*(2), 146–53.

Ekstrom, A. D., Caplan, J. B., Ho, E., Shattuck, K., Fried, I., & Kahana, M. J. (2005). Human hippocampal theta activity during virtual navigation. *Hippocampus*, *15*(7), 881–889.

Elliott, R., Dolan, R. J., & Frith, C. D. (2000). Dissociable functions in the medial and lateral orbitofrontal cortex: evidence from human neuroimaging studies. *Cerebral Cortex (New York, N.Y. : 1991)*, *10*(3), 308–17.

Emsley, R., Rabinowitz, J., & Torreman, M. (2003). The factor structure for the Positive and Negative Syndrome Scale (PANSS) in recent-onset psychosis. *Schizophrenia Research*, *61*(1), 47–57.

Engel, A. K., & Fries, P. (2010). Beta-band oscillations - signalling the status quo? *Current Opinion in Neurobiology*, *20*(2), 156–165.

Eriksen, B. A., & Eriksen, C. W. (1974). Effects of noise letters upon the identification of a target letter in a nonsearch task. *Perception & Psychophysics*, *16*(1), 143–149.

Fervaha, G., Zakzanis, K. K., Foussias, G., Graff-Guerrero, A., Agid, O., & Remington, G. (2014). Motivational deficits and cognitive test performance in schizophrenia. *JAMA Psychiatry*, *71*(9), 1058–65.

Fischl, B., & Dale, A. M. (2000). Measuring the thickness of the human cerebral cortex from magnetic resonance images. *Proceedings of the National Academy of Sciences of the United States of America*, *97*(20), 11050–5.

Fischl, B., Liu, A. K., & Dale, A. M. (2001). Automated manifold surgery: constructing geometrically accurate and topologically correct models of the human cerebral cortex. *IEEE Transactions on Medical Imaging*, *20*(1), 70–80.

Fischl, B., Salat, D. H., Busa, E., Albert, M., Dieterich, M., Haselgrove, C., … Dale, A. M. (2002a). Whole Brain Segmentation. *Neuron*, *33*(3), 341–355.

Fischl, B., Salat, D. H., Busa, E., Albert, M., Dieterich, M., Haselgrove, C., … Dale, A. M. (2002b). Whole brain segmentation: automated labeling of neuroanatomical structures in the human brain. *Neuron*, *33*(3), 341–55.

Fischl, B., Salat, D. H., van der Kouwe, A. J. W., Makris, N., Ségonne, F., Quinn, B. T., & Dale, A. M. (2004). Sequence-independent segmentation of magnetic resonance images. *NeuroImage*, *23 Suppl 1*, S69-84.

Fischl, B., Sereno, M. I., & Dale, A. M. (1999). Cortical surface-based analysis. II: Inflation, flattening, and a surface-based coordinate system. *NeuroImage*, *9*(2), 195–207.

Fischl, B., Sereno, M. I., Tootell, R. B., & Dale, A. M. (1999). High-resolution intersubject averaging and a coordinate system for the cortical surface. *Human Brain Mapping*, *8*(4), 272–84.

Fischl, B., van der Kouwe, A. J. W., Destrieux, C., Halgren, E., Ségonne, F., Salat, D. H., … Dale, A. M. (2004). Automatically Parcellating the Human Cerebral Cortex. *Cerebral Cortex*, *14*(1), 11–22.

Fornito, A., Yoon, J., Zalesky, A., Bullmore, E. T., & Carter, C. S. (2011). General and specific functional connectivity disturbances in first-episode schizophrenia during cognitive control performance. *Biological Psychiatry*, *70*(1), 64–72.

Fornito, A., Zalesky, A., Pantelis, C., & Bullmore, E. T. (2012). Schizophrenia, neuroimaging and connectomics. *NeuroImage*, *62*(4), 2296–2314.

Fox, M. D., Corbetta, M., Snyder, A. Z., Vincent, J. L., & Raichle, M. E. (2006). Spontaneous neuronal activity distinguishes human dorsal and ventral attention systems. *Proceedings of the National Academy of Sciences of the United States of America*, *103*(26), 10046–51.

Fox, M. D., Snyder, A. Z., Vincent, J. L., Corbetta, M., Van Essen, D. C., & Raichle, M. E. (2005). The human brain is intrinsically organized into dynamic, anticorrelated functional networks. *Proceedings of the National Academy of Sciences of the United States of America*, *102*(27), 9673–8.

Fox, P. T., & Raichle, M. E. (1986). Focal physiological uncoupling of cerebral blood flow and oxidative metabolism during somatosensory stimulation in human subjects. *Proceedings of the National Academy of Sciences of the United States of America*, *83*(4), 1140–4.

Fox, P. T., Raichle, M. E., Mintun, M. A., & Dence, C. (1988). Nonoxidative glucose consumption during focal physiologic neural activity. *Science*, *241*(4864), 462–464.

Friederici, A. D., Rüschemeyer, S.-A., Hahne, A., & Fiebach, C. J. (2003). The Role of Left Inferior Frontal and Superior Temporal Cortex in Sentence Comprehension: Localizing Syntactic and Semantic Processes. *Cerebral Cortex*, *13*(2), 170–177.

Garavan, H., Ross, T. J., Murphy, K., Roche, R. A. P., & Stein, E. A. (2002). Dissociable Executive Functions in the Dynamic Control of Behavior: Inhibition, Error Detection, and Correction. *NeuroImage*, *17*(4), 1820–1829.

Garrido, M. I., Barnes, G. R., Kumaran, D., Maguire, E. A., & Dolan, R. J. (2015). Ventromedial prefrontal cortex drives hippocampal theta oscillations induced by mismatch computations. *NeuroImage*, *120*, 362–370.

Gevins, A., Smith, M. E., McEvoy, L., & Yu, D. (1997). High-resolution EEG mapping of cortical activation related to working memory: Effects of task difficulty, type of processing, and practice. *Cerebral Cortex*, *7*(4), 374–385.

Gibson, E. M., Purger, D., Mount, C. W., Goldstein, A. K., Lin, G. L., Wood, L. S., … Monje, M. (2014). Neuronal activity promotes oligodendrogenesis and adaptive myelination in the mammalian brain. *Science*, *344*(6183), 1252304.

Gläscher, J., Adolphs, R., Damasio, H., Bechara, A., Rudrauf, D., Calamia, M., … Tranel, D. (2012). Lesion mapping of cognitive control and value-based decision making in the prefrontal cortex. *Proceedings of the National Academy of Sciences of the United States of America*, *109*(36), 14681–6.

Glover, G. H., & Law, C. S. (2001). Spiral-in/out BOLD fMRI for increased SNR and reduced susceptibility artifacts. *Magnetic Resonance in Medicine*, *46*(3), 515–522.

Goghari, V. M., Rehm, K., Carter, C. S., & MacDonald, A. W. (2007). Regionally specific cortical thinning and gray matter abnormalities in the healthy relatives of schizophrenia patients. *Cerebral Cortex*, *17*(2), 415–424.

Goghari, V. M., Sponheim, S. R., & MacDonald, A. W. (2010). The functional neuroanatomy of symptom dimensions in schizophrenia: a qualitative and quantitative review of a persistent question. *Neuroscience and Biobehavioral Reviews*, *34*(3), 468–86.

Gola, M., Magnuski, M., Szumska, I., & Wróbel, A. (2013). EEG beta band activity is related to attention and attentional deficits in the visual performance of elderly subjects. *International Journal of Psychophysiology*, *89*(3), 334–341.

Gold, J. M., & Dickinson, D. (2013). "Generalized cognitive deficit" in schizophrenia: overused or underappreciated? *Schizophrenia Bulletin*, *39*(2), 263–5.

Gold, J. M., Fuller, R. L., Robinson, B. M., Braun, E. L., & Luck, S. J. (2007). Impaired top-down control of visual search in schizophrenia. *Schizophrenia Research*, *94*(1–3), 148–155.

Goldman, A. L., Pezawas, L., Mattay, V. S., Fischl, B., Verchinski, B. A., Chen, Q., … Meyer-Lindenberg, A. (2009). Widespread reductions of cortical thickness in schizophrenia and spectrum disorders and evidence of heritability. *Archives of General Psychiatry*, *66*(5), 467–77.

Gordon, E. (1999). Brain imaging technologies: How, what, when and why? *Australian and New Zealand Journal of Psychiatry*, *33*(2), 187–196.

Grant, D. A., & Berg, E. A. (1948). A behavioral analysis of degree of reinforcement and ease of shifting to new responses in a Weigl-type card-sorting problem. *Journal of Experimental Psychology*, *38*(4), 404–11.

Gray, C. M., König, P., Engel, A. K., & Singer, W. (1989). Oscillatory responses in cat visual cortex exhibit inter-columnar synchronization which reflects global stimulus properties. *Nature*, *338*(6213), 334–337.

Green, M. F., Harris, J. G., & Nuechterlein, K. H. (2014). The MATRICS consensus cognitive battery: what we know 6 years later. *The American Journal of Psychiatry*, *171*(11), 1151–4.

Green, M. F., Nuechterlein, K. H., Gold, J. M., Barch, D. M., Cohen, J. D., Essock, S., … Marder, S. R. (2004). Approaching a consensus cognitive battery for clinical trials in schizophrenia: the NIMH-MATRICS conference to select cognitive domains and test criteria. *Biological Psychiatry*, *56*(5), 301–7.

Green, R. E. A., Melo, B., Christensen, B. K., Ngo, L.-A., Monette, G., & Bradbury, C. (2008). Measuring premorbid IQ in traumatic brain injury: an examination of the validity of the Wechsler Test of Adult Reading (WTAR). *Journal of Clinical and Experimental Neuropsychology*, *30*(2), 163–72.

Greicius, M. D., Krasnow, B., Reiss, A. L., & Menon, V. (2003). Functional connectivity in the resting brain: a network analysis of the default mode hypothesis. *Proceedings of the National Academy of Sciences of the United States of America*, *100*(1), 253–8.

Grill-Spector, K., Kourtzi, Z., & Kanwisher, N. (2001). The lateral occipital complex and its role in object recognition. *Vision Research*, *41*(10), 1409–1422.

Gross, J., Baillet, S., Barnes, G. R., Henson, R. N. A., Hillebrand, A., Jensen, O., … Schoffelen, J.-M. (2013). Good practice for conducting and reporting MEG research. *NeuroImage*, *65*(100), 349–63.

Gross, J., Kujala, J., Hamalainen, M., Timmermann, L., Schnitzler, A., & Salmelin, R. (2001).

Dynamic imaging of coherent sources: Studying neural interactions in the human brain. *Proceedings of the National Academy of Sciences of the United States of America*, *98*(2), 694–9.

Grundy, J. G., Benarroch, M. F. F., Woodward, T. S., Metzak, P. D., Whitman, J. C., & Shedden, J. M. (2011). The Bivalency effect in task switching: Event-related potentials. *Human Brain Mapping*, *34*(5), 999–1012.

Guitart-Masip, M., Barnes, G. R., Horner, A., Bauer, M., Dolan, R. J., & Duzel, E. (2013). Synchronization of medial temporal lobe and prefrontal rhythms in human decision making. *The Journal of Neuroscience : The Official Journal of the Society for Neuroscience*, *33*(2), 442–51.

Gur, R. E., & Gur, R. C. (2010). Functional magnetic resonance imaging in schizophrenia. *Dialogues in Clinical Neuroscience*, *12*(3), 333–43.

Haddock, G., McCarron, J., Tarrier, N., & Faragher, E. B. (1999). Scales to measure dimensions of hallucinations and delusions: the psychotic symptom rating scales (PSYRATS). *Psychological Medicine*, *29*(4), 879–889.

Hahn, B., Robinson, B. M., Kaiser, S. T., Harvey, A. N., Beck, V. M., Leonard, C. J., … Gold, J. M. (2010). Failure of schizophrenia patients to overcome salient distractors during working memory encoding. *Biological Psychiatry*, *68*(7), 603–609.

Haider, B., & McCormick, D. A. (2009, April 30). Rapid Neocortical Dynamics: Cellular and Network Mechanisms. *Neuron*. NIH Public Access.

Haier, R. J., Karama, S., Leyba, L., & Jung, R. E. (2009). MRI assessment of cortical thickness and functional activity changes in adolescent girls following three months of practice on a visual-spatial task. *BMC Research Notes*, *2*, 174.

Haijma, S. V, Van Haren, N., Cahn, W., Koolschijn, P. C. M. P., Hulshoff Pol, H. E., & Kahn, R. S. (2013). Brain volumes in schizophrenia: a meta-analysis in over 18 000 subjects. *Schizophrenia Bulletin*, *39*(5), 1129–38.

Hall, E. L., Robson, S. E., Morris, P. G., & Brookes, M. J. (2013). The relationship between MEG and fMRI. *NeuroImage*, *102*(1), 80–91.

Hämäläinen, M. S., Hari, R., Ilmoniemi, R. J., Knuutila, J., & Lounasmaa, O. V. (1993). Magnetoencephalography—theory, instrumentation, and applications to noninvasive studies of the working human brain. *Reviews of Modern Physics*, *65*(2), 413–497.

Hampshire, A., Chamberlain, S. R., Monti, M. M., Duncan, J., & Owen, A. M. (2010). The role of the right inferior frontal gyrus: inhibition and attentional control. *NeuroImage*, *50*(3), 1313–9.

Han, X., Jovicich, J., Salat, D. H., van der Kouwe, A. J. W., Quinn, B. T., Czanner, S., … Fischl, B. (2006). Reliability of MRI-derived measurements of human cerebral cortical thickness: the effects of field strength, scanner upgrade and manufacturer. *NeuroImage*, *32*(1), 180–94.

Harris, A., Adolphs, R., Camerer, C., & Rangel, A. (2011). Dynamic construction of stimulus values in the ventromedial prefrontal cortex. *PLoS ONE*, *6*(6), e21074.

Hauser, T. U., Hunt, L. T., Iannaccone, R., Walitza, S., Brandeis, D., Brem, S., & Dolan, R. J. (2015). Temporally Dissociable Contributions of Human Medial Prefrontal Subregions to

Reward-Guided Learning. *The Journal of Neuroscience*, *35*(32), 11209–11220.

Hazlett, E. A., Goldstein, K. E., & Kolaitis, J. C. (2012). A review of structural MRI and diffusion tensor imaging in schizotypal personality disorder. *Current Psychiatry Reports*, *14*(1), 70–8.

Hedge, C., Stothart, G., Todd Jones, J., Rojas Frías, P., Magee, K. L., & Brooks, J. C. W. (2015). A frontal attention mechanism in the visual mismatch negativity. *Behavioural Brain Research*, *293*, 173–181.

Heinrichs-Graham, E., & Wilson, T. W. (2015). Spatiotemporal oscillatory dynamics during the encoding and maintenance phases of a visual working memory task. *Cortex; a Journal Devoted to the Study of the Nervous System and Behavior*, *69*, 121–30.

Heinrichs, R. W., & Zakzanis, K. K. (1998). Neurocognitive deficit in schizophrenia: A quantitative review of the evidence. *Neuropsychology*, *12*(3), 426–445.

Hepp, H. H., Maier, S., Hermle, L., & Spitzer, M. (1996). The Stroop effect in schizophrenic patients. *Schizophrenia Research*, *22*(3), 187–195.

Herdman, A. T., & Cheyne, D. (2009). A Practical Guide for MEG and Beamforming. In *Brain Signal Analysis*. The MIT Press.

Hillebrand, A., & Barnes, G. R. (2005). Beamformer Analysis of MEG Data. *International Review of Neurobiology*, *68*, 149–171.

Hoff, A. L., Svetina, C., Shields, G., Stewart, J., & DeLisi, L. E. (2005). Ten year longitudinal study of neuropsychological functioning subsequent to a first episode of schizophrenia. *Schizophrenia Research*, *78*(1), 27–34.

Honey, C. J., Kötter, R., Breakspear, M., & Sporns, O. (2007). Network structure of cerebral cortex shapes functional connectivity on multiple time scales. *Proceedings of the National Academy of Sciences of the United States of America*, *104*(24), 10240–5.

Honey, C. J., Sporns, O., Cammoun, L., Gigandet, X., Thiran, J. P., Meuli, R., & Hagmann, P. (2009). Predicting human resting-state functional connectivity from structural connectivity. *Proceedings of the National Academy of Sciences of the United States of America*, *106*(6), 2035–40.

Hoogenboom, N., Schoffelen, J.-M., Oostenveld, R., Parkes, L. M., & Fries, P. (2006). Localizing human visual gamma-band activity in frequency, time and space. *NeuroImage*, *29*(3), 764–773.

Horenstein, C., Lowe, M. J., Koenig, K. A., & Phillips, M. D. (2009). Comparison of unilateral and bilateral complex finger tapping-related activation in premotor and primary motor cortex. *Human Brain Mapping*, *30*(4), 1397–1412.

Houck, J. M., Çetin, M. S., Mayer, A. R., Bustillo, J. R., Stephen, J., Aine, C., … Calhoun, V. D. (2017). Magnetoencephalographic and functional MRI connectomics in schizophrenia via intra- and inter-network connectivity. *NeuroImage*, *145*, 96–106.

Hsieh, L.-T., & Ranganath, C. (2014). Frontal midline theta oscillations during working memory maintenance and episodic encoding and retrieval. *NeuroImage*, *85*, 721–729.

Huettel, S. A. (2004). Linking Hemodynamic and Electrophysiological Measures of Brain Activity: Evidence from Functional MRI and Intracranial Field Potentials. *Cerebral Cortex*,

14(2), 165–173.

Hunt, B. A. E., Tewarie, P. K., Mougin, O. E., Geades, N., Jones, D. K., Singh, K. D., … Brookes, M. J. (2016). Relationships between cortical myeloarchitecture and electrophysiological networks. *Proceedings of the National Academy of Sciences of the United States of America*, *113*(47), 13510–13515.

Ikezawa, K., Ishii, R., Iwase, M., Kurimoto, R., Canuet, L., Takahashi, H., … Takeda, M. (2011). Decreased alpha event-related synchronization in the left posterior temporal cortex in schizophrenia: A magnetoencephalography-beamformer study. *Neuroscience Research*, *71*(3), 235–243.

Ishii, R., Canuet, L., Ishihara, T., Aoki, Y., Ikeda, S., Hata, M., … Takeda, M. (2014). Frontal midline theta rhythm and gamma power changes during focused attention on mental calculation: an MEG beamformer analysis. *Frontiers in Human Neuroscience*, *8*(June), 406.

Ishii, R., Shinosaki, K., Ukai, S., Inouye, T., Ishihara, T., Yoshimine, T., … Takeda, M. (1999). Medial prefrontal cortex generates frontal midline theta rhythm. *Neuroreport*, *10*(4), 675–679.

Jablensky, A. (2010). The diagnostic concept of schizophrenia: its history, evolution, and future prospects. *Dialogues in Clinical Neuroscience*, *12*(3), 271–87.

Jensen, O., & Tesche, C. D. (2002). Frontal theta activity in humans increases with memory load in a working memory task. *European Journal of Neuroscience*, *15*(8), 1395–1399.

Jeste, S. D., Patterson, T. L., Palmer, B. W., Dolder, C. R., Goldman, S., & Jeste, D. V. (2003). Cognitive predictors of medication adherence among middle-aged and older outpatients with schizophrenia. *Schizophrenia Research*, *63*(1–2), 49–58.

Jeurissen, B., Leemans, A., Jones, D. K., Tournier, J.-D., & Sijbers, J. (2011). Probabilistic fiber tracking using the residual bootstrap with constrained spherical deconvolution. *Human Brain Mapping*, *32*(3), 461–79.

Jeurissen, B., Leemans, A., Tournier, J.-D., Jones, D. K., & Sijbers, J. (2013). Investigating the prevalence of complex fiber configurations in white matter tissue with diffusion magnetic resonance imaging. *Human Brain Mapping*, *34*(11), 2747–66.

Jovicich, J., Czanner, S., Greve, D. N., Haley, E., van der Kouwe, A. J. W., Gollub, R. L., … Dale, A. M. (2006). Reliability in multi-site structural MRI studies: effects of gradient non-linearity correction on phantom and human data. *NeuroImage*, *30*(2), 436–43.

Kaiser, H. F. (1958). The varimax criterion for analytic rotation in factor analysis. *Psychometrika*, *23*(3), 187–200.

Kane, J. M., & Sharif, Z. (2008). Atypical Antipsychotics: Sedation Versus Efficacy. *The Journal of Clinical Psychiatry*, *69*(suppl 1), 18–31.

Kapur, S. (2003, January). Psychosis as a state of aberrant salience: A framework linking biology, phenomenology, and pharmacology in schizophrenia. *American Journal of Psychiatry*. American Psychiatric Publishing.

Karama, S., Ad-Dab'bagh, Y., Haier, R., Deary, I., Lyttelton, O., Lepage, C., … Brain Development Cooperative Group. (2009). Positive association between cognitive ability and cortical thickness in a representative US sample of healthy 6 to 18 year-olds. *Intelligence*,

37(2), 145–155.

Karlsgodt, K. H., Niendam, T. A., Bearden, C. E., & Cannon, T. D. (2009). White Matter Integrity and Prediction of Social and Role Functioning in Subjects at Ultra-High Risk for Psychosis. *Biological Psychiatry*, *66*(6), 562–569.

Karlsgodt, K. H., Sun, D., Jimenez, A. M., Lutkenhoff, E. S., Willhite, R., van Erp, T. G. M., & Cannon, T. D. (2008). Developmental disruptions in neural connectivity in the pathophysiology of schizophrenia. *Development and Psychopathology*, *20*(4), 1297–327.

Kawaguchi, S., Ukai, S., Shinosaki, K., Ishii, R., Yamamoto, M., Ogawa, A., … Takeda, M. (2005). Information processing flow and neural activations in the dorsolateral prefrontal cortex in the Stroop task in schizophrenic patients. A spatially filtered MEG analysis with high temporal and spatial resolution. *Neuropsychobiology*, *51*(4), 191–203.

Keefe, R. S. E., Eesley, C. E., & Poe, M. P. (2005). Defining a cognitive function decrement in schizophrenia. *Biological Psychiatry*, *57*(6), 688–91.

Keefe, R. S. E., & Harvey, P. D. (2012). Cognitive impairment in schizophrenia. *Handbook of Experimental Pharmacology*, *213*(213), 11–37.

Kerns, J. G., Nuechterlein, K. H., Braver, T. S., & Barch, D. M. (2008). Executive functioning component mechanisms and schizophrenia. *Biological Psychiatry*, *64*(1), 26–33.

Kim, C., Johnson, N. F., Cilles, S. E., & Gold, B. T. (2011). Common and distinct mechanisms of cognitive flexibility in prefrontal cortex. *The Journal of Neuroscience : The Official Journal of the Society for Neuroscience*, *31*(13), 4771–4779.

Kim, J. S., Shin, K. S., Jung, W. H., Kim, S. N., Kwon, J. S., & Chung, C. K. (2014). Power spectral aspects of the default mode network in schizophrenia: an MEG study. *BMC Neuroscience*, *15*(1), 104.

Kim, S.-G., & Ogawa, S. (2012). Biophysical and physiological origins of blood oxygenation level-dependent fMRI signals. *Journal of Cerebral Blood Flow and Metabolism : Official Journal of the International Society of Cerebral Blood Flow and Metabolism*, *32*(7), 1188–206.

Kim, D. Il, Manoach, D. S., Mathalon, D. H., Turner, J. A., Mannell, M., Brown, G. G., … Calhoun, V. D. (2009). Dysregulation of working memory and default-mode networks in schizophrenia using independent component analysis, an fBIRN and MCIC study. *Human Brain Mapping*, *9999*(11), NA.

Kirschfeld, K. (2005). The physical basis of alpha waves in the electroencephalogram and the origin of the " Berger effect " *Biol. Cybern.*

Klimesch, W. Alpha-band oscillations, attention, and controlled access to stored information, 16Trends in Cognitive Sciences 606–617 (2012). Elsevier.

Klimesch, W., Doppelmayr, M., & Hanslmayr, S. (2006). Chapter 10 Upper alpha ERD and absolute power: their meaning for memory performance. *Progress in Brain Research*.

Knöchel, C., Reuter, J., Reinke, B., Stäblein, M., Marbach, K., Feddern, R., … Oertel-Knöchel, V. (2016). Cortical thinning in bipolar disorder and schizophrenia. *Schizophrenia Research*, *172*(1–3), 78–85.

Kochunov, P., Glahn, D. C., Nichols, T. E., Winkler, A. M., Hong, E. L., Holcomb, H. H., …

Blangero, J. (2011). Genetic analysis of cortical thickness and fractional anisotropy of water diffusion in the brain. *Frontiers in Neuroscience*, *5*, 120.

Koechlin, E., Ody, C., & Kouneiher, F. (2003). The architecture of cognitive control in the human prefrontal cortex. *Science (New York, N.Y.), 302*(5648), 1181–5.

Koo, M.-S., Levitt, J. J., Salisbury, D. F., Nakamura, M., Shenton, M. E., & McCarley, R. W. (2008). A Cross-Sectional and Longitudinal Magnetic Resonance Imaging Study of Cingulate Gyrus Gray Matter Volume Abnormalities in First-Episode Schizophrenia and First-Episode Affective Psychosis. *Archives of General Psychiatry*, *65*(7), 746.

Kool, W., & Botvinick, M. M. (2013). The intrinsic cost of cognitive control. *The Behavioral and Brain Sciences*, *36*(6), 697-8-26.

Krause, C. M., Sillanmäki, L., Koivisto, M., Saarela, C., Häggqvist, A., Laine, M., & Hämäläinen, H. (2000). The effects of memory load on event-related EEG desynchronization and synchronization. *Clinical Neurophysiology*, *111*(11), 2071–2078.

Kubicki, M., McCarley, R. W., Westin, C.-F., Park, H.-J., Maier, S., Kikinis, R., … Shenton, M. E. (2007). A review of diffusion tensor imaging studies in schizophrenia. *Journal of Psychiatric Research*, *41*(1–2), 15–30.

Kubicki, M., Park, H.-J., Westin, C.-F., Nestor, P. G., Mulkern, R. V, Maier, S. E., … Shenton, M. E. (2005). DTI and MTR abnormalities in schizophrenia: analysis of white matter integrity. *NeuroImage*, *26*(4), 1109–18.

Kujala, J., Sudre, G., Vartiainen, J., Liljeström, M., Mitchell, T., & Salmelin, R. (2014). Multivariate analysis of correlation between electrophysiological and hemodynamic responses during cognitive processing. *NeuroImage*, *92C*, 207–216.

Kuperberg, G. R., Broome, M. R., McGuire, P. K., David, A. S., Eddy, M., Ozawa, F., … Fischl, B. (2003). Regionally localized thinning of the cerebral cortex in schizophrenia. *Archives of General Psychiatry*, *60*(9), 878–88.

Kustermann, T., Rockstroh, B., Kienle, J., Miller, G. A., & Popov, T. (2016). Deficient attention modulation of lateralized alpha power in schizophrenia. *Psychophysiology*, *53*(6), 776–785.

Kwong, K. K., Belliveau, J. W., Chesler, D. A., Goldberg, I. E., Weisskoff, R. M., Poncelet, B. P., … Turner, R. (1992). Dynamic magnetic resonance imaging of human brain activity during primary sensory stimulation. *Proceedings of the National Academy of Sciences of the United States of America*, *89*(12), 5675–9.

Lavigne, K. M., Menon, M., & Woodward, T. S. (2016). Impairment in subcortical suppression in schizophrenia: Evidence from the fBIRN Oddball Task. *Human Brain Mapping*, *37*(12), 4640–4653.

Lavigne, K. M., Metzak, P. D., & Woodward, T. S. (2015). Functional brain networks underlying detection and integration of disconfirmatory evidence. *NeuroImage*, *112*, 138–151.

Lavigne, K. M., Rapin, L. A., Metzak, P. D., Whitman, J. C., Jung, K., Dohen, M., … Woodward, T. S. (2014). Left-dominant temporal-frontal hypercoupling in schizophrenia patients with hallucinations during speech perception. *Schizophrenia Bulletin*, *41*(1), 259–67.

Lecrubier, Y., Sheehan, D., Weiller, E., Amorim, P., Bonora, I., Harnett Sheehan, K., … Dunbar, G. (1997). The Mini International Neuropsychiatric Interview (MINI). A short diagnostic structured interview: reliability and validity according to the CIDI. *European Psychiatry*, *12*(5), 224–231.

Lee, S.-H., Kubicki, M., Asami, T., Seidman, L. J., Goldstein, J. M., Mesholam-Gately, R. I., … Shenton, M. E. (2013). Extensive white matter abnormalities in patients with first-episode schizophrenia: A diffusion tensor imaging (DTI) study. *Schizophrenia Research*, *143*(2), 231–238.

Lega, B. C., Jacobs, J., & Kahana, M. (2012). Human hippocampal theta oscillations and the formation of episodic memories. *Hippocampus*, *22*(4), 748–761.

Lesh, T. A., Niendam, T. A., Minzenberg, M. J., & Carter, C. S. (2011). Cognitive control deficits in schizophrenia: mechanisms and meaning. *Neuropsychopharmacology : Official Publication of the American College of Neuropsychopharmacology*, *36*(1), 316–38.

Leung, H.-C., & Cai, W. (2007). Common and differential ventrolateral prefrontal activity during inhibition of hand and eye movements. *The Journal of Neuroscience : The Official Journal of the Society for Neuroscience*, *27*(37), 9893–900.

Leung, W. W., Bowie, C. R., & Harvey, P. D. (2008). Functional implications of neuropsychological normality and symptom remission in older outpatients diagnosed with schizophrenia: A cross-sectional study. *Journal of the International Neuropsychological Society : JINS*, *14*(3), 479–88.

Li, C. R., Huang, C., Constable, R. T., & Sinha, R. (2006). Imaging Response Inhibition in a Stop-Signal Task: Neural Correlates Independent of Signal Monitoring and Post-Response Processing. *The Journal of Neuroscience*, *26*(1), 186–192.

Libby, L. A., & Ragland, J. D. (2012). FMRI as a measure of cognition related brain circuitry in schizophrenia. *Current Topics in Behavioral Neurosciences*, *11*, 253–67.

Liddle, E. B., Price, D., Palaniyappan, L., Brookes, M. J., Robson, S. E., Hall, E. L., … Liddle, P. F. (2016). Abnormal salience signaling in schizophrenia: The role of integrative beta oscillations. *Human Brain Mapping*, *37*(4), 1361–74.

Liddle, P. F. (1987). The symptoms of chronic schizophrenia. A re-examination of the positive-negative dichotomy. *The British Journal of Psychiatry*, *151*(2), 145–151.

Liddle, P. F., Ngan, E. T. C., Duffield, G., Kho, K., & Warren, A. J. (2002). Signs and Symptoms of Psychotic Illness (SSPI): a rating scale. *Br J Psychiatry*, *180*, 45–50.

Lien, M.-C., Ruthruff, E., & Johnston, J. C. (2010). Attentional capture with rapidly changing attentional control settings. *Journal of Experimental Psychology: Human Perception and Performance*, *36*(1), 1–16.

Liu, S., Cai, W., Liu, S., Zhang, F., Fulham, M., Feng, D., … Kikinis, R. (2015). Multimodal neuroimaging computing: a review of the applications in neuropsychiatric disorders. *Brain Informatics*, *2*, 167–180.

Liu, X., Lai, Y., Wang, X., Hao, C., Chen, L., Zhou, Z., … Hong, N. (2014). A combined DTI and structural MRI study in medicated-naïve chronic schizophrenia. *Magnetic Resonance Imaging*, *32*(1), 1–8.

Liu, Y., Liang, M., Zhou, Y., He, Y., Hao, Y., Song, M., … Jiang, T. (2008). Disrupted small-world networks in schizophrenia. *Brain*, *131*(4), 945–961.

Logothetis, N. K., Pauls, J., Augath, M., Trinath, T., & Oeltermann, A. (2001). Neurophysiological investigation of the basis of the fMRI signal. *Nature*, *412*(6843), 150–7.

Lopes da Silva, F. (2013). EEG and MEG: relevance to neuroscience. *Neuron*, *80*(5), 1112–28.

Lorig, T., Freeman, W. J., Ahlfors, S. P., & Menon, V. (2009). Combining fMRI with EEG and MEG in order to relate patterns of brain activity to cognition. *International Journal of Psychophysiology*, *73*(1), 43–52.

Lynall, M.-E., Bassett, D. S., Kerwin, R., McKenna, P. J., Kitzbichler, M., Muller, U., & Bullmore, E. (2010). Functional connectivity and brain networks in schizophrenia. *The Journal of Neuroscience : The Official Journal of the Society for Neuroscience*, *30*(28), 9477–87.

MacDonald, A. W. (2000). Dissociating the Role of the Dorsolateral Prefrontal and Anterior Cingulate Cortex in Cognitive Control. *Science*, *288*(5472), 1835–1838.

Maj, M. (1998). Critique of the DSM-IV operational diagnostic criteria for schizophrenia. *The British Journal of Psychiatry*, *172*(6), 458–458.

Makeig, S., Delorme, A., Westerfield, M., Jung, T. P., Townsend, J., Courchesne, E., & Sejnowski, T. J. (2004). Electroencephalographic brain dynamics following manually responded visual targets. *PLoS Biology*, *2*(6), e176.

Martínez, A., Anllo-Vento, L., Sereno, M. I., Frank, L. R., Buxton, R. B., Dubowitz, D. J., … Sereno, M. I. (1999). Involvement of striate and extrastriate visual cortical areas in spatial attention. *Nature Neuroscience*, *2*(4), 364–369.

Mathias, J. L., Bowden, S. C., & Barrett-Woodbridge, M. (2007). Accuracy of the Wechsler Test of Adult Reading (WTAR) and National Adult Reading Test (NART) when estimating IQ in a healthy Australian sample. *Australian Psychologist*, *42*(1), 49–56.

Mayer, A. R., Hanlon, F. M., Teshiba, T. M., Klimaj, S. D., Ling, J. M., Dodd, A. B., … Toulouse, T. (2015). An fMRI study of multimodal selective attention in schizophrenia. *The British Journal of Psychiatry*, *207*(5).

McGurk, S. R., Mueser, K. T., Harvey, P. D., LaPuglia, R., & Marder, J. (2003). Cognitive and Symptom Predictors of Work Outcomes for Clients With Schizophrenia in Supported Employment. *Psychiatric Services*, *54*(8), 1129–1135.

McIntosh, A. M., Job, D. E., Moorhead, T. W. J., Harrison, L. K., Forrester, K., Lawrie, S. M., & Johnstone, E. C. (2004). Voxel-based morphometry of patients with schizophrenia or bipolar disorder and their unaffected relatives. *Biological Psychiatry*, *56*(8), 544–552.

McKiernan, K. A., Kaufman, J. N., Kucera-Thompson, J., & Binder, J. R. (2003). A Parametric Manipulation of Factors Affecting Task-induced Deactivation in Functional Neuroimaging. *Journal of Cognitive Neuroscience*, *15*(3), 394–408.

McTeague, L. M., Huemer, J., Carreon, D. M., Jiang, Y., Eickhoff, S. B., & Etkin, A. (2017). Identification of Common Neural Circuit Disruptions in Cognitive Control Across Psychiatric Disorders. *American Journal of Psychiatry*, appi.ajp.2017.1.

Medendorp, W. P., Kramer, G. F. I., Jensen, O., Oostenveld, R., Schoffelen, J.-M., & Fries, P.

(2007). Oscillatory Activity in Human Parietal and Occipital Cortex Shows Hemispheric Lateralization and Memory Effects in a Delayed Double-Step Saccade Task. *Cerebral Cortex*, *17*(10), 2364–2374.

Meier, B., Woodward, T. S., Rey-Mermet, A., & Graf, P. (2009). The bivalency effect in task switching: General and enduring. *Canadian Journal of Experimental Psychology/Revue Canadienne de Psychologie expérimentale*, *63*(3), 201–210.

Melicher, T., Horacek, J., Hlinka, J., Spaniel, F., Tintera, J., Ibrahim, I., … Hoschl, C. (2015). White matter changes in first episode psychosis and their relation to the size of sample studied: A DTI study. *Schizophrenia Research*, *162*(1), 22–28.

Meltzer, J. A., Zaveri, H. P., Goncharova, I. I., Distasio, M. M., Papademetris, X., Spencer, S. S., … Constable, R. T. (2008). Effects of Working Memory Load on Oscillatory Power in Human Intracranial EEG. *Cerebral Cortex*, *18*(8), 1843–1855.

Menary, K., Collins, P. F., Porter, J. N., Muetzel, R., Olson, E. A., Kumar, V., … Luciana, M. (2013). Associations between cortical thickness and general intelligence in children, adolescents and young adults. *Intelligence*, *41*(5), 597–606.

Menon, V., & Uddin, L. Q. (2010). Saliency, switching, attention and control: a network model of insula function. *Brain Structure & Function*, *214*(5–6), 655–67.

Messé, A., Rudrauf, D., Benali, H., Marrelec, G., & Honey, C. (2014). Relating Structure and Function in the Human Brain: Relative Contributions of Anatomy, Stationary Dynamics, and Non-stationarities. *PLoS Computational Biology*, *10*(3), e1003530.

Metzak, P. D., Feredoes, E., Takane, Y., Wang, L., Weinstein, S., Cairo, T. A., … Woodward, T. S. (2010). Constrained principal component analysis reveals functionally connected load-dependent networks involved in multiple stages of working memory. *Human Brain Mapping*, *32*(6), 856–871.

Metzak, P. D., Meier, B., Graf, P., & Woodward, T. S. (2013). More than a surprise: The bivalency effect in task switching. *Journal of Cognitive Psychology*, *25*(7), 833–842.

Metzak, P. D., Riley, J. D., Wang, L., Whitman, J. C., Ngan, E. T. C., & Woodward, T. S. (2011). Decreased Efficiency of Task-Positive and Task-Negative Networks During Working Memory in Schizophrenia. *Schizophrenia Bulletin*, *38*(4), 803–813.

Miki, A., Liu, G. T., Modestino, E. J., Liu, C. S., Bonhomme, G. R., Dobre, C. M., & Haselgrove, J. C. (2001). Functional magnetic resonance imaging of the visual system. *Current Opinion in Ophthalmology*, *12*(6), 423–431.

Miller, E. K. (2000). The prefrontal cortex and cognitive control. *Nature Reviews. Neuroscience*, *1*(1), 59–65.

Miller, E. K., & Cohen, J. D. (2001). An integrative theory of prefrontal cortex function. *Annual Review of Neuroscience*, *24*, 167–202.

Miller, G. A., & Chapman, J. P. (2001). Misunderstanding analysis of covariance. *Journal of Abnormal Psychology*, *110*(1), 40–48.

Mills, K. L., & Tamnes, C. K. (2014). Methods and considerations for longitudinal structural brain imaging analysis across development. *Developmental Cognitive Neuroscience*, *9*, 172–190.

Minzenberg, M. J., Laird, A. R., Thelen, S., Carter, C. S., & Glahn, D. C. (2014). Meta-analysis of 41 Functional Neuroimaging Studies of Executive Function in Schizophrenia. *Archive of General Psychiatry*, *66*(8), 811–822.

Miyake, A., Friedman, N. P., Emerson, M. J., Witzki, A. H., Howerter, A., & Wager, T. D. (2000). The unity and diversity of executive functions and their contributions to complex "Frontal Lobe" tasks: a latent variable analysis. *Cognitive Psychology*, *41*(1), 49–100.

Mohamed, S., Rosenheck, R., Swartz, M., Stroup, S., Lieberman, J. A., & Keefe, R. S. E. (2008). Relationship of Cognition and Psychopathology to Functional Impairment in Schizophrenia. *American Journal of Psychiatry*.

Moradi, F., Liu, L. C., Cheng, K., Waggoner, R. A., Tanaka, K., & Ioannides, A. A. (2003). Consistent and precise localization of brain activity in human primary visual cortex by MEG and fMRI. *NeuroImage*, *18*(3), 595–609.

Moran, L. V, & Hong, L. E. (2011). High vs low frequency neural oscillations in schizophrenia. *Schizophrenia Bulletin*, *37*(4), 659–63.

Moritz, S., & Laudan, A. (2007). Attention bias for paranoia-relevant visual stimuli in schizophrenia. *Cognitive Neuropsychiatry*, *12*(5), 381–90.

Morris, R., Griffiths, O., Le Pelley, M. E., & Weickert, T. W. (2013). Attention to irrelevant cues is related to positive symptoms in schizophrenia. *Schizophrenia Bulletin*, *39*(3), 575–82.

Narr, K. L., Bilder, R. M., Toga, A. W., Woods, R. P., Rex, D. E., Szeszko, P. R., … Thompson, P. M. (2005). Mapping cortical thickness and gray matter concentration in first episode schizophrenia. *Cerebral Cortex (New York, N.Y. : 1991)*, *15*(6), 708–19.

Nestor, P. G., Kubicki, M., Spencer, K. M., Niznikiewicz, M. A., McCarley, R. W., & Shenton, M. E. (2007). Attentional networks and cingulum bundle in chronic schizophrenia. *Schizophrenia Research*, *90*(1–3), 308–315.

Neuper, C., & Pfurtscheller, G. (2001). Evidence for distinct beta resonance frequencies in human EEG related to specific sensorimotor cortical areas. *Clinical Neurophysiology*, *112*(11), 2084–2097.

Niendam, T. A., Laird, A. R., Ray, K. L., Dean, Y. M., Glahn, D. C., & Carter, C. S. (2012). Meta-analytic evidence for a superordinate cognitive control network subserving diverse executive functions. *Cognitive, Affective & Behavioral Neuroscience*, *12*(2), 241–68.

Nobre, A. C., Coull, J. T., Frith, C. D., & Mesulam, M. M. (1999). Orbitofrontal cortex is activated during breaches of expectation in tasksof visual attention. *Nature Neuroscience*, *2*(1), 11–12.

Ogawa, S., Lee, T. M., Kay, A. R., & Tank, D. W. (1990). Brain magnetic resonance imaging with contrast dependent on blood oxygenation. *Proceedings of the National Academy of Sciences of the United States of America*, *87*(24), 9868–72.

Ogawa, S., Tank, D. W., Menon, R., Ellermann, J. M., Kim, S.-G., Merkle, H., & Ugurbil, K. (1992). Intrinsic Signal Changes Accompanying Sensory Stimulation: Functional Brain Mapping with Magnetic Resonance Imaging. *Proceedings of the National Academy of Sciences of the United States of America*, *89*(13), 5951–5955.

Ohtani, T., Bouix, S., Lyall, A. E., Hosokawa, T., Saito, Y., Melonakos, E., … Kubicki, M.

(2015). Abnormal white matter connections between medial frontal regions predict symptoms in patients with first episode schizophrenia. *Cortex*, *71*, 264–276.

Oostenveld, R., Fries, P., Maris, E., & Schoffelen, J.-M. (2011). FieldTrip: Open source software for advanced analysis of MEG, EEG, and invasive electrophysiological data. *Computational Intelligence and Neuroscience*, *2011*, 156869.

Orellana, G., & Slachevsky, A. (2013). Executive functioning in schizophrenia. *Frontiers in Psychiatry*, *4*, 35.

Otto, W., & McMenemy, R. A. (1965). An appraisal of the Ammons Quick test in a remedial reading program. *Journal of Educational Measurement*, *2*(2), 193–198.

Palaniyappan, L., & Liddle, P. F. (2012). Does the salience network play a cardinal role in psychosis? An emerging hypothesis of insular dysfunction. *Journal of Psychiatry & Neuroscience : JPN*, *37*(1), 17–27.

Panagiotaropoulos, T. I., Kapoor, V., & Logothetis, N. K. (2013). Desynchronization and rebound of beta oscillations during conscious and unconscious local neuronal processing in the macaque lateral prefrontal cortex. *Frontiers in Psychology*, *4*(SEP), 603.

Pasquale, F. de, Penna, S. Della, Snyder, A. Z., Lewis, C., Mantini, D., Marzetti, L., … Corbetta, M. (2010). Temporal dynamics of spontaneous MEG activity in brain networks. *Proceedings of the National Academy of Sciences of the United States of America*, *107*(13), 6040–6045.

Passingham, R. E. (1972a). Non-reversal shifts after selective prefrontal ablations in monkeys (Macaca mulatta). *Neuropsychologia*, *10*(1), 41–46.

Passingham, R. E. (1972b). Visual discrimination learning after selective prefrontal ablations in monkeys (Macaca mulatta). *Neuropsychologia*, *10*(1), 27–39.

Paus, T. (2001). Primate anterior cingulate cortex: Where motor control, drive and cognition interface. *Nat Rev Neurosci*, *2*(6), 417–424.

Periáñez, J. A., Maestú, F., Barceló, F., Fernández, A., Amo, C., & Ortiz Alonso, T. (2004). Spatiotemporal brain dynamics during preparatory set shifting: MEG evidence. *NeuroImage*, *21*(2), 687–695.

Perlstein, W. M., Carter, C. S., Barch, D. M., & Baird, J. W. (1998). The Stroop task and attention deficits in schizophrenia: A critical evaluation of card and single-trial Stroop methodologies. *Neuropsychology*, *12*(3), 414–425.

Peters, S. K., Dunlop, K., & Downar, J. (2016). Cortico-Striatal-Thalamic Loop Circuits of the Salience Network: A Central Pathway in Psychiatric Disease and Treatment. *Frontiers in Systems Neuroscience*, *10*, 104.

Petersen, S. E., & Posner, M. I. (2012). The attention system of the human brain: 20 years after. *Annual Review of Neuroscience*, *35*(1), 73–89.

Petrides, M., & Pandya, D. N. (2002). Comparative cytoarchitectonic analysis of the human and the macaque ventrolateral prefrontal cortex and corticocortical connection patterns in the monkey. *European Journal of Neuroscience*, *16*(2), 291–310.

Petrides, M., Tomaiuolo, F., Yeterian, E. H., & Pandya, D. N. (2012). The prefrontal cortex: comparative architectonic organization in the human and the macaque monkey brains.

Cortex; a Journal Devoted to the Study of the Nervous System and Behavior, *48*(1), 46–57.

Pettersson-Yeo, W., Allen, P., Benetti, S., McGuire, P. K., & Mechelli, A. (2011). Dysconnectivity in schizophrenia: Where are we now? *Neuroscience & Biobehavioral Reviews*, *35*(5), 1110–1124.

Pizzella, V., Marzetti, L., Della Penna, S., de Pasquale, F., Zappasodi, F., & Romani, G. L. (2014). Magnetoencephalography in the study of brain dynamics. *Functional Neurology*, *29*(4), 241–53.

Poldrack, R. A., Wagner, A. D., Prull, M. W., Desmond, J. E., Glover, G. H., & Gabrieli, J. D. E. (1999). Functional Specialization for Semantic and Phonological Processing in the Left Inferior Prefrontal Cortex. *NeuroImage*, *10*(1), 15–35.

Posner, M. I., & Petersen, S. E. (1990). The Attention System of the Human Brain. *Annual Review of Neuroscience*, *13*(1), 25–42.

Potkin, S. G., Turner, J. A., Brown, G. G., McCarthy, G., Greve, D. N., Glover, G. H., … FBIRN. (2009). Working memory and DLPFC inefficiency in schizophrenia: The FBIRN study. *Schizophr Bull*, *35*(1), 19–31.

Power, J. D., Cohen, A. L., Nelson, S. M., Wig, G. S., Barnes, K. A., Church, J. A., … Petersen, S. E. (2011). Functional network organization of the human brain. *Neuron*, *72*(4), 665–78.

Power, J. D., & Petersen, S. E. (2013). Control-related systems in the human brain. *Current Opinion in Neurobiology*, *23*(2), 223–8.

Price, C. J. (2000). The anatomy of language: contributions from functional neuroimaging. *Journal of Anatomy*, *197*(3), 335–359.

Puce, A., Allison, T., Spencer, S. S., Spencer, D. D., & McCarthy, G. (1997). Comparison of cortical activation evoked by faces measured by intracranial field potentials and functional MRI: Two case studies. *Human Brain Mapping*, *5*(4), 298–305.

Pylkkänen, L., & McElree, B. (2007). An MEG Study of Silent Meaning. *Journal of Cognitive Neuroscience*, *19*(11), 1905–1921.

Raichle, M. E. (1994). Visualizing the mind. *Scientific American*, *270*(4), 58–64.

Raichle, M. E., MacLeod, A. M., Snyder, A. Z., Powers, W. J., Gusnard, D. A., & Shulman, G. L. (2001). A default mode of brain function. *Proceedings of the National Academy of Sciences of the United States of America*, *98*(2), 676–682.

Rana, K. D., & Vaina, L. M. (2014). Functional roles of 10 Hz alpha-band power modulating engagement and disengagement of cortical networks in a complex visual motion task. *PLoS ONE*, *9*(10), e107715.

Rapoport, J. L., Giedd, J. N., & Gogtay, N. (2012). Neurodevelopmental model of schizophrenia: update 2012. *Molecular Psychiatry*, *17*(12), 1228–38.

Rau, C., Plewnia, C., Hummel, F., & Gerloff, C. (2003). Event-related desynchronization and excitability of the ipsilateral motor cortex during simple self-paced finger movements. *Clinical Neurophysiology*, *114*(10), 1819–1826.

Reuter, M., Rosas, H. D., & Fischl, B. (2010). Highly accurate inverse consistent registration: a robust approach. *NeuroImage*, *53*(4), 1181–96.

Reuter, M., Schmansky, N. J., Rosas, H. D., & Fischl, B. (2012). Within-subject template estimation for unbiased longitudinal image analysis. *NeuroImage*, *61*(4), 1402–18.

Ribeiro, P. F. M., Ventura-Antunes, L., Gabi, M., Mota, B., Grinberg, L. T., Farfel, J. M., … Herculano-Houzel, S. (2013). The human cerebral cortex is neither one nor many: neuronal distribution reveals two quantitatively different zones in the gray matter, three in the white matter, and explains local variations in cortical folding. *Frontiers in Neuroanatomy*, *7*, 28.

Rietkerk, T., Boks, M. P., Sommer, I. E., Liddle, P. F., Ophoff, R. A., & Kahn, R. S. (2008). The genetics of symptom dimensions of schizophrenia: review and meta-analysis. *Schizophrenia Research*, *102*(1–3), 197–205.

Rimol, L. M., Hartberg, C. B., Nesvåg, R., Fennema-Notestine, C., Hagler, D. J., Pung, C. J., … Agartz, I. (2010). Cortical thickness and subcortical volumes in schizophrenia and bipolar disorder. *Biological Psychiatry*, *68*(1), 41–50.

Roa Romero, Y., Keil, J., Balz, J., Gallinat, J., & Senkowski, D. (2016). Reduced frontal theta oscillations indicate altered crossmodal prediction error processing in schizophrenia. *Journal of Neurophysiology*, *116*(3).

Rosas, H. D., Liu, A. K., Hersch, S., Glessner, M., Ferrante, R. J., Salat, D. H., … Fischl, B. (2002). Regional and progressive thinning of the cortical ribbon in Huntington's disease. *Neurology*, *58*(5), 695–701.

Rosen, H. J., Petersen, S. E., Linenweber, M. R., Snyder, A. Z., White, D. A., Chapman, L., … Corbetta, M. (2000). Neural correlates of recovery from aphasia after damage to left inferior frontal cortex. *Neurology*, *55*(12), 1883–1894.

Rouhinen, S., Panula, J., Palva, J. M., & Palva, S. (2013). Load dependence of β and γ oscillations predicts individual capacity of visual attention. *The Journal of Neuroscience*, *33*(48), 19023–33.

Rubin, O., & Meiran, N. (2005). On the Origins of the Task Mixing Cost in the Cuing Task-Switching Paradigm. *Journal of Experimental Psychology: Learning, Memory, and Cognition*, *31*(6), 1477–1491.

Rubinov, M., Sporns, O., van Leeuwen, C., & Breakspear, M. (2009). Symbiotic relationship between brain structure and dynamics. *BMC Neuroscience*, *10*, 55.

Saha, S., Chant, D., Welham, J., & McGrath, J. (2005). A Systematic Review of the Prevalence of Schizophrenia. *PLoS Med*, *2*(5), e141.

Salat, D. H., Buckner, R. L., Snyder, A. Z., Greve, D. N., Desikan, R. S. R., Busa, E., … Fischl, B. (2004). Thinning of the cerebral cortex in aging. *Cerebral Cortex (New York, N.Y. : 1991)*, *14*(7), 721–30.

Salmelin, R., & Hari, R. (1994). Characterization of spontaneous MEG rhythms in healthy adults. *Electroencephalography and Clinical Neurophysiology*, *91*(4), 237–248.

Sandrini, M., Rossini, P. M., & Miniussi, C. (2008). Lateralized contribution of prefrontal cortex in controlling task-irrelevant information during verbal and spatial working memory tasks: rTMS evidence. *Neuropsychologia*, *46*(7), 2056–63.

Savage, C. R., Deckersbach, T., Heckers, S., Wagner, A. D., Schacter, D. L., Alpert, N. M., … Rauch, S. L. (2001). Prefrontal regions supporting spontaneous and directed application of

verbal learning strategies: evidence from PET. *Brain : A Journal of Neurology*, *124*(Pt 1), 219–31.

Savilla, K., Kettler, L., & Galletly, C. (2008). Relationships between cognitive deficits, symptoms and quality of life in schizophrenia. *Australian and New Zealand Journal of Psychiatry*, *42*(6), 496–504.

Schmiedt, C., Brand, A., Hildebrandt, H., & Basar-Eroglu, C. (2005). Event-related theta oscillations during working memory tasks in patients with schizophrenia and healthy controls. *Cognitive Brain Research*, *25*(3), 936–947.

Schnider, A., & Ptak, R. (1999). Spontaneous confabulators fail to suppress currently irrelevant memorytraces. *Nature Neuroscience*, *2*(7), 677–681.

Scholz, J., Klein, M. C., Behrens, T. E. J., & Johansen-Berg, H. (2009). Training induces changes in white-matter architecture. *Nature Neuroscience*, *12*(11), 1370–1371.

Schomer, D., & Lopes da Silva, F. (2005). *Electroencephalography: Basic Principles, Clinical Applications, and Related Fields*. Lippincott Williams & Wilkins.

Schultz, C. C., Koch, K., Wagner, G., Roebel, M., Schachtzabel, C., Gaser, C., … Schlösser, R. G. M. (2010). Reduced cortical thickness in first episode schizophrenia. *Schizophrenia Research*, *116*(2–3), 204–209.

Ségonne, F., Dale, A. M., Busa, E., Glessner, M., Salat, D. H., Hahn, H. K., & Fischl, B. (2004). A hybrid approach to the skull stripping problem in MRI. *NeuroImage*, *22*(3), 1060–75.

Ségonne, F., Pacheco, J., & Fischl, B. (2007). Geometrically accurate topology-correction of cortical surfaces using nonseparating loops. *IEEE Transactions on Medical Imaging*, *26*(4), 518–29.

Seidman, L. J., Giuliano, A. J., Meyer, E. C., Addington, J., Cadenhead, K. S., Cannon, T. D., … Cornblatt, B. A. (2010). Neuropsychology of the prodrome to psychosis in the NAPLS consortium: relationship to family history and conversion to psychosis. *Archives of General Psychiatry*, *67*(6), 578–88.

Seitz, J., Zuo, J. X., Lyall, A. E., Makris, N., Kikinis, Z., Bouix, S., … Kubicki, M. (2016). Tractography Analysis of 5 White Matter Bundles and Their Clinical and Cognitive Correlates in Early-Course Schizophrenia. *Schizophrenia Bulletin*, *42*(March), sbv171.

Serences, J. T. (2004). A comparison of methods for characterizing the event-related BOLD timeseries in rapid fMRI. *Neuroimage*, *21*(4), 1690–1700.

Sevy, S., & Davidson, M. (1995). The cost of cognitive impairment in schizophrenia. *Schizophrenia Research*, *17*(1), 1–3.

Shamsi, S., Lau, A., Lencz, T., Burdick, K. E., DeRosse, P., Brenner, R., … Malhotra, A. K. (2011). Cognitive and symptomatic predictors of functional disability in schizophrenia. *Schizophrenia Research*, *126*(1–3), 257–64.

Sharot, T., Kanai, R., Marston, D., Korn, C. W., Rees, G. E., & Dolan, R. J. (2012). Selectively altering belief formation in the human brain. *Proceedings of the National Academy of Sciences*, *109*(42), 17058–17062.

Shaw, P., Greenstein, D., Lerch, J., Clasen, L., Lenroot, R., Gogtay, N., … Giedd, J. (2006). Intellectual ability and cortical development in children and adolescents. *Nature*, *440*(7084),

676–679.

Sheehan, D., & Lecrubier, Y. (1998). The Mini-International Neuropsychiatric Interview (M.I.N.I.): the development and validation of a structured diagnostic psychiatric interview for DSM-IV and ICD-10. *The Journal of Clinical Psychiatry*, *59 Suppl 2*, 22–33.

Sherwood, M., Thornton, A. E., & Honer, W. G. (2006). A meta-analysis of profile and time-course of symptom change in acute schizophrenia treated with atypical antipsychotics. *The International Journal of Neuropsychopharmacology*, *9*(3), 357–366.

Siekmeier, P. J., & Stufflebeam, S. M. (2010). Patterns of spontaneous magnetoencephalographic activity in patients with schizophrenia. *Journal of Clinical Neurophysiology : Official Publication of the American Electroencephalographic Society*, *27*(3), 179–90.

Simmonds, D. J., Pekar, J. J., & Mostofsky, S. H. (2008). Meta-analysis of Go/No-go tasks demonstrating that fMRI activation associated with response inhibition is task-dependent. *Neuropsychologia*, *46*(1), 224–232.

Simon, J. R., & Wolf, J. D. (1963). Choice reaction time as a function of angular stimulus-response correspondence and age. *Ergonomics*, *6*(1), 99–105.

Sled, J. G., Zijdenbos, A., & Evans, A. C. (1998). A nonparametric method for automatic correction of intensity nonuniformity in MRI data. *IEEE Transactions on Medical Imaging*, *17*(1), 87–97.

Smith, A. M., Lewis, B. K., Ruttimann, U. E., Ye, F. Q., Sinnwell, T. M., Yang, Y., … Frank, J. A. (1999). Investigation of low frequency drift in fMRI signal. *Neuroimage*, *9*(5), 526–33.

Smith, S. M., Jenkinson, M., Johansen-Berg, H., Rueckert, D., Nichols, T. E., Mackay, C. E., … Behrens, T. E. J. (2006). Tract-based spatial statistics: voxelwise analysis of multi-subject diffusion data. *NeuroImage*, *31*(4), 1487–505.

Smith, S. M., Jenkinson, M., Woolrich, M. W., Beckmann, C. F., Behrens, T. E. J., Johansen-Berg, H., … Matthews, P. M. (2004). Advances in functional and structural MR image analysis and implementation as FSL. *NeuroImage*, *23 Suppl 1*, S208-19.

Smith, S. M., & Nichols, T. E. (2009). Threshold-free cluster enhancement: Addressing problems of smoothing, threshold dependence and localisation in cluster inference. *NeuroImage*, *44*(1), 83–98.

Sohal, V. S., Zhang, F., Yizhar, O., & Deisseroth, K. (2009). Parvalbumin neurons and gamma rhythms enhance cortical circuit performance. *Nature*, *459*(7247), 698–702.

Stephan, K. E., Friston, K. J., & Frith, C. D. (2009). Dysconnection in Schizophrenia: From Abnormal Synaptic Plasticity to Failures of Self-monitoring. *Schizophrenia Bulletin*, *35*(3), 509–27.

Stevenson, C. M., Brookes, M. J., & Morris, P. G. (2011). β-Band correlates of the fMRI BOLD response. *Human Brain Mapping*, *32*(2), 182–197.

Stipacek, A., Grabner, R. H., Neuper, C., Fink, A., & Neubauer, A. C. (2003). *Sensitivity of human EEG alpha band desynchronization to different working memory components and increasing levels of memory load*. *Neuroscience Letters* (Vol. 353).

Strelnikov, K., & Barone, P. (2013). Overlapping Brain Activity as Reflected by the Spatial

Differentiation of Functional Magnetic Resonance Imaging, Electroencephalography and Magnetoencephalography Data. *Journal of Neuroscience and Neuroengineering*, *2*(6), 550–561.

Stroop, J. R. (1935). Studies of interference in serial verbal reactions. *Journal of Experimental Psychology*, *18*(6).

Stuss, D. T., & Alexander, M. P. (2000). Executive functions and the frontal lobes: a conceptual view. *Psychological Research*, *63*(3–4), 289–298.

Sugihara, G., Oishi, N., Son, S., Kubota, M., Takahashi, H., & Murai, T. (2016). Distinct Patterns of Cerebral Cortical Thinning in Schizophrenia: A Neuroimaging Data-Driven Approach. *Schizophrenia Bulletin*, *170*(4), sbw176.

Sundermann, B., & Pfleiderer, B. (2012). Functional connectivity profile of the human inferior frontal junction: involvement in a cognitive control network. *BMC Neuroscience*, *13*(1), 119.

Swettenham, J. B., Muthukumaraswamy, S. D., & Singh, K. D. (2013). BOLD Responses in Human Primary Visual Cortex are Insensitive to Substantial Changes in Neural Activity. *Frontiers in Human Neuroscience*, *7*, 76.

Swick, D., Ashley, V., & Turken, A. U. (2008). Left inferior frontal gyrus is critical for response inhibition. *BMC Neuroscience*, *9*(1), 102.

Swick, D., & Chatham, C. H. (2014). Ten years of inhibition revisited. *Frontiers in Human Neuroscience*, *8*, 329.

Symms, M., Jäger, H. R., Schmierer, K., & Yousry, T. A. (2004). A review of structural magnetic resonance neuroimaging. *Journal of Neurology, Neurosurgery, and Psychiatry*, *75*(9), 1235–44.

Szeszko, P. R., Robinson, D. G., Ashtari, M., Vogel, J., Betensky, J., Sevy, S., … Bilder, R. M. (2008). Clinical and Neuropsychological Correlates of White Matter Abnormalities in Recent Onset Schizophrenia. *Neuropsychopharmacology*, *33*(5), 976–984.

Szeszko, P. R., Robinson, D. G., Ikuta, T., Peters, B. D., Gallego, J. A., Kane, J., & Malhotra, A. K. (2014). White Matter Changes Associated with Antipsychotic Treatment in First-Episode Psychosis. *Neuropsychopharmacology*, *39*(6), 1324–1331.

Takane, Y., & Shibayama, T. (1991). Principal component analysis with external information on both subjects and variables. *Psychometrika*, *56*(1), 97–120.

Tamnes, C. K., & Agartz, I. (2016). White Matter Microstructure in Early-Onset Schizophrenia: A Systematic Review of Diffusion Tensor Imaging Studies. *Journal of the American Academy of Child & Adolescent Psychiatry*, *55*(4), 269–279.

Tandon, R., Gaebel, W., Barch, D. M., Bustillo, J., Gur, R. E., Heckers, S., … Carpenter, W. (2013). Definition and description of schizophrenia in the DSM-5. *Schizophrenia Research*, *150*(1), 3–10.

Tandon, R., Nasrallah, H. A., & Keshavan, M. S. (2009). Schizophrenia, "just the facts" 4. Clinical features and conceptualization. *Schizophrenia Research*, *110*(1–3), 1–23.

Thornton, A. E., Boudreau, V. G., Griffiths, S. Y., Woodward, T. S., Fawkes-Kirby, T., & Honer, W. G. (2007). The impact of monetary reward on memory in schizophrenia

spectrum disorder. *Neuropsychology*, *21*(5), 631–645.

Thulborn, K. R., Waterton, J. C., Matthews, P. M., & Radda, G. K. (1982). Oxygenation dependence of the transverse relaxation time of water protons in whole blood at high field. *Biochimica et Biophysica Acta (BBA) - General Subjects*, *714*(2), 265–270.

Thut, G., Nietzel, A., Brandt, S. A., & Pascual-Leone, A. (2006). α-Band Electroencephalographic Activity over Occipital Cortex Indexes Visuospatial Attention Bias and Predicts Visual Target Detection. *Journal of Neuroscience*, *26*(37).

Tomasi, D., Ernst, T., Caparelli, E. C., & Chang, L. (2006). Common deactivation patterns during working memory and visual attention tasks: an intra-subject fMRI study at 4 Tesla. *Human Brain Mapping*, *27*(8), 694–705.

Tong, F. (2003). Cognitive neuroscience: Primary visual cortex and visual awareness. *Nature Reviews Neuroscience*, *4*(3), 219–229.

Tops, M., & Boksem, M. A. S. (2011). A potential role of the inferior frontal gyrus and anterior insula in cognitive control, brain rhythms, and event-related potentials. *Frontiers in Psychology*, *2*, 330.

Torres, U. S., Duran, F. L. S., Schaufelberger, M. S., Crippa, J. A. S., Louzã, M. R., Sallet, P. C., … Busatto, G. F. (2016). Patterns of regional gray matter loss at different stages of schizophrenia: A multisite, cross-sectional VBM study in first-episode and chronic illness. *NeuroImage: Clinical*, *12*, 1–15.

Tournier, J.-D., Mori, S., & Leemans, A. (2011). Diffusion tensor imaging and beyond. *Magnetic Resonance in Medicine : Official Journal of the Society of Magnetic Resonance in Medicine / Society of Magnetic Resonance in Medicine*, *65*(6), 1532–56.

Trandafir, A., Méary, A., Schürhoff, F., Leboyer, M., & Szöke, A. (2006). Memory tests in first-degree adult relatives of schizophrenic patients: A meta-analysis. *Schizophrenia Research*, *81*(2–3), 217–226.

Tzourio-Mazoyer, N., Landeau, B., Papathanassiou, D., Crivello, F., Etard, O., Delcroix, N., … Joliot, M. (2002). Automated anatomical labeling of activations in SPM using a macroscopic anatomical parcellation of the MNI MRI single-subject brain. *NeuroImage*, *15*(1), 273–89.

Uddin, L. Q., Kelly, A. M., Biswal, B. B., Xavier Castellanos, F., & Milham, M. P. (2009). Functional connectivity of default mode network components: correlation, anticorrelation, and causality. *Hum Brain Mapp*, *30*(2), 625–637.

Ueoka, Y., Tomotake, M., Tanaka, T., Kaneda, Y., Taniguchi, K., Nakataki, M., … Ohmori, T. (2011). Quality of life and cognitive dysfunction in people with schizophrenia. *Progress in Neuro-Psychopharmacology & Biological Psychiatry*, *35*(1), 53–9.

Uludağ, K., & Roebroeck, A. (2014). General overview on the merits of multimodal neuroimaging data fusion. *NeuroImage*, *102*, 3–10.

Vallaghé, S., Papadopoulo, T., & Clerc, M. (2009). The adjoint method for general EEG and MEG sensor-based lead field equations. *Physics in Medicine and Biology*, *54*(1), 135–47.

Van den Oord, E. J. C. G., Rujescu, D., Robles, J. R., Giegling, I., Birrell, C., Bukszár, J., … Muglia, P. (2006). Factor structure and external validity of the PANSS revisited.

Schizophrenia Research, 82(2–3), 213–23.

Van Veen, B. D., & Buckley, K. M. (1988). Beamforming: a versatile approach to spatial filtering. *IEEE ASSP Magazine*, 5(2), 4–24.

Van Veen, B. D., Van Drongelen, W., Yuchtman, M., & Suzuki, A. (1997). Localization of brain electrical activity via linearly constrained minimum variance spatial filtering. *IEEE Transactions on Biomedical Engineering*, 44(9), 867–880.

van Veen, V., & Carter, C. S. (2005). Separating semantic conflict and response conflict in the Stroop task: A functional MRI study. *NeuroImage*, 27(3), 497–504.

Vossel, S., Geng, J. J., & Fink, G. R. (2014). Dorsal and ventral attention systems: distinct neural circuits but collaborative roles. *The Neuroscientist : A Review Journal Bringing Neurobiology, Neurology and Psychiatry*, 20(2), 150–9.

Wagenmakers, E.-J., Ratcliff, R., Gomez, P., & McKoon, G. (2008). A Diffusion Model Account of Criterion Shifts in the Lexical Decision Task. *Journal of Memory and Language*, 58(1), 140–159.

Wallis, G., Stokes, M., Cousijn, H., Woolrich, M. W., & Nobre, A. C. (2015). Frontoparietal and Cingulo-opercular Networks Play Dissociable Roles in Control of Working Memory. *Journal of Cognitive Neuroscience*, 27(10), 2019–2034.

Watrous, A. J., Fried, I., & Ekstrom, A. D. (2011). Behavioral correlates of human hippocampal delta and theta oscillations during navigation. *Journal of Neurophysiology*, 105(4), 1747–1755.

Weiler, M. A., Fleisher, M. H., & McArthur-Campbell, D. (2000). Insight and symptom change in schizophrenia and other disorders. *Schizophrenia Research*, 45(1–2), 29–36.

Weiss, E. M., Siedentopf, C., Golaszewski, S., Mottaghy, F. M., Hofer, A., Kremser, C., … Fleischhacker, W. W. (2007). Brain activation patterns during a selective attention test — a functional MRI study in healthy volunteers and unmedicated patients during an acute episode of schizophrenia. *Psychiatry Research: Neuroimaging*, 154(1), 31–40.

Westen, D. (2012). Prototype diagnosis of psychiatric syndromes. *World Psychiatry : Official Journal of the World Psychiatric Association (WPA)*, 11(1), 16–21.

Whalley, H. C., Harris, J. C., & Lawrie, S. M. (2007). The neurobiological underpinnings of risk and conversion in relatives of patients with schizophrenia. *International Review of Psychiatry*, 19(4), 383–397.

Wheeler, A. L., & Voineskos, A. N. (2014). A review of structural neuroimaging in schizophrenia: from connectivity to connectomics. *Frontiers in Human Neuroscience*, 8, 653.

Whitfield-Gabrieli, S., Thermenos, H. W., Milanovic, S., Tsuang, M. T., Faraone, S. V., McCarley, R. W., … Seidman, L. J. (2009). Hyperactivity and hyperconnectivity of the default network in schizophrenia and in first-degree relatives of persons with schizophrenia. *Proceedings of the National Academy of Sciences*, 106(4), 1279–1284.

Whitford, T. J., Lee, S. W., Oh, J. S., De Luis-Garcia, R., Savadjiev, P., Alvarado, J. L., … Shenton, M. E. (2014). Localized abnormalities in the cingulum bundle in patients with schizophrenia: A Diffusion Tensor tractography study. *NeuroImage: Clinical*, 5, 93–99.

204

Whitman, J. C., Takane, Y., Cheung, T., Moiseev, A., Ribary, U., Ward, L. M., & Woolrich, M. W. (2015). Acceptance of evidence-supported hypotheses generates a stronger signal from an underlying functionally-connected network. *NeuroImage*, *127*, 215–226.

Whitman, J. C., Ward, L. M., & Woodward, T. S. (2013). Patterns of Cortical Oscillations Organize Neural Activity into Whole-Brain Functional Networks Evident in the fMRI BOLD Signal. *Frontiers in Human Neuroscience*, *7*, 80.

Winkler, A. M., Ridgway, G. R., Webster, M. A., Smith, S. M., & Nichols, T. E. (2014). Permutation inference for the general linear model. *NeuroImage*, *92*, 381–97.

Witt, S. T., Laird, A. R., & Meyerand, M. E. (2008). Functional neuroimaging correlates of finger-tapping task variations: an ALE meta-analysis. *NeuroImage*, *42*(1), 343–56.

Woodberry, K. A., Giuliano, A. J., & Seidman, L. J. (2008). Premorbid IQ in schizophrenia: a meta-analytic review. *The American Journal of Psychiatry*, *165*(5), 579–87.

Woodward, T. S., Jung, K., Smith, G. N., Hwang, H., Barr, A. M., Procyshyn, R. M., … Honer, W. G. (2014). Symptom changes in five dimensions of the Positive and Negative Syndrome Scale in refractory psychosis. *European Archives of Psychiatry and Clinical Neuroscience*, *264*(8), 673–682.

Woodward, T. S., Meier, B., Tipper, C. M., & Graf, P. (2003). Bivalency is costly: Bivalent stimuli elicit cautious responding. *Experimental Psychology*, *50*(4), 233–238.

Woodward, T. S., & Menon, M. (2011). Considerations for analysis of source monitoring data when investigating hallucinations in schizophrenia research. *European Archives of Psychiatry and Clinical Neuroscience*, *261*(3), 157–164.

Woodward, T. S., Metzak, P. D., Meier, B., & Holroyd, C. B. (2008). Anterior cingulate cortex signals the requirement to break inertia when switching tasks: A study of the bivalency effect. *NeuroImage*, *40*(3), 1311–1318.

Worden, M. S., Foxe, J. J., Wang, N., & Simpson, G. V. (2000). Anticipatory biasing of visuospatial attention indexed by retinotopically specific alpha-band electroencephalography increases over occipital cortex. *The Journal of Neuroscience*, *20*(6), RC63.

Wotruba, D., Michels, L., Buechler, R., Metzler, S., Theodoridou, A., Gerstenberg, M., … Heekeren, K. (2013). Aberrant Coupling Within and Across the Default Mode, Task-Positive, and Salience Network in Subjects at Risk for Psychosis. *Schizophrenia Bulletin*, sbt161-.

Wright, I. C., Rabe-Hesketh, S., Woodruff, P. W. R., David, A. S., Murray, R. M., & Bullmore, E. T. (2000). Meta-Analysis of Regional Brain Volumes in Schizophrenia. *American Journal of Psychiatry*, *157*(1), 16–25.

Xiao, Y., Lui, S., Deng, W., Yao, L., Zhang, W., Li, S., … Gong, Q. (2015). Altered cortical thickness related to clinical severity but not the untreated disease duration in schizophrenia. *Schizophrenia Bulletin*, *41*(1), 201–210.

Yao, L., Lui, S., Liao, Y., Du, M.-Y., Hu, N., Thomas, J. A., & Gong, Q.-Y. (2013). White matter deficits in first episode schizophrenia: An activation likelihood estimation meta-analysis. *Progress in Neuro-Psychopharmacology and Biological Psychiatry*, *45*, 100–106.

Yücel, M., Volker, C., Collie, A., Maruff, P., Danckert, J., Velakoulis, D., & Pantelis, C. (2002). Impairments of response conflict monitoring and resolution in schizophrenia. *Psychological Medicine*, *32*(7), 1251–1260.

Zeithamova, D., Dominick, A. L., & Preston, A. R. (2012). Hippocampal and Ventral Medial Prefrontal Activation during Retrieval-Mediated Learning Supports Novel Inference. *Neuron*, *75*(1), 168–179.

Zhang, X. Y., Fan, F.-M., Chen, D.-C., Tan, Y.-L., Tan, S.-P., Hu, K., … Soares, J. C. (2016). Extensive white matter abnormalities and clinical symptoms in drug-naive patients with first-episode schizophrenia: a voxel-based diffusion tensor imaging study. *The Journal of Clinical Psychiatry*, *77*(2), 205–11.

Zumer, J. M., Brookes, M. J., Stevenson, C. M., Francis, S. T., & Morris, P. G. (2010). Relating BOLD fMRI and neural oscillations through convolution and optimal linear weighting. *NeuroImage*, *49*(2), 1479–1489.

Zumer, J. M., Scheeringa, R., Schoffelen, J. M., Norris, D. G., & Jensen, O. (2014). Occipital Alpha Activity during Stimulus Processing Gates the Information Flow to Object-Selective Cortex. *PLoS Biology*, *12*(10), e1001965.